ProQuest LLC.
789 East Eisenhower Parkway
P.O. Box 1346
Ann Arbor, MI 48106 – 1346

FACTORS AFFECTING THE MAGNETIC PROPERTIES OF ALLOYS CONTAINING FINE DISPERSIONS OF COBALT

A thesis submitted to the Council for National Academic Awards for the Degree of Doctor of Philosophy

by

Richard Ernest Johnson

PREFACE

The properties of many permanent magnet materials are due to the presence of a finely divided ferromagnetic phase which, in some cases, contains a substantial proportion of cobalt. The most important examples are the alnico alloys, deriving permanent magnet properties from a fine dispersion of a ferromagnetic, b.c.c. phase rich in cobalt and iron.

This thesis is concerned with the magnetic properties of alloys in which the ferromagnetic dispersion is essentially pure cobalt. A large part of the work consists of an examination of an established group of permanent magnet materials, the binary cobalt aluminium alloys known as Malcolloy, in which cobalt is precipitated from super-saturated solid solution during heat treatment. The properties of an alloy in the cobalt titanium system, in which a cobalt precipitate can be induced by a similar process, are also considered and the possibility of producing sufficiently fine dispersions by the eutectic and eutectoid reactions occurring in several binary cobalt alloy systems is examined.

In the course of the investigations various magnetic parameters have been studied and it is perhaps useful, at this stage, to define these and to comment on their significance. Much more detailed discussions of the fundamental basis from which magnetic quantities and properties are derived, the units in which they are measured and the symbols by which they are conventionally represented have been presented by a number of authors. The reviews of McCaig, ("Permanent Magnets and Magnetism", ed. D. Hadfield, Iliffe Books Ltd., p.13, 1962) and Gould ("Cobalt Alloy Permanent Magnets", Cobalt Monograph Series, Centre d'Information du Cobalt, p.1, 1971) are particularly comprehensive. Despite its acceptance in the field of scientific education, the S.I. (or M.K.S.A.) system of units is not yet consistently used in the permanent magnet industry and the majority of current publications continue to express magnetic properties in C.G.S. units. The C.G.S. system has been used

Schematic magnetisation and demagnetisation curves (symbols based on C.G.S. system)

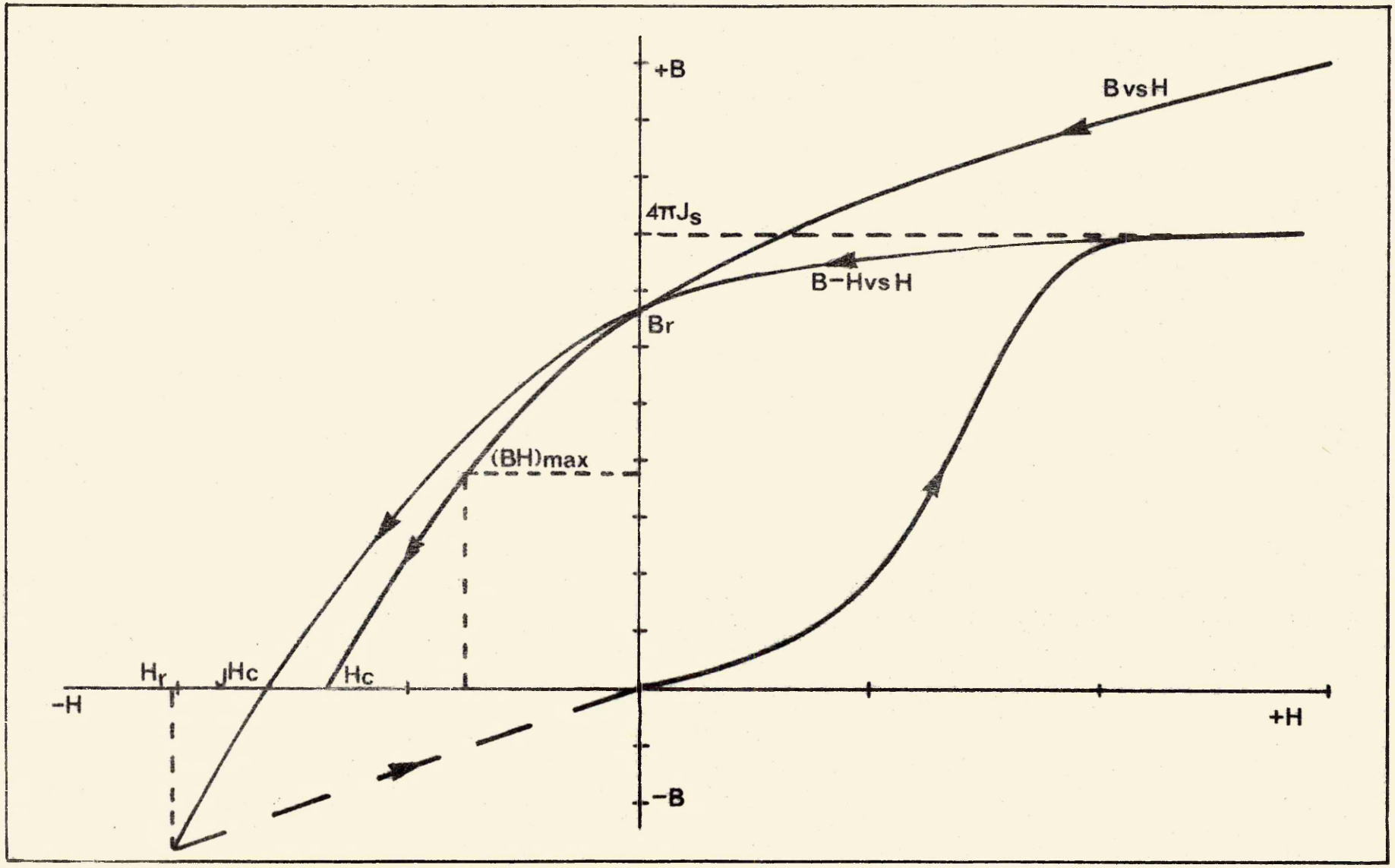

throughout the thesis but the corresponding S.I. units and the factors by which the C.G.S. units must be multiplied in order to convert to S.I. are given in this summary.

The properties, definitions etc., (largely from the work of Gould), are tabulated below and are best understood by reference to the accompanying diagram.

Symbol	Quantity	Units and Relationships C.G.S.	S.I.	C.G.S/S.I. ratio
B	Magnetic flux density	gauss, G	tesla, T	10^{-4}
H	Magnetic field strength	oersteds, Oe	ampère/metre, A/m	$\frac{10^3}{4\pi}$
J	Intensity of magnetisation	e.m.u. = G/4π = dyn/cm^2 Oe	T	$\frac{4\pi}{10^4}$
Bi	Intrinsic flux density	G Bi=4πJ=B-H	T Bi=J=B-μ_oH	10^{-4}
Bi_s	Intrinsic flux density at saturation	G $Bi_s=4\pi J_s$	T $Bi_s=J_s$	10^{-4}
σ	Specific saturation	emug^{-1}=dyn cm/g Oe =4πJ$_s$/4π density	Tm^3/kg σ=J$_s$/density	$\frac{4\pi}{10}$
B_r	Remanence = flux density at zero H after saturation	G	T	10^{-4}
H_c	Coercivity or normal coercivity = H value to reduce B to zero after previous saturation	Oe	A/m	$\frac{10^3}{4\pi}$
J^H_c	Intrinsic coercivity = H value to reduce Bi to zero after previous saturation	Oe	A/m	$\frac{10^3}{4\pi}$
Hr	Remanence coercivity = H value after the application of which Bi recoils to zero	Oe	A/m	$\frac{10^3}{4\pi}$
$(BH)_{max}$	Maximum product in the demagnetising quadrant of the hysteresis loop	mega gauss oersteds, MGO or 10^6 G Oe	kJ/m^3 or kAT/m	$\frac{10^2}{4\pi}$

Saturation magnetisation (σ or Bi_s) is clearly one of the most important parameters in the study of any magnetic material. As a matter of convenience, the measurement of σ rather than Bi_s has been preferred in this work because σ is easily determined using small irregular samples or powders. σ, which is related to composition, can be used, providing certain information regarding the magnetic properties of the phases present is available, as the basis of magnetic phase analysis techniques, (Hoselitz, K., "Ferromagnetic Properties of Metals and Alloys", Oxford, Clarendon Press, 1952). σ may be quoted as $\sigma H, T$, i.e., σ at temperature $T^{o}K$ in field H. Alternatively, (as in this thesis) σ without subscripts is used together with a statement of temperature and magnetising field.

The most significant difference between soft and hard (or permanent) magnet materials is the magnitude of the coercivity, (H_c, $_JH_c$, or H_r). Thus in a soft magnetic material $_JH_c$ may be of the order 10^{-3} Oe whereas permanent magnets with $_JH_c$ of the order 10^4 Oe are known. The most frequently quoted measure of coercivity is H_c, (H value to reduce B to zero). However, since $B = Bi + H$ (in C.G.S.), H_c (in oersteds) cannot exceed B_r (in gauss) and if B_r is low or $_JH_c$ is high the value of H_c may bear no relationship to the field necessary to reverse the magnetisation of the material. In a sample in which the magnetisation of the total volume of magnetic material is reversed at a particular applied field, $_JH_c$ and H_r are equal and represent the fundamental coercivity of the material. In practice, reversal of magnetisation almost invariably occurs over a range of applied fields so that in the presence of a field equal to $_JH_c$ or after the application and removal of a field equal to H_r the magnetisation of a sufficient volume of material has been reversed to make Bi equal in both directions giving a net flux density of zero. When the demagnetising field is removed, the negative contribution to Bi of the lower coercivity volume fraction is reduced and as a result H_r is always greater than $_JH_c$. Neither property

indicates the maximum coercivity present although H_r is clearly closer to the maximum and some information regarding the range of coercivity can be obtained from the ratio $H_r/_JH_c$. In practice, coercivity is important in governing the performance of a magnet in the presence of a demagnetising field, (the self demagnetising field and any externally applied field), and in this respect $_JH_c$ is a more useful parameter and is more frequently quoted than H_r.

Although the factors influencing coercivity are quite well understood in principle, the coercivity of real systems, where several factors act in combination, is not normally predictable with any accuracy and the mechanisms through which known permanent magnet materials derive high coercivity are not always obvious. Remanence (B_r) and maximum energy product ($(BH)_{max}$) are of equal importance to coercivity but the factors controlling these properties are clearly defined and there is normally little difficulty in understanding the level of B_r and $(BH)_{max}$ in terms of saturation magnetisation, coercivity and certain metallurgical factors such as particle orientation. Thus fundamental research into permanent magnets is normally concentrated primarily on coercivity with work at a more practical level endeavouring to combine the conditions necessary to achieve high coercivity with those required to give useful values of B_r and $(BH)_{max}$.

CONTENTS

CHAPTER 1 INTRODUCTION

1.1. Sources of Coercivity in Ferromagnetic Materials

1.1.1. Ferromagnetic domains and domain boundaries.

In ferromagnetic materials the very large internal field, first postulated by Weiss[1], results in domains, spontaneously magnetised to saturation, with magnetisation vectors distributed in a random manner but capable of being aligned on application of an external magnetising field. Between adjacent domains are domain boundaries, otherwise known as domain or Bloch walls, across which the direction of magnetisation changes from that of one domain to that of the other.

Ferromagnetic crystals are strongly anisotropic with respect to ease of magnetisation; iron for example is most easily magnetised along $[100]$[2] whilst in nickel[3] and f.c.c. cobalt[4] $[11\bar{1}]$ directions are preferred. Lattice strain can also give rise to some degree of anisotropy. Domains in ferromagnetic material are spontaneously magnetised in preferred directions but this is not possible within domain boundaries where rotation of the direction of magnetisation takes place. Domain boundaries are therefore regions of high energy. Boundary energy is further increased because exchange forces, tending to make neighbouring spins parallel have to be overcome as rotation is achieved.

1.1.2. Coercivity due to restricted domain boundary movement.

Theories attempting to account for coercivity in terms of restricted domain boundary movement have been reviewed by various authors including Hoselitz[9] and Stoner[10].

The application of an external field normally leads to domain boundary movement such that the volume of domains favourably oriented with respect to the applied field increases at the expense of those less favourably oriented. If this movement is hindered in any way the external field necessary to bring about a change in the overall magnetisation of the material is increased. Various mechanisms have been proposed to

account for the coercivity of permanent magnet materials on this basis.

If a boundary intersects a number of non-magnetic inclusions its area and consequently its energy is reduced. It is feasible that the increase in energy involved in moving such a boundary so that it intersected fewer inclusions would result in high coercivity. Similarly in a crystal containing inhomogeneous strains the contribution of strain anisotropy to boundary energy would vary depending on boundary position. An increased external field would be necessary to move a boundary from a low energy site.

Some early attempts were made using both the above mechanisms to account for the coercivity of ferromagnetic materials including the Alnico permanent magnet alloys in which Bradley and Taylor[5], using X-ray techniques, detected the presence of both strains and precipitate particles. Kersten[6] dealing with non-magnetic inclusions and Becker et al[7] considering the strain mechanism, showed that coercivities of the right levels could be predicted but in both cases a plane domain boundary was assumed together with a regular distribution of either precipitate particles or strains. These assumptions were criticised by Néel[8] who pointed out that an overestimate of coercivity was likely. Thus in Kersten's model a plane boundary intersecting a large number of inclusions was displaced to a position where it intersected none. If the boundary could bend or if the inclusions were less regularly arranged, the variation in the number of inclusions intersected as the boundary moved would be reduced with a consequent reduction in coercivity. The calculations of Becker et al dealing with strain are subject to similar criticism. As an alternative, Néel[8] suggested that if a domain boundary intersected a region of magntic poles associated with non-magnetic or weakly magnetic inclusions or strains the energy of the fields connected with the poles would be reduced. An increased applied field would thus be required to move the boundary away from this region.

1.1.3. The coercivity of single domain particles

The magnetic energy of a ferromagntic particle uniformly magnetised

as a single domain is $-\frac{1}{2} H_d J_s$ per unit volume of the particle, where H_d is the self demagnetising field and J_s is saturation magnetisation. The subdivision of the particle into a number of domains reduces H_d which, if the domains form a complete magnetic circuit within the particle, may, ideally, approach zero. The formation of daomain boundaries thus results in a lowering of particle energy. Domain boundary energy, as discussed above, is however introduced.

Particle energy is proportional to particle volume and, therefore, decreases as the cube of the particle radium, whereas domain boundary energy, which is proportional to boundary area and, therefore, roughly speaking, to particle cross section area, varies with r^2. Thus as the size of a particle is reduced a point is reached at which the reduction in particle energy due to the appearance of a boundary is less than the energy of the boundary. Consequently the total energy is less if the particle remains as a single domain. Went et al[11], using formulae for particle and boundary energy produced by Kittel[12], derived the following expression for the particle diameter at which particle and boundary energy are equal in isolated, single-crystal, spheres, i.e. the critical diameter for single domain behaviour (d_o).

$$d_o = \frac{9\sqrt{K}}{J_s} \sqrt{\frac{k T_c}{a J_o^2}}$$

K = crystal anisotropy constant
J_s = saturation magnetisation
J_o = saturation magnetisation at 0^oK
k = Boltzmann's constant
T_c = Curie temperature
a = lattice constant

In the absence of domain boundaries, changes in the magnetisation of a single domain particle can only occur by rotation of the magnetisation direction. This must take place in opposition to the anisotropy forces and the coercivity of the particle is therefore dependent on the nature and magnitude of these forces.

Anisotropy can arise from crystal structure, strain or particle shape, the preferred direction of magnetisation in the latter case being parallel to the axis of elongation. Stoner and Wohlfarth[13] derived expressions for the coercivities of single domain particles exhibiting crystal, shape or anisotropy as follows.

For a spherical particle exhibiting uniaxial crystal anisotropy -

$$_{J}H_{c} = \frac{2K}{J_s}$$

where K is the crystal anisotropy constant (see section 3.3) and J_s is saturation magnetisation.

For a prolate ellipsoid with only shape anisotropy -

$$_{J}H_{c} = (N_b - N_a)\, J_s$$

where $(N_b - N_a)$ is the difference in the two principal demagnetising factors for a prolate ellipsoid.

For a spherical particle subjected to uniaxial stress

$$_{J}H_{c} = \frac{3\,\lambda\,T}{J_s}$$

where λ is the saturation magnetostriction i.e. the change in length per unit length on magnetisation to saturation and T is the longitudinal strain.

It is clear that the coercivity of an assembly of such particles can only approach the optimum value indicated by these formulae if all the particles are aligned with their easy directions of magnetisation parallel. Stoner and Wohlfarth proceed to show that in a random assembly of particles coercivity is reduced by a little more than half, so that the above expressions become -

$$H_c = \frac{0.958K}{J_s}, \quad H_c = 0.479\,(N_b - N_a)\,J_s, \quad H_c = \frac{1,437\,\lambda\,T}{J_s}$$

The hysteresis curves calculated by Stoner and Wohlfarth also indicate that remanence, which in a fully aligned assembly is equal to saturation magnetisation, is reduced by half if the orientation is random.

Fig. 1 - a Spin Rotations During Uniform Rotation [15]
b Vector Rotation During Fanning [14]
c Spin Rotations During Buckling [15]
d Spin Rotations During Curling [15]

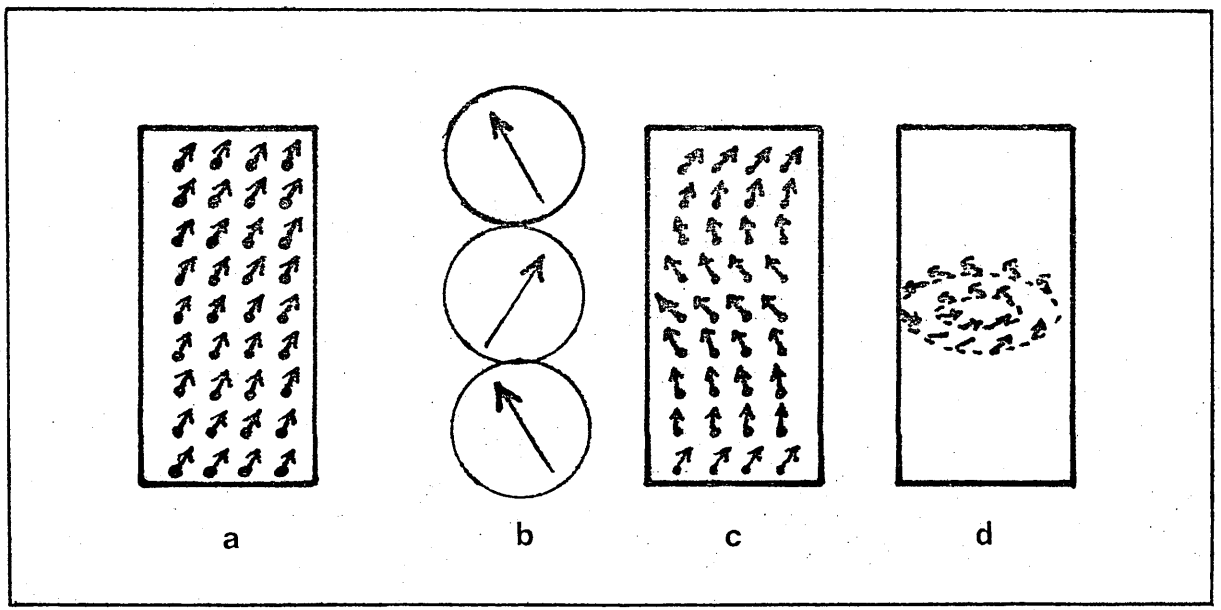

1.1.4. Factors affecting the properties of single domain particles

The single domain hypothesis accounts for the coercivity of many of the more important permanent magnet materials, (e.g. Alnico, barium ferrite). In general, however, properties measured in practice are considerably less than those predicted by theory and a number of factors must be considered to account for these discrepancies.

(a) Mechanisms for incoherent rotation. The expressions derived by Stoner and Wohlfarth[13] deal with particles or assemblies or particles which are anisotropic single domains in which coherent rotation of the magnetisation vector takes place uniformly in opposition to the anisotropy forces. There are, however, alternatives to uniform rotation which in certain circumstances may require less energy and thus lead to lower coercivity. Bean and Jacobs[14] showed that elongated iron particles, with coercivity less than half that predicted on the basis of uniform rotation, were, in fact, chains of spheres in which rotation occurred by a fanning mechanism such that the magnetisation of adjacent spheres rotated in different directions and to differing extents (Figure 1.b). In regular particles Frei, Shtrickman and Treves[15] proposed two processes by which rotation could occur at lower fields than those necessary to cause coherent rotation. These were buckling, (a similar mechanism to fanning) and curling. The spin rotations occurring in both are shown in figures 1.c. and 1.d. The fields necessary to bring about the onset of buckling and curling are dependent on various factors including particle size. Calculations show[15] that, in a sufficiently small particle, uniform rotatin and buckling are nucleated by similar fields and are energetically preferred to curling. As particle size increases, however, the energy to bring about buckling and curling decreases until the first buckling and then curling are favoured. Thus except in the case of extremely small particles coercivity is likely to be considerably lower than that predicted by Stoner and Wohlfarth[13]. Furthermore, any irregularity in particle shape is likely to facilitate the onset of non-uniform rotational processes such as fanning and buckling and lead to further reduction in coercivity.

(b) Mixed anisotropies. The formulae of Stoner and Wohlfarth deal individually with the three types of anisotropy. In practice, one type may predominate but some influence from the others is likely and if this acts in a different direction, rotation will be easier and coercivity reduced. The properties of particles with mixed anisotropies have been considered by Wohlfarth and Tonge[16].

Various authors, including Rathenauet al[17], Aharoni[18] and Brown[19], have shown that the reduced anisotropy associated with crystalline imperfections would lower the coercivity of ferromagnetic particles. In general this may be due either to the nucleation of domain boundaries in what otherwise would be a single domain, or to the encouragement of the incoherent rotational processes discussed above. In either case coercivity would be reduced.

(c) Mixed coercivities. When an assembly of ferromagnetic particles is produced, either by powder metallurgical techniques or as a component of a multi-phase alloy, some variation in particle size and shape and in the nature and concentration of defects is inevitable. Variations in the coercivities of the particles are therefore likely. The effect on the coercivity of the assembly is clearly dependent on the range of coercivities and on the coercivity distribution. Wohlfarth[20] reviews a number of attempts to understand the properties of assemblies with varying coercivities. The main conclusion to be reached is that the mixture coercivity is lower than a simple mean and that it falls rapidly as the amount of lower coercivity material increases. This matter has been considered more recently by McCurrie[21] in connection with cobalt rare-earth alloys and is discussed in more detail elsewhere in the present work. It is sufficient at this stage to point out that the coercivity of particle assemblies and therefore of real permanent magnets is always likely to be considerably lower than that predicted by theory for a single particle.

(3) Packing density. Another important consideration in connection with the properties of shape anisotropic particle assemblies is the packing density. As such particles are brought closer together interaction leads to a reduction in anisotropy and therefore in coercivity. Néel[22a] suggested the relationship $H_{c(p)} = H_{c(o)}(1-p)$ where p is the packing factor $\left(\frac{\text{total volume of particles present}}{\text{volume occupied by the dispersion}}\right)$. This was in reasonable agreement with some of the effects observed in practice. Wohlfarth[20] modified this formula as follows –

$$H_{c(p)} = H_{c(o)} - ApJ_o$$

where A depends on particle distribution and may be of either sign. Thus certain distributions may be envisaged in which particle interaction would increase coercivity. A simple example is a chain of spheres tending to act as an elongated particle. In general, however, a reduction in coercivity of the order indicated by Néel's formula is more likely. In addition to high coercivity a permanent magnet ideally requires the highest possible saturation and remanent magnetication and thus a high degree of packing. In practice a compromise between perfect packing, to give maximum magnetisation, and infinite dilution, to give maximum coercivity, is necessary so that reasonable values of each property and, therefore, of maximum energy product $((BH)_{max})$, are obtained. The coercivity of particles with high uniaxial crystal anisotropy are unaffected by packing because the anisotropy is inherent in their structure. Packing density may, therefore, approach 100% without loss of coercivity providing the single domain character of the particles is preserved.

1.1.5. The properties of some significant permanent magnet materials.

Amongst the most important and best known permanent magnet materials are the Alnico alloys. Some indication of the range of compositions and properties is given in Table 1. In these alloys, suitable heat treatment leads to spinodal decomposition into two b.c.c. phases; one, rich in iron and cobalt, is ferromagnetic, the other, rich in nickel and aluminium, is not. Many authors notably de Vos[23] have published photomicrographs of this

TABLE 1

COMPOSITIONS AND PROPERTIES OF SOME OF THE ALNICO ALLOYS

Alloy	Composition									Properties		
	Al %	Ni %	Co %	Cu %	Nb %	Ti %	Si %	S %	Fe %	B_r G	$(BH)_{max}$ MGO	H_c Oe
Alni*	12.5	25.5		4.5					Bal	6200	1.25	480
Alnico*	9.2	16.4	12.3	5.0				0.2	"	8000	1.7	500
Alcomax III	8.0	13.5	24.5	3.0	0.6		0.2	0.2	"	12600	5.4	650
Columax**	8.0	13.5	24.5	3.0	0.6		0.2	0.2	"	13500	7.5	740
Hycomax III	7.0	14.5	35.5	3.0		5.2			"	9000	5.5	1600
Hycomax III**	7.0	14.5	35.5	3.0		5.2		0.25	"	10400	8.0	1600
								Te %				
Hycomax IV	7.5	14.5	37.0	3.0		7.5				7800	5.8	1900
Hycomax IV**	7.5	14.5	37.0	3.0		7.5		2.0		9500	10.0	2000
de Vos [23]***	7.5	14.9	34.8	2.4		5.4				11500	13.4	1525

* isotropic properties, all others anisotropic

** cast with columnar crystal structure

*** single crystal

structure showing elongated particles of about the right size for single domain behaviour (shortest axis ≈200 Å). There is no doubt that these particles act as shape anisotropic single domains and are responsible for the permanent magnet properties of the alloys. Elongation of the ferromagnetic particles occurs parallel to <100> directions in the matrix and if a magnetic field is applied during heat treatment, those <100> directions most nearly parallel to the field direction are preferred. A considerable degree of anisotropy is, therefore, induced with superior properties in the field direction. The effect is even more marked if the alloy is prepared with a columnar crystal structure such that the <100> directions in all the crystals are parallel and if during heat treatment a magnetic field is applied parallel to the columnar axis.

Using a carefully controlled process, Luborsky et al[24] prepared elongated single domain (E.S.D.) particles or iron and iron cobalt alloy. The particles, produced by electrodeposition into a liquid mercury cathode, had diameters between 100 and 200 Å and length much greater than diameter although electron micrographs showed chains of spheres rather than regular cylinders. Aligned compacts of these powders, bonded with plastic or lead or tin alloys, are produced commercially in the U.S.A. and are known as Lodex. The best reported properties are -

$$B_r = 9{,}050\ G,\ (BH)_{max} = 5.04\ M.G.O.,\ H_c = 1{,}025\ Oe.$$

Although having only limited application, these materials are of interest as examples of permanent magnets based on shape anisotropic single domain particles and were developped as a direct result of the theoretical work of Stoner and Wohlfarth[13] and others, referred to earlier.

Barium ferrite ($BaFe_{12}O_{19}$) is the most important of the ceramic or oxide permanent magnet materials. This group characteristically has low value of saturation and remanent magnetisation coupled with relatively high coercivity. Typical properties of a barium ferrite magnet are as follows

$$B_r = 3{,}500\ G,\ (BH)_{max} = 3.0\ M.G.O.,\ H_c = 2{,}500\ Oe.$$

The ferrites have hexagonal crystal structures with strong uniaxial crystal anisotropy such that the c axis ([0001]) is the preferred direction of magnetisation. Went et al[11] calculate d_o (single domain diameter) as 1.2 μm. Magnets are prepared by compacting and sintering particles of about this size to about 90% of theoretical density. The properties are attributed to the single domain behaviour of these highly crystal anisotropic particles. Particle alignment so that the easy directions of magnetisation are parallel is normally achieved by the application of a magnetic field during compaction.

Permanent magnets based on the compound $R Co_5$, where R is a rare earth metal, notably samarium, are at present the subject of a great deal of research throughout the world. The best properties are obtained on aligned sintered compacts of powdered material; $(BH)_{max}$ values of around 20 M.G.O., B_r in excess of 9000 G and H_c around 9000 Oe, have been reported by a number of workers including Buschow et al[25], Tsui and Strnat[26], Benz and Martin[27] and the present author in collaboration with Fellows[28]. The intrinsic coercivity of powdered and compacted material is around 30 - 40 k Oe. The precise mechanism by which these alloys derive their properties is not clear at present. The compounds are hexagonal with extremely high crystal anisotropy. The anisotropy field (i.e. that necessary to cause uniform rotation is in excess of 300 kOe which is an order of magnitude greater than the observed intrinsic coercivity. Furthemore, the best properties are achieved when particle size is much greater than any reasonable estimate of d_o. It seems likely therefore, that in this case we are not dealing with single domain particles. Zijlstra[29], on the basis of hysteresis measurements carried out on a single particle of $Sm Co_5$ only a few microns in diameter, suggested that domain boundaries are present and that movement is restricted, particularly close to the particle surface. This view is supported by Schweizer et al[30] working with material slightly removed from the stoichiometric composition

R Co_5, who found that phase changes occurring at the particle surface during sintering could result in lattice strain and the pinning of domain boundaries. Thus in these materials it appears that a mechanism based on restricted boundary movement is responsible for an extremely high level of coercivity.

Another alloy in which a very high coercivity is attributed to restricted domain boundary movement is the equiatomic cobalt platinum alloy. Its properties are inferior to those of Sm Co_5 but have the advantage of being isotropic. By suitable heat treatment it is possible to produce in this alloy a partially ordered structure consisting of a mixture of disordered face centred cubic and ordered face centred tetragonal lattices. The two are coherent but the degree of disregistry involved leads to strain which is thought to be responsible for the development of a high coercivity.

1.2. Magnetic Properties of Finely Divided Cobalt.

1.2.1. Potential properties.

In an ideal permanent magnet the value of $_JH_c$ (intrinsic coercivity) is equal to or greater than $4\pi J_s$ (saturation magnetisation), Br (remanence) is equal to $4\pi J_s$ and the intrinsic demagnetisation curve is square, i.e. on application of a demagnetising field there is no reduction in intrinsic magnetisation until the applied field exceeds the value of Br. In such a magnet B_r is equal to H_c (coercivity) and $(BH)_{max}$ is given by $B_r^2/4$. Only in the cobalt rare-earth alloys is this ideal achieved in practice and in most materials, particularly those based on shape anisotropic particles, properties are much less than the ideal. It is useful, however, to begin this account of the properties of finely divided cobalt by assessing the maximum properties which can be anticipated.

The $4\pi J_s$ value of cobalt is 17,500 G; maximum possible $(BH)_{max}$ is therefore about 77.0 M.G.O. Both a, f.c.c. cobalt and c, h.c.p. cobalt

Fig. 2 - Variation of the Anisotropy Constants K_1 and K_2 for Cobalt [32]

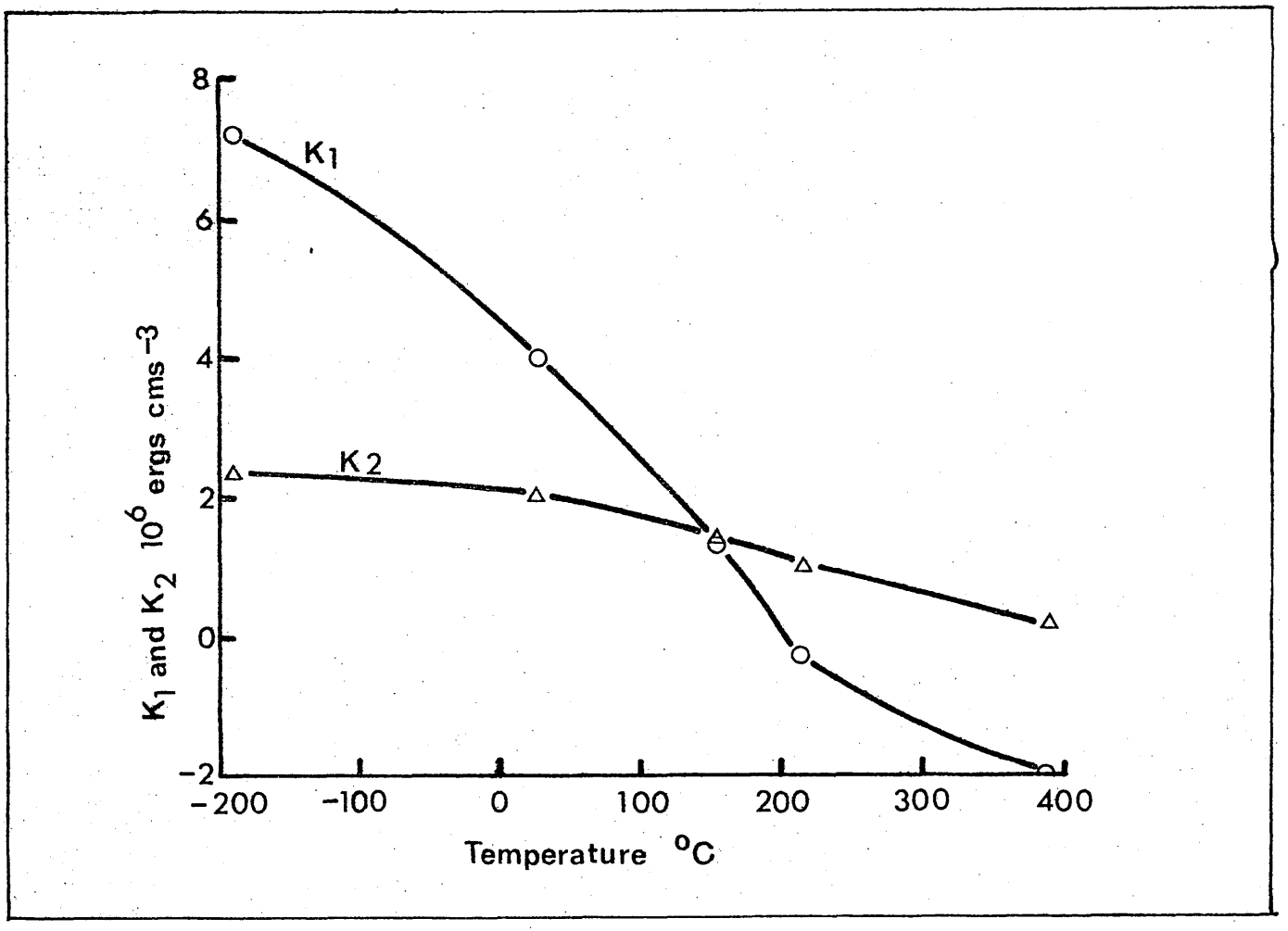

can exist at room temperature, and there is little difference in $4\pi J_s$ but a large difference in crystal anisotropy. The mechanisms leading to a high coercivity in each are therefore quite different and they must be considered seperately in making a more realistic estimate of potential magnetic properties.

Consider first c (f.c.c.) cobalt). The magnetocrystalline anisotropy is low with <111> preferred[4]. A high coercivity is most likely to be achieved therefore if single domain particles with shape anisotropy are produced. Single domain size is similar to that of iron, i.e. around 200 Å. If an assembly of perfect ellipsoids with an axial ratio greater than 10 are assumed to undergo uniform rotation the coercivity, according to the formula of Stoner and Wohlfarth[13], $[H_c = J_s\ (Nb-Na)]$ is around 8000 Oe. if alignment is perfect. However, it has already been shown that the coercivity of shape anisotropic particles is reduced by about half at a packing density of 50%. Maximum $4\pi J_s$ and $_JH_c$ of an aligned compact with 50% packing are therefore 8,750 G and 4,000 Oe respectively. Disregarding any further reduction in $_JH_c$ due to non-uniform rotation $(BH)_{max}$ is given by (8,750 - 4,000) x 4,000 = 19.0 M.G.O. Such a material would be an extremely useful permanent magnet but the value of $(BH)_{max}$ for b.c.c. iron worked out on a similar basis is 33.5 M.G.O. There is thus no obvious advantage in the use of f.c.c. cobalt as compared to iron, particularly since the former is more expensive.

The situation is quite different in the case of ε(h.c.p. cobalt), the permanent magnet properties of which have been discussed by McCaig[31] ε has high crystal anisotropy and the energy of magnetisation is given by

$$E = K_o + K_1 \sin^2\theta + K_2 \sin^4\theta$$

where θ is the angle between the magnetisation vector and the easy direction of magnetisation [0001]. Values of the anisotropy constants K_1 and K_2 have been determined at various temperatures by Honda and Masumoto[32] and are shown in Figure 2. Stoner and Wohlfarth[13], using K_1

on a first approximation for K in the expression

$$H_c = \frac{2K}{Js}$$

calculate a value of about 6000 Oe for the coercivity of single domain particles of ε. Because coercivity is based on crystal anisotropy packing density of the particles can approach 100%. Assuming perfect packing and alignment therefore B_r = 17,500 G, H_c = 6,000 Oe and $(BH)_{max}$ = 69.0 M.G.O. Using similar reasoning to that of McCaig[31] it is possible to assess the properties if packing and alignment are not perfect. Suppose the packing density was only 50%, as might be the case in an unsintered powder compact or if cobalt was precipitated from solid solution. The values of $4\pi J_s$ and B_r would be reduced to 8,750 G, and since H_c is greater than ½ B_r, $(BH)_{max} = B_r^2/4$ = 19.2 M.G.O. If, at the same time, alignment was random B_r would be reduced to 4,375 G and $_JH_c$ (intrinsic coercivity) would become 2,960 Oe. H_c, which in an imperfectly aligned assembly is less than $_JH_c$, and $(BH)_{max}$, can be estimated from a curve given by Stoner and Wohlfarth[13] as about 1,800 Oe and 2.0 M.G.O. respectively. Gerling[33] derived a rather more accurate relationship for the coercivity of randomly oriented crystal anisotropic particles. Using this, $_JH_c$ = 3,300 Oe, H_c = 2,000 Oe and $(BH)_{max}$ = 2.25 M.G.O. Finally, if $_JH_c$ was further reduced, due to the various factors discussed in section 1.14, to say 1,500 Oe, B_r would remain at 4,375 G, H_c would be about 1,250 Oe and $(BH)_{max}$ about 1.4 M.G.O.

From these results it can be seen that h.c.p. cobalt is, potentially, a useful permanent magnet material providing that a high degree of alignment and packing can be achieved. Because they have high crystal anisotropy, particles of ε need not be elongated, as is the case with cubic iron or cobalt, and single domain size is, according to Went et al[11] about 0.25 μm, i.e. an order of magnitude greater than that of the cubic materials. Particles with high coercivity should therefore be more easily produced.

1.2.2. Properties observed in practice.

The magnetic properties of finely divided cobalt, both α and ε, as powders and as components of two phase alloys, have been reported by various workers.

Meiklejohn[34] examined particles of iron and cobalt, produced by electro-deposition into mercury. Coercivity was dependant on particle size with, for both metals, a peak of 1,000 Oe (measured at liquid nitrogen temperature) at about 200 Å. The stable crystal structure of cobalt below about 400°C is h.c.p. (ε) and d_o, according to theory is about 2,500 Å. Meiklejohn comments on the fact that peak coercivity and presumably single domain size for his cobalt powder occurred at a particle size an order of magnitude smaller than this. He does not appear, however, to establish the hexagonal nature of the particles and, as discussed in section 1.3 and in Appendix I, it is quite possible for cobalt, particularly if it is finely divided, to have the cubic structure at temperatures far below the equilibrium transformation temperature. It may be that in this case the cobalt particles had a largely f.c.c. structure. Behaviour similar to that of iron would then be expected.

Cobalt powders with coercivity up to about 600 Oe were examined by Weil[35]. In this case the cobalt was hexagonal. As was expected for a material with high crystal anisotropy packing density had no effect on coercivity. Furthermore, although coercivity was an order of magnitude less than that calculated from $2K/J_s$, it was shown to vary in a logical manner as K and J_s were altered by varying the temperature, (the effect of temperature on the anisotropy of ε is shown in Figure 2).

More recently Lavin[36] reported the preparation, by an evaporation technique, of cobalt fibres, with coercivity as high as 2,200 Oe. Electron microscopy showed these to be chains of spheres, not unlike those produced by Luborsky et al[24]. The crystal structure was largely f.c.c. and it was thought that a trace of h.c.p. cobalt detected by X-ray and electron diffraction was due to stacking faults in the f.c.c. structure. Thus the

coercivity was assumed to be due to shape rather than crystal anisotropy.

Bate et al[37] and Bucksmith[38] measured the properties of copper cobalt Alloys in which a precipitate of cobalt was produced by heat treatment. The alloys were rich in copper with cobalt between 0.7% and 4.0%. After solution treatment and quenching the alloys were aged to bring about precipitation of cobalt. Although the highest ${}_{J}H_{c}$ measured did not exceed 250 Oe, various other observations indicated that a certain amount of material with a much higher coercivity was present. For instance saturation magnetisation is normally achieved in an applied field of the order 3 - 5 times greater than the coercivity; in these alloys no approach to saturation was observed in fields up to 15,000 Oe. Measurements were also made of the field necessary to reduce remanent magnetisation to zero (H_r). This is normally not much greater than ${}_{J}H_{c}$ but in these alloys values of $H_r/{}_{J}H_{c}$ approaching 50 were obtained. These results were taken to indicate the presence of a large range in the coercivity of the precipitate with maximum values in excess of 1,500 Oe. It was not possible to determine the crystal structure of the cobalt. It was pointed out, however, that the matrix was f.c.c. and that there is a tendency for finely divided cobalt to retain the f.c.c. structure. It is likely, therefore, that the precipitate was f.c.c.

A considerable amount of work has been reported dealing with the possibility of producing elongated single domain particles by the controlled directional solidification of eutectic alloys. In most cases the ferromagnetic component was iron rich, although in a few cases alloys with nickel or cobalt have been examined. This work has been reviewed by Calasso[39]. In most cases ${}_{J}H_{c}$ was low, frequently around 20 Oe, but in the work of Livingston[40] a more useful level of properties was achieved. Livingston found that the coercivity of a directionally solidified gold cobalt eutectic alloy increased with increased growth rate and related this to a finer eutectic structure. The best ${}_{J}H_{c}$, as grown, was 330 Oe using a growth rate of 2.1×10^{-1}cm/sec. A specimen grown at 9.3×10 cm/sec had ${}_{J}H_{c}$

Fig. 3 - Cobalt Aluminium Phase Diagram (After Scarum [50])

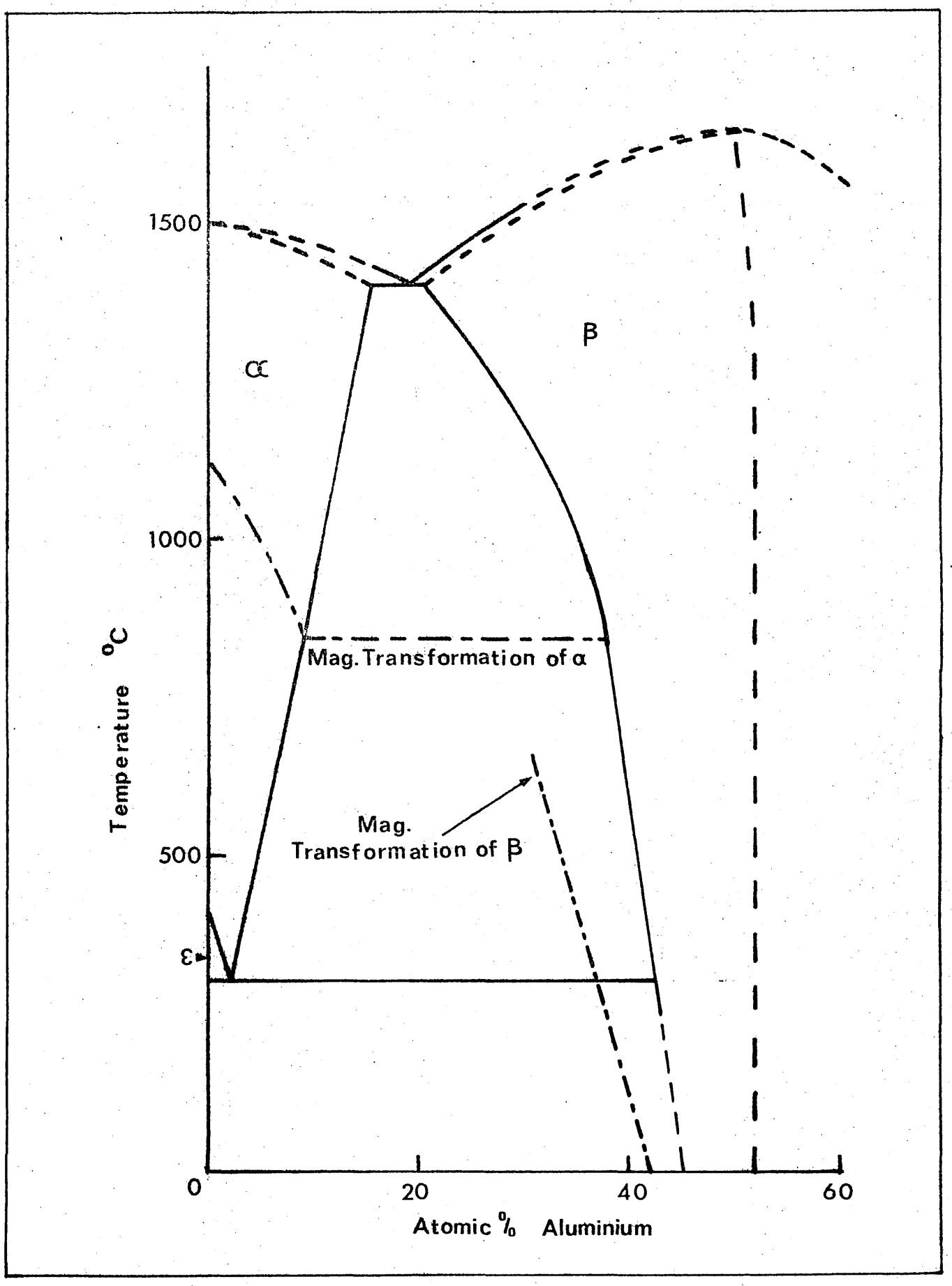

of 200 Oe but this was increased to 925 Oe by cold drawing to reduce the sample diameter from 0.177 in to 0.010 in. The increase in coercivity was attributed to a reduction in particle diameter and to particle elongation. In the as grown condition the cobalt precipitate was shown by X-ray diffraction to be f.c.c. After drawing, however, the temperature dependence of the coercivity was consistent with the presence of h.c.p. cobalt with its easy axis of magnetisation ($[000\bar{1}]$) inclined to the axis of elongation of the particles. It was suggested that coercivity after drawing could be to some extent reduced due to the formation of h.c.p. cobalt because its crystal anisotropy, acting at an angle to shape anisotropy, would reduce the overall anisotropy of the particles.

In 1965 Masumoto et al[41-49] reported permanent magnet properties of a group of cobalt aluminium alloys which they named 'Malcolloy' (magnetic Al Co alloy). After heat treatment to produce a precipitate of cobalt, coercivity (H_c) was between 600 and 1,200 Oe, dependent on composition and heat treatment, and $(BH)_{max}$ values up to 2.11 M.G.O. were achieved. The authors concluded that the observed properties were due to the single domain behaviour of the precipitate particles. The properties of Malcolloy are far superior to those of any other material based on finely divided cobalt and since a study of these alloys constitutes a large part of the present work the results of Masumoto et al will be discussed in some detail.

The Malcolloy alloys have compositions between 20 and 40 wt % (10-25 wt %) aluminium. The phase diagram after Schramm[50] (Figure 3) shows that alloys within this range can be solution treated at temperatures up to 1400°C and, if cooling is sufficiently rapid to retain the solution, subsequently aged to precipitate a cobalt rich phase. Masumoto et al[41] showed that a water quench after solution treatment was necessary in order to obtain the highest coercivity on ageing. The effect on coercivity (H_c)

Fig. 4 - Effect of ageing on the properties of a 28% (15 wt.%) Fe-Co-Mo alloy after quenching from 1380°C according to Nesumoto et al [41]

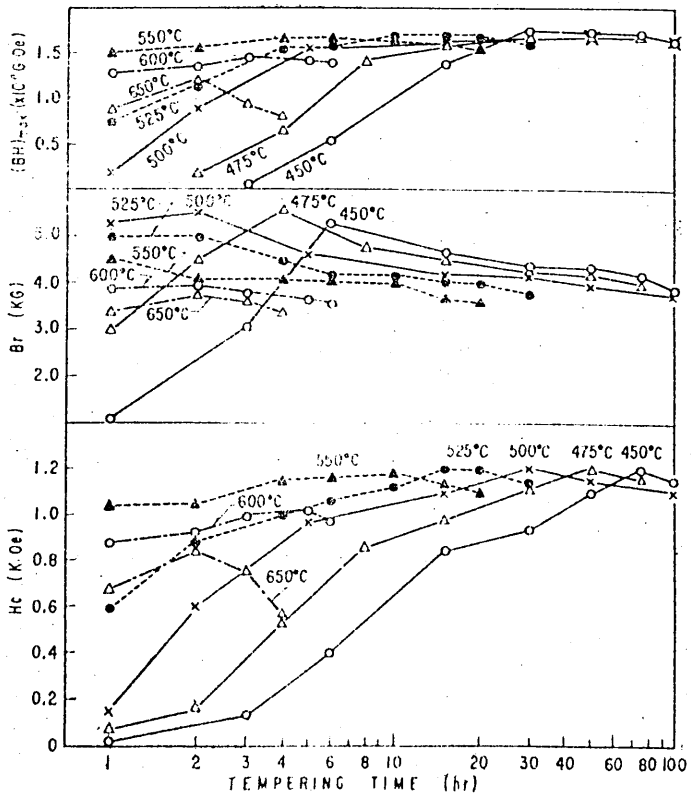

TABLE 2

THE PROPERTIES OF BINARY ALCOLLOY ALLOYS

(from Masumoto et al [41])

all samples water quenched from 1380°C

Al wt.%	Ageing Temp. °C	Ageing Time hrs.	Magnetic Properties B_r G	H_c Oe	$(BH)_{max}$ MGO	$4\pi J_s$ G
11.32	550	4	6000	600	1.40	9060
12.64	550	6	5450	860	2.00	7550
15.02	500	30	4200	1200	1.71	6250
17.99	500	30	2400	1160	0.90	4800
22.00	*		1200	400	0.15	2200

* treatment described as that giving maximum coercivity

of ageing an alloy containing 25 at% (15 wt%) aluminium at various temperatures is shown in Figure 4. Peak coercivity was achieved more quickly at higher ageing temperatures but above 525°C the peak reduced with increasing temperature. In general coercivity increased and remanence decreased as the cobalt content was reduced. The best properties and optimum heat treatments for various compositions are shown in Table 2. Best $(BH)_{max}$ values were observed at intermediate levels of remanence and coercivity.

In the as cast condition a Widmanstätten structure was observed; its components were identified by X-ray diffraction as the b.c.c. Co Al phase, β, and the f.c.c. cobalt rich solid solution α. Solution treatment produced entirely β and ageing resulted in the appearance of a precipitate identified as a mixture of α and ε cobalt. It was suggested that the coercivity was due to single domain particles with a combination of crystal and shape anisotropy.

In further work by the same authors the effect of additions of other elements was investigated[42-48]. The results are summarized in Table 3, which includes the best $(BH)_{max}$ and coercivity associated with each addition. With the exception of manganese[48], all the additions had the effect of increasing coercivity (H_c) and reducing saturation magnetisation ($4\pi J_s$) and remanence (B_r). For a given aluminium content the decrease in B_r was sometimes offset by the increase in H_c to give a small improvement in $(BH)_{max}$. The highest values of H_c observed, however, were associated with inferior values of $(BH)_{max}$. The general effect of manganese was to increase B_r at the expense of H_c giving some improvement in $(BH)_{max}$ at the optimum composition. In a patent specification dealing with these alloys[49] the effect of additions of iron, copper, tin, antimony and zinc are mentioned. Only copper gave an improvement in comparison with the binary alloys. Its effect was similar to that of manganese and it gave a $(BH)_{max}$ of 2.6 M.G.O., the best reported value on this type of alloy.

TABLE 3

THE EFFECT OF THE ADDITION OF THIRD ELEMENTS ON THE MAGNETIC PROPERTIES OF MALCOLLOY (FROM NASUNOTO ET AL [42-46])

Composition			Heat Treatment			Magnetic Properties			
	Addition		Solution	Ageing					
% Al	Element	%	Temp. °C	Temp. °C	Time hrs.	B_r G	H_c Oe	$(BH)_{max}$ MGO	$4\pi J_s$ G
12.79	Ni[42]	2.63	1360-1400	550	5	4900	1020	2.08	7350
14.74	"	19.80	1360-1400	550	6	3200	1500	1.45	4500
12.14	Mo[43]	1.88	1360-1400	550	12.5	4900	1150	2.10	7250
13.96	Mo[43]	5.53	1360-1400	600	20	2750	1600	1.34	4600
13.21	V[44]	0.52	1300-1400	550	8	4950	1040	2.00	7000
13.42	"	4.65	1300-1400	550	15	3209	1450	1.40	4660
12.30	Ti[45]	1.32	1120-1380	550	8	4800	1150	2.20	7250
14.82	Ti[45]	4.63	1120-1380	550	20	2850	1550	1.40	4220
13.01	Cr[46]	1.98	1350-1400	525	10	4800	1180	2.40	6400
14.12	Cr[46]	3.77	1350-1400	550	15	3150	1450	1.42	5220
12.29	W[47]	0.97	1350-1400	550	6	5150	920	2.04	7530
13.55	W[47]	10.56	1350-1400	525	150	3100	1450	1.40	4360
15.99	Mn[48]	1.02	1300-1380	525	15	3800	1160	1.27	5500
12.81	Mn[48]	2.60	1300-1380	525	20	5900	860	2.50	7960

Also quoted in the patent are coercivities of 1,650 Oe for alloys containing molybdenum and a $(BH)_{max}$ of 2.34 M.G.O. for a binary alloy containing 27.8 at% (14.9 wt%) aluminium.

An interesting feature of these results is the high value of $B_r/4\pi J_s$. According to Stoner and Wohlfarth[13], in a random assembly of particles $B_r/4\pi J_s = 0.5$. Masumoto et al do not claim to have induced any alignment but their quoted results give $B_r/4\pi J_s$ always greater than 0.5 and sometimes approaching 0.6. Another comment which can be made is in connection with particle size. The authors state that mean particle diameter was around 300 Å. Examination of the published photo micrographs, however, indicates a particle diameter closer to 1,000 Å and length 2 or 3 times greater. The difference is important because, whereas a f.c.c. particle with a diameter of 300 Å might approach single domain behaviour, one of 1,000 Å diameter could only be single domain if its structure was h.c.p. Discrepancies of this kind can arise due to enlargement or reduction of photographs for publication. In the present case, however, the magnification of one of the photographs[46] is indicated by a superimposed scale which eliminates this possibility.

1.3 The Allotropic Transformation in Cobalt.

Because of the importance of the crystal structure of cobalt in relation to its magnetic properties, the nature of the allotropic transformation and any influencing factors must be considered in endeavouring to understand the properties of magnets based on cobalt. The literature dealing with the allotropes and the transformation is reviewed in Appendix I but it is useful at this stage to emphasise certain significant points.

The thermodynamically stable crystal structure at room temperature is h.c.p. (ε). There is, however, considerable hysteresis and the transformation is influenced by various factors. The extent of sub-division into grains or discrete particles is one such factor, the f.c.c. form (α) being likely to be present at room temperature in increasing amounts as the

degree of sub-division is increased. Owen and Madoc-Jones[51] consider α to be the stable form at room temperature if the particle size is very fine. Newkirk and Geissler[52], however, conclude that ε is retained as a metastable phase on cooling if the particles are sufficiently small to inhibit the transformation mechanism. Since it has been shown that the best potential magnetic properties are associated with small particles of ε this matter is obviously of considerable importance.

Ness and Barrett[53] investigated the effect of mechanical work on the transformation. A small amount of deformation reduced the amount of hysteresis between the heating and cooling transformation giving a transformation temperature of 417 ± 7°C. Severe deformation lowered the α - ε transformation temperature, whilst moderate deformation at room temperature was found to convert retained α to ε.

The structure of cobalt produced by electrolysis is affected by the nature of the electrolytic cell and particularly by the pH of the electrolyte. For instance according to Kerston[54] cobalt deposited from the sulphate was h.c.p. at high pH with increasing amounts of f.c.c. as the pH was lowered.

The complex effects of impurities and alloy additions on the stability of the allotropes have been reviewed by Krajewski et al[55]. In In general a majority of elements tend to restrict the ε field giving α at room temperature.

1.4 Present Work

From the foregoing it can be seen that only in the case of the Malcolloy alloys has any real success been achieved in the preparation of permanent magnets based on finely divided cobalt. Although an extensive empirical examination of the effects of heat treatment and compositional variations has been reported by Masumoto et al[41-49] the observed properties are understood only in that they can be attributed to the presence of a cobalt precipitate exhibiting crystal or shape anisotropy or a mixture of the two. In the present work the alloys are examined in some detail

and the mechanisms responsible for the permanent magnet properties are evaluated.

A number of methods by which the properties of Malcolloy might be improved are investigated and the properties of a cobalt titanium alloy, in which a cobalt precipitate can be induced by a similar process to that used for Malcolloy, are examined.

The work has been extended to include a study of a number of cobalt based eutectic and eutectoid alloys. Properties in the bulk condition and after comminution are considered in terms of the crystal structure and particle size of the cobalt rich component.

2.1. General

The alloys studied in this work were, in most cases, prepared and heat treated by conventional methods, details of which are included in the account of the work carried out on each alloy. A description of the techniques used for testing and examination of the alloys is, however, conveniently presented at this stage.

2.2. Magnetic Testing

2.2.1. Saturation magnetisation

Saturation magnetisation was measured as specific saturation σ. Values at room temperature were obtained in a magnetising field of about 19k Oe, provided by a large permanent magnet. The intensity of magnetisation was determined from the deflection on a ballistic galvanometer as the sample was pulled out of the magnetising field through a special search coil as described by Kittsing[56]. A Sucksmith ring balance, in which the force acting on a sample in a field gradient is related to intensity of magnetisation[57], was used to determine σ at elevated temperatures. The magnetising field was about 10k Oe. Using this apparatus, it was possible to determine σ at intervals of 5°C whilst heating, under vacuum, from room temperature to the Curie temperature.

Because ferromagnetic crystals are anisotropic with respect to magnetic properties σ is most accurately determined on powdered samples such that each particle is a single crystal free to move in the magnetising field. Thus each particle rotates until an easy direction of magnetisation is parallel to the field. In the present work, however, it was found that, in the case of the Nelcolloy alloys, changes in the amount and composition and, therefore, the magnetic properties of the phases present, were induced by the process of powdering, and it was necessary to measure σ on small solid samples.

2.2.2. Intrinsic coercivity ($_JH_c$) and remanence coercivity (H_r)

$_JH_c$ and H_r were determined by similar techniques. Prior to testing, samples were magnetised in the highest available field which was a pulse of about 50 k Oe with a duration of 0.01 sec. Increasing demagnetising fields were then applied, and using an oil cooled solenoid, until there was no deflection on a ballistic galvanometer as the sample was pulled out of a search coil.

$_JH_c$ is the demagnetising field in the presence of which the intrinsic magnetisation of the sample is reduced to zero. When this property was required, therefore, the applied fields were maintained while deflection was measured and the field corresponding to zero deflection was equal to $_JH_c$. After the application and removal of a field equal to H_r the magnetisation of the sample recoils to zero. To obtain H_r, therefore, deflections were measured after the removal of the demagnetising field.

By incorporating, inside the solenoid, a small non-inductively wound furnace, it was possible to measure $_JH_c$ at temperatures up to 600°C.

2.2.3. Properties determined using a recording hysteresigraph

A recording hysteresigraph, as described by Scholes [58], was used to determine remanence (B_r), maximum energy product ($(BH)_{max}$), coercivity (H_c) and, occasionally intrinsic coercivity ($_JH_c$). This instrument provides magnetising fields of the order of 20 k Oe. Applied field (H) is measured by a Hall probe and flux density (B) by an air flux compensated search coil. The magnetic properties are recorded as a demagnetisation curve, plotted by an X-Y recorder.

2.2.4. Reproducibility of magnetic tests.

Magnetic measurements were reproducible to better than 2% except in the case of $(BH)_{max}$ where results could vary by up to 5%

2.3. X-Ray Diffraction Examination

X-ray phase analysis of conventional powder samples was carried out in a 9 cm Unicam camera. Alternatively a Beaumaris camera, shown in Figure 5 was used. This instrument, by providing facilities for the

a

showing
specimen holder

b

with cylindrical film cassette
for the production of powder
type patterns

c

with plate cassette
for back reflection
technique

d

heated specimen holder
(½ actual size)

1. specimen
2. furnace
3. thermocouple
4. refractory cement
5. water cooling
6. brass support

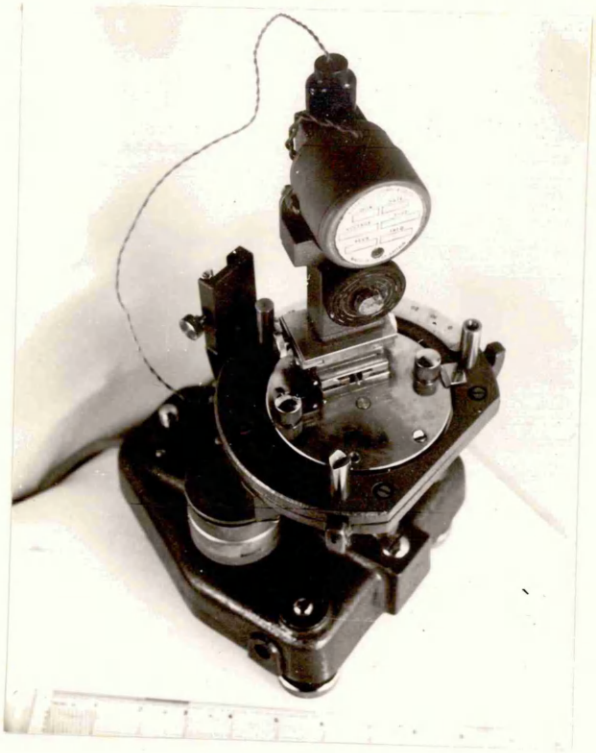

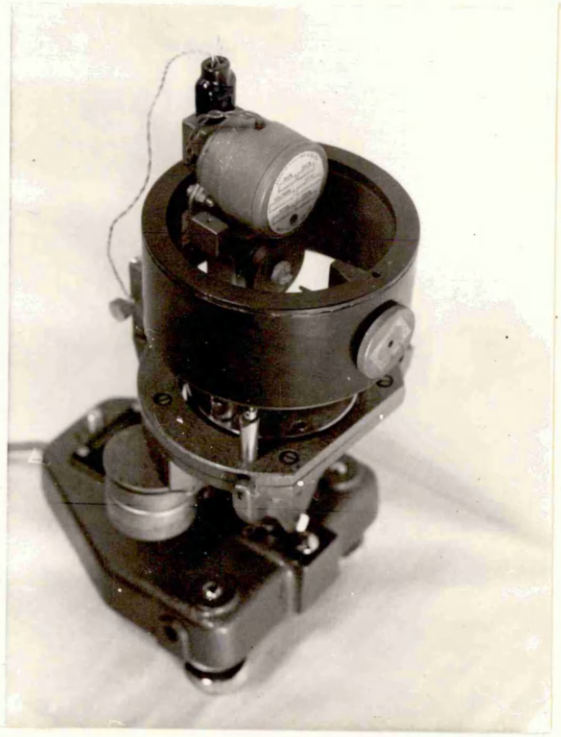

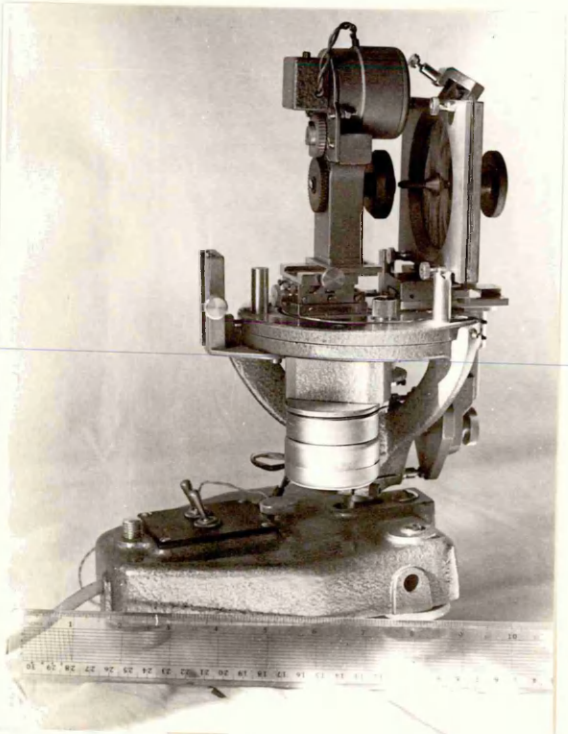

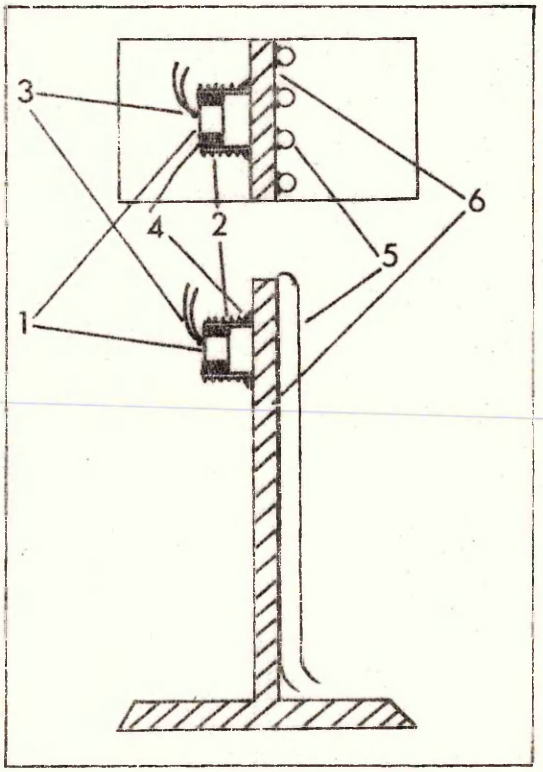
3
6
4
2
5
1

rotation and oscillation of the sample, enables powder type diffraction photographs to be obtained from solid samples. The main advantage of this technique was that the risk of phases observed in powder samples failing to be representative of those present in the bulk material was avoided. This was particularly important because of the effect of particle size on the allotropic transformation in cobalt (see section 1.3 and Appendix I). Surfaces for examination were normally prepared by mechanical polishing followed by chemical etching although on a few occasions exactly similar results were obtained from electropolished and fracture surfaces.

By constructing a special specimen holder incorporating a small heater and thermocouple (Figure 5d) it was possible to adapt the Beaumaris camera for elevated temperature work. The technique was used only for the Nalcolloy alloys (Chapter 3) the very high oxidation resistance of which allowed the production of satisfactory diffraction patterns up to 550°C without atmospheric protection.

The Beaumaris camera was also used to determine precipitate orientation in the Nalcolloy alloys. The technique, which resembled the rotating crystal method is described in section 3.4.3.

2.4. Other Techniques

2.4.1. Metallographic examination

Samples for both optical and electron microscopy were ground on emery paper and polished using 1μm diamond paste. The Nalcolloy samples and the eutectic alloys were etched using a mixture of 4-5 parts ethanol, 5 parts concentrated H Cl, and 1 part Br, and the cobalt titanium alloy in a mixture of 3 parts 30% HF, 1 part HNO_3. Electron metallography was carried out using conventional carbon replica techniques.

2.4.2. Determination of particle size

The particle size of powder materials was determined using optical microscopy. The powders were mixed with metallurgical mounting

plastic and ground and polished as micro samples. Average particle diameter was assessed by the standard technique, i.e. all the particles in a particular field of view were compared with a calibrated eye-piece graticule and the number of particles in each of a series of size ranges was counted. From these counts average particle diameter in terms of frequency of occurrence was calculated. For each sample several fields of view were examined and the values quoted are the overall average diameters.

3.1. Preparation and Heat Treatment of the Alloys

Two series of cobalt aluminium alloys were prepared covering the range of Malcolloy compositions (see section 1.2.2.) For the first series, three casts of 500g were prepared from materials of commercial purity (cobalt 99.5wt.%, aluminium 99.9 wt.%.) Melting was carried out by induction heating under a slight positive pressure of argon. After solidification each cast was broken up and re-melted to ensure adequate mixing. Table 4 shows the analysed compositions, including the amount of iron which is seen to be the major impurity. The homogeneity of these casts was established magnetically as described in 3.2.2. The alloys are conveniently identified by their nominal aluminium contents. i.e. 23, 28 and 38 at.%, (in this work atomic % is subsequently used unless otherwise stated.) The second series of alloys consisted of a number of small castings, also made from commercial purity materials, which were prepared by non-consumable arc melting at a pressure of half an atmosphere of argon. Compositions were as shown in Table 5 and Figure 6. These alloys were used only to determine the variation of saturation magnetisation with aluminium content. To check important observations on such features as the crystal structure of the cobalt precipitate a further alloy, with a nominal composition of 28% Al was prepared, from higher purity materials (cobalt 99.9 wt.%, aluminium 99.995 wt.%), by induction melting under argon. The analysed composition is in Table 4 with iron again the major contaminant.

Samples (about 5 x 5 x 10 mm) from each of the casts were solution treated for 30 minutes at 1300°C under purified hydrogen and water quenched. Those from the 23, 28 and 38 % Al casts and from the higher purity 28% Al cast, (materials are of commercial purity unless otherwise stated), were then aged isothermally for various times at

TABLE 4

ANALYSED COMPOSITIONS OF THE BINARY HALCOLLOY ALLOYS USED IN THE INVESTIGATIONS

Aluminium		Iron (impurity)		Cobalt (by difference)	
Wt. %	At. %	Wt. %	At. %	Wt. %	At. %
12.1	23.1	0.3	0.25	87.6	76.55
14.9	27.7	0.3	0.2	84.8	72.1
22.5	38.2	0.2	0.2	77.3	61.6
15.0	27.85	0.05	0.05	84.95	72.1 (higher purity)

TABLE 5

SATURATION MAGNETISATION (σ) of ARC MELTED COBALT-ALUMINIUM ALLOYS AFTER SOLUTION TREATMENT AT 1380°C AND WATER QUENCHING

Aluminium	σ
at. % analysed	emu_g^{-1}
50.1	0
48.8	0
47.5	0
45.0	0
43.4	0
41.5	15.8
39.2	30.0
37.6	38.3
36.1	47.2
34.2	59.1
31.3	72.9
28.7	82.3
27.0	92.2
24.6	102.2

TABLE 6

MAGNETIC PROPERTIES OF HALCOLLOY ALLOYS IN THE AS CAST CONDITION

Alloy	σ emu_g^{-1}	J^H_c Oe
23% Al	92.0	98
26% Al	73.5	110
38% Al	29.6	163
28% Al (higher purity)	74.8	140

Fig. 6 - Variation of the Saturation Magnetisation (σ) of β with composition

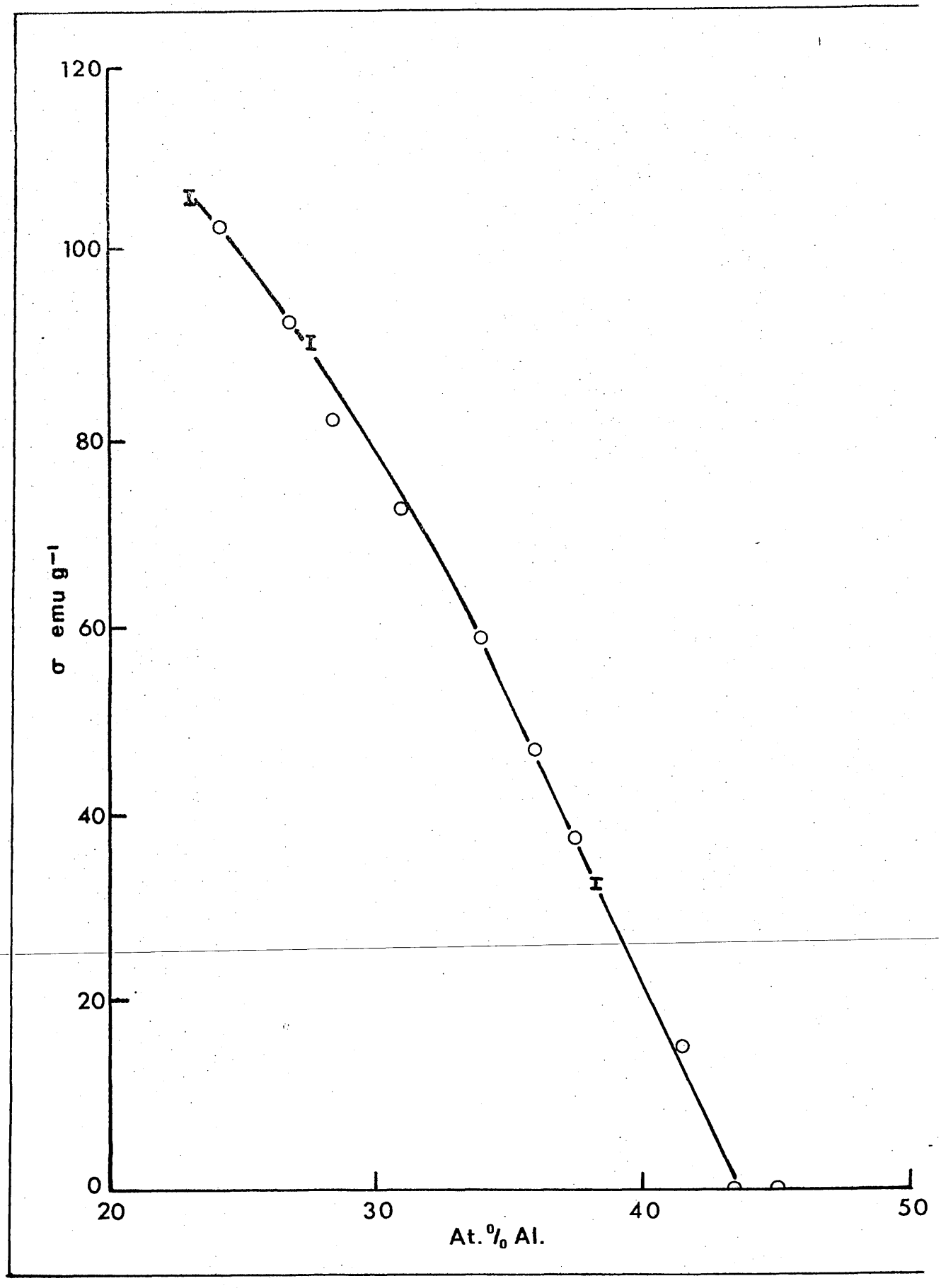

temperatures between 450°C and 750°C. Ageing was carried out either in air, with no appreciable sign of oxidation or, for treatments of less than 30 minutes, where rapid heat transfer was important, in a salt bath. Ageing temperatures were controlled to ± 2°C and the solution treatment temperature to ± 5°C. Powder samples for X-ray examination were solution treated either in sealed, evacuated silica tubes or under pure hydrogen, as above. In either case, subsequent ageing was carried out in evacuated silica tubes. All samples were quenched to room temperature after ageing.

3.2. Structure and Magnetic Properties at Room Temperature

3.2.1. The as-cast condition

In the as-cast condition σ and $_{J}H_{c}^{as}$ of the 23, 26 and 28% Al alloys and the higher purity 28% Al alloy were/shown in Table 6.

Samples from each cast were examined metallographically and by X-ray diffraction. The latter was carried out using bulk samples in the Beaumaris camera with filtered cobalt radiation. In all the casts a Widmanstätten precipitate of α cobalt was present in a b.c.c. matrix. The lattice parameter of the matrix in the 23, 26 and 28% Al casts was 2.855 Å, 2.857 Å and 2.856 Å respectively. This phase was identified as the Co Al intermediate phase β; the lattice parameter of which, according to Cooper[59], first increases with increasing aluminium content, reaching a peak of 2.861 Å at about 49% Al, and then decreases. The amount of α observed was fairly constant within individual casts but decreased with increasing aluminium content. The microstructure of the 28% Al alloy is shown in Figure 7a.

3.2.2. The solution treated condition

Examination, using the Beaumaris camera, of bulk samples solution treated for 30 minutes at 1300°C and water quenched, indicated for all the alloys complete solution of α and retention of supersaturated β at room temperature. The single phase nature of these samples was confirmed metallographically (Figure 7b). Powder samples, which were heat treated in sealed evacuated silica tubes, prior to X-ray examination

Fig. 7 - 2% Al Malcolloy Alloy

a

as cast

x 200

b

solution treated ½ hour 1380°C
and water quenched

x 200

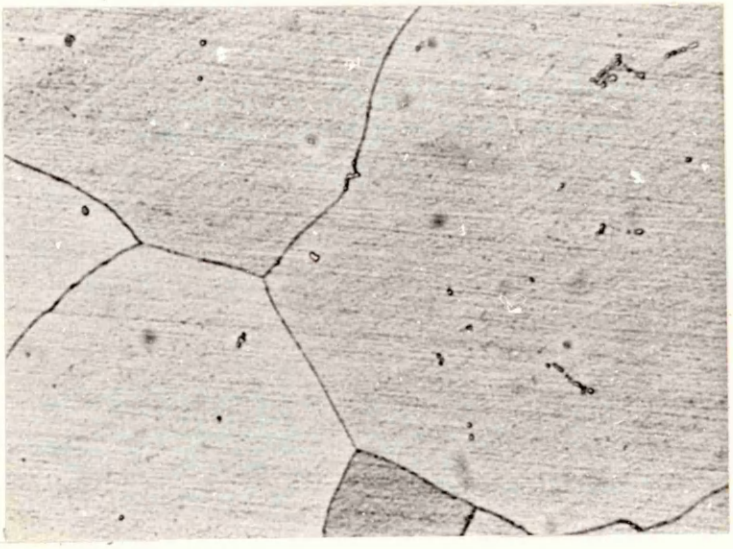

α and ε after similar ageing treatments. The observation was, therefore, confirmed using bulk and powder X-ray diffraction samples from the commercial and higher purity alloys. Identical results were obtained in each case.

The absence of α was surprising since, according to the phase diagram (Figure 3), this modification is the stable form for precipitation above 300°C. The possibility that the precipitate formed initially as α and underwent complete transformation to ε on cooling was unlikely in view of the extreme sluggishness of the reaction, particularly in finely divided cobalt, (see section 1.3. and Appendix I). This was, however, checked using the high temperature specimen holder in the Beaumaris camera. Solution treated samples from each cast were heated to 550°C in the camera. This temperature was maintained for 16 hours in the case of the 23% Al and 28% Al alloys (both commercial and higher purity) and for 48 hours in the case of the 38% Al alloy. A diffraction pattern was then obtained with the specimen still at the ageing temperature. In each case, only ε and β were detected.

Two samples from the 28% Al cast were subjected to prolonged ageing treatments, one at 500°C and one at 600°C. No α was detected at 500°C after 2000 hours but at 600°C a trace of α was observed after 400 hours and after 2000 hours the allotropes were estimated to be present in approximately equal quantities.

It was concluded, therefore, that ε formed as a metastable phase on precipitation from β under conditions for which α was thermodynamically stable.

in the Unicam camera, showed a tendency for σ to reprecipitate on quenching. This occurred even when the silica tube was broken during the quench. The supersaturated solid solution was, however, fully retained in powder samples, solution treated, as was the bulk material, in refractory boats under a stream of purified hydrogen and water quenched. Specimens treated in this manner were used for investigating the effects of subsequent heat treatments.

Figure 6 shows the relationship between σ and analysed aluminium content for the series of arc melted alloys after solution treatment to give a β structure. These alloys became non-magnetic at room temperature above about 43% aluminium which is in fair agreement with the magnetic transformation for β shown in Figure 3. Values of σ were also obtained for ten samples from each of the 23, 28 and 38% Al casts in the solution treated condition. The range of values, indicated on Figure 6, proves the maximum composition variation within any alloy to be ± 0.2% aluminium. In each case σ was significantly greater than that observed in the as cast condition (Table 6). $_{J}H_{c}$ of all the alloys was reduced, by solution treatment, to a level too low to be measured using available apparatus, i.e. less than 2 Oe.

3.2.3. The effect of ageing

a. Structure: Precipitates of a cobalt-rich phase with crystal structure varying with ageing time and temperature were obtained in all the alloys and identified by X-ray diffraction using bulk samples in the Beaumaris camera.

Ageing isothermally at 650°C, 700°C and 750°C resulted initially in the precipitation of a mixture of α and ε. The amount of α increased as the ageing time or temperature was increased and after one hour at 750°C only α was detected.

After ageing within the range 450°C - 600°C for less than about 400 hours only ε precipitation was detected. This was not in agreement with the results of Masumoto et al[41] who reported a mixture of

Fig. 8 - 28% Al Malcolloy Alloy

a

½ hour 1380°C
water quench
aged 1½ hours 450°C

x 40,000

b

½ hour 1380°C
water quench
aged ½ hour 500°C

x 40,000

c

½ hour 1380°C
water quench
aged 12½ hours 500°C

x 40,000

d

½ hour 1380°C
water quench
aged 17 hours 500°C

x 40,000

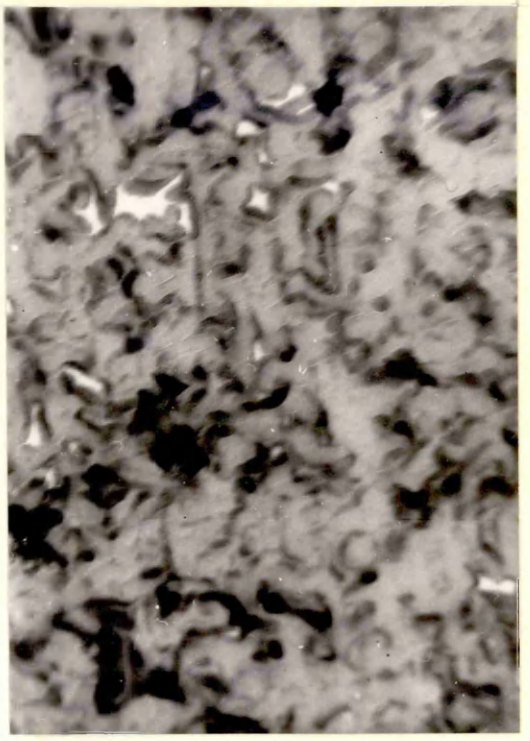

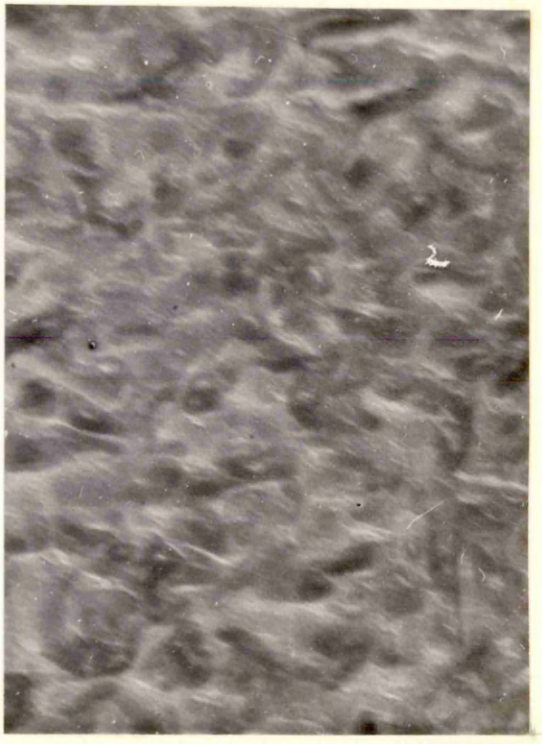

Fig. 8 - 28% Al Malcolloy Alloy

e

½ hour 1380°C
water quench
aged 10 minutes 700°C

x 10,000

f

½ hour 1380°C
water quench
aged 1 hour 700°C

x 2,000

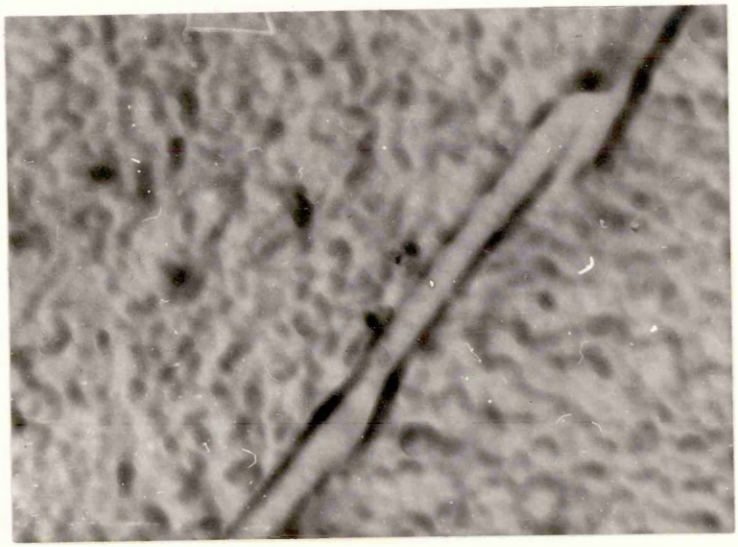

Some degree of line broadening was observed in the diffraction of both ε and β. This effect was not present in the lines representing α and when only α and β were detected the β lines were also relatively sharp.

Electron micrographs, obtained by a normal carbon replica technique, of the precipitate in the 28% Al alloy after various ageing treatments are shown in Figure 8. Figures 8a and 8b show the precipitate in the early stages of ageing at 450°C and 500°C respectively, 8c and 8d show later stages at 500°C, in these four samples the precipitate was ε. 8e and 8f show early and late stages at 700°C; the precipitate in 8e was a mixture of ε and α while that in 8f was entirely α. There is a tendency in Figures 8c (12½ hours at 500°C) and 8d (17 hours at 500°C) for the precipitate particles to be elongated. This is, however, not particularly evident in any other case. As might be expected particle size tends to increase as ageing time and temperature are increased.

b. Magnetic properties: The effect of ageing on ${}_{J}H_{c}$ and σ of the 23, 28 and 36% Al alloys is shown in Figures 9 - 13 and Tables 7, 8 and 9. Each experimental value shown represents one sample aged continuously for the time and at the temperature indicated. In every case ageing caused a decrease in σ and an initial increase in ${}_{J}H_{c}$ which in most cases reached a peak value and subsequently decreased. In the case of the 28% Al alloy the properties at each temperature were confirmed after several ageing times using the higher purity material. No significant difference was observed.

It is at first sight surprising that σ should decrease during the precipitation of the ferromagnetic cobalt rich phase. It has been shown, however, that these alloys are strongly magnetic in the solution treated (β) condition with σ of β decreasing as its cobalt content decreases (Figure 6). The σ of supersaturated β is greater than that of material of the same composition after full precipitation of cobalt

Fig. 9 - The effect of ageing on $_{J}H_{c}$ and σ of the 23% Al alloy

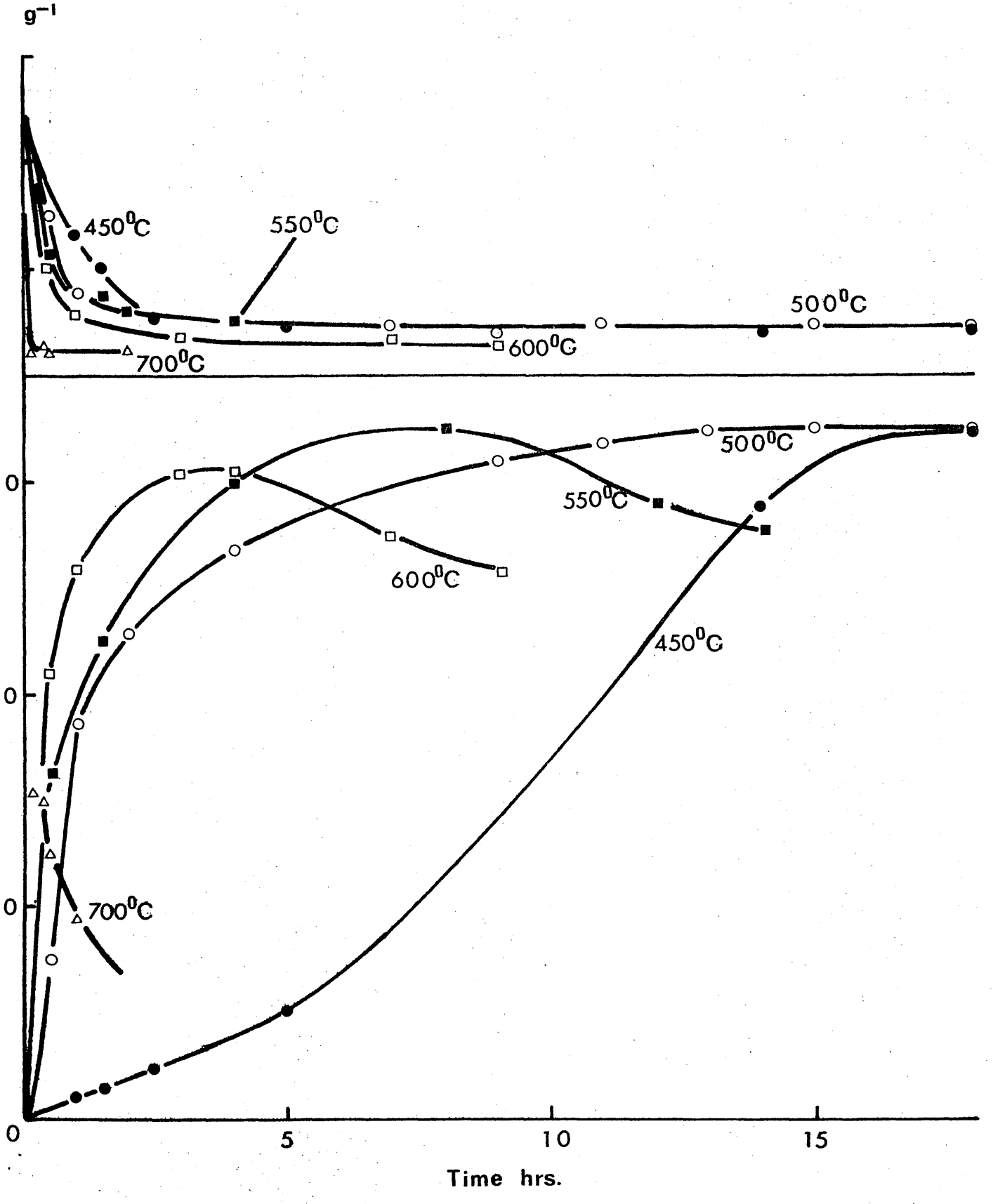

TABLE 7

THE EFFECT OF AGEING ON $_{J}H_{c}$ AND σ OF THE 23% Al ALLOY

450°C			500°C			550°C			600°C			700°C	
J^{H}_{Oe}	σ emug^{-1}	Time hrs.	J^{H}_{Oe}	σ emug^{-1}	Time hrs.	J^{H}_{Oe}	σ emug^{-1}	Time hrs.	J^{H}_{Oe}	σ emug^{-1}	Time hrs.	J^{H}_{Oe}	σ emug^{-1}
<2	105	0	<2	105	0	<2	105	0	<2	105	0	<2	105
20	93.0	¼	150	95	¼	325	92.1	¼	420	90.0	10 mins*	308	82.2
31	90.0	1	375	87.5	1	410	87.8	1	514	85.7	20 mins*	300	82.8
49	85.3	2	459	-	1½	450	87.5	3	610	83.8	¼*	250	82.0
105	84.9	4	536	85.1	4	600	85.0	4	609	-	1	189	-
575	84.0	7	583	84.9	8	649	83.5	5	-	82.6	2	136	82.3
648	83.9	9	618	84.0	12	580	84.0	7	548	83.4			
650	83.4	11	636	84.9	14	550	84.5	9	514	82.3			
		13	649	84.1									
		15	651	84.8									
		18	648	84.5									

* treatment in salt bath

Fig. 10 - The effect of ageing on the $_{J}H_{c}$ and σ of the 28% Al alloy (see also Fig. 11)

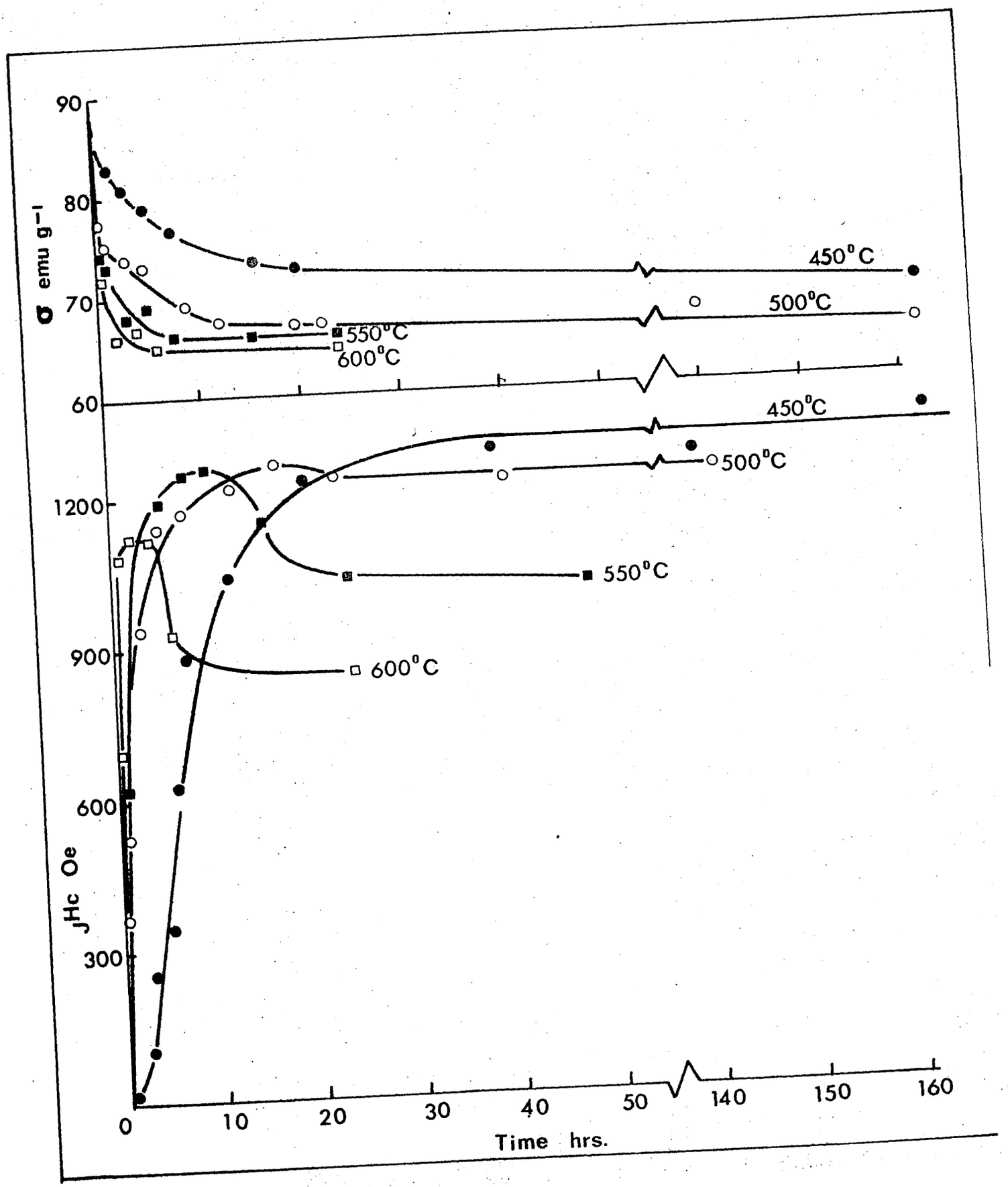

Fig. 11 - The effect of ageing between 450°C and 750°C on $_JH_c$ of the 28% Al alloy (as Fig. 10 but with expanded time scale)

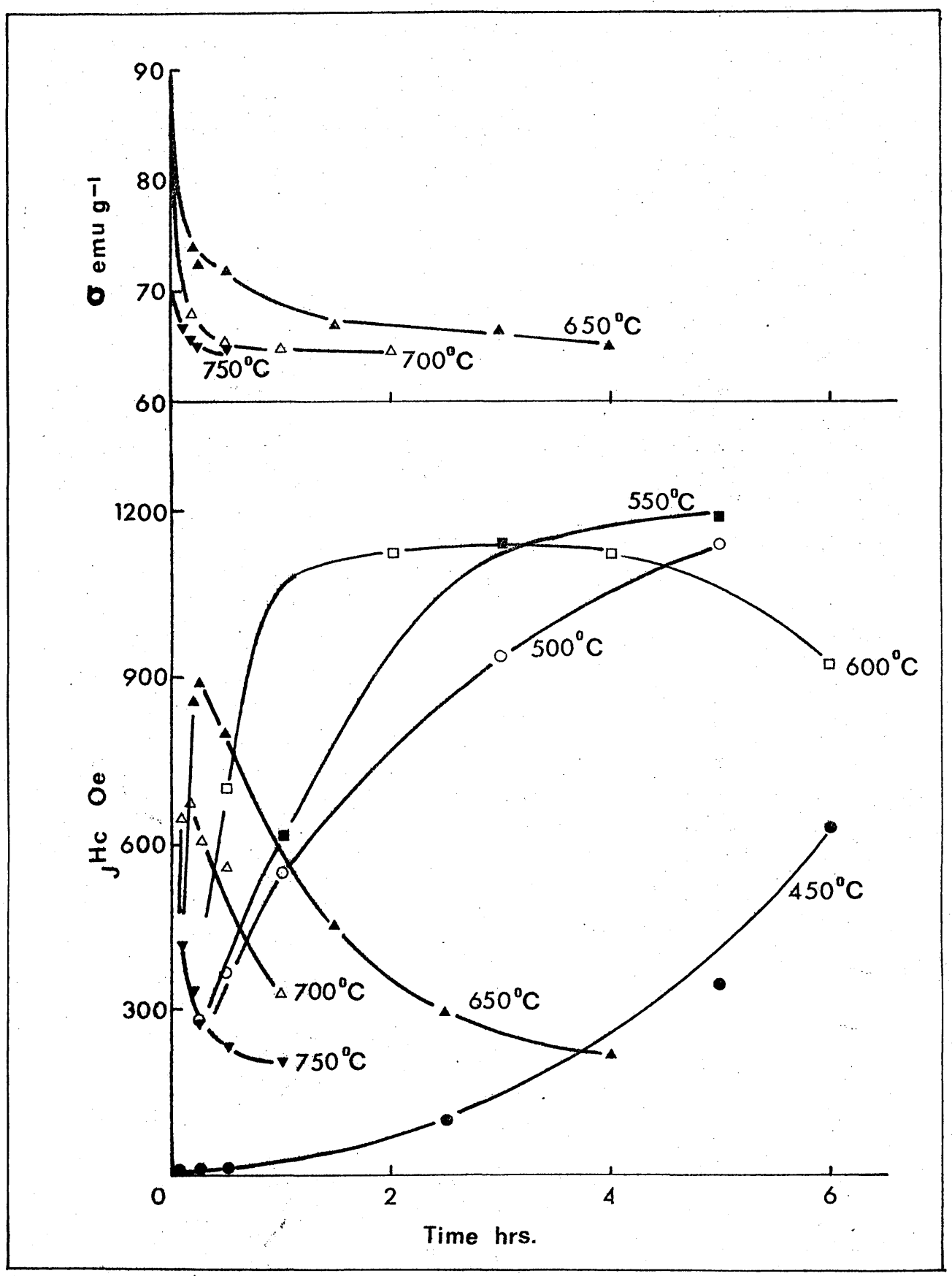

TABLE 8

THE EFFECT OF AGEING ON THE J_c^H AND σ OF THE 28% Al ALLOY

a) Commercial Purity

	450°C		500°C		550°C		600°C		650°C		700°C		750°C	
Time hrs.	J_c^H Oe	σ emug^{-1}	J_c^H Oe	σ emug^{-1}	J_c^H Oe	σ emug^{-1}	J_c^H Oe	σ emug^{-1}	J_c^H Oe	σ emug^{-1}	J_c^H Oe	σ emug^{-1}	J_c^H Oe	σ emug^{-1}
0	<2	90	<2	90	<2	90	<2	90	<2	90	<2	90	<2	90
5 mins*	8	87	150	81.0	143	78.8	207	77.0	[illegible]	[illegible]	651		419	67.0
10 mins*	3	86.6	202	79.5	252	77.3	309	75.3	863	74.0	678	68.0	339	66.1
½*	10	85.6	280	78.0	260	75.4	-	75.0	892	72.7	602	-	272	65.0
¾*	9	86.0	360	77.2	-	74.6	700	72.0	803	72.2	538	65.7	232	64.6
1			524	75.0	613	73.0	1081	-			330	65.0	201	64.7
1½	40	82.8							452	67.0				
2							1126	66.0			248	64.9		
2½	100	82.0							300	66.5				
3	256	81.0	935	73.8	1140	68.0								
4							1126	66.8	219	65.0				
5	346	79.0	1140	73.0	1193	69.0								
6	630						926	65.0						
7½	885	76.7	1172		1252	66.2								
9				69.0	1250									
12	1040													
12½			1215	67.5										
15½					1150	65.8								
16	1104	73.3												
17			1260	67.3										
20	1226	72.4	1250	66.5										
23			1230	66.5										
24					1037	66.0	847	64.4						
25									163	65.2				
39	1280	-	1220											
48					1015									
66	1293	70.6												

TABLE 8 continued

a) Commercial Purity

	450°C		500°C		550°C		600°C		650°C		700°C		750°C	
Time Hrs.	J^{H}_{Oc} Oe	σ emug^{-1}	J^{H}_{Oc} Oe	σ emug^{-1}	J^{H}_{Oc} Oe	σ emug^{-1}	J^{H}_{Oc} Oe	σ emug^{-1}	J^{H}_{Oc} Oe	σ emug^{-1}	J^{H}_{Oc} Oe	σ emug^{-1}	J^{H}_{Oc} Oe	σ emug^{-1}
69			1240	66.5										
90	1270	-												
93			1249											
114	1305	69.9												
138	1260	67.7												
141			1230	66.3										
162	1330	69.5	1250	65.0										
169			1250	65.2										

b) Higher Purity (26% Al)

0	<2	90	< 2	90	<2	90	<2	90	<2	90	<2	90	<2	90
10 mins*									870	75.0	670	69.0	328	66.8
2½	123	82.3												
3			950	74.1	1126	67.1	1135	67.0						
7½					1255	66.4								
17			1270	70.0										
114	1295	68.5												

* treatment in salt bath

Fig. 12 - Effect of ageing of $_{J}H_{c}$ and σ of the 30% Al alloy

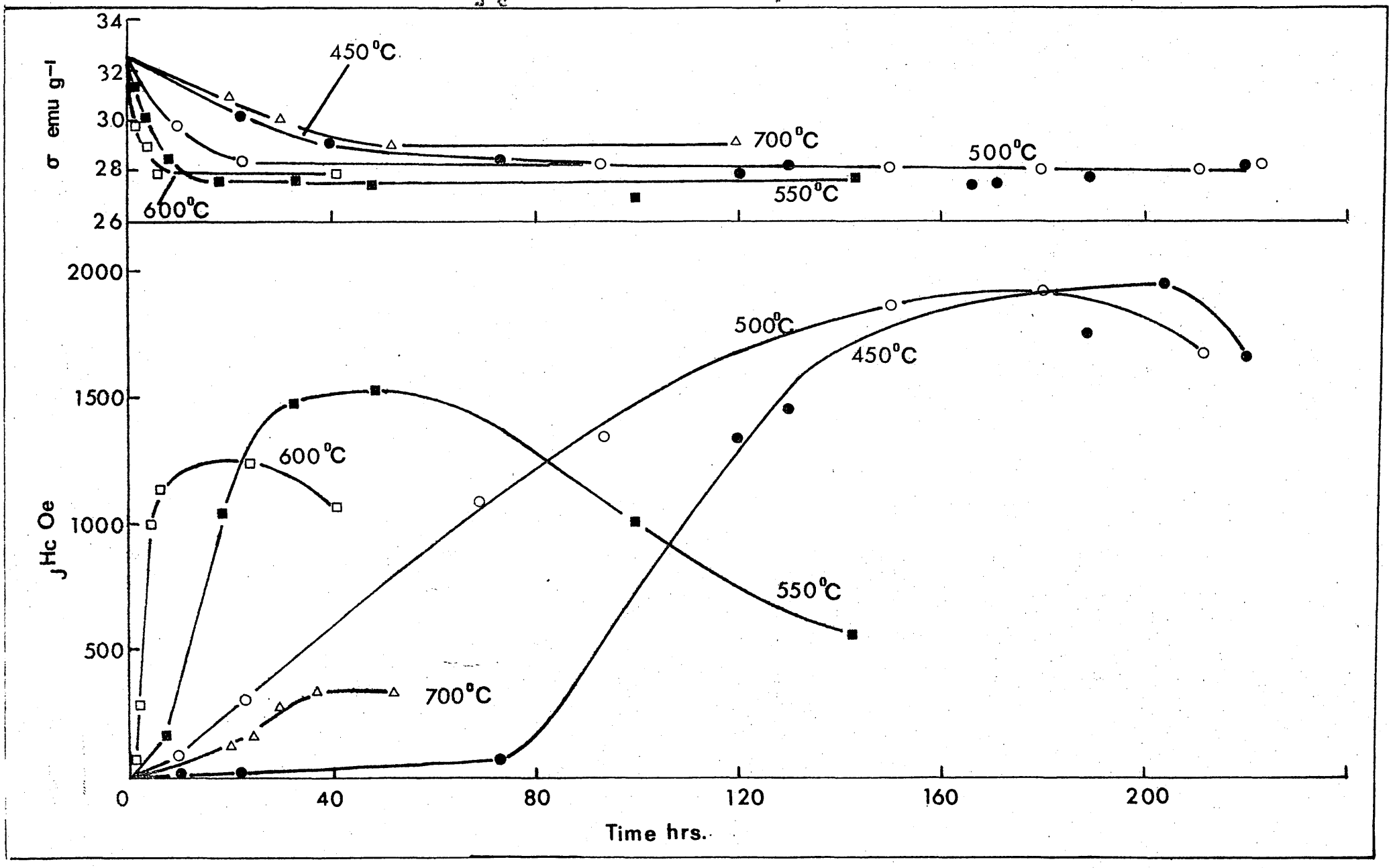

TABLE 9

THE EFFECT OF AGEING ON J^H_c AND σ OF THE 38% Al ALLOY

450°C			500°C			550°C			600°C			700°C		
J^H_c Oe	σ emug^{-1}	Time hrs.	J^H_c Oe	σ emug^{-1}	Time hrs.	J^H_c Oe	σ emug^{-1}	Time hrs.	J^H_c Oe	σ emug^{-1}	Time hrs.	J^H_c Oe	σ emug^{-1}
≤2	32.5	0	≤2	32.5	0	≤2	32.5	0	≤2	32.5	0	≤2	32.5
10	32.4	10	100	29.8	1½	18	30.2	1	67	30.2	1	32	-
35	31.6	23	300	28.4	8	170	28.5	2	290	29.8	2	24	31.5
27	30.3	69	1095	-	18	1048	27.6	4	992	29.0	4	28	-
52	29.2	93	1349	28.3	33	1482	27.7	6	1137	27.9	20	116	30.9
72	28.5	150	1873	28.1	48	1516	27.5	24	1238	28.3	24	161	-
1340	28.0	180	1930	28.1	100	1005	27.0	41	1070	27.9	30	280	30.0
1470	28.3	211	1680	28.1	143	573	27.8				37	340	-
-	27.5										52	340	29.0
1760	27.8										120	-	29.2
1970	27.9												
1673	28.2												

Fig. 13 - Effect of ageing 23%, 28% and 38% Al alloys at 500°C

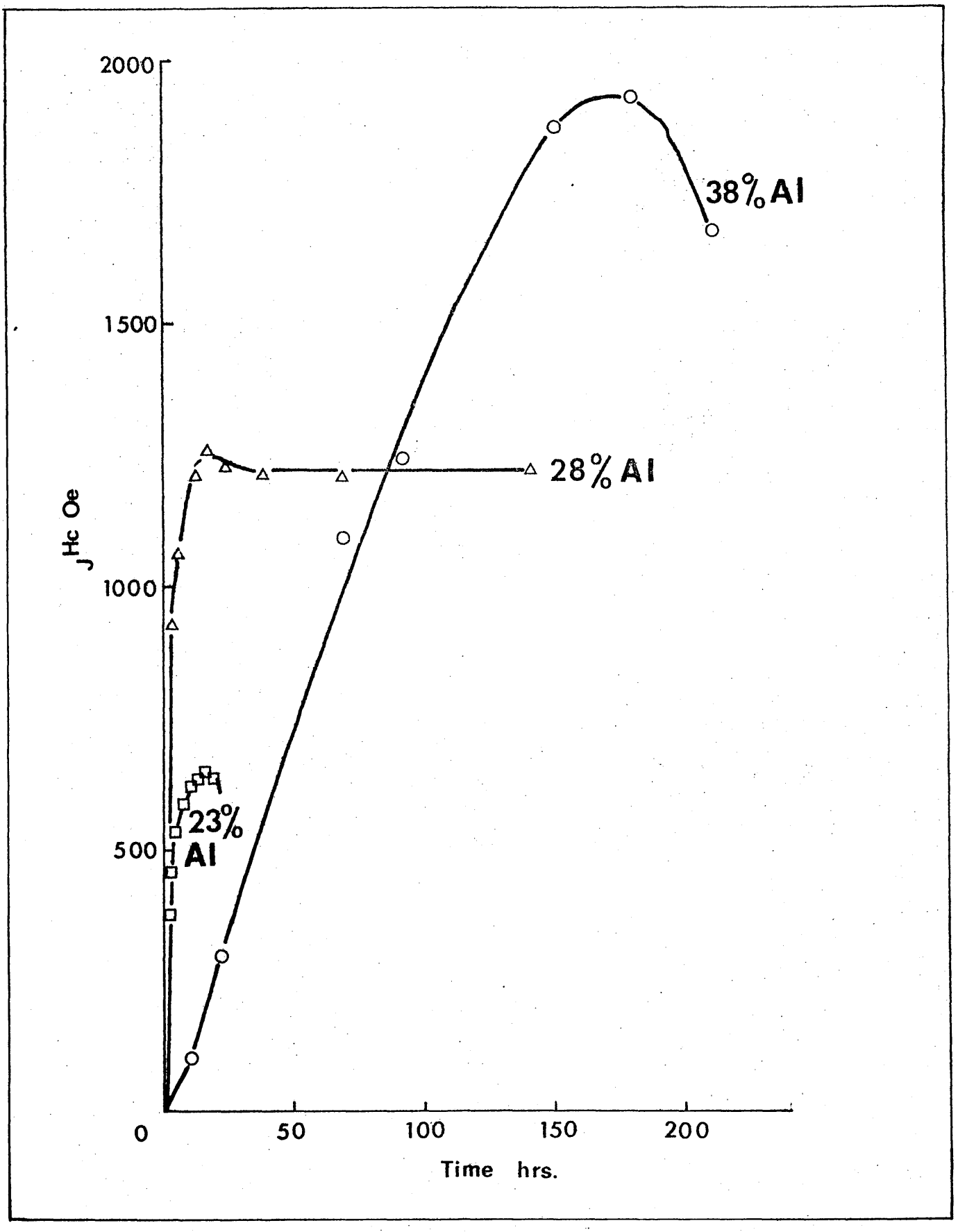

to give a non-magnetic β matrix. A progressive decrease from the σ of supersaturated β to that of diluted cobalt is therefore observed on ageing. With regard to the effect of ageing on $_{J}H_{c}$, the 23 and 28% Al alloys responded in a similar manner but the peak values of $_{J}H_{c}$ in the latter were about twice as great as those in the former. In both alloys, increasing the ageing temperature caused peak $_{J}H_{c}$ to be reduced and the peaks to be achieved more quickly. This effect was particularly marked above 600°C. The 38% Al alloy reached significantly higher values of $_{J}H_{c}$ than the other materials. Peak $_{J}H_{c}$ in this alloy again decreased as ageing temperature increased but the approach to the peak was very slow in comparison with the other alloys. The change in both σ and $_{J}H_{c}$ on ageing the 38% Al alloy at 700°C was somewhat anomalous in that the initial decrease in σ and increase in $_{J}H_{c}$ were slower than at the lower temperatures.

Values of B_r, H_c and $(BH)_{max}$ were measured on samples from each cast after ageing to maximum coercivity at 500°C; these are shown in Table 10 together with comparable figures from the work of Masumoto et al[41]. The high values of $B_r/4\pi J_s$ obtained by these authors have been mentioned in section 1.2.2. From Table 10 it can be seen that similarly high values were obtained in the present work in the case of the 23 and 38% Al alloys, although a ratio much closer to the expected value of 0.5 was observed for the 28% Al material. In general, properties obtained in the present work were rather lower than those reported by Masumoto et al.

c. Relationship between properties and structure: In general the association of a large increase in $_{J}H_{c}$ over a range of compositions and ageing treatments, with the appearance of a finely divided cobalt precipitate, clearly supports the conclusion of Masumoto et al[41] that the coercivity of these alloys is derived from single domain particles of this precipitate.

TABLE 10

PERMANENT MAGNET PROPERTIES OF HALCOLLOY - COMPARISON OF THE PRESENT RESULTS WITH THOSE OF MASUMOTO ET AL [41]

Composition % Al	Treatment	Source	Saturation Magnetisation $emu\,g^{-1}$ σ	Saturation Magnetisation $4\pi J_s$ G	B_r $4\pi J_s$	B_r G	$(BH)_{max}$ MGO	H_c Oe	$_jH_c$ Oe
23.1	30 mins.1380°C W.Q. + 14 hrs.500°C	Present work	85	7500	0.73	5450	0.9	620	650
23.3	7 mins.1380°C W.Q. + 30 hrs.500°C	Masumoto et al [41]	92	8500	0.67	5700	1.5	600	-
27.7	30 mins.1350°C W.Q. + 1 hr.500°C	Present work	75	6900	0.62	4300	0.82	490	524
27.7	30 mins.1380°C W.Q. + 12½ hrs.500°C	Present work	67.5	6200	0.57	3550	1.30	1100	1215
27.7	30 mins.1380°C W.Q. + 70 hrs.500°C	Present work	68	6300	0.55	3450	1.25	1125	1230
27.7	30 mins.1380°C W.Q. + 169 hrs.500°C	Present work	65.2	6100	0.56	3400	1.16	1100	1250
27.9	7 mins.1380°C W.Q. + 30 hrs.500°C	Masumoto et al [41]	69	6250	0.67	4200	1.71	1200	-
36.2	30 mins.1380°C W.Q. + 180 hrs.500°C	Present work	28	2250	0.69	1550	0.40	1030	1920

$4\pi J_s$ calculated from σ using the relationship, $4\pi J_s = 4\pi\sigma\rho$. Using ρ (density) as given by Masumoto et al [41].

The present work has shown that the highest values of $_JH_c$ (up to 1570 Oe in the 38% Al alloy) are obtained when the precipitate is c and that the appearance of c is associated with significantly reduced $_JH_c$, (340 Oe in the 38% Al alloy). Reference to the electron micrographs in Figure 8 shows that in the 26% Al alloy maximum coercivity at 500°C, achieved after about 17 hours (8d), was associated with precipitate particles, showing some tendency to be elongated, with a mean length of the order 0.3μ and mean thickness around 0.1μ. This is in good agreement with the published photo-micrographs of Masumoto et al although not with the values they quote in the text. (see section 1.2.2.). Furthermore, since the precipitate has been shown by X-ray diffraction to have the h.c.p. c structure (3.2.3a), particles of this size should, according to Went et al[11], be single domain and exhibit high $_JH_c$. The properties of this sample can, therefore, be readily understood in general terms as arising from the presence of single domain particles of c. Such particles will derive high coercivity from the crystal anisotropy of the h.c.p. structure.

The position is less straightforward when the properties and structures of samples in the early stages of ageing are considered. The particles in these samples, Figures 8a (1½ hours at 450°C), 8b (½ hour at 500°C), 8c (12½ hours at 500°C) are smaller than those in 8d (17 hours at 500°C) and should, therefore, be single domains and have coercivities at least as high as those in the 17 hour sample. In fact, the coercivities of these samples are lower.

If particles of ferromagnetic materials are sufficiently small, their direction of magnetisation is influenced by thermal agitation. The properties of such particles are similar to those of paramagnetic materials and the condition is known as super-paramagnetism. According to Néel[22b]

Fig. 16 - Ideal Variation of Coercivity with Particle Size

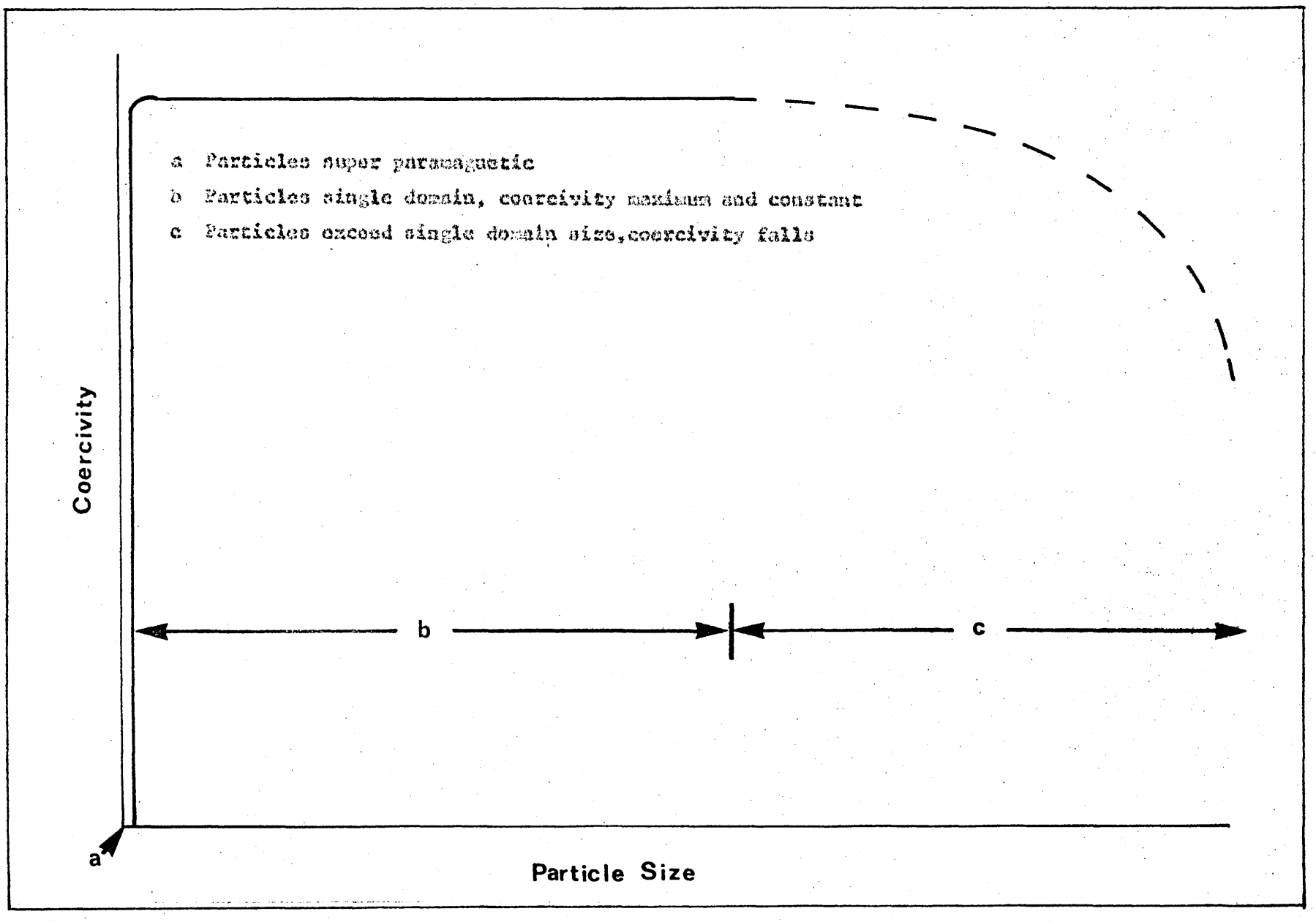

the critical volume below which a particle becomes super-paramagnetic is given by:-

$$\frac{1}{r_o} = f_o \exp\left[-\left(\frac{VK}{kT}\right)\right]$$

where r_o is relaxation time, i.e. the time required for thermal agitation to rotate the magnetisation of the particle into a preferred direction

K is the anisotropy energy

T is absolute temperature

k is Boltzmann's constant

V is particle volume

f_o is a frequency factor of the order of 10^9

Using this relationship the critical radius for super-paramagnetic behaviour in ε is about 30 Å. In the present case, therefore, where particle radius is of the order of 1000 Å it is clear that super-paramagnetism cannot be responsible for the low values of coercivity observed.

The type of variation of coercivity with particle size which might be expected, in principle, is shown in Figure 14. Coercivity rises suddenly from a low value to the maximum for single domain behaviour as the material passes from the super-paramagnetic to the ferromagnetic condition. It subsequently remains constant until single domain size is exceeded after which domain wall movements lead to a substantial reduction. It is obvious that in practice only an approximation to this curve should be anticipated because, at any stage, considerable variation in particle size is likely. In the present case, however, the observed relationship between particle size and coercivity is difficult to understand unless some other factor is involved. Section 3.6 deals with this problem and shows that coercivity is influenced by the magnetic properties of the matrix phase β.

After ageing for 1 hour at 700°C (Figure 8f) the crystal structure of the precipitate was almost entirely f.c.c. (α) with only a trace of ε. The particle size was too large for single domain behaviour to occur in either phase and the observed low coercivity ($_JH_c$ = 201 Oe) was thus to be expected. After only 10 minutes at 700°C a much greater coercivity ($_JH_c$ = 678 Oe) was associated with a mixture of α and ε, with α the majority component. It is possible that the coercivity of this sample was due to α. The particle diameter (Figure 8e) however, can be estimated at about 0.1μ which is of the right order for single domain behaviour in ε but much too large for α. It seems likely, therefore, that the coercivity arises in this case from the minority component, ε.

Two tentative conclusions can be drawn at this stage,

I It is likely that the coercivity of these alloys is derived from the crystal anisotropy of a metastable precipitate of ε, the particles of which exist as single magnetic domains. This may apply even if the precipitate is, in part, α.

II Coercivity does not vary in a completely logical manner with particle size and some other factor or factors must be considered before the relationship can be understood.

Note:

An investigation of the crystallography of this type of alloy was reported by Arbuzov et al (Fizika Metallov I Metallovedenie 28 1969 (21)) and came to the attention of the present author when published in English translation in 1971, at which time the present work was largely completed. This study, which is discussed in Appendix II, completely confirms the above findings relating to the crystal structure of the precipitating phase.

3.3. The Influence of the Crystal Anisotropy of ε on the Coercivity of Malcolloy

3.3.1. Introduction

From the fact that high coercivity in these alloys is associated with the presence of a precipitate of ε or ε + α with particle size too great for single domain behaviour in α it has been inferred that the crystal anisotropy of the h.c.p. ε structure has a significant influence on the observed properties. For a complete understanding of the behaviour of the alloys it is necessary to evaluate this influence.

3.3.2. The variation of the crystal anisotropy of ε with temperature

The crystal anisotropy energy in a hexagonal structure is given by

$$E = K_o + K_1 \sin^2\theta + K_2 \sin^4\theta + \text{-------}$$

where K_o, K_1 and K_2 are anisotropy constants

and θ is the angle between the magnetisation vector and $[000\bar{1}]$

If the magnetisation vector is parallel to $[000\bar{1}]$ the energy required to magnetise to saturation is

$$E_o = K_o$$

but during reversal of magnetisation the magnetisation vector must, at some stage, be perpendicular to $[000\bar{1}]$. The energy is a maximum at this point and is given by

$$E = K_o + K_1 + K_2$$

Since K_o is constant regardless of the direction of magnetisation the energy required to bring about reversal is

$$E = K_1 + K_2$$

It can be seen from Figure 2 that K_1 and K_2 for ε are dependent on temperature, their sum falling from about 6×10^6 erg cm^{-3} at 20°C to zero at 250°C and becoming negative at higher temperatures. These values

are due to Honda and Masumoto[32] who also show that above about 250°C the principal directions in the basal plane of the c structure ($[11\bar{2}0]$ and $[10\bar{1}0]$) are more easily magnetised than $[000\bar{1}]$. The structure becomes increasingly anisotropic as the temperature is raised to 400°C. It is clear, therefore, that coercivity arising from the crystal anisotropy of c must have a strong reversible temperature dependance.

This was demonstrated in practice by Weil et al[35,60] using cobalt powders with varying mixtures of c and α. In some of the powders tested only a trace of α was present and coercivity decreased from about 350 Oe at room temperature to between 100 and 200 Oe at about 200°C. There was a substantial increase in coercivity below room temperature and a small increase above 200°C. The authors commented on the difference between the temperature at which minimum coercivity was observed (200°C) and the temperature at which, according to theory, the anisotropy of c is zero (250°C). This they attributed to the presence of impurities in the cobalt powder.

3.3.3. The variation of the $_JH_c$ of Malcolloy with temperature

The temperature dependence of $_JH_c$ of a number of Malcolloy samples was determined, as part of the present work, as follows.

The measurements were carried out using the apparatus described in 2.2.2. The samples were magnetised at the test temperature before progressive demagnetisation as described for room temperature measurements. The magnetising field was about 5000 Oe. The samples tested and the results obtained are shown in Table 11 and in Figures 15 (commercial and high purity 28% Al alloys) and 16 (23% Al and 30% Al alloys).

With the exception of the sample from the 28% Al alloy aged for ½ hour at 750°C, (Figure 15), the results obtained showed $_JH_c$ to vary significantly with temperature. The extent to which the changes were reversible was established by subsequent tests at room temperature as shown in the table. In more than half the samples temperature dependence

Fig. 15 - Variation of $_{J}H_{c}$ with temperature of samples from the commercial and high purity 28% Al alloys

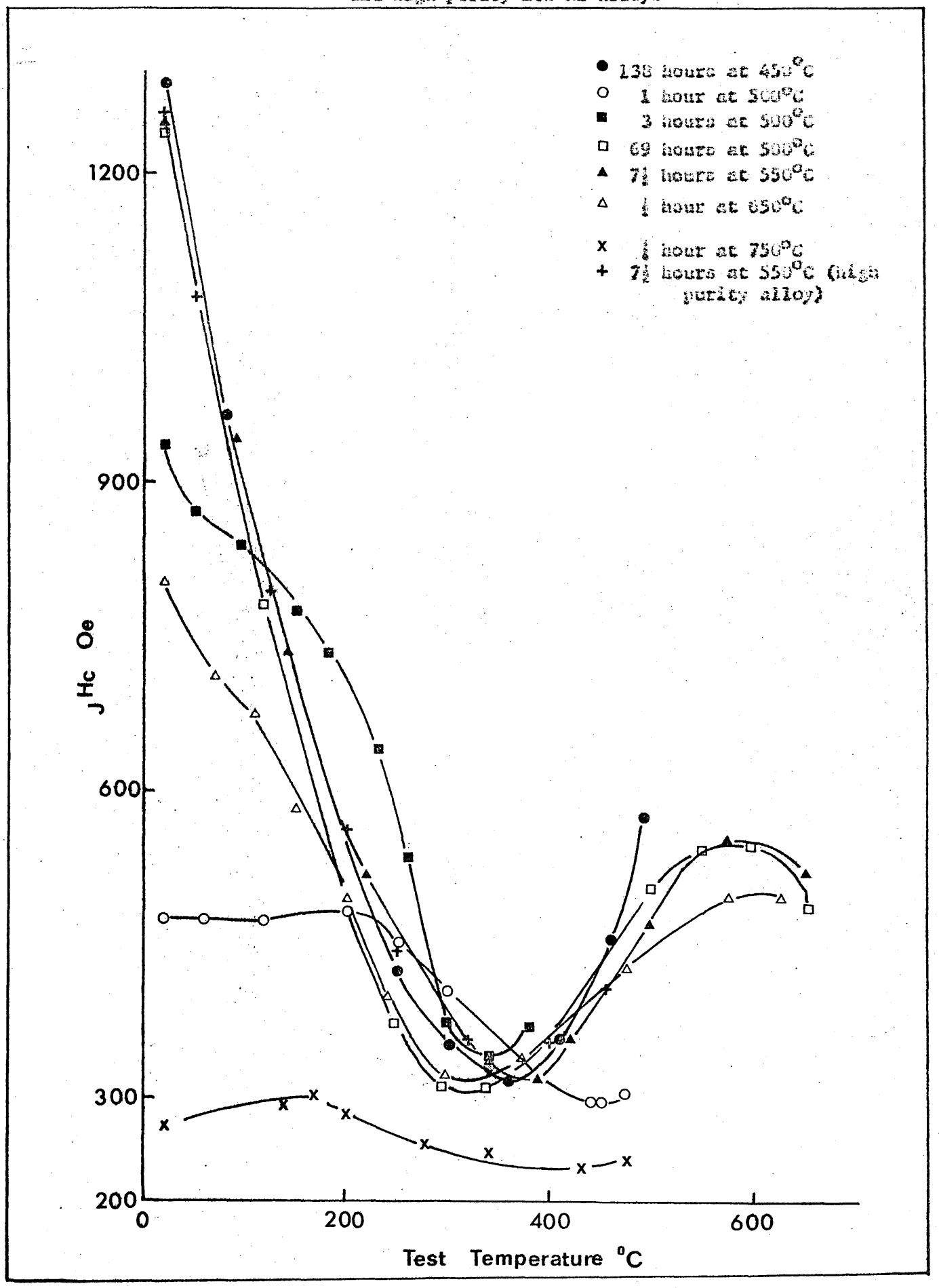

Fig. 16 - Variation of $_{J}H_{c}$ with temperature of samples from the 23% and 38% Al alloys

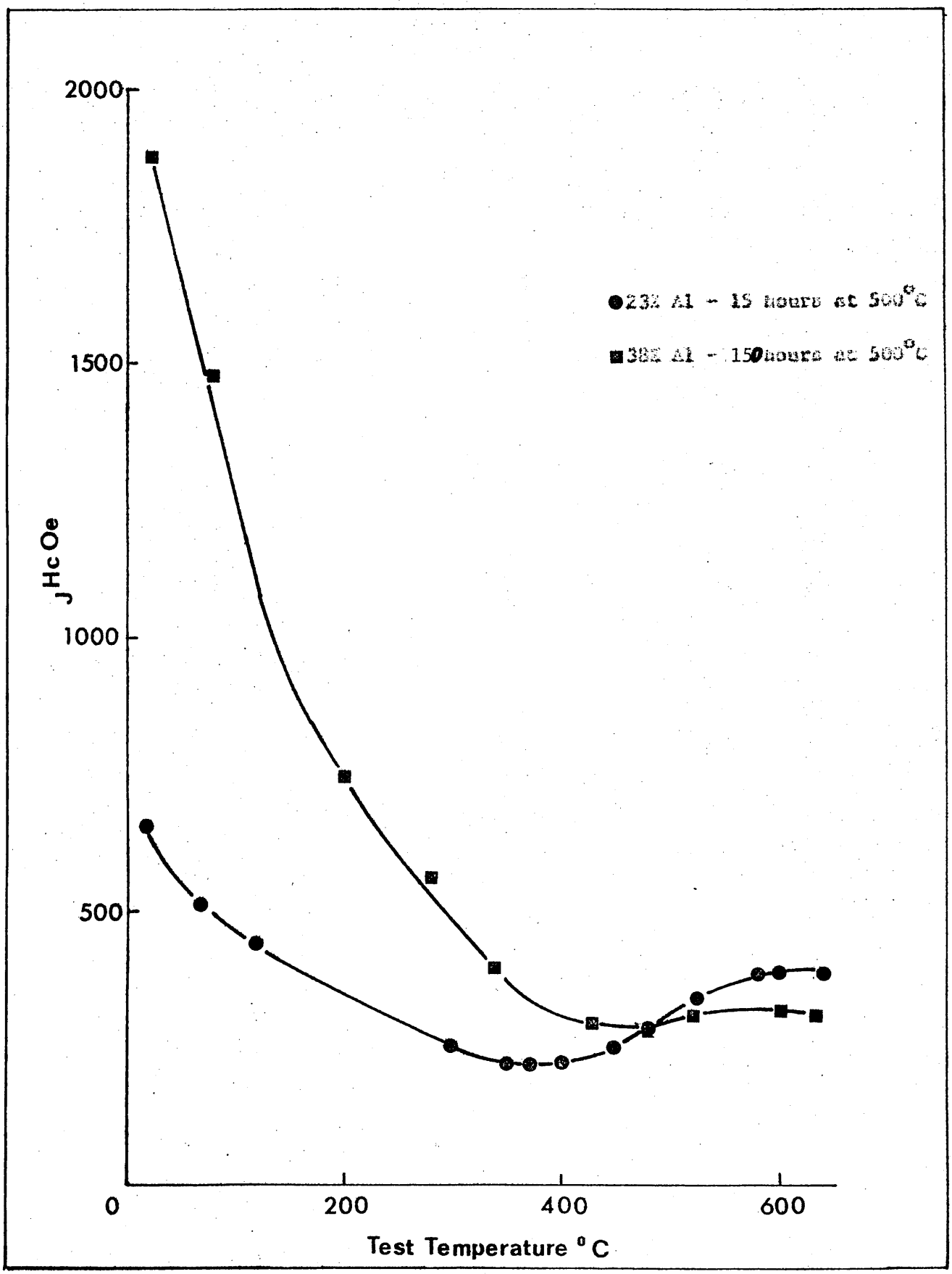

TABLE 11

VARIATION OF J_c^H OF ALCOLLOY WITH TEST TEMPERATURE

23% Al Alloy

15 hours at 500°C		15 hours at 500°C	
Temp. °C	$J_{Oe}^{H_c}$	Temp. °C	$J_{Oe}^{H_c}$
20 (RT)	651	450	250
70	510	480	290
120	446	525	340
300	252	580	385
350	220	600	395
370	220	640	365
400	225	20 (RT)	649

28% Al Alloy

138 hours at 450°C		1 hour at 500°C		3 hours at 500°C	
Temp. °C	$J_{Oe}^{H_c}$	Temp. °C	$J_{Oe}^{H_c}$	Temp. °C	$J_{Oe}^{H_c}$
20 (RT)	1290	20 (RT)	479	20 (RT)	935
80	965	60	475	50	870
200	558	120	475	95	839
250	424	200	486	150	772
300	351	250	453	180	735
360	319	300	402	230	637
410	359	360	351	260	535
460	455	390	325	300	375
490	574	440	297	340	342
20 (RT)	1285	450	297	390	370
		475	305	20 (RT)	940
		20 (RT)	495		

69 hours at 500°C		7¼ hours at 550°C		¼ hour at 650°C	
Temp. °C	$J_{Oe}^{H_c}$	Temp. °C	$J_{Oe}^{H_c}$	Temp. °C	$J_{Oe}^{H_c}$
20 (RT)	1240	20 (RT)	1252	20 (RT)	803
120	781	90	941	70	710
250	375	140	734	110	678
295	309	220	518	150	562
340	311	340	335	200	495
360	327	390	319	240	399
20 (RT)	1239	420	359	300	320
400	360	20 (RT)	1255	375	340
450	432	500	470	475	425
500	504	575	552	575	499
550	644	650	520	625	495
600	550	20 (RT)	1193	20 (RT)	710
650	488				
20 (RT)	1168				

TABLE 11 continued

28% Al Alloy	Temp. °C	H_{Oe}^{c}	½ hour at 750°C
	20 (RT)	272	
	30	279	
	140	295	
	170	303	
	200	287	
	280	255	
	340	247	
	430	231	
	475	240	
	20 (RT)	279	

28% Al High Purity Alloy	Temp. °C	H_{Oe}^{c}	7½ hours at 550°C
	20 (RT)	1255	
	50	1080	
	125	792	
	200	560	
	250	445	
	320	352	
	350	320	
	400	355	
	455	410	
	20 (RT)	1262	

38% Al Alloy	Temp. °C	H_{Oe}^{c}	150 hours at 500°C
	20 (RT)	1873	
	80	1472	
	130	992	
	200	740	
	280	560	
	340	384	
	480	288	
	520	304	
	550	320	
	600	320	
	630	312	
	20 (RT)	1504	

was completely reversible. When permanent differences were observed they were small and could be attributed to predictable changes in the nature of the precipitate taking place during testing. For example, the sample from the 26% Al alloy aged for 1 hour at 500°C was effectively aged for a further time of about 1 hour at temperatures between room temperature and 475°C during testing. As might be expected from the curves in Figure 10 this resulted in a small increase in $_JH_c$. On the other hand the sample from the same alloy aged for 138 hours at 450°C underwent no significant permanent change; presumably because the additional heat treatment during testing was insignificant in comparison with the previous ageing treatment. The irreversible changes observed in samples which were tested up to 650°C were probably associated with the change in the crystal structure of the precipitate from c to c + a the occurrence of which above 600°C has been described in section 3.2.3.

3.3.4. Comparison of the experimental temperature dependence of $_JH_c$ with theory

The curves obtained for the 26% Al alloy aged for 3 hours and 69 hours at 500°C and those from the 23 and 38 % Al alloys aged for 15 hours and 180 hours respectively at 500°C are compared in Figure 17 with the relationship which can be predicted from the temperature dependence of the crystal anisotropy of c. The theoretical curve is derived for randomly oriented single crystal spheres acting as single domains using the expression of Stoner and Wohlfarth[13] (see section 1.3.3.),

$$_JH_c = \frac{0.958K}{J_s}$$

This expression assumes that magnetisation changes take place by coherent rotation of the magnetisation vector. The crystal anisotropy constant, K, was taken as the sum of K_1 and K_2 the variation with temperature of which is shown in Figure 2. Values of J_s (saturation magnetisation) were taken from a curve shown by Bozorth[61]. Above 250°C the calculated change in coercivity is shown as a broken line. The nature of the anisotropy of c above 250°C is such that $[11\bar{2}0]$ and $[10\bar{1}0]$ are mutually preferred directions

FIG.17 - Temperature dependance of $_JH_c$ of Heicolloy samples and calculated temperature dependance of $_JH_c$ of h.c.p. cobalt

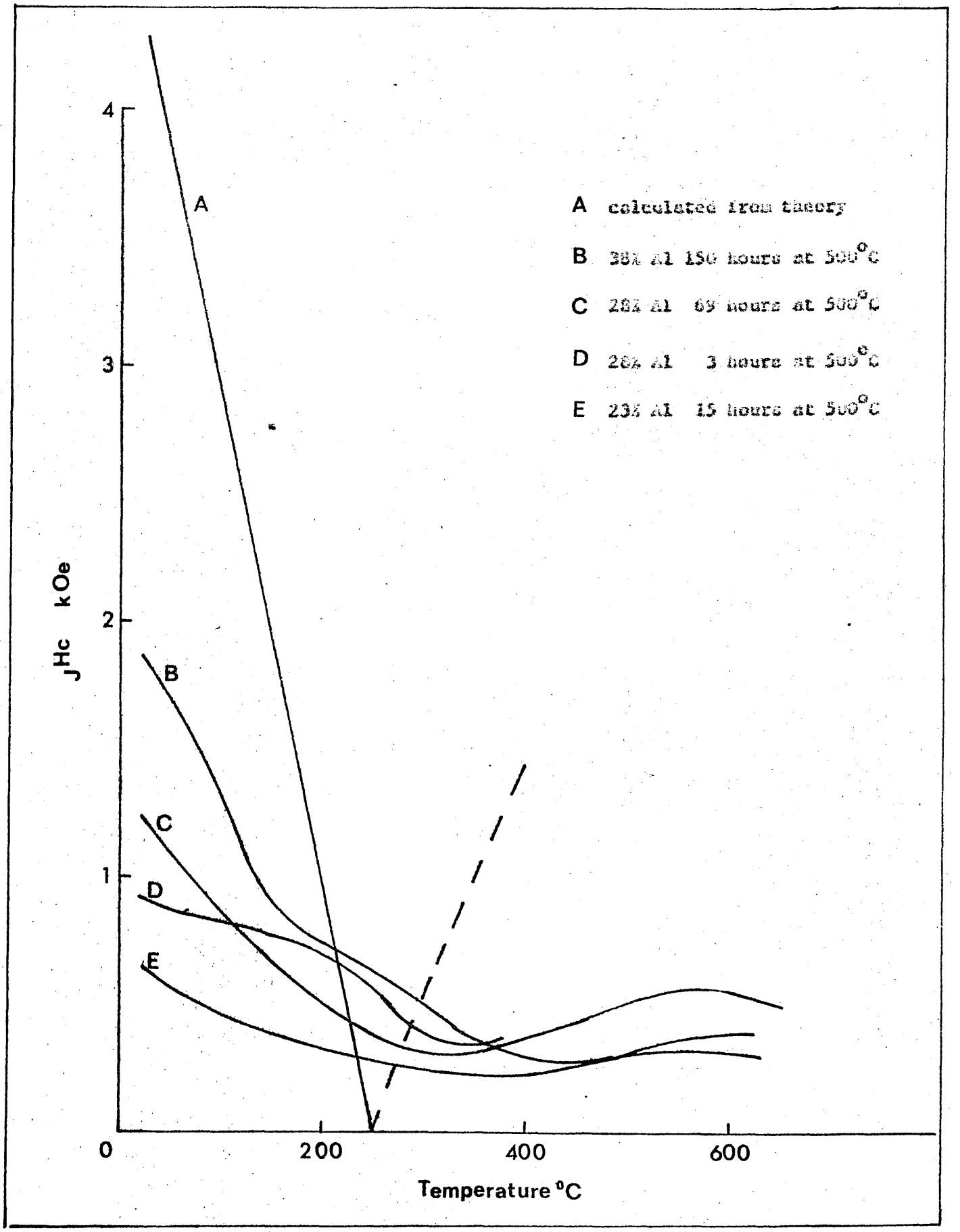

of magnetisation; i.e. the anisotropy is not uniaxial. The preferred directions lie in the (0001) plane of the c structure. The magnetisation of a single domain particle exhibiting this type of anisotropy can, therefore, rotate quite easily within (0001). There is thus no necessity for the anisotropy forces involved in rotation through the $[000\bar{1}]$ direction to be overcome. The broken line in the Figure was calculated using the above expression for ${}_{J}{}^{H}{}_{c}$ based on uniaxial anisotropy, i.e. making the assumption that the magnetisation vector must pass through $[000\bar{1}]$. For the reasons outlined above this assumption is not believed to be valid but the change in coercivity calculated on this basis was, to some extent comparable with that observed in practice.

c. Qualitative similarities between experimental and theoretical temperature dependence of ${}_{J}{}^{H}{}_{c}$

From Figures 15, 16 and 17 it is clear that the experimental results differ considerably from the ideal relationship. Nevertheless, in the case of the samples from the 20% Al alloy aged for 136 hours at 450°C, 69 hours at 500°C and 7½ hours at 550°C and those from the 23% Al and 38% Al alloys aged for 15 hours and 150 hours at 500°C respectively all containing c + β, a substantial continuous decrease in ${}_{J}{}^{H}{}_{c}$ with increasing temperature was observed. A reversible temperature dependence of this magnitude is explicable only in terms of crystal anisotropy and it must be concluded that these samples derived their coercivity from this factor. The decrease in ${}_{J}{}^{H}{}_{c}$ with temperature of the 38% Al alloy aged for 3 hours at 500°C (containing c + β), is similarly difficult to understand unless crystal anisotropy is involved but the form of curve differs from that of the previous group of samples. This curve and those for the samples aged for 1 hour at 500°C (containing c + β), and ½ hour at 650°C (containing α + c + β) are discussed in section 3.6. and are found to be influenced by the magnetic properties of β. Allowing for this influence the curves are shown to be consistent with a coercivity derived from the crystal anisotropy of c, a result which is particularly interesting in the case of

the sample aged at 650°C which contained both c and α. In every case, therefore, except the sample aged for ½ hour at 750°C (containing α + β and a trace of c), where the change in $_JH_c$ was small and inconclusive it is possible to conclude that coercivity arose largely from the crystal anisotropy of c.

b. Departure of the experimental temperature dependence of $_JH_c$ from that predicted by theory

The difference between the experimental and theoretical results can be considered under three headings

i) The magnitude of $_JH_c$ between room temperature and about 200°C

ii) The increase in measured $_JH_c$ in the higher temperature range (above about 350°C)

iii) The magnitude of the minimum $_JH_c$ and the temperature at which the minimum occurs.

i) The difference between theoretical and measured $_JH_c$ between room temperature and 200°C is not surprising. Various factors which can account for the reduced values obtained in practice, (e.g. incoherent rotation of magnetisation, particle size variation, structural defects, etc.), are outlined in section 1.1.4. Furthermore, it is shown in section 3.6 that the $_JH_c$ at room temperature of the samples from the 28% Al alloy aged for 1 and 3 hours at 500°C and for ½ hour at 650°C is reduced by the influence of the matrix phase β which is magnetic in samples aged for short times.

ii) According to theory the crystal anisotropy of c approaches zero at 250°C. At higher temperatures the structure becomes anisotropic but, as pointed out earlier, the anisotropy is essentially planar rather than uniaxial. The broken line in Figure 17, representing calculated coercivity above 250°C, was derived on the assumption that the anisotropy was uniaxial. This assumption is clearly invalid and yet a corresponding increase in measured coercivity was observed at temperatures above about 350°C. It is

possible that there might be a small increase in coercivity as the material passes from the isotropic state at 250°C to the planar anisotropic state at higher temperatures but the small effect observed for the 38% Al alloy (Figure 16) is more easily explained on this basis than the much greater increases occurring in the 23% and 28% Al alloys (Figures 15 and 16).

The increases are even more difficult to understand when the effect of the change in crystal anisotropy on single domain size is considered. According to Went et al[11] (section 1.1.3.) single domain size is proportional to $\sqrt{K}/J_s$ where K is the crystal anisotropy constant and J_s is saturation magnetisation. On heating to 250°C, K approaches zero while there is only a small decrease in J_s. Single domain size is, therefore, reduced and if, as a result, some of the particles become multi-domain there will be a tendency for coercivity to be reduced which will be additional to the straightforward influence of decreasing crystal anisotropy. Above 250°C anisotropy increases but because rotation of the magnetisation vector between adjacent domains can occur easily in the basal plane, the energy of domain boundaries will be low. The formation of boundaries will thus be energetically favoured in relatively small particles (see section 1.1.3.). It is likely, therefore, that multi-domain particles would be present above 250°C in a precipitate which at room temperature consisted largely of single domains.

It is possible that particles which have planar crystal anisotropy might exhibit uniaxed anisotropy due to their shape. Single domain, shape anisotropic particles have high coercivity, but there is no reason why this effect should vary with temperature and the coercivity of such particles would, of course, be low if the particles were multi-domain due to low crystal anisotropy.

It is difficult, therefore, to account for the increasing coercivity of Melcolloy above 350°C. However, in section 3.4 it is

shown that the crystallographic relationship between the ε precipitate and the β matrix is such that both are likely to be subjected to coherency strains. (Note that line broadening, in the X-ray diffraction patterns of the two phases, which was mentioned in section 3.2.3., can be attributed to mutual strain). Elastic strain could influence the anisotropy of the precipitate in two ways. The distortion of the crystal structure of the particles might significantly alter the crystal anisotropy and, possibly the variation of crystal anisotropy with temperature. In addition, some degree of strain anisotropy may be introduced. The combined influence of these effects on the coercivity and the temperature dependence of coercivity of the precipitate is impossible to predict. It can be suggested, however, that some directions in $\{0001\}_\varepsilon$ might, due to distortion of the crystal structure, become preferred directions of magnetisation relative to others in the same plane, at temperatures when the unstrained structure has planar anisotropy (above 250°C). Rotation of the magnetisation vector within {0001} would thus be hindered, resulting in increased domain boundary energy and single domain size and in increased coercivity. Since this effect would be due to the crystal anisotropy of the distorted structure some variation with temperature might be anticipated. The observed increase in $_JH_c$ at temperatures above about 350°C may, therefore, be explicable in these terms.

It should also be noted that h.c.p. cobalt is not normally stable above about 420°C. Data relating to the anisotropy at higher temperatures is consequently not available. It has been assumed in the above discussion that the observations of Honda and Masumoto[32] regarding the anisotropy of ε between 250 and 400°C, can be extrapolated to higher temperatures. It is conceivable that this might not be true in which case the increased $_JH_c$ in the higher temperature range might be associated with some unexpected form of anisotropy in the ε precipitate.

iii) At 250°C c is isotropic (Figure 2). Since single domain size decreases with anisotropy an c dispersion which was a system of anisotropic single domains at room temperature would consist largely of isotropic multi domain particles at 250°C. The coercivity of such a system would clearly be low. In Figure 17 coercivity at 250°C, calculated purely from crystal anisotropy, is zero; this would not be the case in practice because even when domain boundaries are present some energy is required to bring about magnetisation changes by domain boundary movement. The coercivity of such a system is impossible to predict but the coercivity of c particles on heating would be expected to reach a minimum value when anisotropy was a minimum i.e. at 250°C. The results obtained for the Nalcolloy alloys give minima at higher temperatures varying, depending on composition and heat treatment, between 300°C and 450°C.

Weil et al[60] attributed similar effects to the presence of impurities. In the present case, however, no difference was observed between the high purity and commercial purity 28% Al alloys (Figure 15). It seems likely that the difference between the observed and theoretical minima can be attributed to the unpredictable effect of coherency strains on the anisotropy of c as discussed above.

c. Conclusions

With the exception of the sample from the 28% Al alloy aged ½ hour at 750°C, the $_JH_c$ of the Nalcolloy alloys has been found to be extremely temperature dependent. After ageing for ½ hour at 750°C the precipitate was largely α and the change in coercivity with temperature was small and inconclusive. In all the other samples tested the precipitate consisted either entirely of c or of α plus a substantial proportion of c; the reversible temperature dependance of $_JH_c$ of these samples is explicable only in terms of the crystal anisotropy of c.

The change in coercivity with temperature differed considerably from the theoretical relationship. The differences are not understood but it may be that coherency strains in the c precipitate might have some influence.

3.4. The Formation of the Metastable ε Precipitate in Halcolloy

3.4.1. Introduction

It has been shown that the ε precipitate, present in the Halcolloy alloys, is a metastable constituent produced under conditions for which α is the stable allotrope. The properties of the alloys have been shown to arise from the crystal anisotropy of the ε particles and when α was present the coercivity was reduced. It is clear, therefore, that the mechanism by which ε is formed and retained is of some interest and an investigation of the nature of the precipitation process has been carried out.

Experiments to examine two possible processes by which ε might be precipitated are described below.

3.4.2. Growth of ε from h.c.p. nuclei produced on quenching

In section 3.2.2. it was stated that in encapsulated powder samples there was some difficulty in completely retaining cobalt in solid solution by water quenching from the solution treatment temperature. This problem was easily overcome but it was possible that even in bulk samples there might be some undetected precipitation occurring during quenching which might take place, in part, at temperatures at which ε was the stable modification of cobalt. It was feasible, therefore, that h.c.p. nuclei could be produced and that, on subsequent ageing, growth of these nuclei would result in the development of an ε precipitate

In examining this possiblity a sample from the 28% Al alloy was solution treated for ½ hour at 1380°C and quenched into molten tin at 500°C. The sample was then transferred directly to a furnace, already at the ageing temperature of 500°C, and aged for 20 hours. Thus the temperature of the sample was never allowed to fall below that at which ε becomes stable in this system (390°C). X-ray examination at room temperature showed that, as with the water quenched and aged samples, the precipitate was ε.

It has been shown previously that ε was not produced by transformation from α on cooling from the ageing temperature. Thus ε was both nucleated and grown at temperatures for which α was the equilibrium phase and it was not possible that the precipitate developed from h.c.p. nuclei produced as a thermodynamically stable component during quenching.

3.4.3. The formation of ε due to the crystallographic relationship between precipitate and matrix

It was possible that the ε precipitate was nucleated and grown due to a more favourable lattice correspondence, between ε and the matrix, on certain crystallographic planes, than existed with equilibrium α; i.e. the surface energy was lower if the precipitate was ε than if it was α. In this case ε could be described as a transition phase analogous to the coherent or semi-coherent metastable precipitates found in various age hardening alloys.(e.g. Duralumin).

a. Determination of the crystallographic relationship

To evaluate the above hypothesis it was first necessary to determine the orientation relationship between ε and β.

The Nalcolloy alloys are extremely brittle and attempts to prepare thin foils, from which the precipitate orientation could have been determined by electron diffraction, were unsuccessful. The grain size of the material was sufficiently large (1-2 mm diameter) for Laue back reflection photographs to be obtained from single grains in aged samples. These photographs, although revealing clear patterns representing the β matrix, contained no reflections arising from the ε precipitate and thus gave no indication of the relationship between the two phases. It was concluded that the ε particles were oriented at a variety of angles to the incident beam; and a number of different Laue patterns should, therefore, have been produced but presumably these multiple reflections were too weak to be recorded. This view was substantiated when the orientation relationship was successfully

Fig. 16 - Exothermic Mould and Chill Assembly

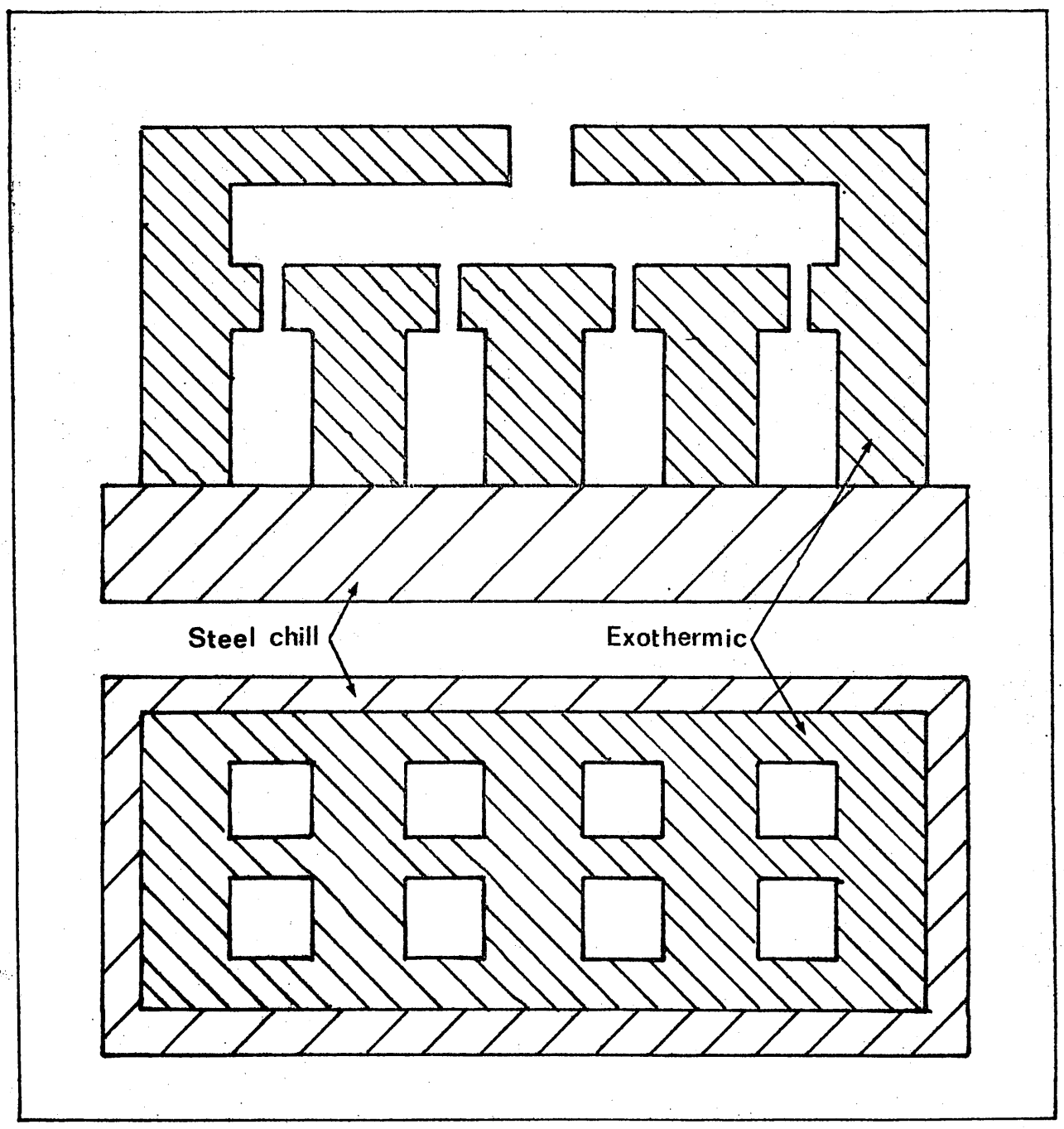

established using the Debye-Scherrer X-ray camera as described below.

I The preparation of samples with known matrix orientation

A cast of commercial purity, with an analysed composition of 27.7% Al, was poured into a mould and chill assembly as shown in Figure 18. The mould, prepared by the CO_2 technique, consisted of the following mixture of materials and reacted exothermically upon ignition.

70 wt % silica sand

15 " aluminium powder

7.5 " sodium nitrate

2.5 " sodium silico-fluoride

5 " sodium silicate

After ignition was complete the molten alloy was poured into the mould and allowed to solidify. The mould temperature immediately prior to casting was estimated to be in excess of 1500°C. There was thus little tendency for heat extraction except in the direction of the chill and the result was a columnar crystal structure with the long axes of the crystals perpendicular to the chill face. This technique of exothermic casting is used commercially in the preparation of crystal oriented permanent magnets.

A sample (1 cm x 1 cm x 2 cm) from this cast was solution treated at 1380°C and water quenched to retain β. It was then sectioned perpendicular to the columnar axis and etched to reveal cross sections through about 50 crystals. The orientations of 10 crystals near the centre of the section were determined by Laue back reflection (see Figure 5c) to show that in every case <100> was within 2° of the normal to the section. The sample was next aged at 500°C for 15 hours to induce precipitation of ε. After ageing $_{J}H_{c}$ was 1200 Oe (the magnetic properties of columnar Malcolloy samples are examined in Chapter 4).

II Determination of precipitate orientation

The orientation relationship commonly observed between h.c.p. and b.c.c. structures, the Burgers relationship[63], is for the closest packed planes and directions in each structure to be parallel; i.e. {0001} h.c.p. parallel to {110} b.c.c. and <11$\bar{2}$0> h.c.p. parallel to <111> b.c.c.

Assuming that the Burgers relationship existed between the h.c.p. precipitate and b.c.c. matrix in Maleolloy it was possible, using the Seemanis camera and the columnar specimen of known matrix orientation, to establish conditions for diffraction, from a particular plane in the c particles, such that if the assumption was valid, diffraction from the selected plane only would be recorded on the film.

The camera was set up so that the normal to the columnar specimen cross section (i.e. <001>β), the incident beam of monochromatic chromium Kα radiation and a cylindrical film strip, were in the same plane, which can be described as the plane of the camera. The c plane selected for study in the first instance was (10$\bar{1}$1)c. Figure 19 shows the anticipated relationship between (001)β (the specimen section), (011)β, (0001)c, and those (10$\bar{1}$1)c poles associated with (0001)c parallel to (011)β. Since (011) planes contain two <111> directions there are, in each (011)β plane, two possible orientations for <11$\bar{2}$0>c and, therefore, two possible positions in the stereographic projection for each (10$\bar{1}$1)c pole. There are thus 24 possible positions for (10$\bar{1}$1)c poles associated with each (0001)c pole, (only 12 are shown in the Figure, a further 12 are on the reverse side of the projected sphere). The broken line in the Figure represents the plane of the camera and it can be seen that if the specimen rotates about [00$\bar{1}$]β (10$\bar{1}$1)c poles move through this plane.

Using Cr Kα radiation the Bragg angle θ for (10$\bar{1}$1)c is 37°. The two possible positions of (1 $\bar{1}$01)c poles in Figure 19 are at 18° to the pole of the specimen section (i.e. (001)β). Therefore, if the incident beam makes an angle of 19° (i.e. 37° - 18°) to the specimen section (i.e. 71° to the (001)β pole in the Figure), and if the assumed orientation relationship exists, conditions are established for diffraction from (1 $\bar{1}$01)c

Fig. 19 - (001)β projection with {0001}α and {10$\bar{1}$1}α poles superimposed according to the Burgers relationship (only those {10$\bar{1}$1}α poles associated with {0001}α parallel to (011)β are shown)

The broken line represents the plane of the camera, as defined in the text, and the point marked X is the position of the X-ray beam incident on (001)β at 19°. The circles show the movement of {10$\bar{1}$1}α poles on rotation about [$\bar{0}$01]β

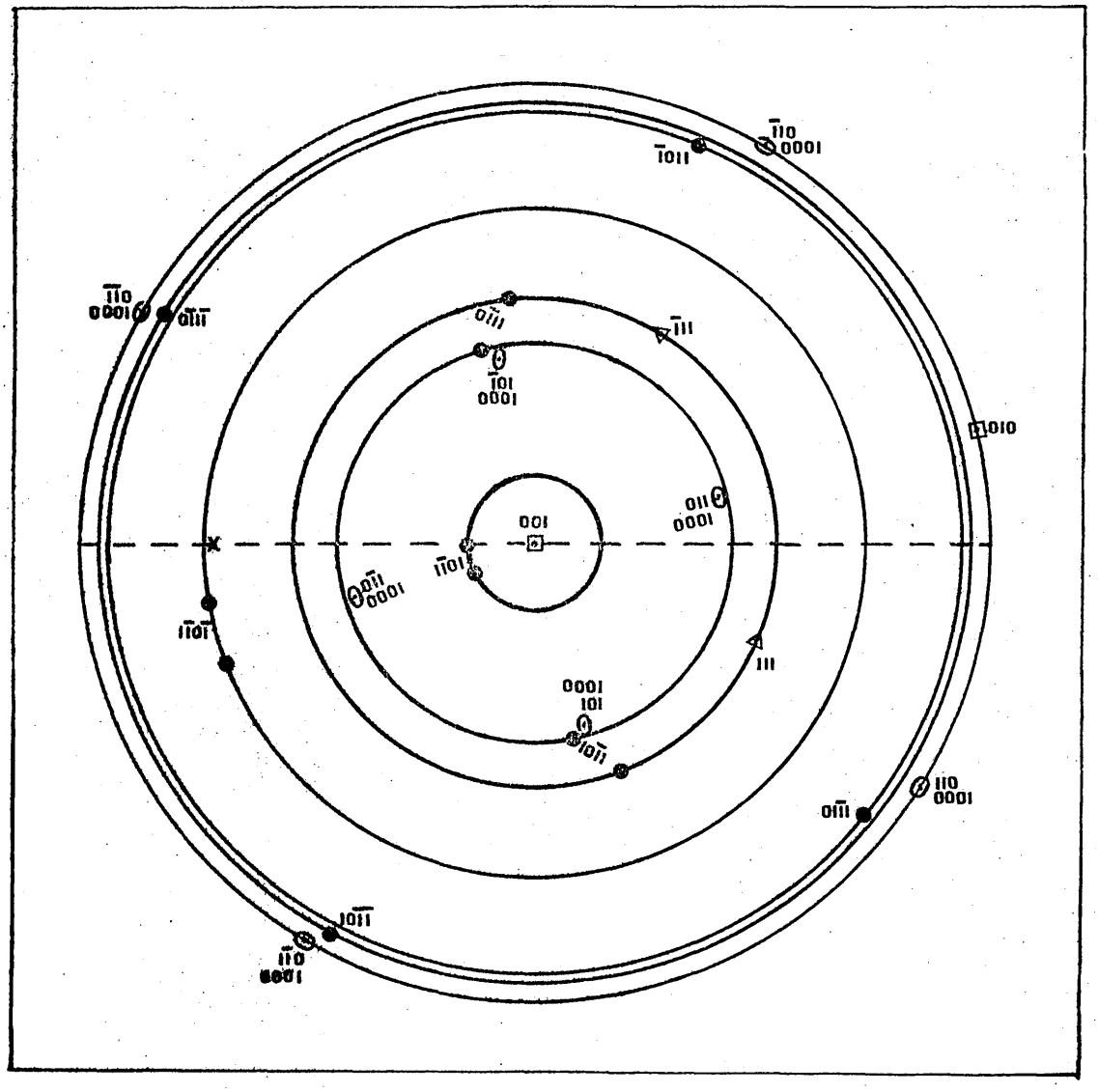

Fig. 20 - (001)$_\beta$ projection with {0001}$_\alpha$ and {11$\bar{2}$0}$_\alpha$ poles superimposed according to the Burgers Relationship (only those {11$\bar{2}$0}$_\alpha$ poles associated with {0001}$_\alpha$ parallel to ($\bar{1}$01)$_\beta$ are shown)

The broken line represents the plane of the camera, as defined in the text, the point marked X is the X-ray beam incident on (001)$_\beta$ at 59°. The circles show the movement of the poles on rotation of the specimen

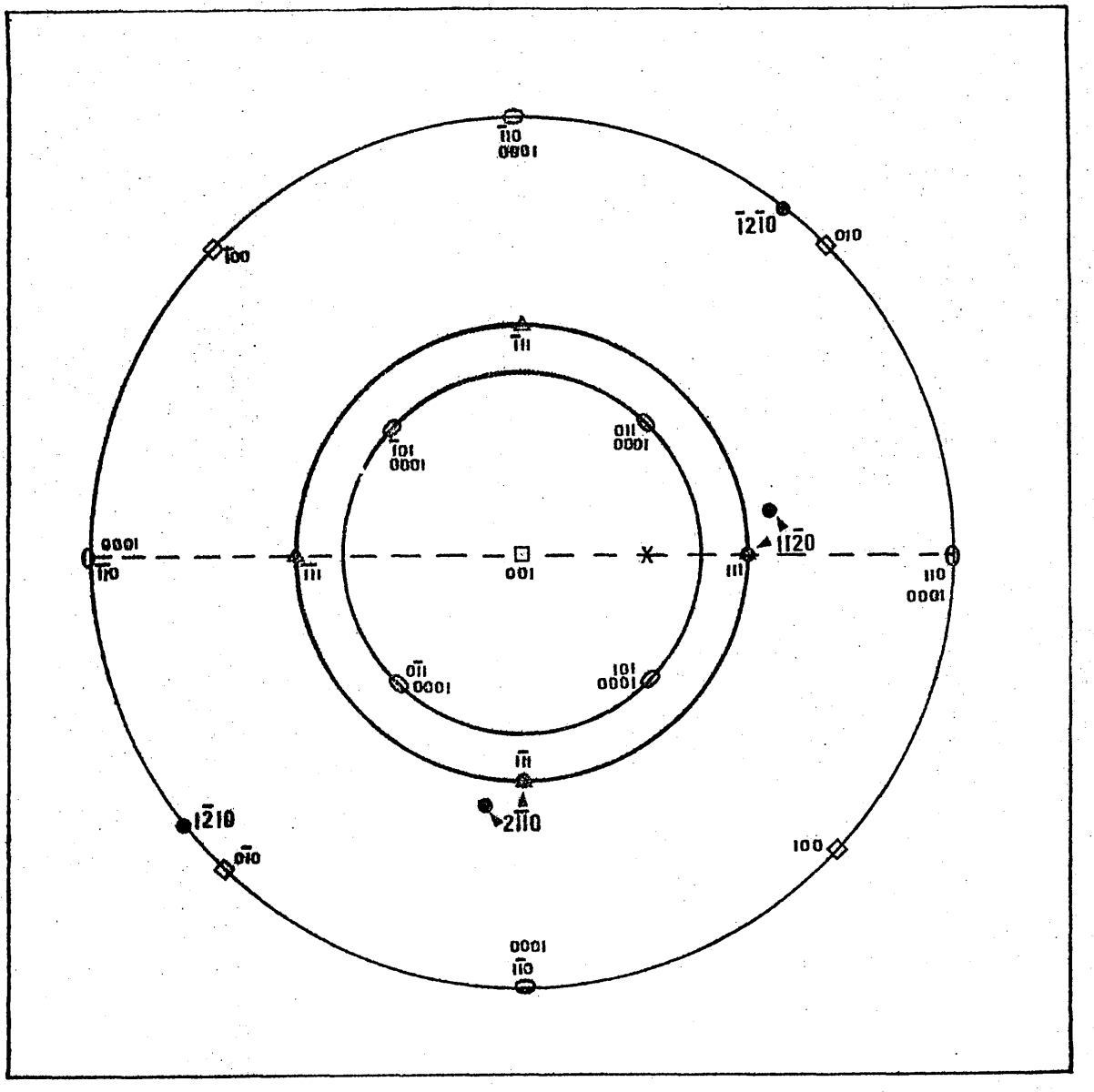

as the normal to this plane rotates into the plane of the camera. The diffracted beam will also be in the plane of the camera and will be recorded on the film. There are twelve possible orientations of $(0001)_c$ planes; i.e. parallel to $(011)_\beta$ (only eight are shown in the Figure, four being on the reverse side of the projected sphere). On rotation, four of these move into positions such that diffraction, in the plane of the camera, from two of the associated $(10\bar{1}1)_c$ planes will occur. Assuming that all the possible orientations described by the Burgers relationship are present, conditions for diffraction from $(10\bar{1}1)_c$ are thus established eight times during rotation through 360°. (Those $(10\bar{1}1)_c$ planes associated with the $(0001)_c$ planes whose poles are on the reverse of the projected sphere, and those associated with $(0001)_c$ planes which are at 90° to $(001)_\beta$ make angles with the incident beam which do not approach the Bragg angle in or near the plane of the camera).

A diffraction pattern was, therefore, obtained with the incident beam at a constant angle of 19° to the specimen section and with the specimen rotating about the columnar axis in order to obtain diffraction from $(10\bar{1}1)_c$. Rotation was eccentric with respect to the point of incidence with the X-ray beam so that a number of grains were irradiated. The area examined was near the centre of the section and contained those grains, the matrix orientation of which had been determined as described earlier. Only one line from the diffraction pattern of c appeared on the film, the anticipated $(10\bar{1}1)_c$ reflection at a d value of 1.91Å.

The angle between the incident beam and the specimen section was then adjusted to 59° in order to establish conditions for diffraction from $(11\bar{2}0)_c$, $(\theta = 66.5^\circ)$, as shown in Figure 20. The resulting diffraction pattern contained a single line which was the anticipated $(11\bar{2}0)_c$ reflection.

III Discussion of the technique

The fact that the anticipated reflections appeared in both

experiments is consistent with the existence of the Burgers relationship. It could be argued, however, that these reflections might conceivably occur even if some other orientation relationship existed. If the precipitate was oriented in some unexpected manner the incident beam would be incident on planes in the precipitate at a variety of angles and conditions for diffraction from some c planes, including those sought, might be established by chance. We are concerned only with diffraction occurring when the normal to the diffracting plane and, therefore, the diffracted beam, is in the plane of the camera. The possibility of such reflections occurring by chance is clearly dependent on the number of different angles which the plane makes with the incident beam within the plane of the camera. This number can, in these experiments, be quite large; for example, it is easily shown that $\{10\bar{1}1\}_c$ planes make 24 different angles with the incident beam within the plane of the camera when the precipitate is oriented according to the Burgers relationship. In either of the experiments it is, therefore, conceivable that the plane sought might be detected, by chance, in the absence of the anticipated orientation relationship. It is extremely unlikely, however, that coincidence could be responsible for the appearance of reflections from the selected planes in both experiments. Diffraction from both selected planes could only be expected if the orientation was, either as anticipated or was such that c planes made a great many angles with the incident beam in the plane of the camera. In the latter case, reflections would inevitably be recorded from planes other than those sought in the experiments. Such additional reflections were not observed and it can be concluded, therefore, that the results of the two experiments confirm an approximate correspondence with the Burgers relationship.

Because the experiments were designed to promote diffraction only when the normals to the anticipated planes and, therefore, the

<001>β axis. (The scale is 5x that of Fig. 13).

The broken line is the plane of the camera and X marks the incident beam. The circles A and B show the possible spread of (001)β and (1101)α poles respectively.

The arc C shows the movement of the most extreme (1$\bar{1}$01)α pole on rotation about (001)β and the points D show the stages during rotation at which diffraction from (1$\bar{1}$01)α will take place, i.e. about 9° above and below the plane of the camera.

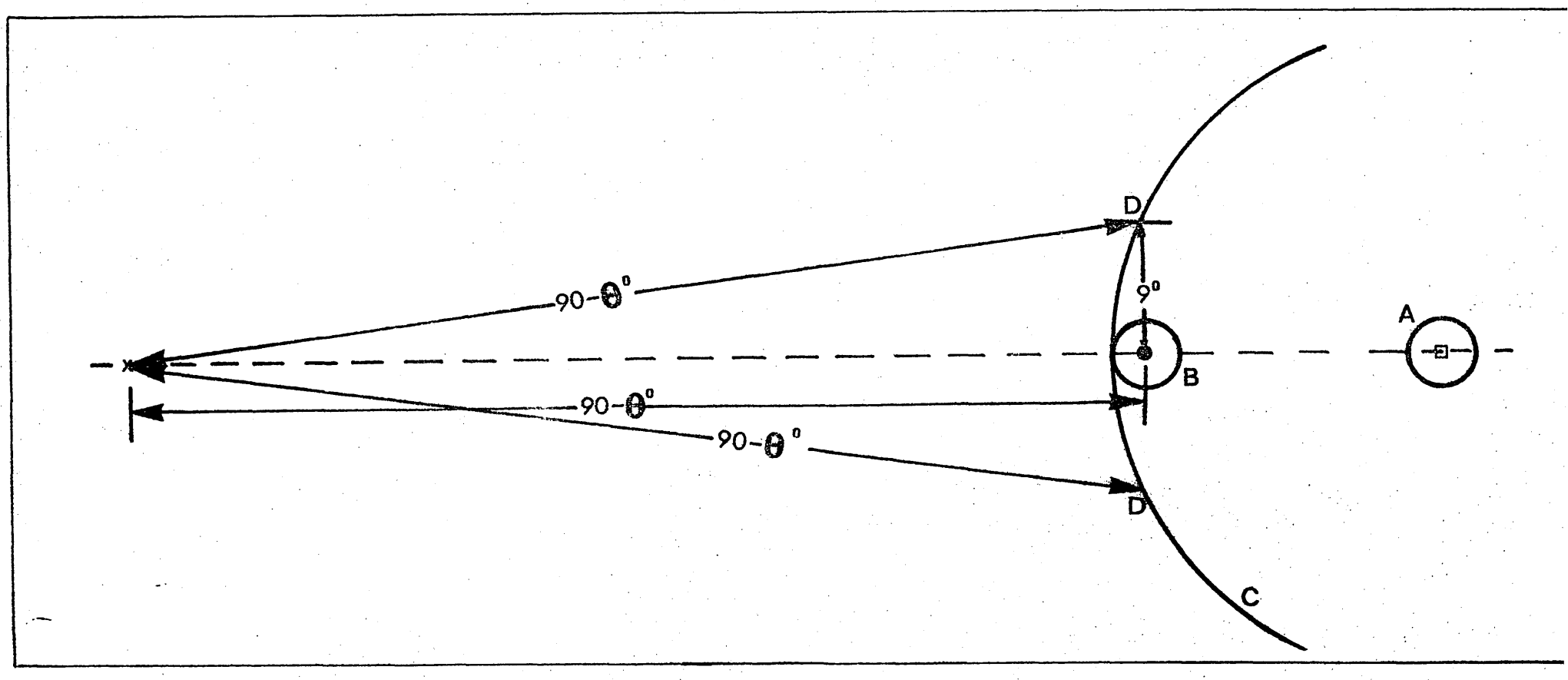

diffracted beams, were in the plane of the camera, the reflections should have been detected as a spot. In fact a line was recorded in both cases. Figure 21, using the first experiment as an example, shows that this can be attributed to the fact that on rotation a number of grains in the specimen were irradiated. As shown earlier, the <001>β axes of the columnar grains could deviate by up to 2° from the normal to the surface. The position of (001)β poles is, therefore, more correctly represented, as in Figure 21 within a circle of radius equivalent to 2°, than as in Figure 19 where the deviation of <001>β from the specimen normal has been disregarded. It can be seen from Figure 21 that due to the deviation of <001> axes the Bragg condition could be satisfied when the normals to $(10\bar{1}1)$ c were up to about 9° above or below the plane of the camera. By plotting the diffracted beam on the stereographic projection it can be shown that the resulting reflection could be up to 11° above the plane of the camera. By simple trigonometry, therefore, the reflection recorded on the cylindrical film strip (radius 5.73 cm) could be elongated by up to about 1.1 cm on either side of this plane; i.e. to give a line 2.2 cm long bisected by the centre line of the film strip.

Because of the differences in the orientations of the matrix grains the technique is not sensitive to small deviations from the anticipated orientation relationship. The extent to which deviation could occur while the observed lines were produced is examined below.

Consider the first experiment. In Figure 19 the specimen is positioned so that the normal to $(1\bar{1}01)$ c lies in the plane of the camera. If the orientation of c deviated from that anticipated so that (0001) c was not parallel to (011)β but was rotated towards $(\bar{1}11)$ β, so that at this stage of rotation the pole of $(1\bar{1}01)$ c was above or below the plane of the camera, conditions for diffraction in the plane of the camera would not exist. Figure 22 (neglecting the spread of (001)β poles) shows the position if (0001) c is inclined at 10° to (011) β so that, at the stage of rotation shown in Figure 19, the $(1\bar{1}01)$ c pole is 10° above

Fig. 22 - Stereographic projection on [illegible]
so that, at the stage of rotation shown in Fig. 19, $(1\bar{1}01)_c$ is 10^o above the plane of the camera. The arc c is 5x that of Fig. 19).

The broken line is the plane of the camera and X is the incident beam.

The arc A shows the movement of the $(1\bar{1}01)_c$ pole on rotation about $(001)_\beta$ and the points B show the stages during rotation at which diffraction from $(1\bar{1}01)_c$ will take place, i.e. about 8.5^o above and below the plane of the camera.

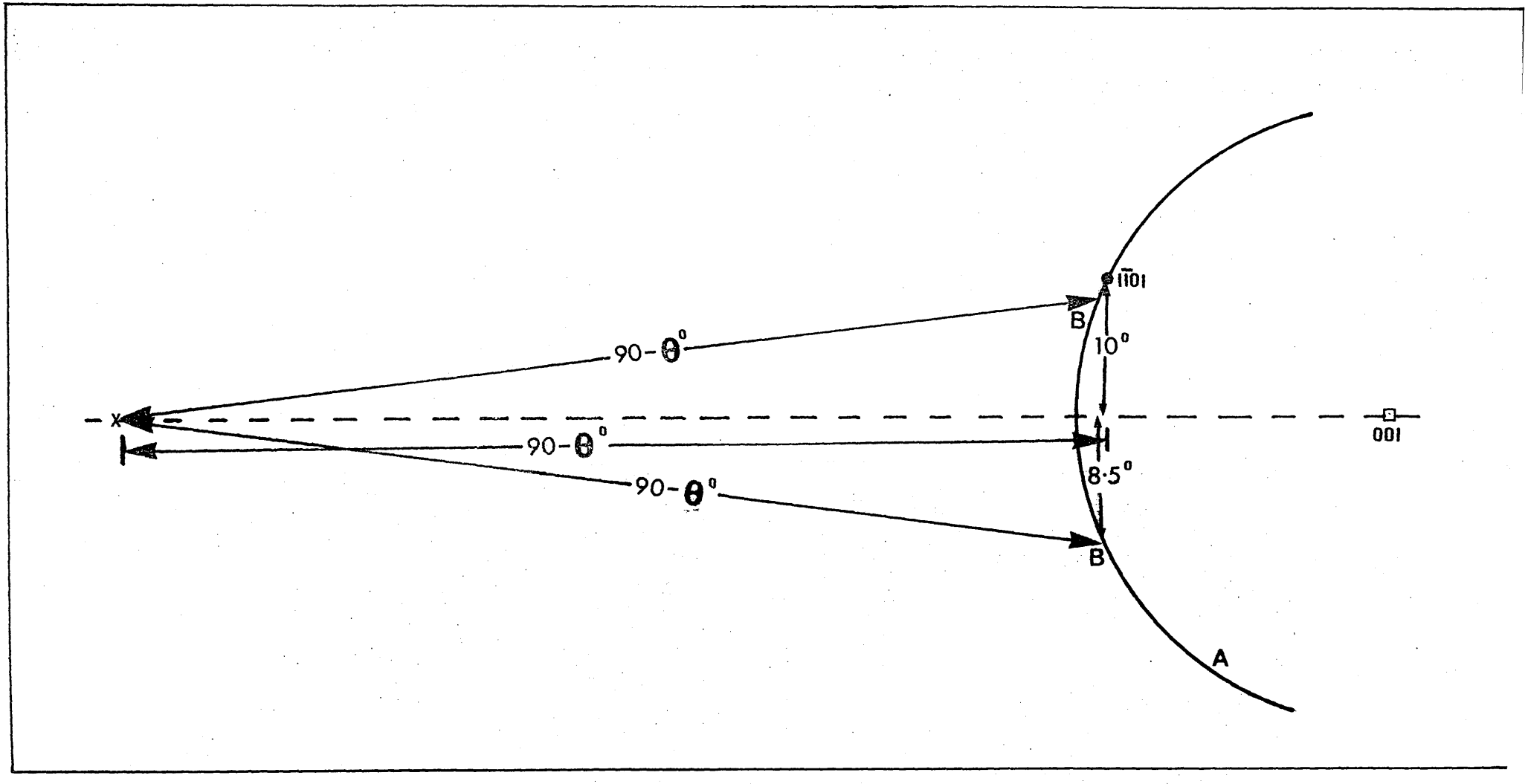

the plane of the camera. As rotation proceeds it can be seen that in the plane of the camera the angle between $(1\bar{1}01)$ c and the beam is less than 0 but that when the normal to $(1\bar{1}01)$ c is 8.5° above or below the plane of the camera, conditions for diffraction are established. Thus the diffracted beam will intersect the film at positions about 1.1 cm above and below the centre line. Due to the deviation of {001} β planes from the specimen section, as discussed earlier, the points of intersection will be elongated to give lines about 2.2 cm in length. These reflections will, therefore, meet at the centre of the film giving a continuous line. If (001) c rotated by more than 10° towards $(\bar{1}11)$ β the line would be discontinuous at the centre of the film. Since no such discontinuity was observed, it follows that this angle was not exceeded.

Similar analysis of the effect, on the result of the first experiment, of the rotation of (0001) c away from (011) β towards $(\bar{1}01)$ β, (110) β, (001) β or (010) β, shows that the observed pattern would not have been obtained if rotation exceeded 3°. According to the Burgers relationship $<11\bar{2}0>$ c should be parallel to <111> β. Consideration of the influence on the diffraction pattern obtained in the first experiment of variation from this directional relationship shows that deviation of up to 10° was possible. Thus deviations of up to 10° from both the planar and directional aspects of the Burgers relationship could not be excluded.

Analysis of the extent to which deviation from the Burgers relationship could occur while producing the line observed in the second experiment ($\{11\bar{2}0\}$c) shows that rotation of (0001) c towards $(1\bar{1}0)$ β, $(\bar{1}10)$ β, $(\bar{1}00)$ β or (001) β could be up to 5°, i.e. a little more than in the first experiment. All other deviations, however, including the rotation of (0001) c towards $(\bar{1}11)$ β and the rotation of the directional relationship, both of which could approach 10° in the first experiment, were restricted to less than 3° in the second.

It is clear that the accuracy of the technique would be

improved if the X-ray beam was incident on only one matrix grain so that the spread of matrix orientations was eliminated. As stated earlier, the matrix grain size was sufficiently large (diameter around 1 - 2 mm) for Laue photographs to be obtained from individual grains, i.e. for single grains to be irradiated. For this purpose, however, the incident beam was perpendicular tothe specimen surface and the specimen was stationary. In order to determine the precipitate orientation it was necessary, for the reasons described above, to rotate the specimen and to set the incident beam at an angle to the specimen surface. As a result the cross section of the incident beam, at its intersection with the specimen surface, was an elipse with a principal axis of length similar to a grain diameter. On rotation of the specimen it did not prove possible to restrict irradiation to a single grain and a diffraction pattern, obtained with the incident beam at 59° to the specimen surface (as in the second experiment described above), consisted of a line, (the $(11\bar{2}0)$ ε reflection as in the second experiment). If only one grain had been irradiated, this reflection should have been recorded as a spot. It was not possible, therefore, to improve the sensitivity of the technique by this approach.

From the combined results of the experiments discussed above it follows that the orientation relationship between the ε precipitate and the β matrix did not deviate by more than 3° from that anticipated. It can be concluded, therefore, that the Burgers relationship or a close approximation to it existed; i.e. (0001) ε approximately parallel to (110) β and $\langle 11\bar{2}0\rangle$ ε approximately parallel to $\langle 111\rangle$ β.

b. The formation of the h.c.p. ε precipitate

Having established the approximate orientation of the ε precipitate in the β matrix it is possible to consider whether the nature of the orientation relationship might be expected to favour the formation of an h.c.p. rather than an f.c.c. structure.

It can be suggested that nucleation of the precipitate occurs in small regions of the matrix which, due to micro-inhomogeneity or

agglomeration prior to precipitation, are rich in Co. The structural change in such regions is, therefore, essentially the transition of "b.c.c. cobalt" to h.c.p. cobalt. Burgers[63], in a study of zirconium crystals, shows that the b.c.c. to h.c.p. transition, leading to the orientation relationship observed in the present work, can occur by a series of shear operations. It may be useful to relate this type of mechanism to the precipitation of cobalt in Malcolloy.

Burgers' mechanism involves three basic steps:

1. A shear along an(112) b.c.c. plane parallel to $[\bar{1}11]$ b.c.c. directions in this plane, such that the angle of $70^{\circ}\ 32'$ between $[\bar{1}11]$ b.c.c. directions in the (110) b.c.c. plane which is perpendicular to the plane of the shear is changed to the angle between $[11\bar{2}0]$ h.c.p. directions (60°) (Figure 23a).

2. The movement of the central atom of the resulting unit cell over $^{1}/_{6}$ of the length of the long diagonal of the base of the unit cell, to give a lattice approximating to h.c.p. (Figure 23 b).

3. Alterations in the dimensions of the lattice obtained in 1 and 2 to give the exact parameters of the new h.c.p. structure.

Of these three steps the second is the most difficult to accomplish because this involves the movement of every atom in alternate (110) b.c.c. or (0001) h.c.p. planes. Burgers shows that the necessary movement can be accomplished in two further shearing operations.

2a. A shear parallel to (011) b.c.c. planes in the direction of the long diagonal of the base of the cell produced in step 1 above, (a-d Figure 23b) so that successive planes are moved with respect to each other over $^{1}/_{6}$ of the length of the diagonal.

2b. A shear in the same plane as 2a and in exactly the opposite direction, such that pairs of planes move simultaneously, successive pairs moving relative to each other over $^{1}/_{3}$ of the length of the diagonal.

Fig. 23a - First shear in Burger's mechanism for the transition of b.c.c. to h.c.p.

○ = atoms in {011} b.c.c.

● = atoms after shear to change the angle between [111] from 70° 32′ to 60°

a,b,c,d indicate the atoms in the base of the unit cell shown in Fig. 23b

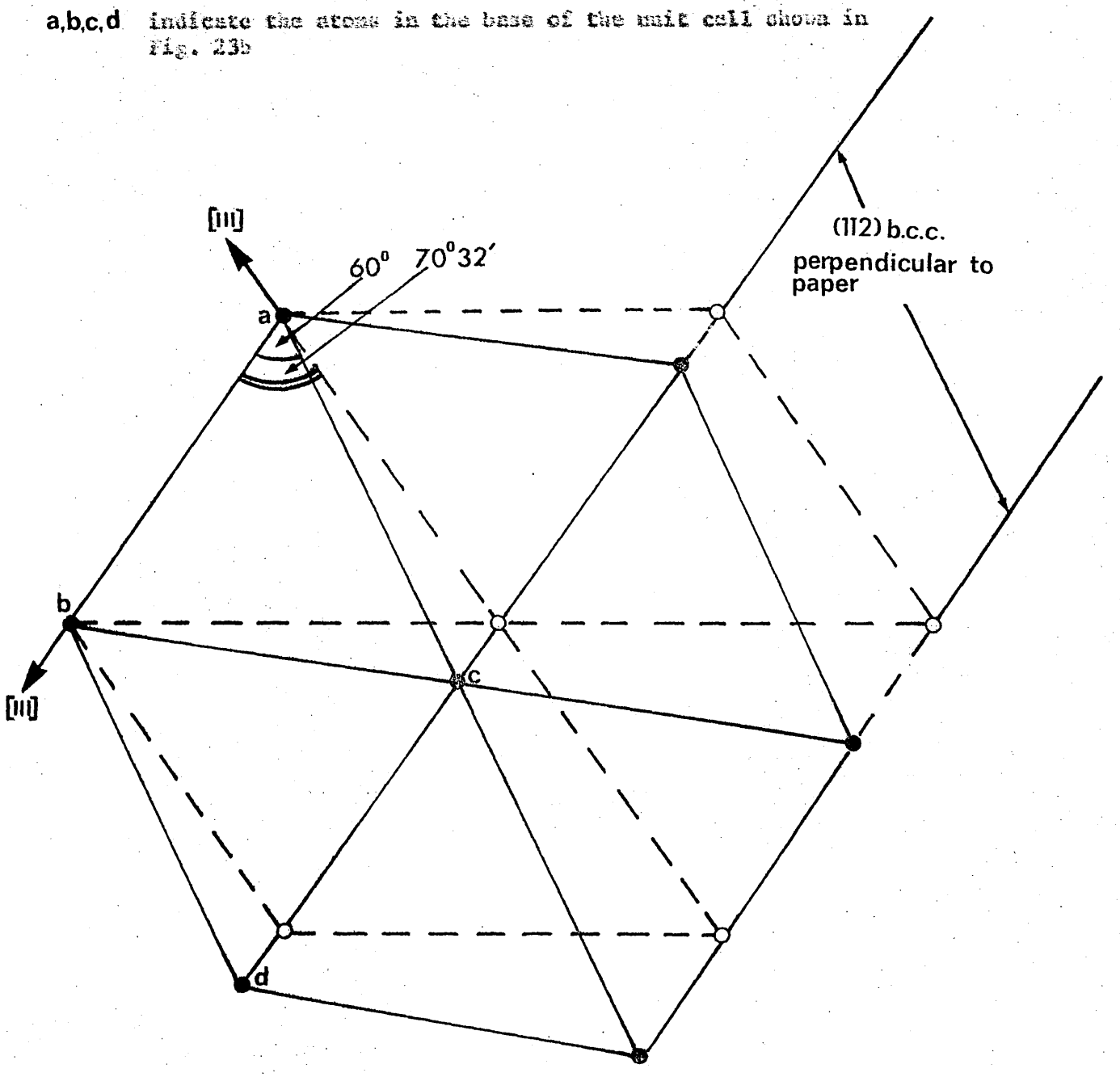

Fig. 23b - The second step in Burger's mechanism for the transition of b.c.c. to h.c.p.

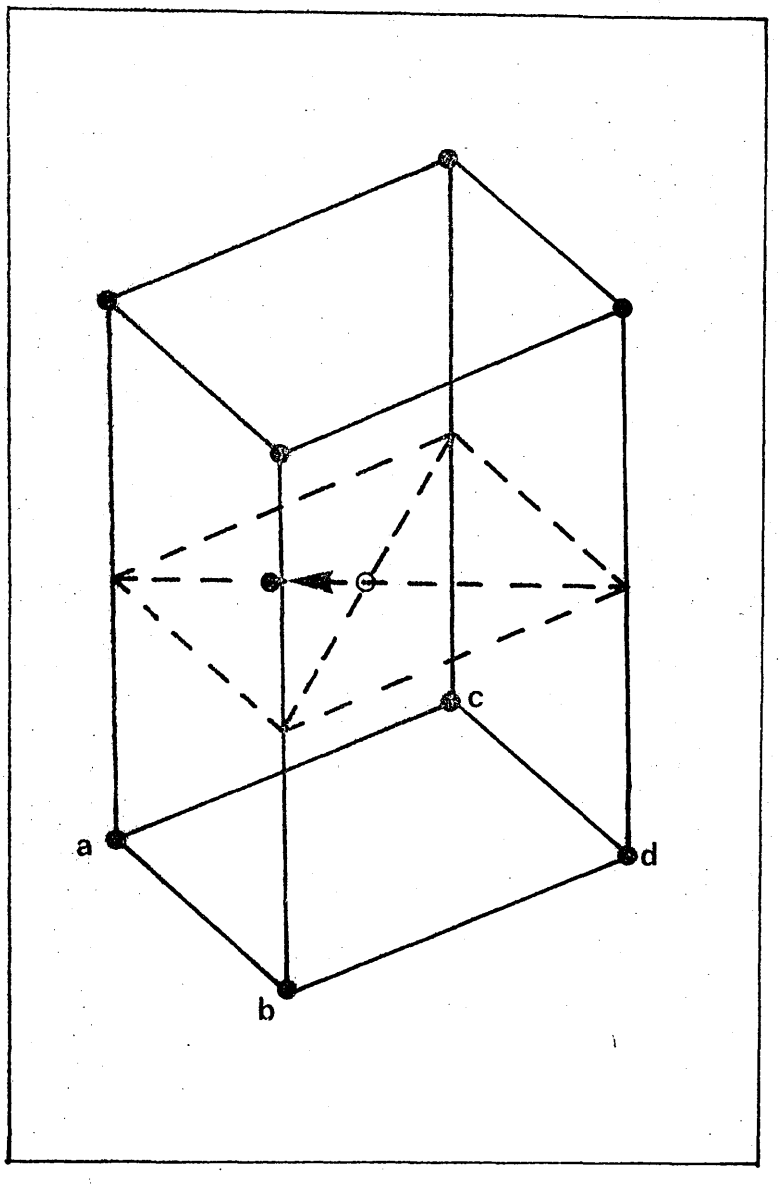

The significant point is that step 2a results in a structure containing a face centred unit cell. Small alterations to the dimensions of this lattice would give a face centred cubic cell and Burgers suggests that the b.c.c. to h.c.p. transition in zirconium might proceed via an intermediate f.c.c. structure. (Note that the mechanism embodied in steps 1 and 2a to transform b.c.c. to f.c.c. is the reverse of the well known Kurdjumow and Sachs mechanism[64] for the transition of austenite to martensite in carbon steel.)

In the case of the precipitation of cobalt in Nalcolloy the stable form of the precipitate is f.c.c. α and we are attempting to account for the appearance of h.c.p. ε. Since the mechanism outlined above produces an intermediate structure approximating to f.c.c. it would, presumably, result in the formation of stable f.c.c. α as a precipitate in Nalcolloy. It is interesting, however, to consider the nature of the interface between a transforming region and the matrix, as the steps outlined above take place. Step 1 results in a region with crystal structure differing from that of the matrix but {112} matrix planes form a coherent interface with the sheared region. If step 2 proceeds indirectly via step 2a this coherency is destroyed, resulting in an increase in interfacial energy. If, on the other hand, the necessary movement of alternate planes of atoms (step 2) takes place directly, it is possible for atoms of the undisturbed planes to maintain complete coherency with the matrix. After the adjustments to the parameters of the transformed lattice, step 3, to give a h.c.p. ε nucleus in a b.c.c. β matrix, the planes at the coherent interface are $(1\bar{1}00)$ ε and {112} β. Figure 24 shows that the atomic arrangements on {112} β and $(1\bar{1}00)$ ε planes are similar; mismatch does not exceed 2%. The persistence of the coherent interface when a h.c.p. nucleus is established is therefore likely. Thus if nucleation is considered to occur by a shear process it is reasonable to suggest that the mechanism leading to the f.c.c. structure would be inhibited due to the necessity for creating an

Fig. 24 - Comparison of the atomic arrangement on $\{1\bar{1}00\}\varepsilon$ and $\{112\}\beta$

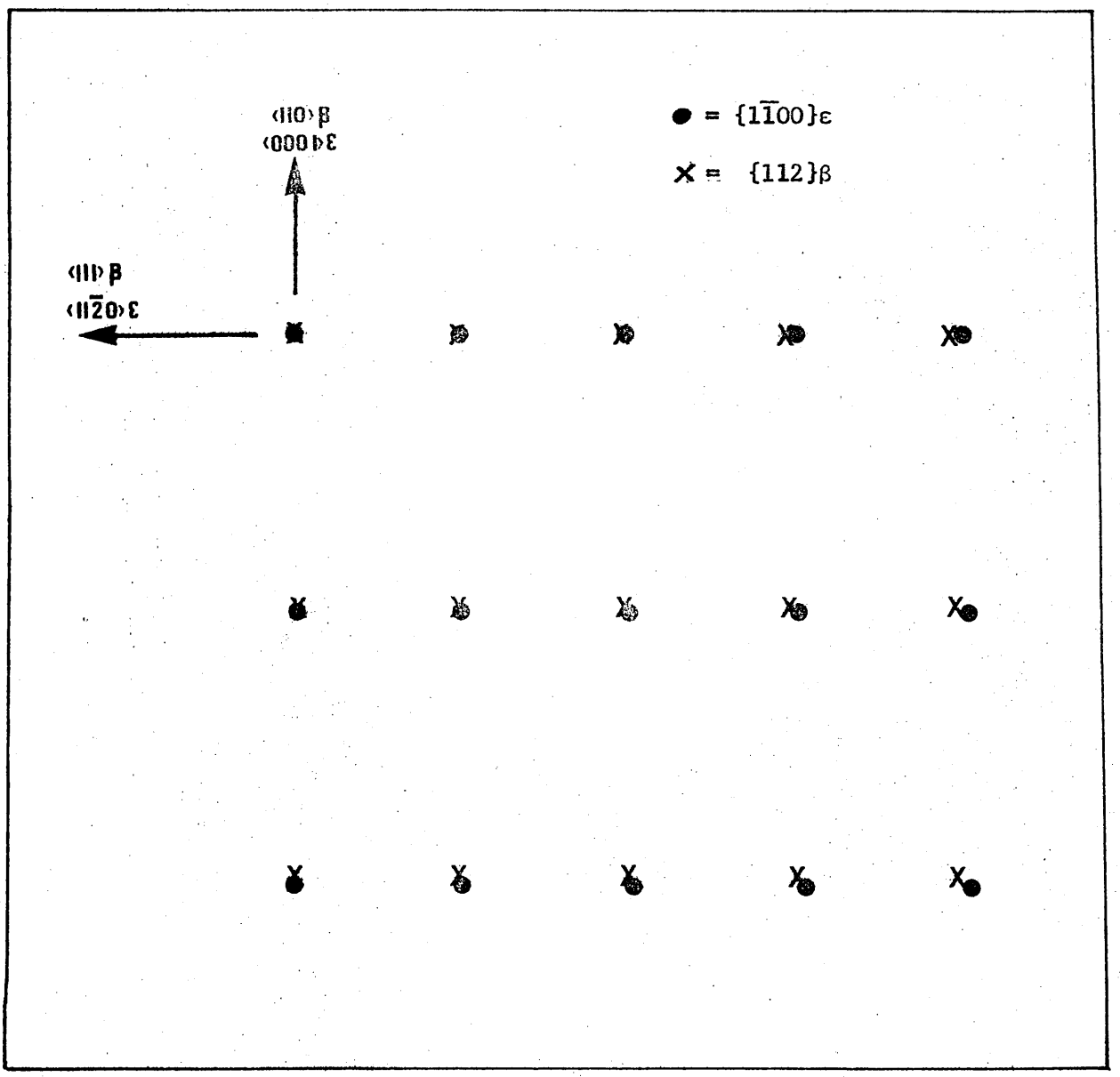

incoherent interface and that the process leading to an h.c.p. nucleus would be preferred.

The above discussion shows that at least one mechanism can be envisaged by which the formation of metastable ε can be understood. It cannot be assumed, however, that the postulated shear mechanism is in fact responsible for nucleation of the precipitate. It may be, for example, that nucleation takes place simply by the assembly of Co atoms in the form of an h.c.p. structure, the necessary re-arrangement of atoms occurring simultaneously with the migrations of cobalt and aluminium atoms needed to establish the change in composition from β to ε. For any nucleation mechanism, however, the argument regarding coherency between $\{1\bar{1}00\}$ ε and {112} β is valid. It is reasonable to suggest, therefore, that a particle of ε could exist with a partially coherent and low energy interface with the β matrix, and thus have low surface energy.

As particle size increases surface energy increases as the square of the radius while bulk free energy increases as r^3. Thus the importance of surface energy relative to the total energy associated with a precipitate particle decreases with increasing radius. Nevertheless, surface energy is significant in small particles where the surface to volume ratio is high and the structure of a small particle or nucleus may well be influenced by surface energy considerations. As a result, the formation of a metastable but coherent ε structure might be favoured. Examination of the atomic arrangement on planes of low indices, (up to {221}), and, therefore, high reticular density in f.c.c. ε and b.c.c. β shows that in no case is mismatch less than about 12%. The possibility of the existence of coherency planes with higher indices than {221} cannot be excluded but because the packing density of atoms on such planes is low the advantage in terms of surface energy would be less than that associated with coherency between $\{1\bar{1}00\}$ ε and {112} β.

It can thus be concluded that whatever the nucleation mechanism, the metastable ε precipitate in Malcolloy is probably produced because of the ability of the h.c.p. structure to form a partially coherent and low energy interface with the β matrix.

c. ε to α transition

It has been shown, in section 3.2.3., that initially the precipitate was completely or partially ε at all the ageing temperatures studied (450 - 750°C). Ageing above 600°C, or for prolonged times at 600°C, however, resulted in transformation of ε to α. If, as concluded above, metastable ε is produced because it is partially coherent with β, transformation to stable α will eventually occur when one of the following criteria is satisfied.

It has been pointed out that the relative contribution of surface energy to the total energy of a precipitate decreases as the particle size increases. During growth of the precipitate, therefore, a stage may be reached where the increased bulk free energy, associated with the presence of the metastable structure outweighs the decrease in surface energy due to the existence of the low energy interface. At this stage the total energy of the system will be reduced by transformation to the stable phase. It may be, on the other hand, that the ε → α transition begins when, due to increasing particle size, coherency strains in either β or ε become intolerable. The coherent interface will then be destroyed with a consequent increase in surface energy. Total energy will thus be reduced by transformation to stable α.

Both these possibilities assume that transition will take place at some critical particle size. The much more rapid transition of ε to α at temperatures above 600°C can, therefore, be attributed to the greater rate of particle growth during ageing in the higher temperature range. Furthermore, as the ageing temperature is increased the difference between the free energies of the allotropes becomes greater. The driving force

for transition is, therefore, increased and after either of the above criteria is satisfied, the transformation will proceed more rapidly than at temperatures just above the equilibrium transition temperature

d. Particle shape and lattice strain

If the ε precipitate is coherent with {112} β planes the particles would be expected to form thin plates extending parallel to {112} β in order to minimise surface energy. The electron-micrographs in Figure 8 show signs of particle elongation and to some extent support this view. If this is the case it follows since $\{1\bar{1}00\}$ ε is the coherent plane in the precipitate, that this plane and, therefore, <0001> ε directions (the preferred direction of magnetisation with respect to crystal anisotropy) will be parallel to the plane of the plate. In a plate-like particle, in the absence of any crystal anisotropy, directions lying in the planeof the plate are more easily magnetised than the perpendicular direction,but rotation of the magnetisation vector within the plane of the plate is easily accomplished. Since, in the present case, the easy direction of magnetisation with respect to crystal anisotropy, (<0001> ε) lies in the plane of the plate, the shape anisotropy of the particle will have little influence on coercivity.

More important with respect to coercivity is the fact that coherency will result in some degree of strain in the lattices of either the ε precipitate or the β matrix or both. The X-ray diffraction patterns of both phases (see section 3.2.3.) showed some degree of line broadening which could be interpreted as indicating the existence of strain. Since this was observed in both the ε and β patterns, it could not be a particle size effect and the fact that broadening disappeared from both the precipitate and matrix patterns when the precipitate was entirely α strongly suggests that coherency strains between ε and β were responsible. Distortion of the ε lattice would affect the anisotropy of the structure and, therefore, the coercivity. The existence of coherency strains might, therefore, account to some extent for the various departures from theoretical coercivity,

both at room temperature and at elevated temperatures, discussed in section 3.3.

c. Conclusions.

It can be concluded that the observed orientation relationship, {0001} ε approximately parallel to {110} β, <11$\bar{2}$0> ε approximately parallel to <111> β, is compatible with the existence of a partially coherent interface between the ε precipitate and β matrix. It is probable that the lower interfacial energy associated with ε results in the nucleation of ε rather than thermodynamically stable α.

Presumably transformation from ε to α takes place either when coherency is lost or the particle size is such that the total energy of the system is reduced by the transformation.

If the coherency hypothesis is accepted it follows that the particles will take the form of thin plates in order to minimise surface energy. The proposed crystallographic orientation of the particles with respect to their shape is, however, such that shape anisotropy will have little influence on coercivity, although this property might be affected by coherency strains within the particles.

FOOTNOTE: Subsequent to the completion of this work, a study of the crystallography of cobalt-aluminium alloys (Arbuzov et al, Fizika Metallov. I. Metallovedenie, 28, 21, 1969) came to the attention of the present author when published in an English translation in 1971. This work, referred to at the end of section 3.2. and discussed in Appendix II, confirms the orientation relationship established above and reports the existence of strain in the matrix lattice. The latter point supports the hypothesis postulated in the present work regarding probable coherency between ε and β.

3.5. The Metastable Co-Al Phase Diagram

3.5.1. Introduction

In attempting to understand the magnetic properties of any alloy it is obviously desirable that the compositions and amounts of the phases present should be predictable. This information can normally be derived from the equilibrium phase diagram. In the case of the Malcolloy alloys, however, ageing below 600°C results in the precipitation of ε as a metastable constituent and it is possible that the equilibrium phase diagram for the cobalt-aluminium system (Figure 3) will not accurately represent either the proportions or the compositions of the phases present after heat treatment in this temperature range. It was necessary, therefore, in studying the properties of the Malcolloy alloys, to establish the nature of the metastable equilibrium between ε and β.

3.5.2. The composition of the ε precipitate.

According to the equilibrium phase diagram (Figure 3) ε, when present as a thermodynamically stable phase below about 400°C, contains little or no aluminium in solid solution. Bradley and Seager[65] state that the solubility of aluminium in ε is negligible. The solubility of aluminium in α is, on the other hand, quite significant, increasing from 2% at 300°C to 15.5% at 1400°C. Within the range 450-600°C, shown in the present work to give metastable ε, the solubility of aluminium in stable α is between 4 and 6%. The first requirement, therefre, was to determine the solubility of aluminium in metastable ε at these temperatures. This was conveniently carried out by measuring the variation of specific saturation (σ) with temperature (σ, T curves).

Figure 25 shows three σ, T curves. Curve A is the relationship for pure cobalt (according to Bozorth[61]) reduced by 60%; this can therefore be regarded as the curve for pure cobalt in the presence of 60% by weight of non-magnetic material. Curves B and C are heating

Fig: 23 - σ - T curves for pure cobalt and Alcolloy

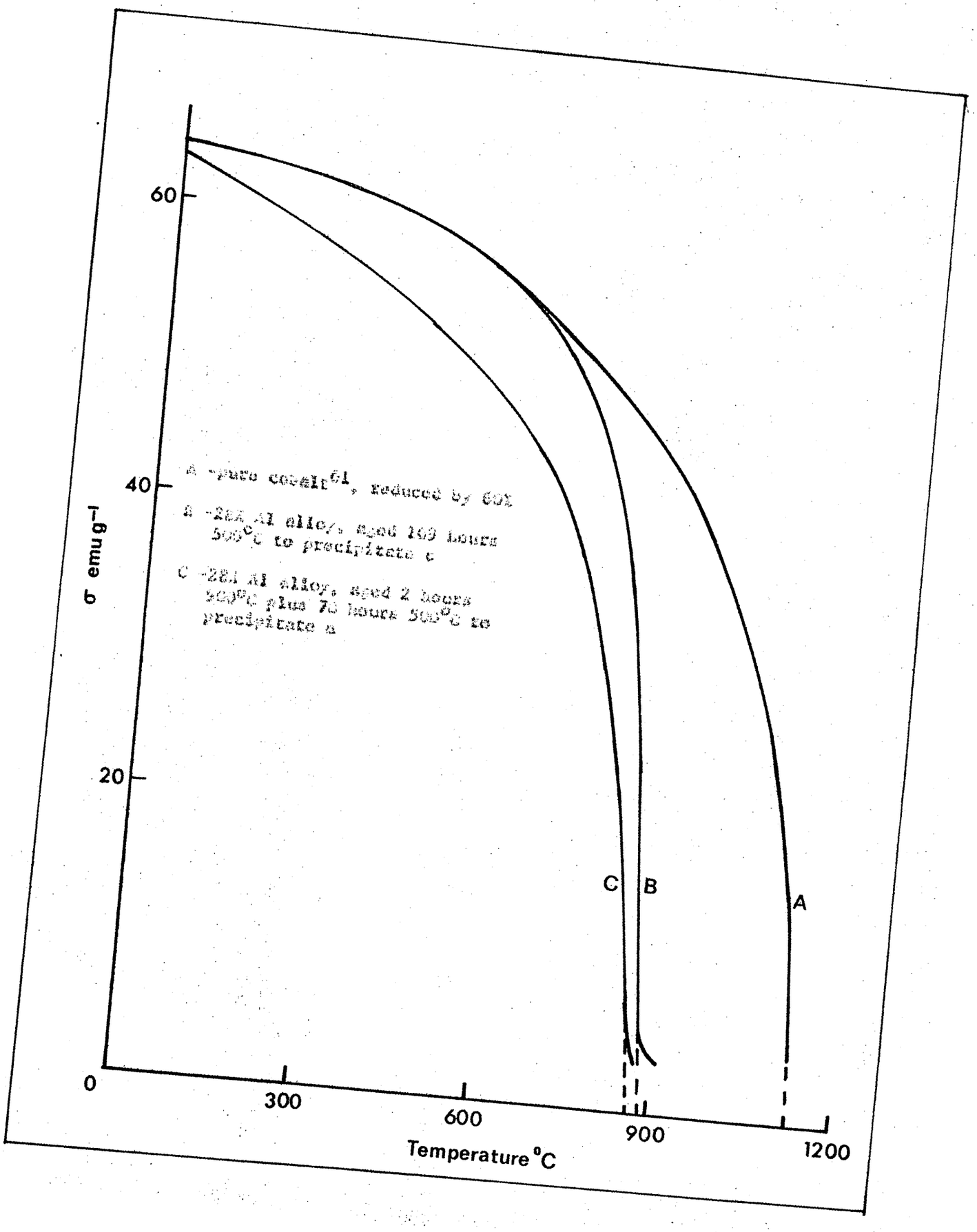

curves determined using a Sucksmith balance, and show the change in σ with temperature for two samples from the 28% Al alloy. One of these samples (B) had previously been aged for 169 hours at 500°C to precipitate ε. The other (C) contained substantially σ precipitated at 900°C and brought into equilibrium at 500°C by subsequent ageing for 70 hours at that temperature. In both cases the matrix phase, β, was non-magnetic at and above room temperature. The difference between curves B and C cannot be attributed directly to the crystal structure of the cobalt precipitate because the change in σ associated with the allotropic transformation is very small, (Myers and Sucksmith[66] detected 1.5% increase in σ during the h.c.p. to f.c.c. transition in pure cobalt). It can be assumed, however, that in the case of the sample represented by curve C, aluminium is in solution in the σ precipitate causing substantial deviation from curve A (pure cobalt). It follows, since curve B (ε precipitate) and curve A (pure cobalt) are identical up to 600°C, that the ε precipitate did not contain a significant amount of aluminium in solution. At temperatures above 600°C the precipitate has been shown to become a mixture of σ and ε (section 3.2.3.) and the observed deviation of curve B from curve A at these temperatures can be attributed to the solution of aluminium in σ. The variation of σ with temperature was also determined for a sample from the 28% Al alloy aged for 20 hours at 600°C. The resulting σ, T curve was virtually identical to curve B. It can be concluded, therefore, that aluminium displays little or no solubility in ε at temperatures up to 600°C.

3.5.3. The composition of β in metastable equilibrium with ε

From the equilibrium phase diagram (figure 3) it can be seen that the composition of β in equilibrium at 600°C is such that the phase is magnetic at room temperature with T_c (Curie temperature) of about 100°C. The presence of magnetic β would have resulted in an inflection in the σ,

T curve (as in Figures 29 and 30) but the measurements discussed above showed no inflection, indicating β in metastable equilibrium with ε at 600°C to be non-magnetic at room temperature (i.e. T_c less than room temperature). Furthermore, the amount of cobalt precipitated at 600°C should, according to the equilibrium phase diagram, be less than that produced at 500°C. After ageing at 600°C, therefore, σ of the alloy at room temperature should, if β is non-magnetic, be lower than after ageing at 500°C. In fact, the σ, T curves for samples aged at 500°C and 600°C were identical suggesting the presence of similar quantities of precipitate. The implications are that β in metastable equilibrium with ε at 600°C has a composition richer in aluminium than that predicted by the equilibrium phase diagram, (i.e. the position of the β phase field boundary is shifted towards higher aluminium contents), the composition of β in equilibrium with ε at various temperatures was determined by X-ray diffraction techniques as follows.

a. The effect of composition on the lattice parameter of β

First the variation in the lattice parameter of β with composition was determined. Samples from several of the arc melted casts referred to in section 3.1. were crushed to - 200 mesh powder, solution treated for ½ hour at 1380°C and water quenched to retain β. The lattice parameter 'a' of β was then measured, for each sample, from X-ray diffraction patterns obtained in the Unicam camera. Unfiltered chromium radiation was used and lattice parameters, derived by extrapolation against the Nelson-Riley-Taylor-Sinclair function, were reproducible to within ± 0.0005Å. The relationship between lattice parameter and composition is shown in Figure 26 and in Table 12, (values of 'a' are quoted to the nearest 0.0005Å). In Figure 26 the results obtained are compared with those reported by Bradley and Seager[65] and Cooper[59]. The differences observed may be attributable to impurities in the material used in the present work (see section 3.1.).

Fig. 26 - Variation of the lattice parameter (a) of β with composition

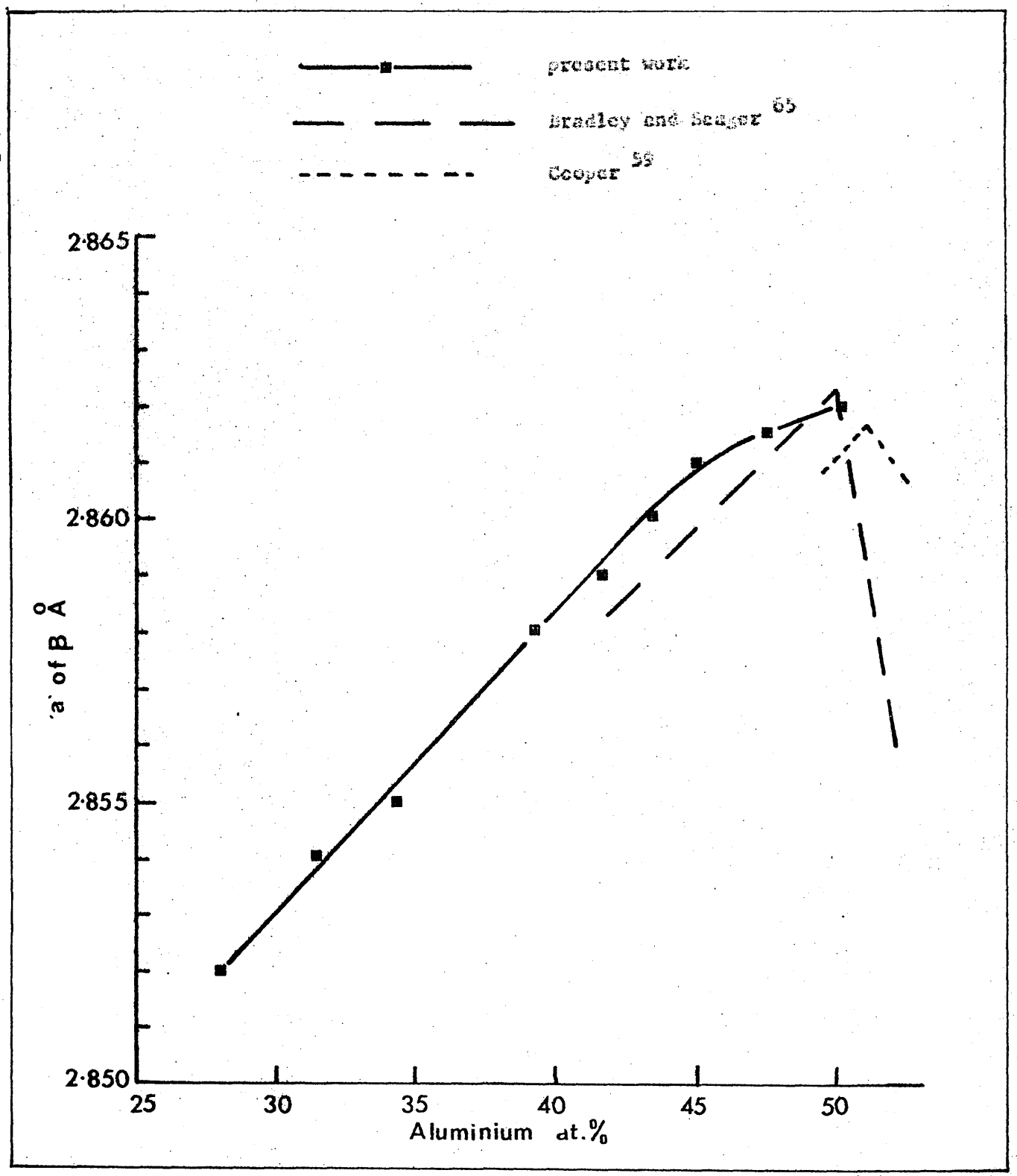

TABLE 12

THE INFLUENCE OF COMPOSITION ON THE LATTICE PARAMETER 'a' OF β

(all samples water quenched from 1380°C)

Analysed Composition at.% Al	Lattice parameter 'a' of β Å
50.1	2.862
48.8	2.8615
47.5	2.8613
45.0	2.861
43.4	2.860
41.5	2.859
39.2	2.858
34.2	2.855
31.3	2.854

TABLE 13

THE LATTICE PARAMETER AND COMPOSITION OF β AFTER AGEING

Ageing Treatment		Precipitated	Lattice Parameter of β	Composition of β
Time hrs.	Temp. °C	phase	Å	at.% Al ±1.0%
200	450	ε	2.860	43.3
150	500	ε	2.8605	44.3
150	525	ε	2.860	43.3
50	550	ε	2.860	43.3
50	600	ε	2.860	43.3
20	650	largely α	2.858	39.3
20	700	α	2.858	39.3
20	750	α	2.8575	38.3
15	900	α	2.857	37.5

b. The lattice parameter of β in the presence of the cobalt precipitate

Small solid samples from the 25% Al cast were solution treated at 1300°C and water quenched. The lattice parameter of the retained β, determined using the Guinier camera, was 2.852 Å which is in good agreement with an extrapolation of the previous results as shown in Figure 26. Samples were then aged to allow β to come into metastable equilibrium with ε and water quenched. Ageing temperatures and times are shown in Table 13, (note that ageing time was more prolonged at the lower ageing temperatures in order to ensure complete precipitation). The lattice parameter of the β present in each sample was measured and the composition of β was determined by reference to the curve shown in Figure 26. Lattice parameters and the derived compositions of β are shown in Table 13. Lattice parameter values were again reproducible to within ± 0.0005 Å, giving a possible variation in the derived composition of β of about 1% aluminium (see Figure 26).

Thus the lattice parameter and, by implication, the composition of β in metastable equilibrium with ε (aged between 450°C and 600°C) did not vary (within the accuracy of the technique) with ageing temperature. At higher ageing temperatures when the precipitate was of the lattice parameter and the aluminium content of β decreased with increasing ageing temperature.

3.4.4. The metastable phase diagram

In Figure 27 the compositions of precipitate and matrix, derived above, are superimposed on the equilibrium cobalt-aluminium phase diagram. The metastable β phase field boundary is shown at 43.3% at all temperatures between 300°C and 600°C. Because of the possible error in composition determination this boundary could be moved to higher or lower aluminium contents, within the range shown and the solubility of cobalt in β might vary with temperature. It should also be noted that work described in section 3.4.3. suggests that ε and β are partially coherent

Fig. 27 - Compositions of α and β in the 28% Al alloy aged at various temperatures (superimposed on the phase diagram according to Schramm [30])

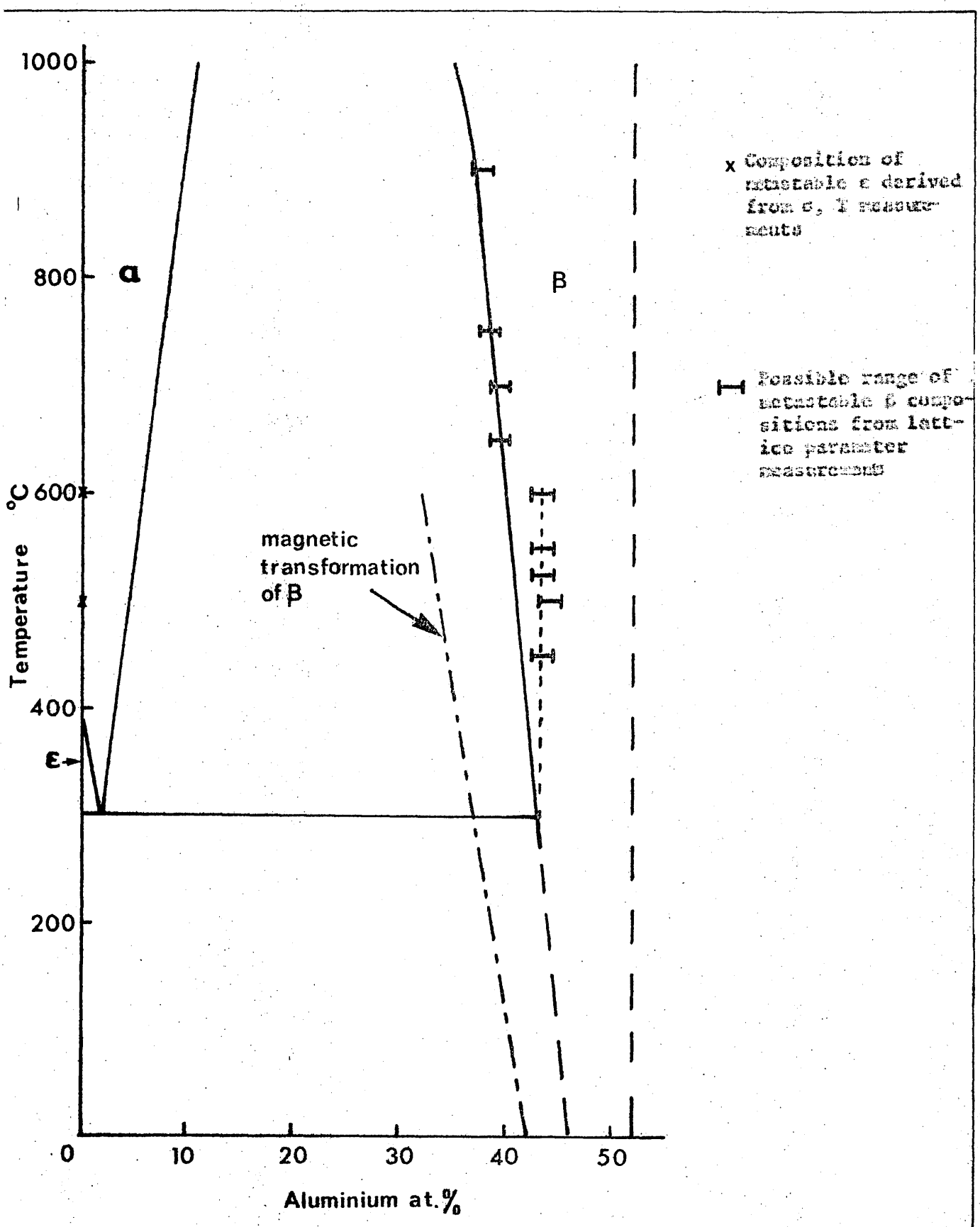

and are thus subjected to some degree of uniaxial strain which tends to expand the β lattice parallel to <111> β, (Figure 24). To what extent this elastic strain influences the lattice parameter of β and, therefore, the accuracy of the positioning of the metastable β boundary in Figure 27, is difficult to assess. However, the vertical boundary shown is compatible with the σ, T curves referred to earlier, in that β of the composition which is in metastable equilibrium at 600°C would have T_c below room temperature while the amount of α precipitated at 600°C would be similar to that present at 500°C.

Ageing at temperatures above 600°C to give α precipitate resulted in β with composition in fair agreement with the phase boundary in the equilibrium phase diagram.

3.6. The Influence of the Magnetisation of the Matrix Phase β On the Properties of Kelcalloy

3.6.1. Introduction

From the equilibrium phase diagram (Figure 2) and from the variation of the saturation magnetisation of β (σ_β) with composition (Figure 6) it can be seen that $T_{c\beta}$ and σ_β decrease with increasing aluminium content. On ageing to precipitate cobalt, β is enriched in aluminium and, therefore, σ_β (at room temperature) decreases. According to the metastable β boundary, derived in section 3.5. (Figure 27) ageing at temperatures below 600°C to precipitate α will result, when the reaction is complete, in β with T_c below room temperature and, therefore, σ_β at room temperature of zero. However, in samples in which precipitation is incomplete, the cobalt precipitates in in the presence of magnetic β. The influence of the magnetisation of this phase on the permanent magnet properties of such samples must be considered.

When coercivity arises from elongated particles with low crystal anisotropy, the presence of a magnetic matrix effectively reduces the shape anisotropy and, therefore, the coercivity of the particles[67].

Fig.26 - Schematic hysteresis loops of two materials with widely differing coercivities (solid lines) and the resulting loop if the two materials are mixed in equal proportions (broken line)

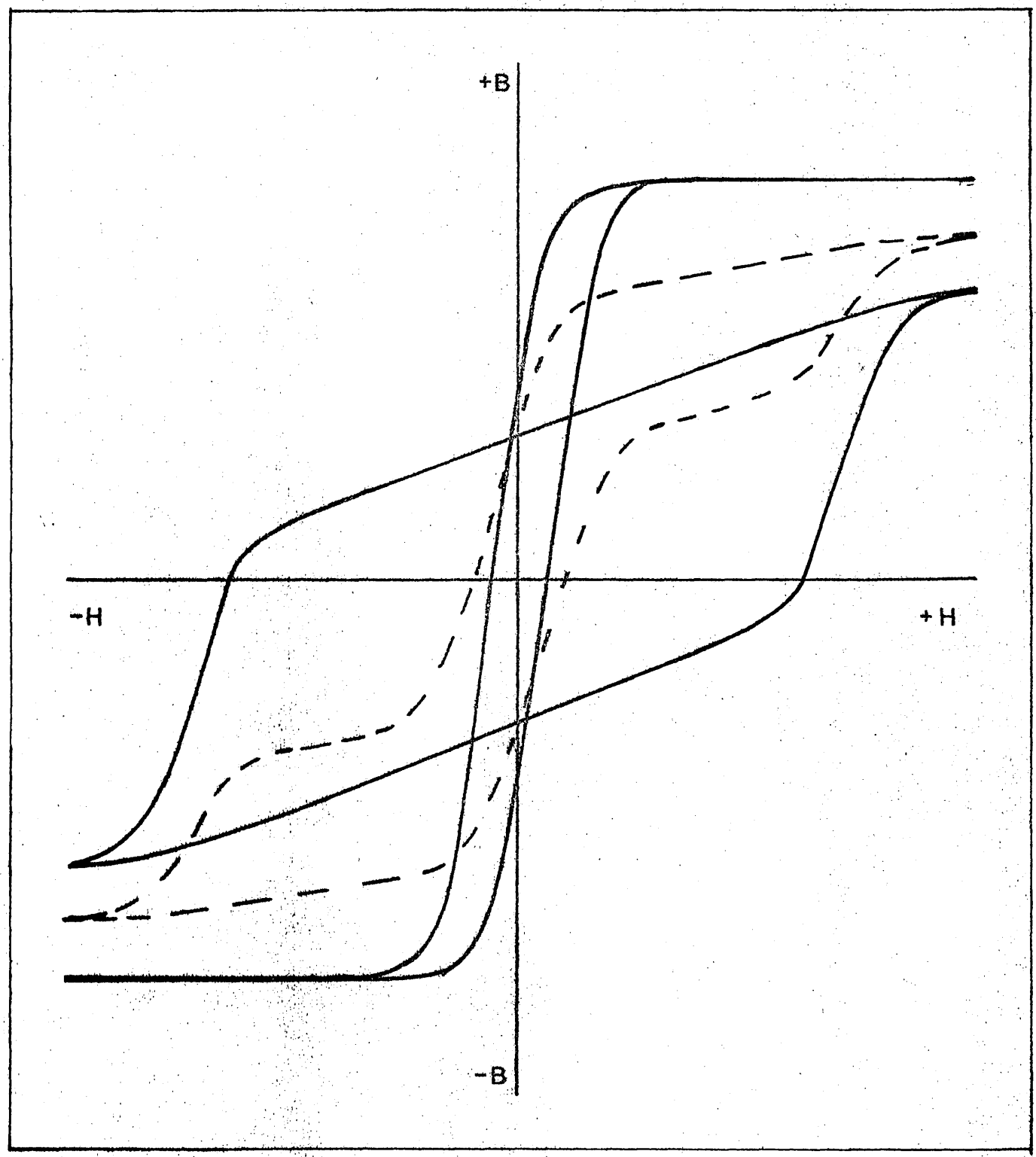

Crystal anisotropy, on the other hand, is inherent in the structure of the material and the coercivity of crystal anisotropic single domain particles is not affected by a magnetic matrix phase.

It is clear, however, that the properties of a mixture of magnetic phases must be influenced by the properties of all the constituents. It is necessary, therefore, to examine the effect of mixing phases of differing individual properties.

Gerlach[68], Neiklejohn[34], Wohlfarth[69], Bean[70] and other authors have discussed the properties of ferro-magnetic materials containing a range of coercivities. The principle is summarised by Bean[70] who states that the method of calculating the hysteresis loop of a mixture is to add the magnetisations of the components for a given field, weighting them in proportion to their fraction of the total.

The total intensity of magnetisation of a mixture of α and magnetic β is the sum of their individual contributions, each being dependent on the intensity of magnetisation and the fraction of the phase present. Figure 28 shows schematically the hysteresis loop (broken line) of a mixture of two phases, 50% of each, with coercivities differing by an order of magnitude (solid lines). It can be seen that the coercivity of the mixture is determined not only by individual coercivities of the phases present but also by the contribution of each phase to the total magnetisation. In the case of the Malcolloy alloys the coercivity of β in the solution treated condition is <2 Oe (section 3.2.1.). Assuming the coercivity of the matrix does not change significantly during precipitation this phase will probably be saturated in a field of 3 to 5 x coercivity, i.e. <10 Oe. The contribution of magnetic β in any applied field greater than a few oersteds can, therefore, be regarded as σ_s x weight fraction β. In studying the properties of samples containing magnetic β it is useful, therefore, to determine σ_s and weight fraction β and to relate the product of these factors to the coercivity of the

Fig. 29 - σ, T curve (heating and cooling) for the 25% Al alloy after ageing 3 hours at 500°C

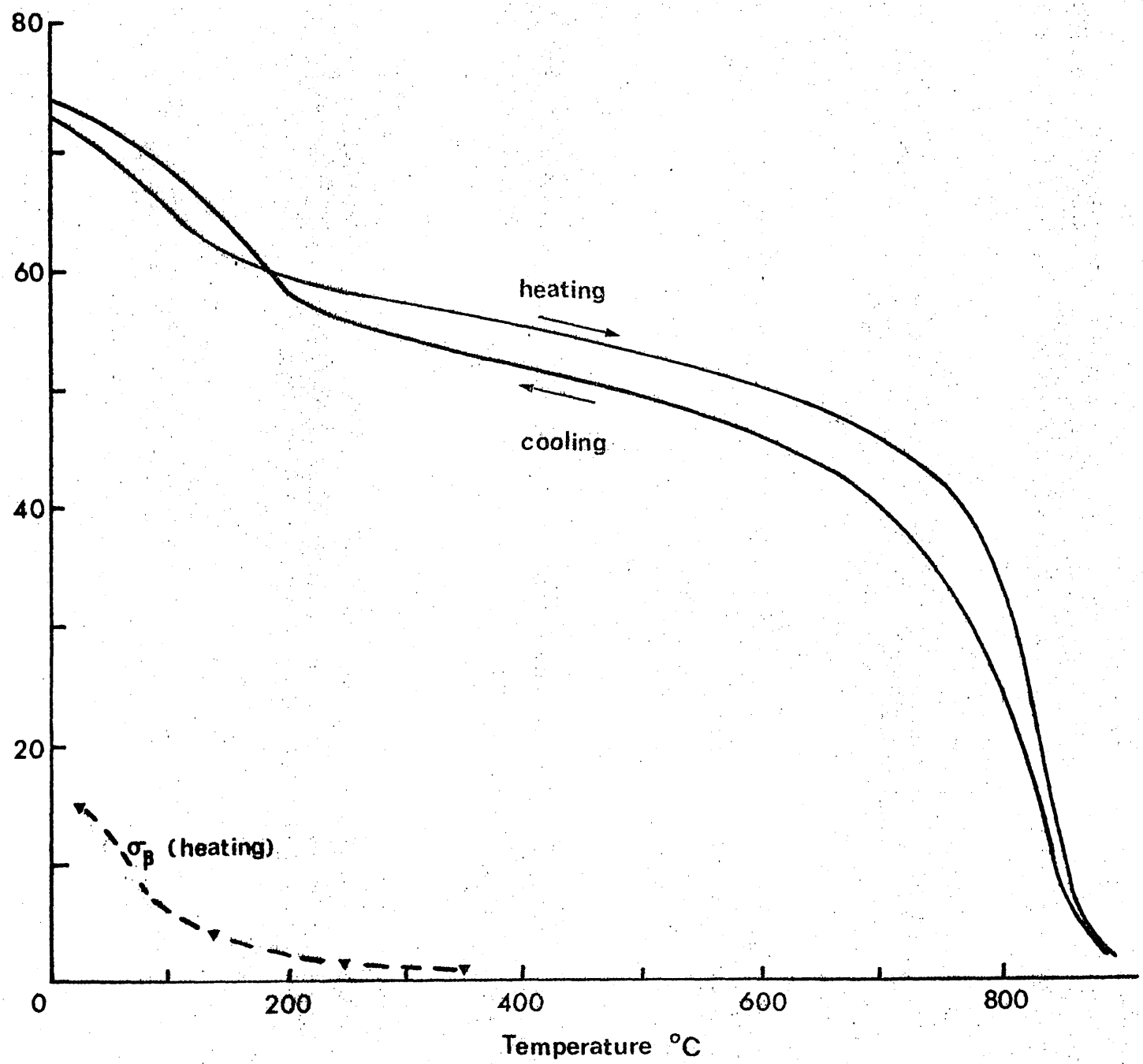

sample as a whole.

3.6.2. Experimental relationship between σ_β x weight fraction β and $_JH_c$

a. Determination of σ_β and weight fraction β in variously aged samples

Weight fraction β and σ_β of samples from the 28% Al alloy aged for various times at 500°C were derived using σ, T curves. These were determined by first heating to 500°C (the previous ageing temperature) and cooling to room temperature, this process being complete in about 1 hour, followed by reheating either to 600°C or the Curie temperature (about 900°C). No difference in the heating, cooling and reheating curves over the first 500°C was observed, even for the sample previously aged for only 1 hour at 500°C. When samples were reheated to the Curie temperature and then cooled, however, the cooling curve deviated from the heating curve. Figure 29 shows heating and cooling curves between room temperature and T_c, for the sample aged 3 hours at 500°C and is typical of the effect observed. The difference was largely due to the transition of the ε precipitate to α at temperatures above about 600°C, and the consequent solution of aluminium in α (see section 3.2.3. and 3.5.2.). In general, since the structure and composition of the phases present in the higher temperature range were not representative of the as aged condition, measurements were discontinued after heating to 600°C. Heating curves between room temperature and 600°C are shown in Figure 30. The curve for the sample aged for 169 hours at 500°C is typical of a material with only one magnetic phase, i.e. the ε precipitate in the presence of non-magnetic β. In all other cases an inflection in the curve showed both the precipitate and the matrix to be magnetic.

In a mixture of phases σ of the mixture is given by:-

$$\sigma = \sigma_A W_A + \sigma_B W_B$$

where W_A and W_B are the weight fractions of phases A and B respectively. Therefore, if β is non-magnetic ($\sigma_\beta = 0$) and σ of the precipitate is known, the weight fractions of the phases present can be readily determined. In

Fig. 30 - σ, T curves (heating, room temperature to 600°C) for samples from the 28% Al alloy

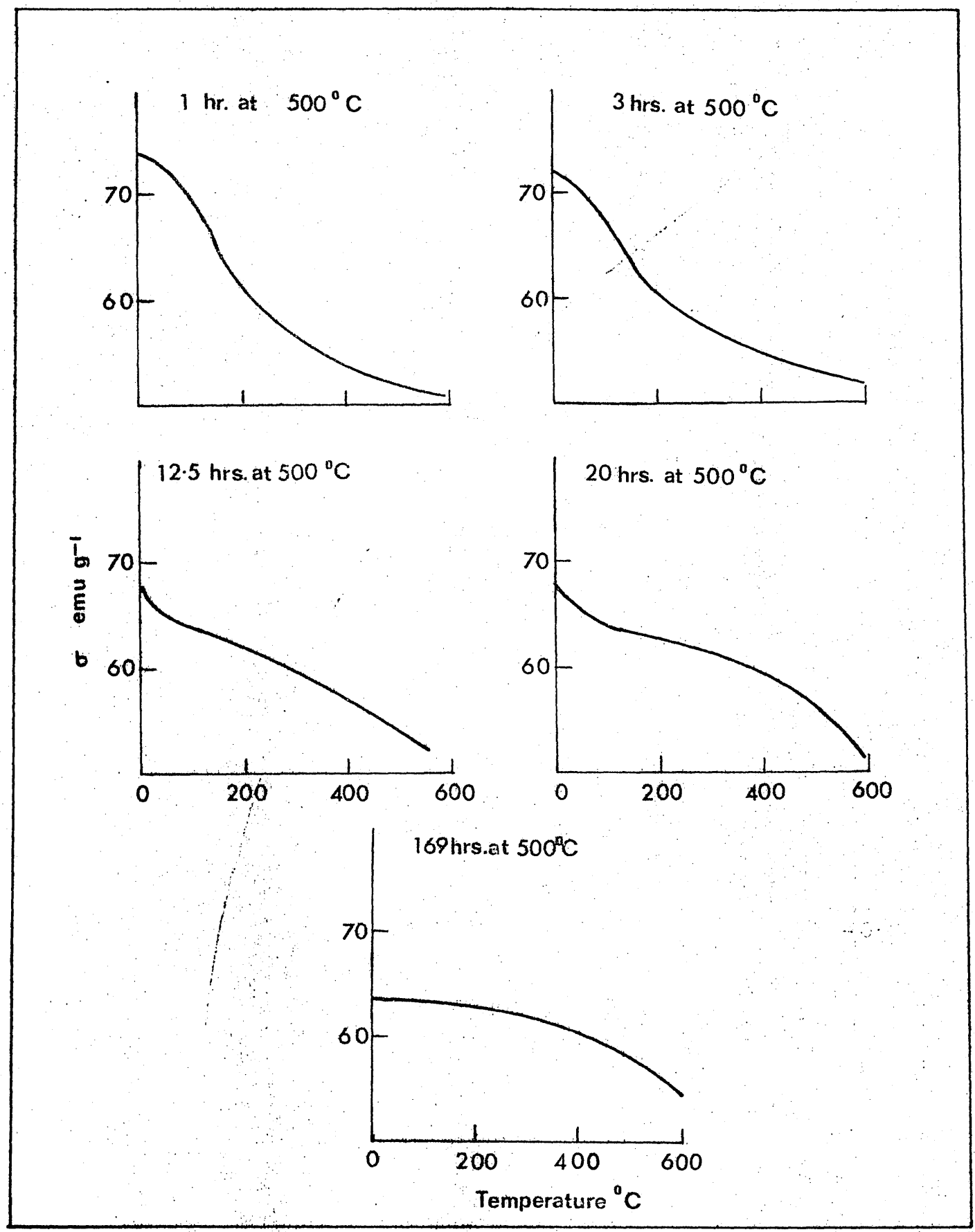

all the curves in Figure 30, T_c of β is below about 300°C thus, at any higher temperature, σ_β is zero. The σ of the ε precipitate has been shown in section 3.5.2. to be equal to that of pure cobalt at temperatures up to 600°C. Therefore, analysis of the curves in Figure 30 to find σ_β and the weight fractions of β and ε was easily carried out.

Consider the σ, T curve for the sample previously aged for 1 hour at 500°C. At a temperature of 500°C, σ of the sample is 51.5 $emug^{-1}$. (This temperature is high enough to ensure that β is non-magnetic but low enough to avoid the appearance of α precipitate with consequent solution of aluminium.) At the same temperature σ for pure cobalt is 144 $emug^{-1}$.[61] The weight fraction of ε present is, therefore, 0.358 and, by difference, the fraction of β is 0.642. At room temperature σ of pure cobalt is 161 $emug^{-1}$ and σ of the sample is 74 $emug^{-1}$. Using the fractions of the phases present it is easily shown that σ_β at room temperature is 25 $emug^{-1}$.

The various curves in Figure 30 were analysed in the same manner giving fractions of β and σ_β at room temperature as shown in Table 14. σ_β at various elevated temperatures was also calculated. The results obtained for the sample aged for 3 hours at 500°C, are typical and are plotted in Figure 29. The resulting curve does not have the form of a normal σ, T relationship (c.f. Figure 25) but can be understood on the assumption that β was inhomogeneous, as might be expected when precipitation is incomplete, so that the observed σ_β, T curve is the sum of a family of curves with a range of Curie temperatures. Since β was apparently inhomogeneous σ_β at room temperature, derived from the σ, T curves, can only be an approximate mean value.

b. The observed relationship between $_JH_c$ and $\sigma_\beta W_\beta$.

In Figure 31 the contribution of β to the total magnetisation of the material (σ_β x weight fraction β) is plotted against $_JH_c$ (the figure also includes a calculated relationship, the derivation of which is described later). It was, unfortunately, not possible to obtain further

TABLE 14

CHANGE IN σ_β AND WEIGHT FRACTION β IN THE 28% AL ALLOY ON AGEING AT 500°C

Time aged at 500°C hours	Weight fraction β	σ_β at room temperature emu_g^{-1}	Weight fraction $\beta \times \sigma_\beta$ emu_g^{-1}
1	0.642	25.0	16.2
3	0.640	18.8	12.0
12½	0.625	12.3	7.7
20	0.610	6.5	4.0
169	0.600	0.0	0.0

Fig. 31 - Variation of $_{J}H_{c}$ of the 283 Al alloy with magnetic contribution of β ($\sigma\beta$ x weight fraction β)

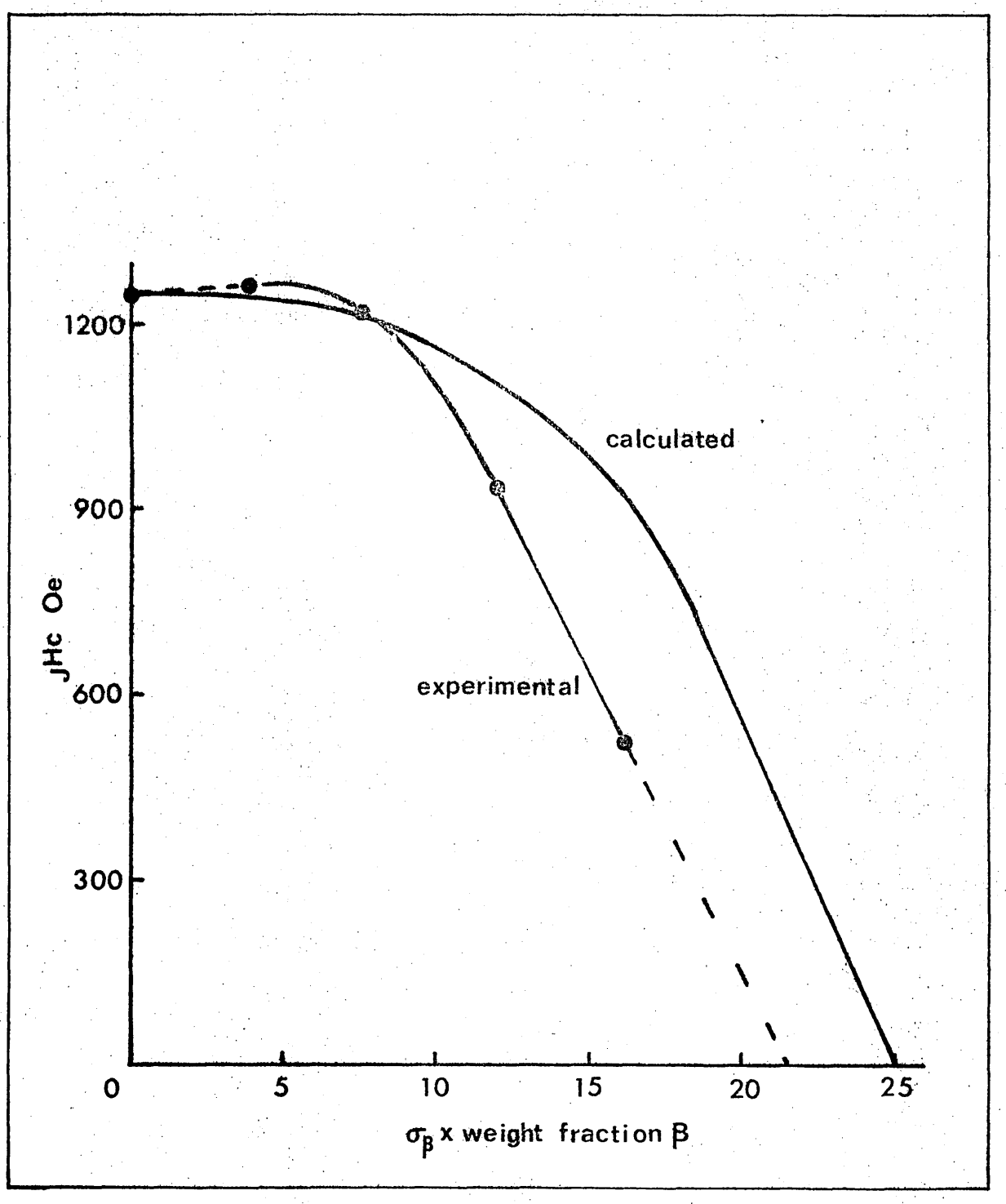

points representing samples aged for shorter times where the contribution of β was greater. Such samples were subject to phase changes during the course of the σ, T test and meaningful values of σ_β and fraction β could not be obtained. According to the extrapolation in Figure 31, $_J{}^{H}{}_c$ begins to increase only when σ_β x weight fraction β is below about 22 $emug^{-1}$. Since prior to ageing σ_β x weight fraction β was about 90 $emug^{-1}$ the implication is that $_J{}^{H}{}_c$ began to increase only in the later stages of the precipitation process.

In the very early stages of ageing the precipitate would be superparamagntic and have low coercivity. Using Néels relationships[22b], however, it was calculated, in section 3.2.3., that particles of ε would pass from the superparamagnetic to the ferromagnetic state when particle diameter exceeded about 60 Å. Since particle diameter, after ageing the 28% Al alloy for 17 hours at 500°C to give maximum $_J{}^{H}{}_c$ at that temperature, was of the order of 2000 Å, (Figure 8d) it is reasonable to suggest that during most of the precipitation process the majority of the ε particles were too large for superparamagnetic behaviour. The particles were therefore, ferromagnetic single domains. It must be concluded that the associated high coercivity was suppressed, according to the principle summarised in Figure 28, by the presence of the low coercivity magnetic β matrix. The effect would, of course, disappear in the later stages of precipitation as σ_β approached zero.

3.6.3. The theoretical influence of magnetic β

In order to confirm that the coercivity of the ε precipitate is suppressed by magnetic β and to ensure that no other factor is involved, it is necessary to determine the exact manner in which magnetic β would be expected to influence the properties and to compare the results with the experimental observations.

Consider a fully magnetised sample containing ε and magnetic β.

If a demagnetising field of about 10 Oe is applied, β is saturated in the opposite direction to make a negative contribution to the total magnetisation which can be expressed as σ_β x weight fraction β. This small demagnetising field will not significantly affect the high coercivity precipitate, the magnetisation of which will, therefore, remain approximately at remanence. In a randomly oriented system of particles exhibiting uniaxial anisotropy remanent magnetisation is approximately half saturation magnetisation[13]. A close approximation to the contribution of the precipitate is, therefore, $\underline{\sigma Co}$ x weight fraction cobalt, i.e. 80 $emug^{-1}$ x weight fraction cobalt[2]. In practice local fields due to each phase will influence the magnetisation and, therefore, the contribution of the other phase. For the purpose of a simple analysis, however, it can be assumed that the phase distribution is such that these local fields are equal in all directions and thus have no net effect. How closely the real system approximates to this ideal is difficult to predict but it is interesting to compare results derived making this simplifying assumption with those observed in practice.

If, as in the early stages of ageing, σ_β and the amount of β present are large so that the contribution of β is greater than that of the precipitate, the total magnetisation will be reversed in a field of less than 10 Oe (i.e. the field required to magnetise β to saturation). The sample as a whole thus has a coercivity of less than 10 Oe despite the fact that the cobalt precipitate remains magnetised to remanence in the original direction. If, as ageing proceeds, the amount of cobalt precipitate increases, its contribution to the total magnetisation increases. At the same time, the contribution due to β decreases, since not only is the amount of β less but, due to its lower cobalt content, σ_β is reduced. A point is reached at which the contribution due to the precipitate exceeds that due to β If a sample in this condition is subjected to a demagnetising field of about 10 Oe, (i.e. the magnetisation of β is reversed) the greater contribution of the precipitate will cause the overall

Fig. 32 - Calculated magnetic contributions of β and ε as precipitation proceeds

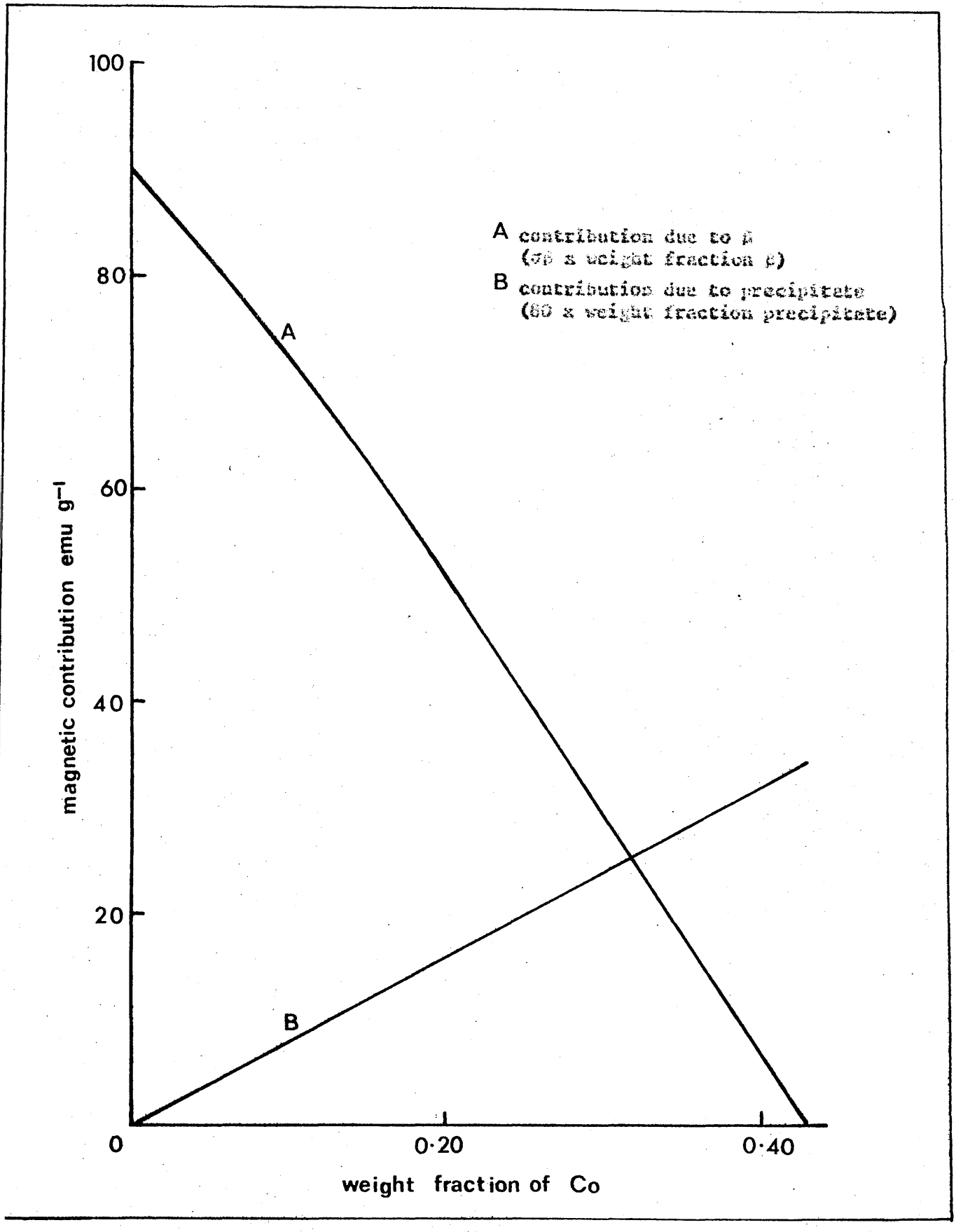

magnetisation to remain in the original direction. A considerably higher field will have to be applied before the magnetisation of the cobalt particles starts to reverse, i.e. there is an increase in coercivity. The stage at which $_JH_c$ begins to increase can thus be regarded as that at which the contribution from the cobalt precipitate becomes equal to that from β.

The calculated change in the contributions from the two phases as precipitation proceeded in the 28% Al alloy are plotted against weight fraction of precipitate in Figure 32. The contribution due to β was obtained as follows. The change in the composition of β, as cobalt precipitated, was calculated and σ_β was derived according to the relationship between composition and σ_β given in section 3.1. (Figure 6). Contribution was then σ_β x weight fraction β. The contribution of the precipitate was calculated as $\frac{\sigma \text{ Co}}{2}$ x V Co i.e. 80 x weight fraction of precipitate.

In Figure 32, the two contributions are equal at a value of 25 $emug^{-1}$ when the cobalt precipitate fraction is 0.315. Thus at this stage of precipitation an increase in coercivity may be anticipated. This is shown in Figure 31 to be in reasonable agreement with the measured results where $_JH_c$ begins to increase when the contribution from β is 22 $emug^{-1}$. According to Figure 32, this value corresponds to a precipitate fraction of 0.33.

Thus, almost complete suppression of the coercivity of the ε particles until late in the precipitation process can be satisfactorily understood in terms of the influence of magnetic β

If the ε precipitate was an ideal single domain system, in which the same field was required to reverse the magnetisation of every particle, the true coercivity of the precipitate would be exhibited as soon as the contribution due to ε exceeded that from β; i.e. the coercivity would rise immediately from less than 10 Oe to a value equal to the coercivity of the ε particles and would remain at that level

Fig. 33 - Intrinsic demagnetisation curve for Cu 20% Ni alloy after ageing for 100 hours at 500°C

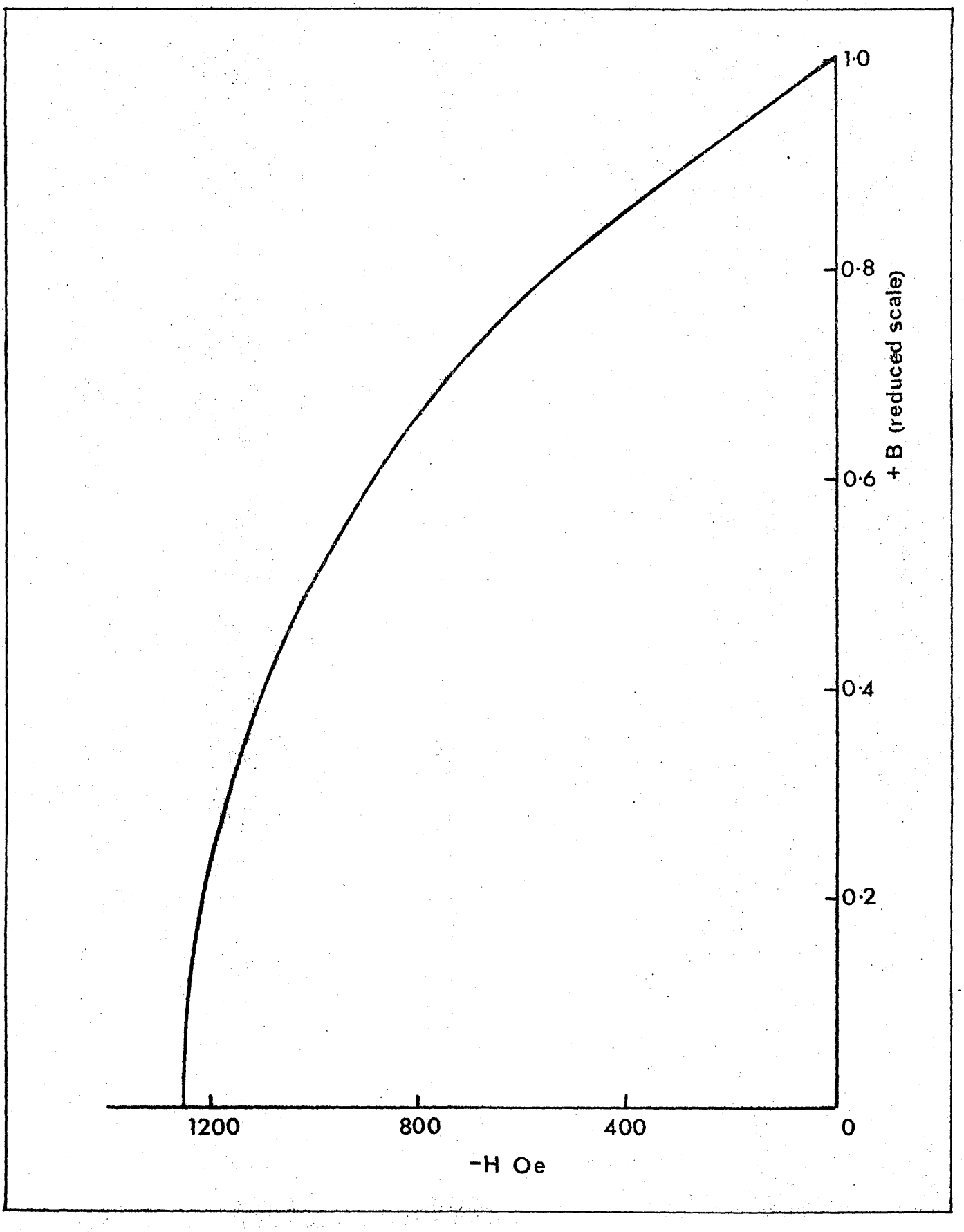

throughout the remainder of the precipitation process until single domain size was exceeded. In practice, the ε dispersion is likely to contain a minority of very small (superparamagnetic) and large (multi domain) particles which will have low coercivity. Furthermore, according to Stoner and Wohlfarth[13], the field required to rotate the magnetisation of an anisotropic single domain particle is dependent on the orientation of the easy direction of magnetisation with respect to the field. Thus, since the ε precipitate is, in a poly-crystalline sample, oriented at random, it follows that some particles, either because of their low coercivity or because of their orientation, will be reversed by a lower field than the coercivity of the ε dispersion as a whole. Their contribution will be additive to the reverse contribution from β and at some field less than the coercivity of the ε precipitate the overall magnetisation will be reversed. Therefore, as ageing proceeds and the contribution from β is reduced, the coercivity of the material as a whole will rise at a rate dependent on the demagnetisation characteristics of the precipitate.

The rate of this increase can only be predicted accurately using the demagnetisation curve for the ε dispersion in the presence of magnetic β, i.e. while precipitation remains incomplete. The form of this curve is not known but it is possible to obtain some indication of the rate of increase using the demagnetisation curve for the ε dispersion after complete precipitation, i.e. the curve for a sample aged to give non-magnetic β.

Figure 33 shows the intrinsic demagnetisation curve determined using the recording hysteresigraph as described in section 2.1., for the sample from the 28% Al alloy aged at 500°C for 169 hours to give non-magnetic β. The remanence of this sample was 3,500 G but if the curve is assumed to represent the properties of the cobalt dispersion throughout the precipitation process remanence will increase from zero to3,500 G as

precipitation proceeds. It is convenient, therefore, to use a reduced B scale so that, as in Figure 33, remanence is unity. The contribution of β expressed in the same terms I_β therefore

$$\frac{\sigma_\beta \times \text{weight fraction } \beta}{80 \times \text{weight fraction Co}}$$

When the β contribution in these terms is less than 1, a field sufficient to saturate β will not bring about reversal of the overall magnetisation because of the greater contribution from the precipitate. As the field is increased the magnetisation of low coercivity and badly oriented precipitate particles will begin to reverse, making a negative contribution to the overall magnetisation so that the total contribution of the precipitate decreases along the demagnetisation curve shown in Figure 33; when the precipitate contribution becomes less than the contribution from β the overall magnetisation will be reversed. Thus, coercivity is that field which reduces the precipitate contribution to equal that of β. To determine coercivity at any stage of precipitation it is necessary, therefore, to calculate contribution due to β, as above, the coercivity can then be derived from Figure 33 as the H co-ordinate corresponding to a B value equal to the β contribution.

The calculated curve in Figure 31 was derived using this approach and it can be seen that the form of the measured curve is similar to that obtained from theory. The difference between the two curves is not surprising in view of the simplifying assumptions made in deriving the theoretical curve, i.e. that local fields associated with each phase do not influence the magnetisation of the other and that the curve in Figure 33 represents the demagnetisation curve of ε throughout the precipitation process. Furthermore, the accuracy of the measured values of $\sigma_\beta \times$ weight fraction β is limited due to the inhomogeneity of β during precipitation.

It can be concluded, therefore, that the presence of magnetic β suppresses the coercivity of the ε precipitate so that the coercivity of

Fig. 34 - Intrinsic demagnetization curves (B-H vs B) for the 25% Al alloy aged 1 hour (curve A) and 169 hours (curve B) at 500°C

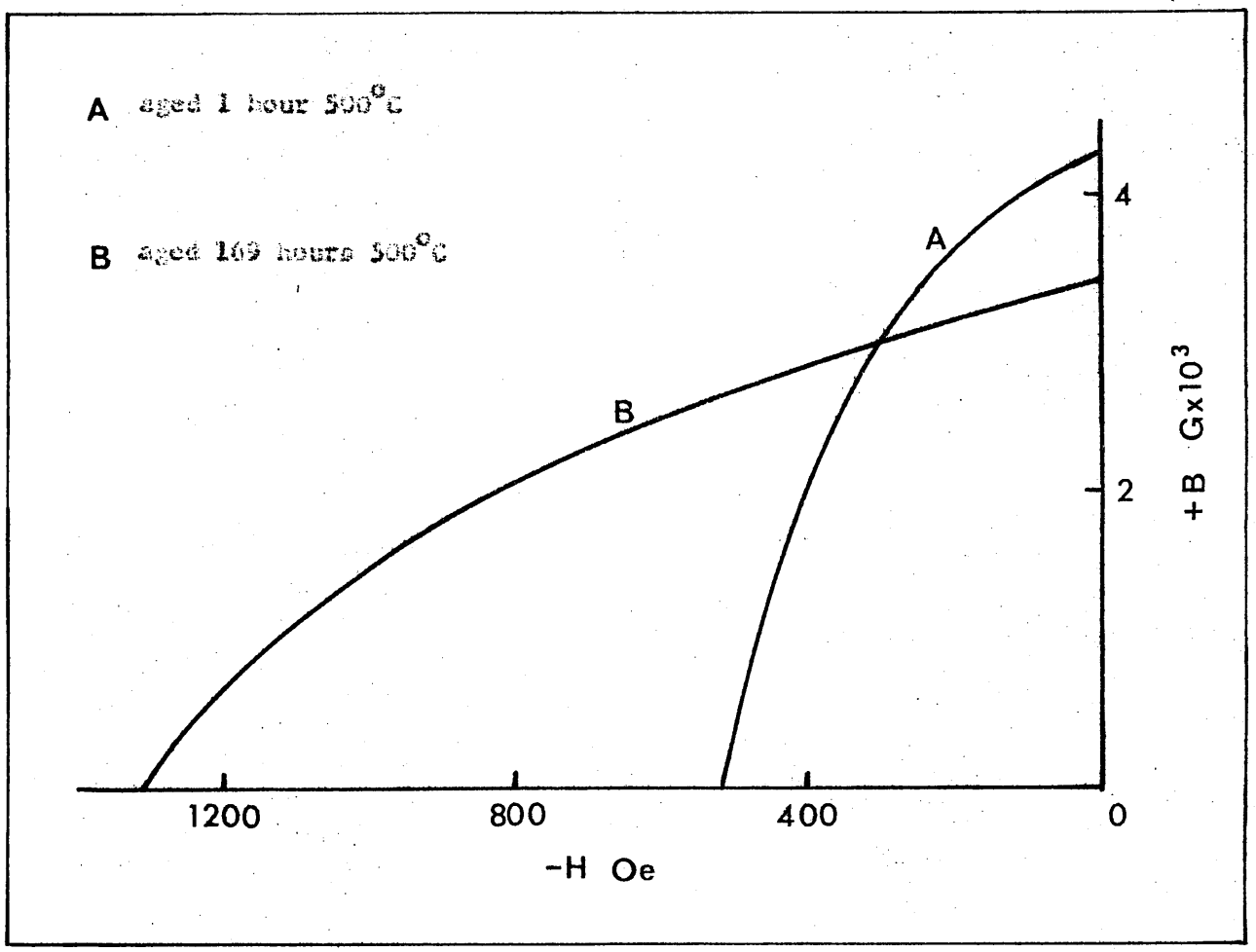

the material as a whole does not begin to increase until the later stages of precipitation. The rate of increase is then dependent on the form of the demagnetisation curve of the precipitate.

3.6.4. The influence of local fields

a. The influencejof local fields on the form of the demagnetisation curve

As discussed in section 3.6.1. the magnetisation of β will be reversed by demagnetising fields of only a few oersteds and the phase will probably be saturated in fields greater than 10 Oe giving a contribution to the overall magnetisation which is negative with respect to that of the precipitate. Thus, the demagnetisation curve for a sample in which β is magnetic, but where the contribution of the precipitate to the total magnetisation is greater than that of β, should show a rapid decrease in magnetisation as the applied field is increased from 0 to 10 Oe, followed by a much slower decrease as the field is further increased to reverse the magnetisation of the high coercivity precipitate. The intrinsic demagnetisation curve (B-H vs H) in Figure 34 for a sample from the 28% alloy aged at 500°C for 1 hour (containing ε and magnetic β) is not of this form, a continuous decrease in magnetisation being observed between a positive field of 100 Oe and the intrinsic coercivity of about 500 Oe. Furthermore, comparing this curve with that from a sample aged for 169 hours at 500°C to give non-magnetic β, (Figure 34), it is seen that, in the presence of demagnetising fields up to 300 Oe, the magnetisation of the sample aged for 1 hour is greater than that of the sample aged for 169 hours. Since after ageing for 1 hour a smaller volume fraction of precipitate is present than after ageing for 169 hours (Table 14), it must be concluded that the greater magnetisation of the sample aged for 1 hour is due to a positive contribution from magnetic β. This can be understood if the assumption made earlier, that local fields associated with each phase do not influence the magnetisation of the other, is taken to be invalid. Thus, if the fields due to the ε particles tend to magnetise the matrix

in the same direction as the magnetisation of the particles the contributions of ε and β will be additive.

b. The influence of local fields on coercivity

When a demagnetising field is applied to a sample containing ε and magnetic β its influence on the magnetisation of the β will, in the absence of any effect due to local fields, be in the opposite direction to that of the ε particles. The theoretical variation of coercivity with β contribution (Figure 31) was derived on this basis and agrees reasonably well with the experimental results. Presumably, therefore, during that part of the precipitation process covered by these results, i.e. the later stages, the fields due to the ε particles are overcome by low applied fields and have little effect on coercivity.

In the early stages of ageing, when the β contribution to the total magnetisation outweighs that of the precipitate the simple model (neglecting local fields) predicts that $_JH_c$ will be <10 Oe and remain at this level, as precipitation proceeds, until the contribution of the precipitate becomes greater than that of β. Thus, during precipitation, a delay would be expected before any increase in $_JH_c$ was observed. In practice it was possible, for all the casts at all the ageing temperatures explored, to extrapolate a plot of $_JH_c$ v.s. ageing time to approximately zero $_JH_c$ at zero time (Figures 10, 11 and 12). Even during ageing at the lowest temperature (450°C), when there was, for all the alloys, a sigmoidal relationship between $_JH_c$ and time, a continuous increase in $_JH_c$ was indicated. Thus, no significant delay, prior to the increase of $_JH_c$ on ageing, was detected. Since, particularly at the higher temperatures, the decrease in ε on ageing was quite rapid, it may be that the anticipated delay, prior to the increase in $_JH_c$, was masked by an initially high rate of precipitation. In addition, however, it seems likely that, because of the influence of local fields, the simple model is not applicable in the initial stages of ageing when the contribution of β to the magnetisation is greater than

Fig. 35 - σ, T curve for the 38% Al alloy aged for 180 hours at 500°C

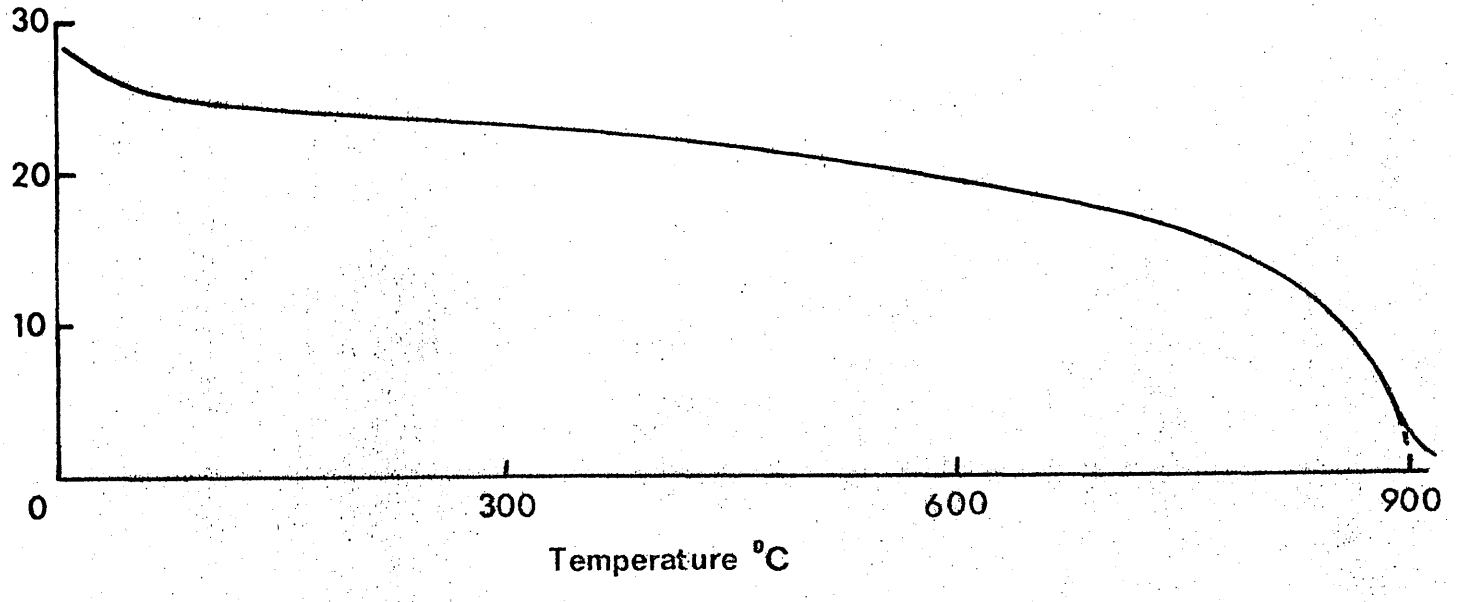

that of the precipitate. A continuous increase in $_JH_c$ from zero time can be understood qualitatively if it is supposed that the volume of β influenced by local fields increases with the volume fraction of precipitate. Thus, as the amount of precipitate increases, larger applied demagnetising fields are necessary to give a negative contribution from β equal to the positive contribution of the high coercivity precipitate plus that from a certain volume of β which remains magnetised in a positive direction due to the influence of local fields.

c. The influence of local fields in remanence

In section 1.2.2. it was pointed out that the ratio of B_r to $4\pi J_s$ (saturation magnetisation), obtained by Masumoto et al[41] for Malcolloy was much higher than would be expected for isotropic material. ($B_r/4\pi J_s$ for isotropic material should be approximately 0.5[13] but Masumoto et al reported values up to 0.8). Similarly, as shown in Table 10, $B_r/4\pi J_s$ for samples from the 23% and 38% Al alloys, examined in the present work, was around 0.7. It may be possible to explain these results in terms of the influence of local fields on the magnetisation of β. If it is assumed that ageing was discontinued while σβ remained greater than zero at room temperature and if, as suggested above, the net magnetisation of β by local fields, is in the same direction as that of the ε particles then, when the sample is at remanence the magnetisation of β may be greater than half saturation. As a result $B_r/4\pi J_s$ for the sample as a whole will be greater than 0.5. Clearly this mechanism can only apply while β is magnetic. σ, T measurements carried out on the 38% Al alloy after ageing 180 hours at 500°C, ($B_r/4\pi J_s$ = 0.69, see Table 10), showed β to be weakly magnetic at room temperature (Figure 35, σβ being about 5 $emug^{-1}$. It is also consistent with the hypothesis that the sample from the 28% Al alloy aged for 1 hour at 500°C which had σβ of 25 $emug^{-1}$ (Figure 30 and Table 14) had $B_r/4\pi J_s$ of 0.62 while a sample from the same cast aged for 169 hours at 500°C to give σβ of zero had $B_r/4\pi J_s$ rather closer to that expected for isotropic material, ie. 0.56 .

Fig. 36 - Relationship between J_c^{μ} and σ in the 23, 28, and 38% Al alloys on ageing at 500°C

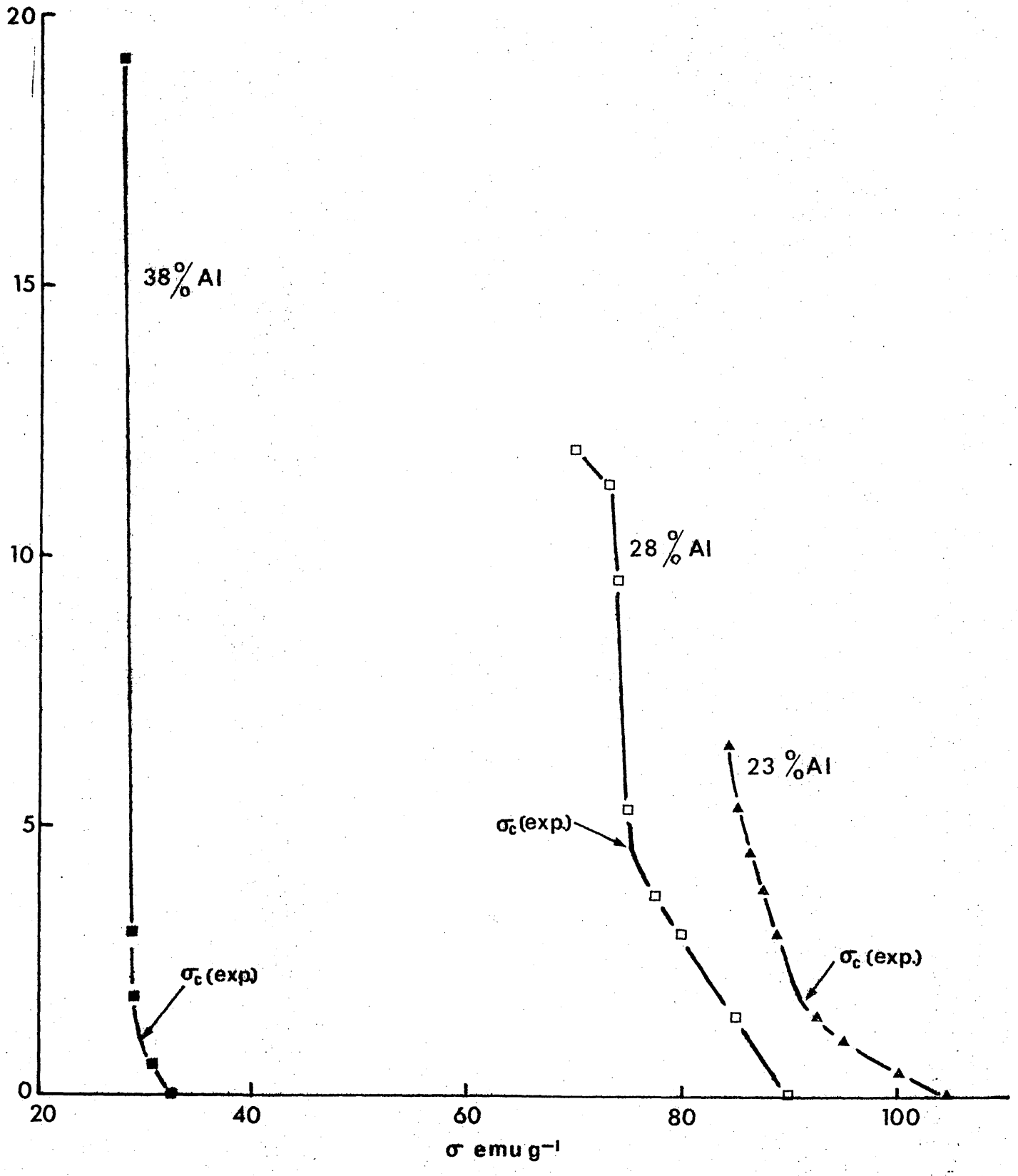

3.6.7. The relationship between $_JH_c$ and σ on ageing

Although the majority of the foregoing results deal with the influence of magnetic β on the properties of the 20% Al alloy it is reasonable to suppose that the mechanisms indicated are applicable to all alloys of the Malcolloy type. That this is the case can be deduced from the relationship between $_JH_c$ and σ of the 23%, 28% and 38% Al alloys on ageing. This relationship, during ageing the three alloys at 500°C, is shown in Figure 36. It can be seen that decreasing σ is always accompanied by increasing $_JH_c$, but that late in the precipitation process, there is a large increase in $_JH_c$ associated with only a small fall in σ, this effect becoming less obvious as the aluminium content decreases. The initial increase in $_JH_c$, occurring while the majority of the decrease in σ takes place, must be induced while the amount and σ of β present are such that the β contribution outweighs that of the precipitate. Increasing $_JH_c$ at this stage can be understood in terms of the influence of local fields as discussed in 3.6.4. (b). The final increase in $_JH_c$, associated with only small changes in σ, is compatible with the simple model in section 3.6.3. if it is assumed to be initiated when the contribution of the precipitate, $(\frac{\sigma\ Co}{2}$ x weight fraction cobalt), exceeds that of β, ($\sigma\beta$ x weight fraction β).

It is interesting to compare the σ of each alloy at the point during ageing when the final increase in $_JH_c$ begins, (i.e. points designated σ_c (exp.) in Figure 36), with values of σ derived from theory, at which the contribution from precipitate and matrix should be equal (see section 3.6.3.). Figure 37 shows the calculated contributions due to precipitate and β in the three alloys as precipitation proceeds and includes calculated curves for the change in σ of each alloy. (Contributions of the two phases were calculated as for Figure 32, section 3.6.3., while σ of the alloys is given by $\sigma\beta$ x weight fraction β + σ_{Co} x weight fraction cobalt). Values of σ corresponding to the stage of precipitation at which the contributions of precipitate and β are equal (designated $\sigma_{c(calc.)}$ in Figure 37) are compared below with values of $\sigma^{c(exp.)}$ from Figure 36.

Fig. 37 - Calculated variation of σ and the magnetic contributions of β and precipitate as precipitation proceeds in the 23%, 28% and 38% Al alloys

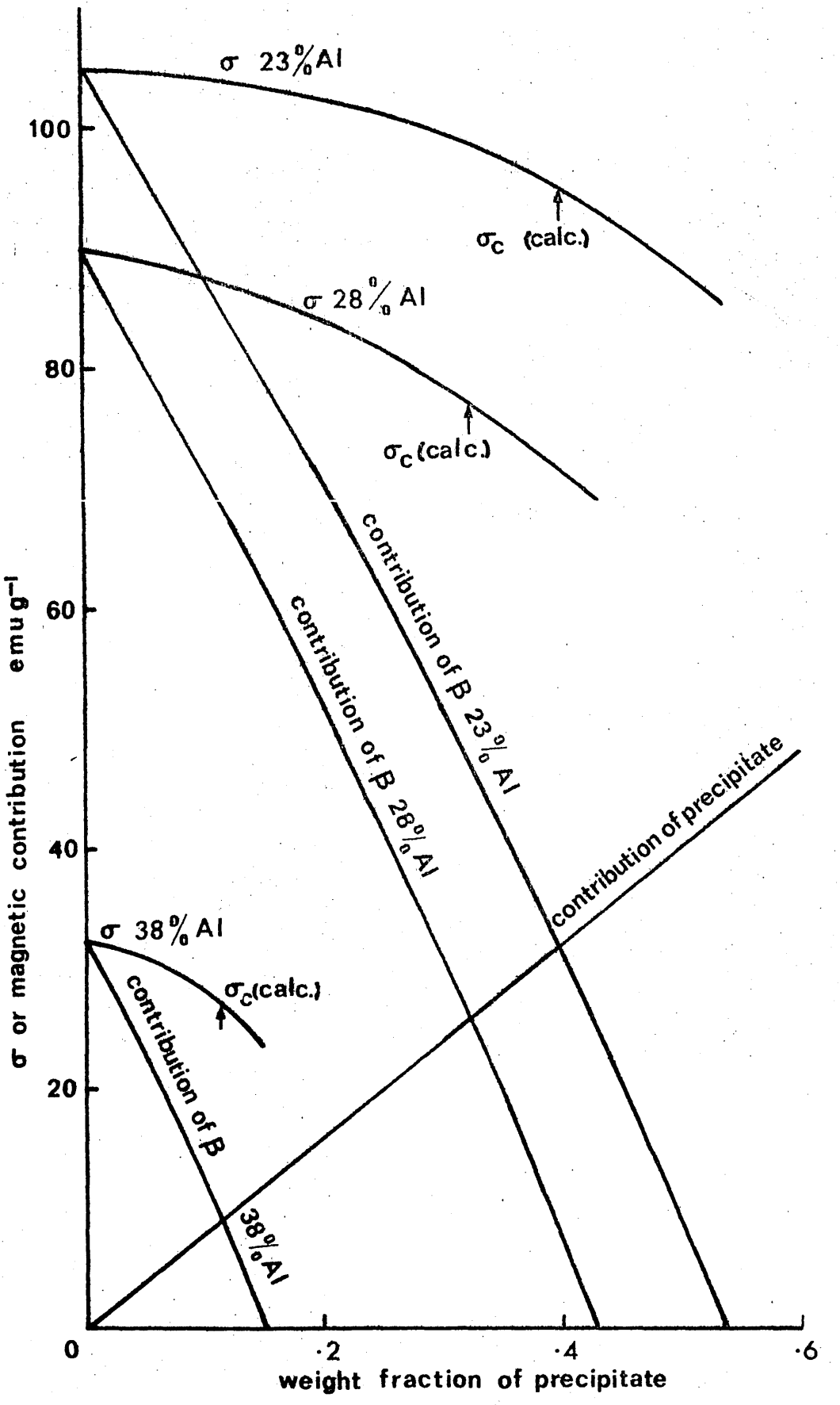

23% Al alloy, $\sigma_{c(calc.)} = 95$ emug^{-1}, $\sigma_{c(exp.)} = 91$ emug^{-1}

28% Al alloy, $\sigma_{c(calc.)} = 77$ emug^{-1}, $\sigma_{c(exp.)} = 76$ emug^{-1}

38% Al alloy, $\sigma_{c(calc.)} = 27$ emug^{-1}, $\sigma_{c(exp.)} = 29$ emug^{-1}

There is thus good agreement between theory and practice in the 28% and 38% Al alloys while the discrepancy in the case of the 23% Al material may arise because of the form of the $_JH_c$ versus σ curve which makes the precise value of $\sigma_{c(exp.)}$ difficult to estimate for this alloy.

3.6.6. The coercivity of the ε precipitate during ageing

a. Deductions from the temperature dependence of $_JH_c$.

The cobalt precipitate will have maximum coercivity at some stage during ageing but there is no reason to suppose that this stage will correspond to complete demagnetisation of β. Thus maximum coercivity of the cobalt dispersion may be suppressed by magnetic β. That this is the case in the 28% Al alloy aged at 500°C can be deduced from the temperature dependence of $_JH_c$, shown in Figure 15. After ageing for 3 hours at 500°C β remained magnetic and $_JH_c$ at room temperature was lower than after more prolonged ageing to give non-magnetic β. As the temperature of the 3 hour sample was raised the magnetisation of β decreased according to the σ, T curve in Figure 30. The influence of magnetic β on coercivity was, therefore, reduced until at T_c of β (about 250°C, see Figure 30) the true coercivity of the ε precipitate was exhibited. The form of the $_JH_c$, T curves for the samples aged for ½ hour at 650°C and 1 hour at 500°C can also be explained in this way. The sample aged for 3 hours at 500°C is particularly interesting because at temperatures above about 125°C, $_JH_c$ is greater than that of the sample aged for 69 hours at 500°C to give non-magnetic β. The inference is that in the absence of magnetic β, $_JH_c$ of the precipitate was higher after ageing for 3 hours at 500°C than after ageing for 69 hours. Extrapolation of the curve for the 3 hour sample from temperatures above 250°C suggests that $_JH_c$ of the precipitate at room temperature was in excess of 1500 Oe.

Fig. 38 - Variation of $_{J}H_{c}$ and H_{r} on ageing the 20% Al alloy at 500°C

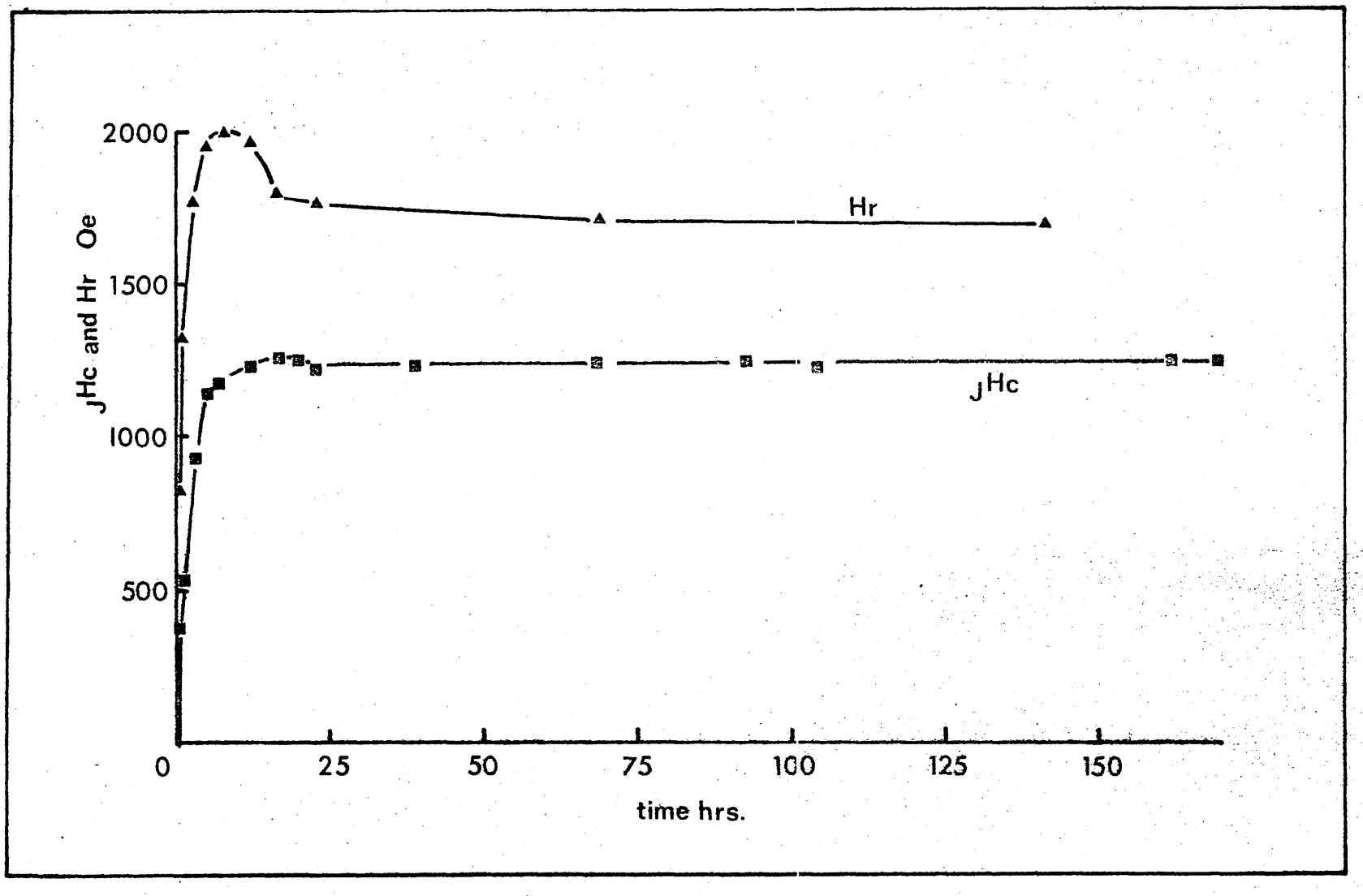

TABLE 15

CHANGE IN J_c^{II} AND H_r ON AGEING THE 28% AL ALLOY AT 500°C

Time Aged	J_c^{II}	H_r
hours	Oe	Oe
½	368	803
1	524	1316
3	935	1770
5	1140	1960
7½	1172	2020
12½	1215	1962
17	1200	1784
20	1250	
23	1230	1762
39	1220	
69	1240	1717
93	1249	
141	1230	1700
162	1250	
169	1250	

b. H_r tests

It has been shown that the coercivity of a mixture of α and magnetic β is reduced when β is saturated by the applied field, in the reverse direction to the magnetisation of α. During the measurement of $_JH_c$ (see section 2.2.2.), the total magnetisation remaining after the application of a demagnetising field, is measured while the fild is maintained, i.e. while β is saturated in the reverse direction to the original magnetisation. If the applied field is removed, the magnetisation of β will be reduced and in the absence of local fields associated with the precipitate particles the self demagnetising field of β would cause the magnetisation of β to approach zero. In practice, local fields are thought to have some influence but it is likely that the magnetisation of β and, therefore, its influence on coercivity will be reduced in the absence of the applied field. Therefore, if H_r is determined i.e., if the magnetisation at each step is measured after the demagnetising field is switched off (see section 2.2.2.), a closer approximation to the coercivity of the α precipitate will be obtained. Values of H_r for the 28% Al alloy aged for various times at 500°C are shown in Table 15 and Figure 38 along with corresponding $_JH_c$ measurements.

It can be seen that during ageing peak H_r is achieved before peak $_JH_c$. Large differences between $_JH_c$ and H_r can arise due to particle size variation within a ferromagnetic dispersion if some particles are larger than single domain size. Such particles influence $_JH_c$ and H_r in much the same way as a low coercivity magnetic matrix as discussed above. The significance of the H_r measurements is, therefore, difficult to assess but the results are consistent with the conclusion that the coercivity of the dispersion is a maximum early in the precipitation process while β is still magnetic and coercivity of the material as a whole is lost.

Fig. 39 - Particle size distribution necessary to give a single domain dispersion of a c (h.c.p.) cobalt b a (f.c.c.)cobalt

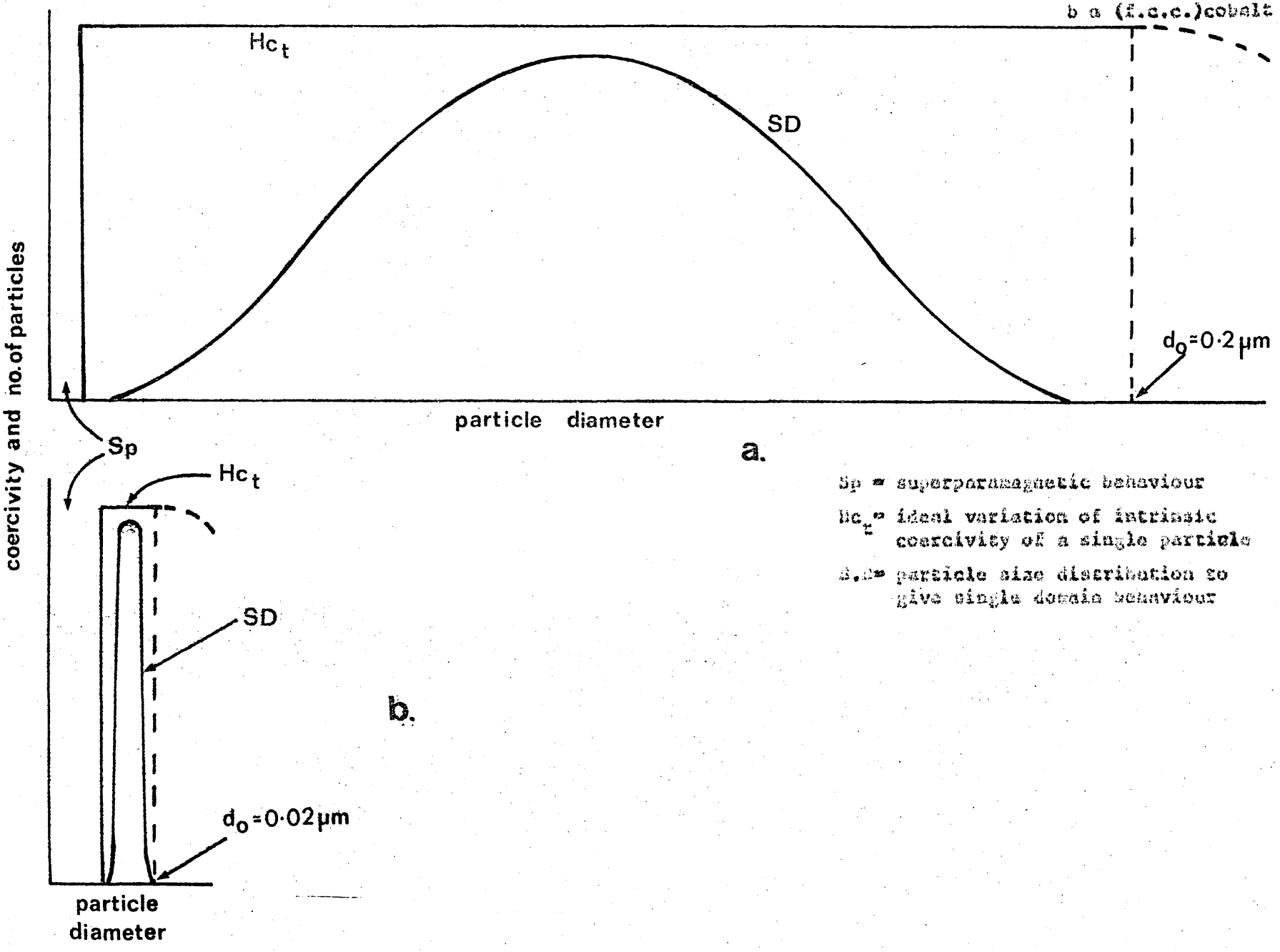

Sp = superparamagnetic behaviour

Hc_t = ideal variation of intrinsic coercivity of a single particle

S.D = particle size distribution to give single domain behaviour

3.7. The Relationship Between The Kinetics Of The Precipitation Process And Coercivity

3.7.1. The relevance of kinetic considerations

The permanent magnet properties of any magnetic dispersion are dependent on particle size. In practice a range of particle sizes is always likely and for optimum properties all particles must be sufficiently large to be outside the superparamagnetic range and small enough to be single domains. According to Went et al[11] (section 1.1.3.), the critical size for single domain behaviour, d_o, is given by:-

$$d_o = \frac{9\sqrt{K}}{J_s} \sqrt{\frac{kT_c}{aJ_o}}$$

whilst according to Neel[22] (section 3.2.3.) the conditions for superparamagnetic behaviour are given by:-

$$\frac{1}{\tau_o} = f_o \exp \frac{-VK}{kT}$$

where a particle with volume smaller than V will be superparamagnetic.

Therefore, as the crystal anisotropy K is increased the critical size for single domain behaviour increases while the size at which superparamagnetic behaviour occurs is reduced. Thus the range of particle size over which ferromagnetic single domains exist is increased. Figure 39 shows schematically the ideal variation in $_jH_c$ with particle size for h.c.p. (α) cobalt (39a) and f.c.c. (β) cobalt (39b), with high and low crystal anisotropy respectively, and the type of particle size distribution which would give optimum permanent magnet properties in each case. Clearly, the conditions for the formation of a high coercivity precipitate of ϵ are far more flexible in terms of mean particle size and particle size distribution than if the precipitate is α. In either case, however, it can be seen that assuming a normal size distribution of the type shown in the figure, the majority of particles must be appreciably smaller than maximum single domain size if the presence of a certain number of multi

Fig. 40 - Schematic representation of the proposed changes in composition of β and particle size of cobalt on ageing the 23 and 38% Al alloys

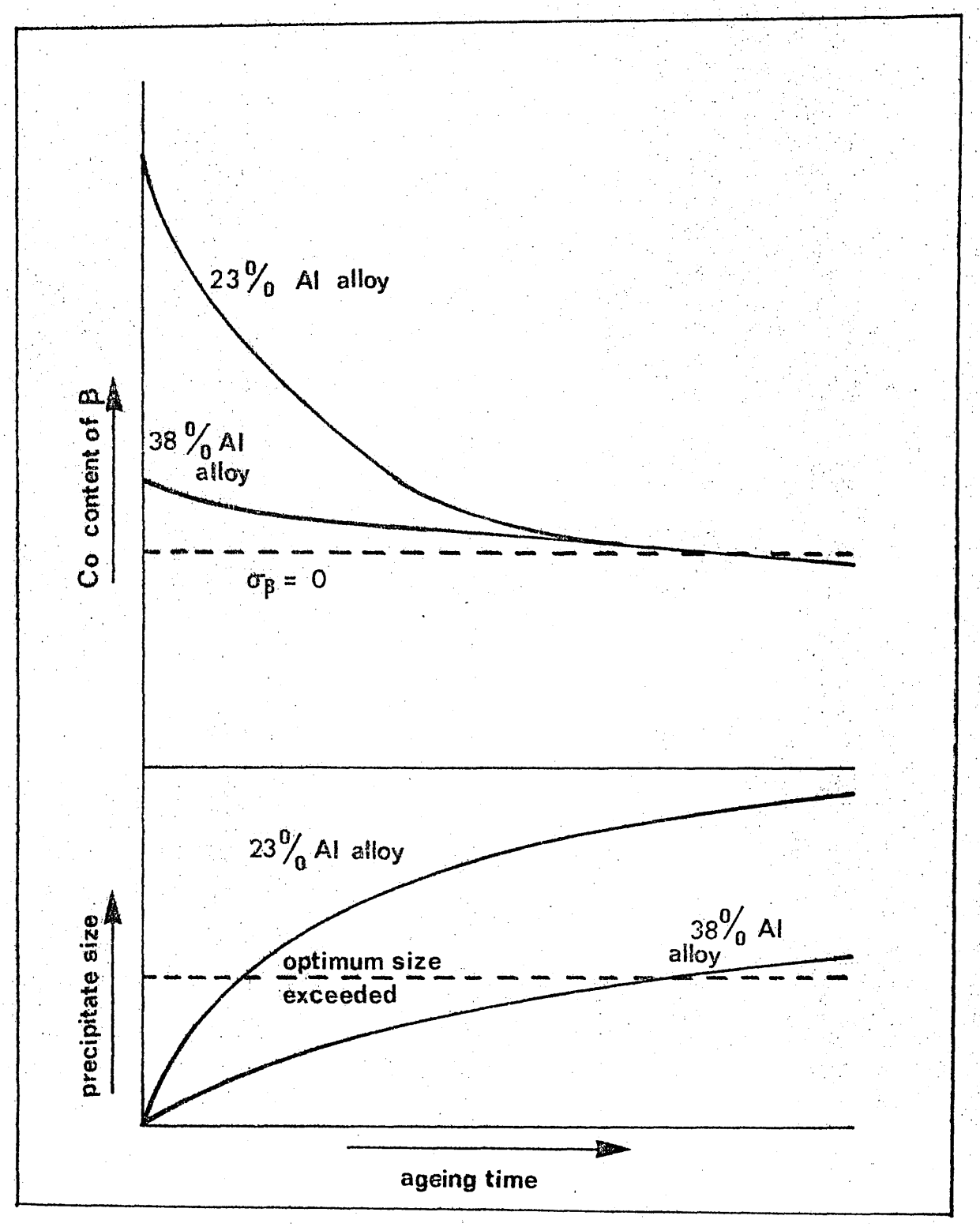

domain, low coercivity particles, is to be avoided. If the size range is narrow, the majority of the particles need only be a little smaller than maximum single domain size whereas if there is a wide range the majority must be much smaller to exclude the presence of a low coercivity fraction. Thus both particle size and size distribution are of fundamental importance in determining the properties of fine particle permanent magnets. If the magnetic dispersion is produced as a precipitate in an alloy by heat treatment, both factors are influenced by the kinetics of the precipitation reaction.

In the case of the Malcolloy alloys, the variation of particle size and size distribution during ageing is particularly important because of the influence of magnetic δ. It has been shown in section 3.2.3. that the maximum coercivity of the three alloys examined increases substantially as aluminium content is increased. Thus on ageing at 500°C (Figure 13) maximum coercivity of the 23% Al alloy was 651 Oe, that of the 28% Al alloy was 1260 Oe and that of the 33% Al alloy was 1930 Oe. Further results in section 3.6. indicate maximum coercivity of the alloys to be the resultant of two effects. The ϵ dispersion achieves optimum particle size at some stage during ageing but, if σ_β is high the alloy as a whole exhibits low coercivity. Further growth may result in particle growth beyond optimum size and thus a fall in the true coercivity of the precipitate but at the same time the reduction in σ_β will tend to increase the coercivity of the alloy. At some stage the resultant coercivity is a maximum but the maximum true coercivity of the precipitate may never be exhibited. It has been shown that maximum coercivity of the ϵ dispersion is never exhibited in the 28% Al alloy (3.6.6.) and it is reasonable to suggest that the difference in the maximum coercivity of the three alloys is largely due to differences in the relationship between the precipitate particle size and σ_β during ageing.

Figure 40 demonstrates this effect schematically. In the lower (23%) aluminium alloy, the availability of a large amount of cobalt for

precipitation will lead to rapid growth and thus the development of a precipitate of optimum size and size range while the cobalt content and σ of β are still high. By the time the cobalt content of β is reduced sufficiently for σ_β to approach zero, the particle size of the precipitate has grown to such an extent that optimum coercivity can no longer be expected. When the amount of precipitating cobalt is less, as in the 38% Al alloy, the tendency for precipitate growth is reduced and the achievement of optimum precipitate size will correspond more closely to the approach of σ_β to zero.

Thus the variation in ${}_JH_c$ with composition can be understood in general terms but it is interesting to examine the relationship between the kinetics of the precipitation reaction and coercivity.

3.7.2. The activation energy of the ϵ precipitation process

Approximate values of activation energy, E_A, for the precipitation of ϵ in the three alloys were obtained from plots of log t (logarithm of the time to precipitate a given fraction) versus $1/T^\circ K$ (reciprocal of the absolute ageing temperature). σ and ${}_JH_c$ during ageing (Figures 9-12 and Tables 7-9), were used as a measure of the fraction of precipitate present. Thus in each alloy t was first taken as the time for about half the total decrease in σ to take place, i.e. the time for σ to fall to 94 $emug^{-1}$ in the 23% Al alloy, to 77 $emug^{-1}$ in the 28% Al alloy and to 30 $emug^{-1}$ in the 38% Al alloy. The value of E_A obtained was checked taking t as the time for ${}_JH_c$ to rise to about half the maximum value observed for each alloy, i.e. ${}_JH_c$ values of 325 Oe, 650 Oe and 1000 Oe in the 23%, 28% and 38% Al alloys respectively. The resulting plots of log t v.s. $1/T^\circ K$ shown in Figure 41 (a), (b), (c).

Using σ as an indication that the same fraction of precipitate was present, the graphs are linear between 450°C and 600°C (the temperature range studied) for the 23% and 38% Al alloys (Figures 41 (a) and (c)) and between 500°C and 600°C for the 28% Al alloy (Figure 41 (b)). The departure from a linear relationship in the 28% Al alloy below 500°C is surprising

Fig. 41a- log t vs $1/T^{\circ}K$ for the 23% Al alloy

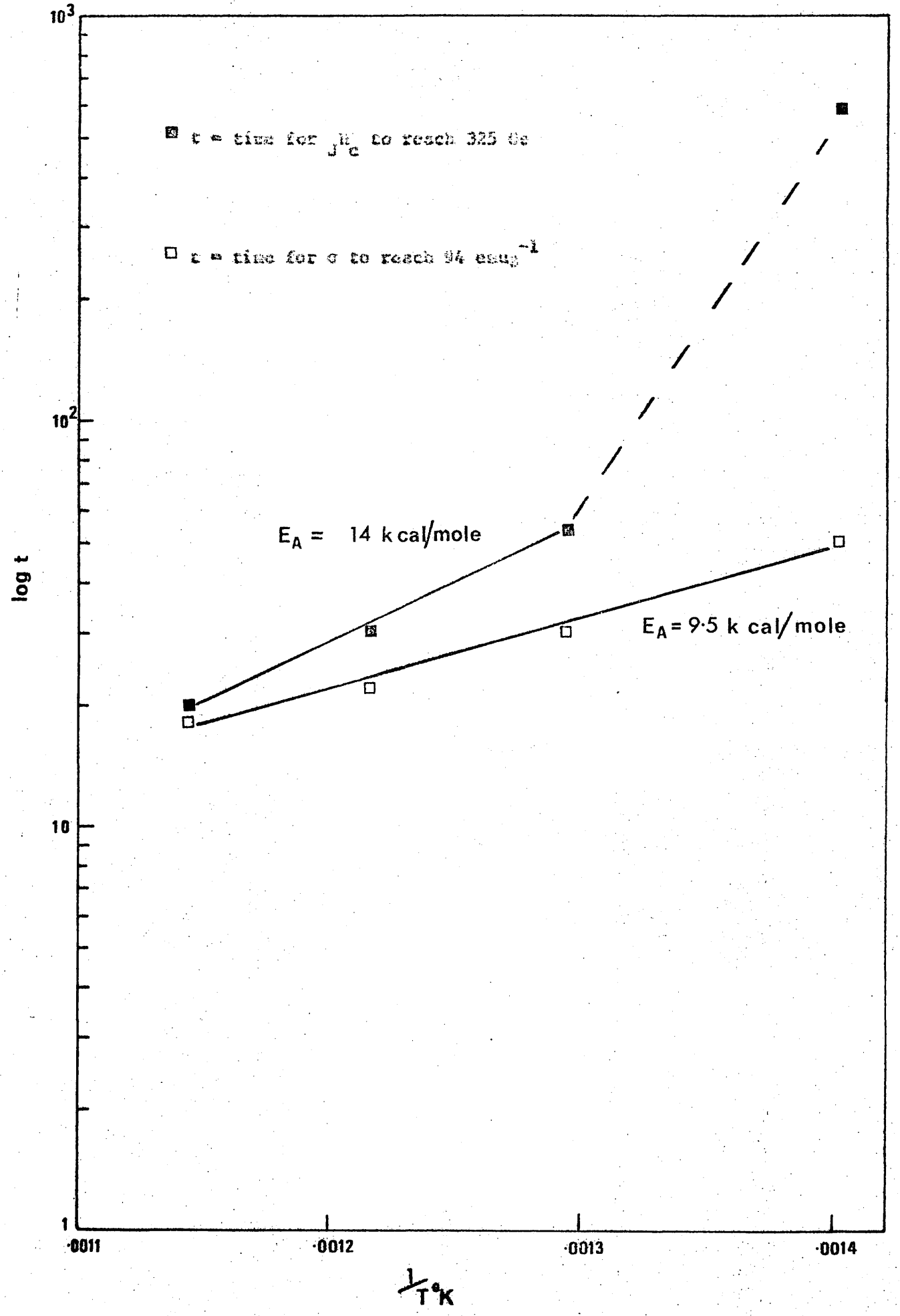

Fig. 41b - log t vs 1/T°K for the 28% Al alloy

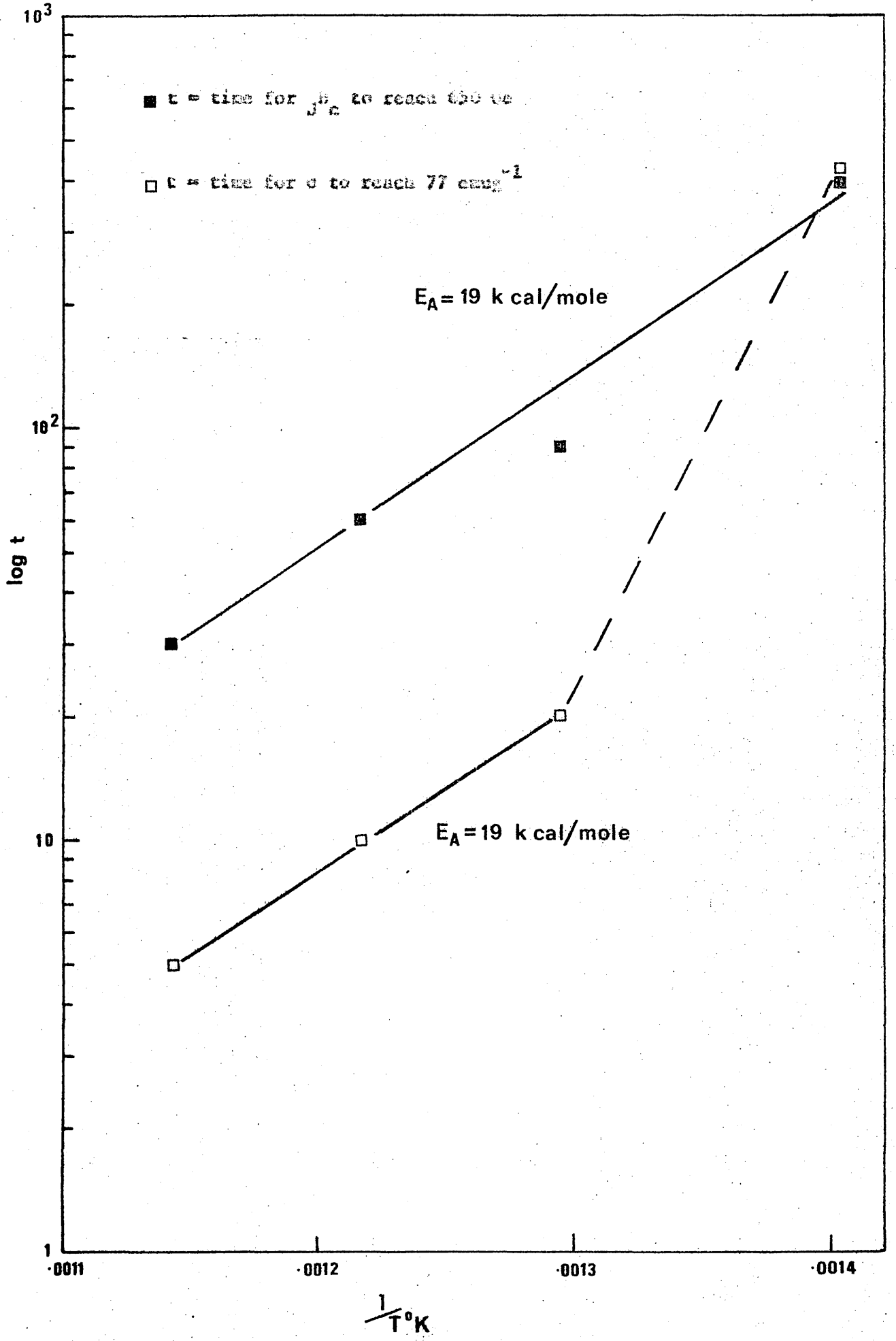

Fig. 41c - $\log t$ vs $1/T^{\circ}K$ for the 38% Al alloy

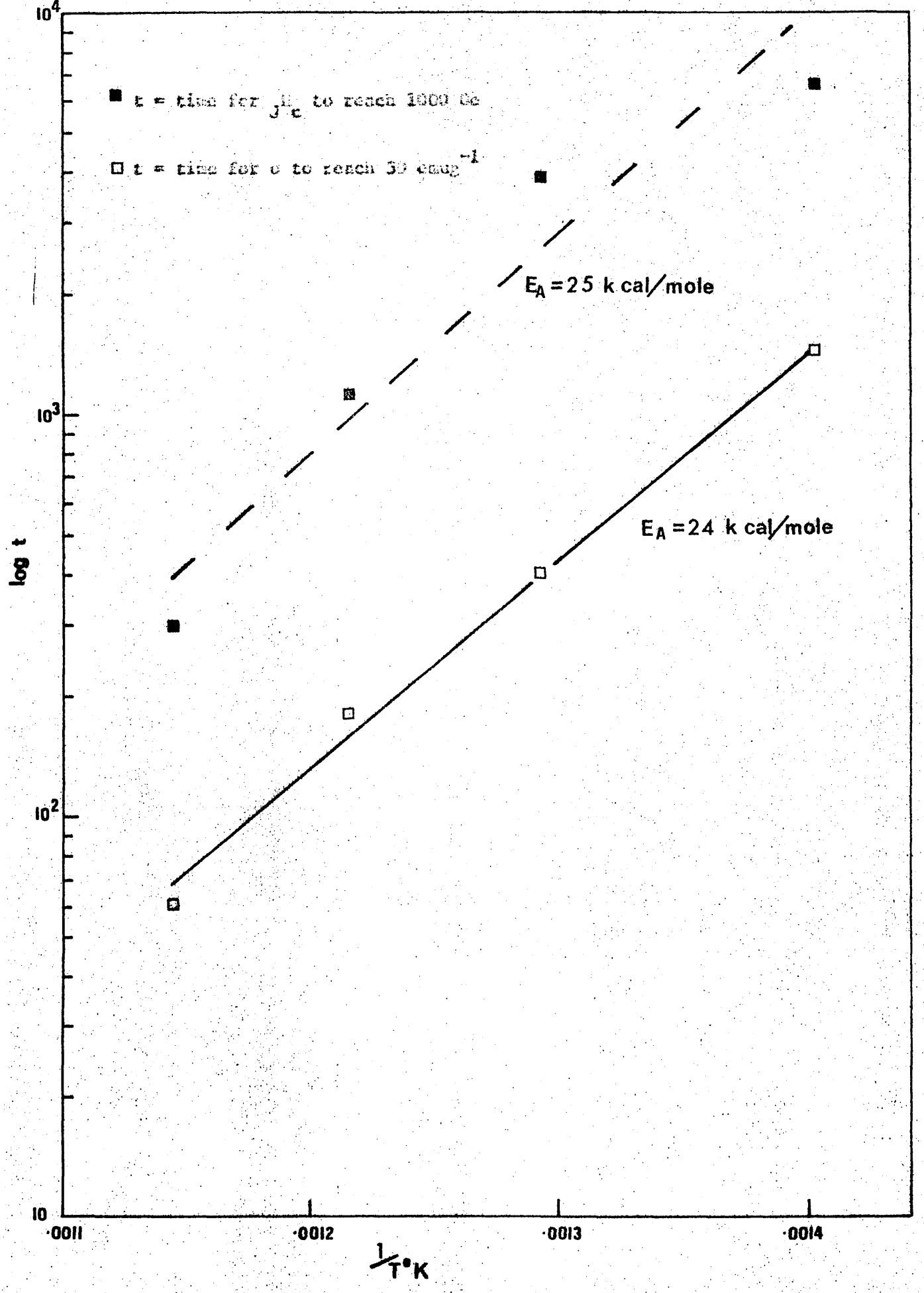

and infers that E_A below 500°C differs from that at higher temperatures. This seems unlikely but it is clear from the changes in σ and the $_JH_c$ of the alloy with ageing that precipitation proceeds much more slowly at 450°C than at higher temperatures (Figures 9 and 10). Unlike σ which is determined by the amounts and σ values of the phases present, $_JH_c$ is influenced by particle size and thus would be expected to give a less accurate indication of the stage to which the reaction had progressed than one based on σ. However, it has been shown in section 3.6. that providing the particle size of the precipitate does not exceed single domain size, $_JH_c$ is primarily controlled by the amount and σ of β present which are directly related to the stage reached in the precipitation process. In the Malcolloy alloys, therefore, the use of $_JH_c$ as an indication of fraction transformed is believed to be justified. It can be seen from Figure 41 that the values obtained basing t on $_JH_c$ can be interpreted as linear but with a greater scatter than is the case using σ. The plots are linear over the full temperature range (450-600°C) in the 28% and 38% Al alloys (Figures 41 (b) and (c) and between 500°C and 600°C in the 23% Al alloy, (Figure 41 (a)).

Values of E_A (activation energy), calculated from Figure 41 as gradient x 2.3 R (R = the gas constant) were as follows:-

23% Al alloy E_A (based on σ) = 9,500 cal/mole

E_A (based on $_JH_c$) = 14,000 cal/mole

28% Al alloy E_A (based on σ) = 19,000 cal/mole

E_A (based on $_JH_c$) = 19,000 cal/mole

38% Al alloy E_A (based on σ) = 24,000 cal/mole

E_A (based on $_JH_c$) = 25,000 cal/mole

Thus, for the 28% and 38% Al alloy, the data derived from $_JH_c$ could be

interpreted to give values of E_A very similar to those based on σ. In the 23% Al alloy there was some difference between the two values obtained. The figure derived using σ (9,500 cal/mole) was, however, surprisingly low for a reaction occurring in a solid metal and, since it was not confirmed by that based on $_JH_c$, may be regarded as suspect.

3.7.3. Relationship between activation energy and coercivity

From the relatively small particle size of the precipitate in these alloys and the very rapid decrease in σ early in the ageing process, it can be deduced that nucleation of the precipitate takes place easily, i.e. the activation energy of nucleation is low. This view is consistent with the hypothesis presented in section 3.5. regarding partially coherent nucleation. It is reasonable to suggest, therefore, that observed differences in E_A are due to variations in the activation energy associated with precipitate growth rather than nucleation, (i.e. variations in the activation energy of diffusion through the matrix or across the matrix-precipitate interface).

It is significant that the increase in maximum $_JH_c$ of the three alloys as aluminium content is increased corresponds to an increase in E_A. In an alloy in which E_A for growth is high it can be suggested that particle growth would be restricted and that the formation of fresh nuclei would be favoured. The resulting precipitate would, therefore, have a small particle size and a narrow size range. If E_A is low, growth would be less restricted and a relatively large particle size with a wide size distribution would result. Thus, in the Malcolloy alloys, high E_A favours the retention of a dispersion with optimum properties until late in the precipitation process when σ_β is reduced. When E_A is lower the greater tendency for particle coarsening will result in a wide size range and a reduction in the coercivity of the precipitate before σ_β is sufficiently reduced for a high coercivity to be exhibited.

The extent to which the properties of Malcolloy are, in fact,

influenced by E_A is difficult to determine and the amount of cobalt available for precipitation, as discussed earlier, may be a more significant factor. Nevertheless, it seems certain that high values of E_A will tend to favour the retention of a finely divided dispersion and thus the development of high coercivity.

4.1. Introduction

4.1.1. Comparison of the properties of Malcolloy with common permanent magnet materials

Although Malcolloy is the best known magnet material based on finely divided cobalt, the properties of the alloy are poor when considered in relation to those of other materials at present in commercial production. Thus, Malcolloy (Tables 2, 3 and 10) compares unfavourably with barium ferrite (B_r = 3,500 G, H_c = 2,500 Oe, $(BH)_{max}$ = 1.0 - 3.0) and with most of the Alnico alloys (Table 1). Because of their high cobalt content the Malcolloy alloys are relatively expensive; it seems unlikely, therefore, that these materials will become commercially useful unless considerable improvement in their properties can be achieved.

4.1.2. Possibility of increasing coercivity

It has been shown in section 3.3. that the energy to rotate the magnetisation vector of a single domain particle through 180° is given by -

$$E = K_1 + K_2$$

where K_1 and K_2 are crystal anisotropy constants, values for which at various temperatures have been determined by Honda and Masumoto[32] (Figure 2).

Stoner and Wohlfarth[13] used K_1 as a first approximation for K in the relationship -

$$J^{H}_{c} = \frac{2K}{J_s} \qquad \text{(see section 1.2.1.)}$$

to calculate a value of 6,000 Oe for the J^{H}_{c} of an assembly of spherical single domain particles of c aligned with their [0001] axes parallel. If as in section 3.3., K is taken to be the sum of K_1 and K_2, J^{H}_{c} (at 20°C) according to the above expression is 9,000 Oe in a fully aligned dispersion and about 4,300 Oe if alignment is random.

Thus the coercivity of the Malcolloy alloys is much lower than

that predicted by theory. It has been shown that in these alloys coercivity is influenced not only by the properties of the c dispersion but also by the presence of magnetic β (section 3.6.) The highest coercivity observed was in the 38% Al alloy with $_{J}H_{c}$ approaching 2,000 Oe. Whether this represents the maximum $_{J}H_{c}$ of the c dispersion has not been determined but it is thought that the coercivities of the 23% and 28% Al alloys are reduced relative to the 38% Al alloy by the influence of magnetic β. It is likely, therefore, that at some stage during ageing, the coercivity of the precipitate in the lower aluminium casts was at least as high as 2,000 Oe (the maximum $_{J}H_{c}$ of the 38% Al alloy) which is about half the ideal coercivity for random c particles predicted above.

It would seem on this basis, that there is considerable scope for improving the coercivity of the c dispersion. It is known, however, that coercivity is always much less than the ideal value. There are many possible reasons; the expressions of Stoner and Wohlfarth[13], which predict the coercivity of single domain particles (see section 1.1.2.) assume coherent rotation of the magnetisation vector, whereas in practice rotation can take place by lower energy processes such as curling and buckling (section 1.1.4.). A small number of large, multi domain particles may be present, the existence of structural or surface defects may lead to the nucleation of domain boundaries in particles smaller than theoretical single domain size and various factors such as strain or stacking faults may reduce the crystal anisotropy of the material. These, and other factors, reduce the measured coercivity of barium ferrite to less than half, and that of the cobalt rare-earth permanent magnet alloys to one tenth of the ideal value. It must be concluded that there is little possibility of significantly improving the coercivity of the c dispersion in Malcolloy. It may, however, be possible to increase the coercivity of the material as a whole if optimum properties of the precipitate can be made to coincide with, or be preceded by, the approach of σ_{β} to zero.

4.1.3. Possibility of increasing remanence

In the 38% Al alloy $4\pi J_s$ (saturation magnetisation) and B_r are low (2250 G and 1550 G respectively, see Table 10) so that despite the high $_JH_c$ of the material (1930 Oe) the overall properties are poor (B_r = 1550 G, H_c = 1030 Oe, $(BH)_{max}$ = 0.40 MGO) in comparison with those of the 28% Al alloy (B_r = 3550 G, $(BH)_{max}$ = 1.3 MGO, H_c = 1215 Oe). In order to improve the overall properties of the alloys it is necessary, therefore, to increase the coercivity of the higher remanence compositions as discussed above. However, even if the coercivity of the 23% Al alloy (with remanence about 5300 G, Table 10) was increased to 2,000 Oe the properties would remain inferior to the cheaper Hycomax alloys (Table 1). It is clear, therefore, that B_r as well as $_JH_c$ must be increased if the Malcolloy alloys are to become useful permanent magnet materials.

Various modifications to the preparation, treatment and composition of Malcolloy, aimed at improving these properties are discussed below.

4.2. Modifications aimed to increase coercivity

4.2.1. Effect of solution treatment, time and temperature

It has been shown (section 3.2.) that the maximum $_JH_c$ attained on ageing the Malcolloy alloys decreases with decreasing aluminium content. In the as cast condition, Malcolloy contains a coarse Widmanstätten precipitate of cobalt (Figure 7a) which is dissolved during solution treatment. All the samples previously discussed were solution treated for ½ hour at 1380°C. It is possible that this treatment, although resulting in the solution of the cobalt precipitate, is not sufficient to homogenise the alloy completely; i.e. regions with high cobalt content may exist in the single phase β. In such regions, therefore, conditions similar to those in a higher cobalt alloy would exist and the ε precipitate would grow rapidly on ageing so that when σ_β approached zero, the precipitate size would be large and coercivity would be low. Some

Fig. 42 - Effect of Solution Treatment Temperature on $_{J}H_{c}$ after subsequent ageing at 450°C (28.3% Al alloy)

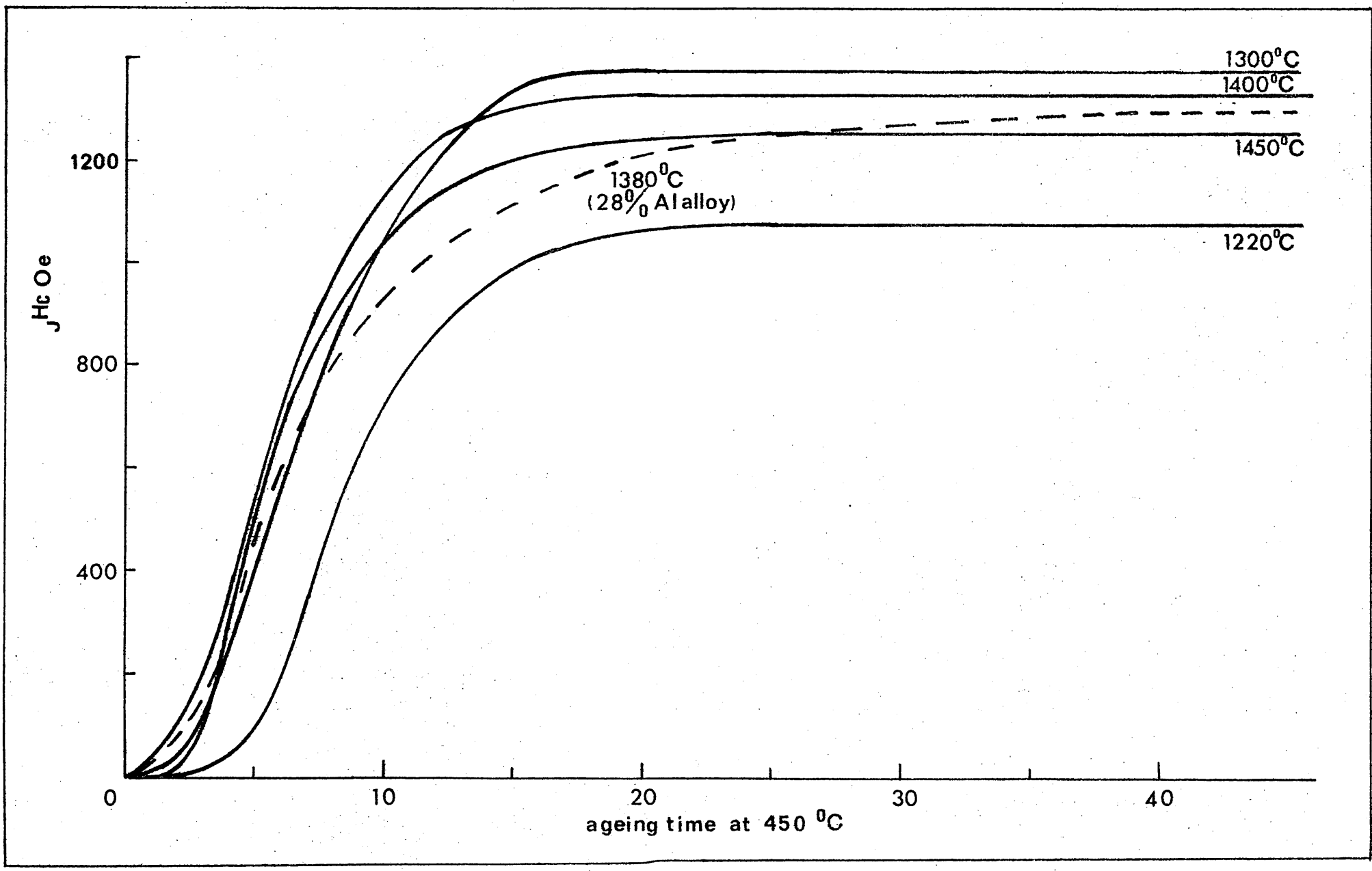

TABLE 16

THE EFFECT OF AGEING THE 28.3% AL ALLOY AT 450°C AFTER VARIOUS SOLUTION TREATMENTS

Time at 450°C hours	½ hour at 1220°C		½ hour at 1300°C		½ hour at 1400°C		½ hour at 1450°C	
	J^{H}_{c} Oe	σ emug^{-1}	J^{H}_{c} Oe	σ emug^{-1}	J^{H}_{c} Oe	σ emug^{-1}	J^{H}_{c} Oe	σ emug^{-1}
0	<2	90	<2	90	<2	90	<2	90
2½	5	81	20	82	100	82	15	80
4	40	76	300	77	200	79	290	76
6½	232	77	762	78	765	77	853	76
9	620	74	1018	75	1055	74	1010	76
11	780	74	1136	74	1191	72	1007	74
13	909	72	1255	72	1270	70	1195	73
19	1061	70	1380	69	1332	70	1245	67
24	1066	68	1386	67	1330	69	1220	69
30	1070	67	1350	66	1315	67	1250	66
42	1090	67	1380	67	1340	66	1260	66

	1 hour at 1300°C		2 hours at 1300°C		16 hours at 1300°C	
	J^{H}_{c} Oe	σ emug^{-1}	J^{H}_{c} Oe	σ emug^{-1}	J^{H}_{c} Oe	σ emug^{-1}
0	<2	90	<2	90	<2	90
2½	30	82	5	84	130	79
4	62	79	90	78	290	77
6½	624	77	939	75	906	76
9	932	75	1080	76	1097	76
11	1121	74	1180	75	1058	74
13	1235	74	1276	70	1150	72
19	1385	70	1415	69	1284	72
24	1380	67	1400	67	1230	67
30	1375	67	1420	67	1300	68
42	1380	68	1410	67	1290	66

indication that the form of a precipitate can be influenced by the previous solution treatment is contained in the results of Merica et al[71]. These authors showed that the mechanical properties attainable on ageing aluminium-copper alloys, with around 4% copper, were increased if the solution treatment temperature was as high as possible. An investigation of the effect of solution treatment temperature and time on the $_JH_c$ of Vacolloy, after subsequent ageing was, therefore, worthwhile.

Insufficient of the original alloys remained for this work to be carried out; a new cast was, therefore, prepared. As with the previous casts, the constituents were of commercial purity (Cobalt 99.6 wt%, aluminium 99.9 wt%), and melting was carried out by induction heating under argon. The aimed composition was 28% Al, but in order to distinguish this material from the earlier 28% Al alloy it will be referred to by the analysed Al content of 28.3% Al. The analysed composition was as follows -

Co 71.5% (by difference), Al 28.3%, Fe 0.2% (impurity)

Groups of samples were solution treated for ½ hour at different temperatures, (1220°C, 1300°C, 1400°C and 1450°C) and water quenched. Measurements on five samples from each group showed that there was no consistent variation in σ with solution treatment temperature, the total range in σ was from 89.5-91. The samples were aged for various times at 450°C to give $_JH_c$ and σ values as shown in Table 16 and Figure 42. The Figure also includes the variation of $_JH_c$ on ageing at 450°C of the original 28% Al alloy (broken line).

It can be seen that as solution treatment temperature was increased from 1220°C to 1300°C the maximum $_JH_c$ on ageing increased from 1080-1380 Oe. Further increase in solution treatment temperature, however, resulted in a decrease in maximum $_JH_c$. The change in σ on ageing did not vary with solution treatment temperature.

Two further groups of samples were solution treated at 1300°C. Treatment was prolonged for two hours in one case and for 16 hours in the other. The results of subsequent ageing at 450°C are shown in Figure 43.

Fig. 43 - Effect of solution treatment time at 1300°C on $_jH_c$ after subsequent ageing at 450°C (28.3% Al alloy)

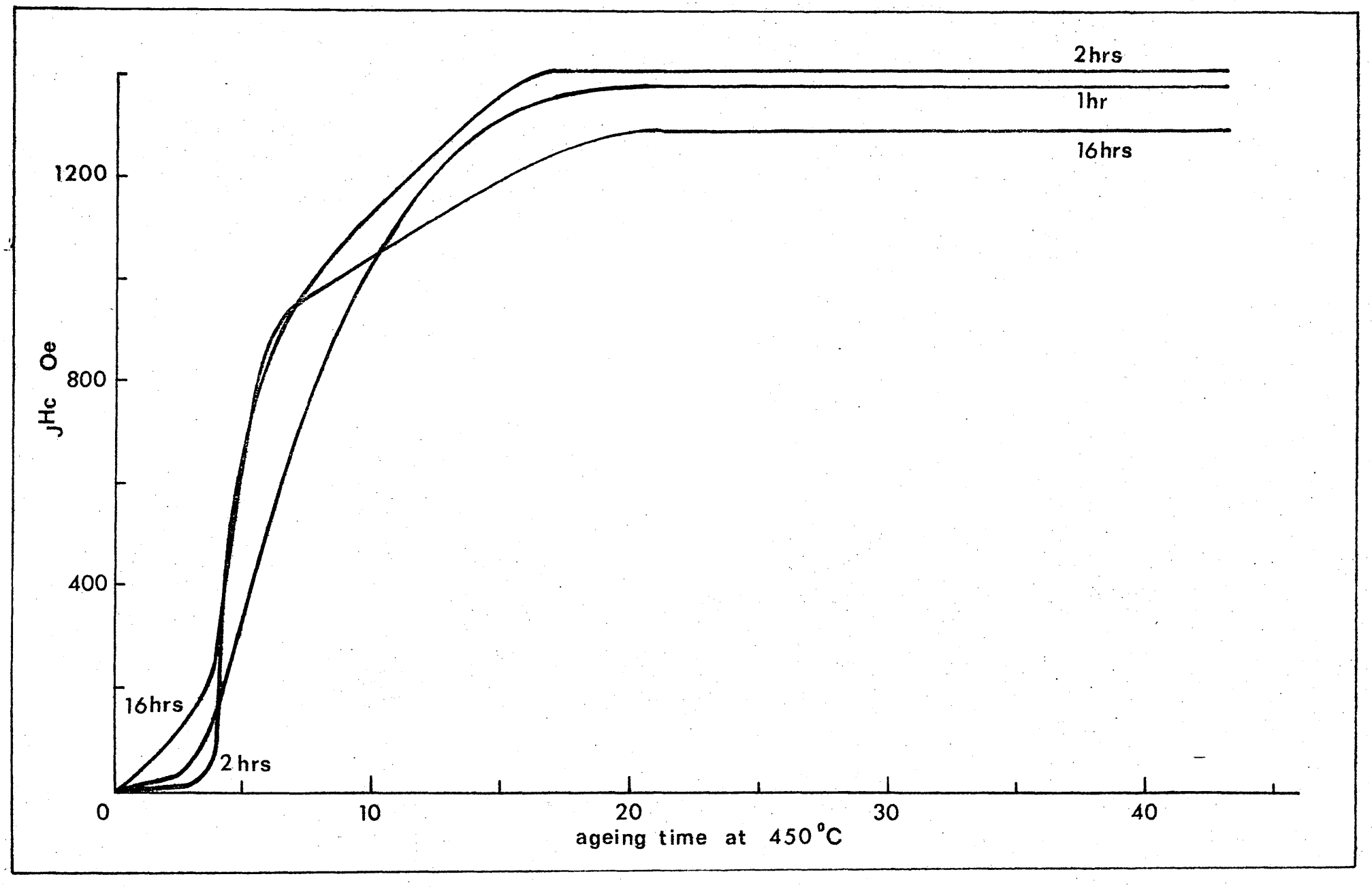

The material solution treated for 2 hours is seen to have a slightly higher maximum $_{J}H_{c}$ than that treated for $\frac{1}{2}$ hour but after 16 hours maximum $_{J}H_{c}$ decreased. Again, σ during ageing was not dependent on solution treatment.

Thus maximum $_{J}H_{c}$ attainable on ageing first increased and then decreased as both solution temperature and time were increased. This effect can be understood as follows. As solution treatment temperature and/or time is increased, the β phase becomes more homogenous and $_{J}H_{c}$ is increased due to elimination of regions with high cobalt content as discussed above. It is known, however, that the equilibrium vacancy concentration increases with temperature and that the activation energy for precipitation is reduced when vacancy concentration is high[72]. Thus, as solution treatment temperature is increased, the number of vacancies retained on quenching will increase and diffusion and particle growth on ageing will be easier. The coercivity of the c dispersion will, therefore, be reduced. At higher temperatures, vacancy concentration will be higher and subsequent coercivity will be less. At lower temperatures, the vacancy concentration will be less and the time required to reach equilibrium will be increased. A short solution treatment time may, therefore, result in a low, non-equilibrium vacancy concentration and a higher maximum $_{J}H_{c}$ on ageing. From this hypothesis optimum solution treatment temperature can be understood as the resultant of two opposing effects. Treatment must be sufficiently prolonged and at a high enough temperature to homogenise the β phase but for as short a time and at as low a temperature as possible to minimise the vacancy concentration.

Solution treatment conditions could be optimised by carrying out a detailed examination of different combinations of time and temperature but it seems doubtful, in view of the relatively small effect observed, whether any great benefit in terms of maximum $_{J}H_{c}$ would arise from such a study.

4.2.2. The addition of third elements

Masumoto et al[42-48] succeeded in increasing the coercivity of Alcolloy by making additions of third elements. One such alloy had the composition -

Co 67.6% (60.55 wt.%), Al 27.4% (14.82 wt.%), Ti 5.0% (4.63 wt.%)

and properties, after solution treatment at 1365°C and ageing 20 hours at 550°C -

B_r 2850 G, H_c 1550 Oe. $(BH)_{max}$ 1.40 MGO

This alloy is typical of the various high coercivity ternary alloys described by Masumoto et al in that the increase in coercivity is accompanied by a decrease in B_r and $(BH)_{max}$ (Table 3). An alloy of similar composition has been examined as part of the present work to determine the reason for the increased coercivity.

The material was prepared from constituents of the following purity -

cobalt 99.5 wt.%, aluminium 99.9 wt.% and Ti 99.9 wt.%

melting was carried out by induction heating under argon. After solidification the cast was broken up and re-melted to ensure adequate mixing. The analysed composition including iron, present as impurity, was -

Co 67.5% (by difference), Al 27.3%, Ti 5.0%, Fe 0.2%

A number of samples were solution treated at 1365°C, under a protective atmosphere of hydrogen, and water quenched. In this condition σ ranged between 65.4 $emug^{-1}$ and 66.6 $emug^{-1}$, indicating a fair degree of homogeneity, and $_jH_c$ was too small to be measured, i.e. <2 Oe. X-ray diffraction examination, using the Debye-Scherrer camera, and optical metallography revealed a single phase structure which was identified as b.c.c. β.

Samples were aged at temperatures between 450°C and 700°C. As with the binary alloys, the precipitate was found to be ϵ on ageing up to 600°C and a mixture of α and ϵ at 700°C. During ageing at the latter temperature the amount of α increased until after 12 hours only a trace of

Fig. 44 - Effect of ageing on $_jH_c$ and σ of the Co-Al-Ti Alloy

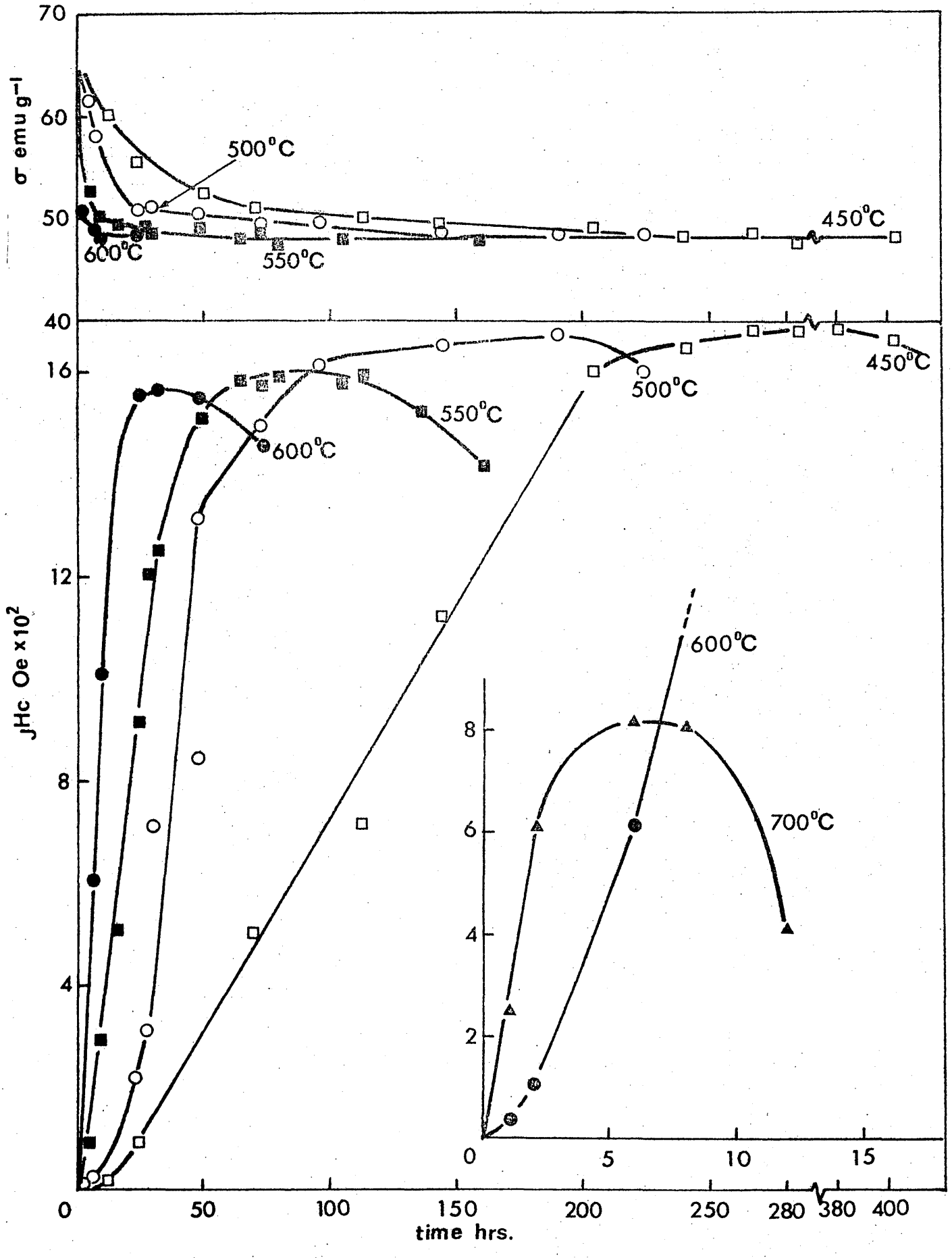

TABLE 17

EFFECT OF AGEING ON $_{J}{}^{H}{}_{c}$ AND σ OF THE Co-Al-Ti ALLOY

450°C			500°C			550°C		
Time hrs.	$_{J}{}^{H}{}_{c}$ Oe	σ emug^{-1}	Time hrs.	$_{J}{}^{H}{}_{c}$ Oe	σ emug^{-1}	Time hrs.	$_{J}{}^{H}{}_{c}$ Oe	σ emug^{-1}
0	<2	66	0	<2	66	0	<2	66
2	<2	65.2	1¼	<2	64.2	1	5	57.0
7	<2	63.0	2	<2	63.0	4	92	52.8
10	5	59.2	4	7	61.5	8	93	50.0
12	10	60.0	7	22	58.1	15	502	49.6
24	94	55.5	23	220	50.2	24	910	49.1
50	-	52.3	27	310	51.1	26	1202	48.5
70	502	51.0	30	714	51.0	31½	1257	-
112	915	50.2	47	1316	50.1	48	1510	49.0
143	1125	49.5	72	1494	49.5	64	1580	48.0
204	1004	49.1	96	1616	49.4	72	1573	48.5
240	1647	48.2	144	1650	48.6	88	1599	47.6
267	1650	48.5	190	1673	48.3	104	1581	48.0
284	1677	47.5	224	1600	47.5	112	1587	-
302	1660	-				136	1543	-
380	1664	-				160	1412	47.6
402	1662	47.9						
444	1672	48.2						

600°C			700°C		
0	<2	66	0	<2	64
1	30	56.2	1	250	49.2
2	102	50.5	2	603	43.1
6	603	49.1	6	612	43.2
8	1005	47.9	8	803	42.7
24	1552	46.1	12	407	42.1
32½	1560	47.7			
48	1553	48.2			
72	1455	47.9			

Fig. 45 - Variation of peak $_{J}H_{c}$ and minimum σ with atomic cobalt content for the binary Halcolloy alloys and the Co-Al-Ti alloy

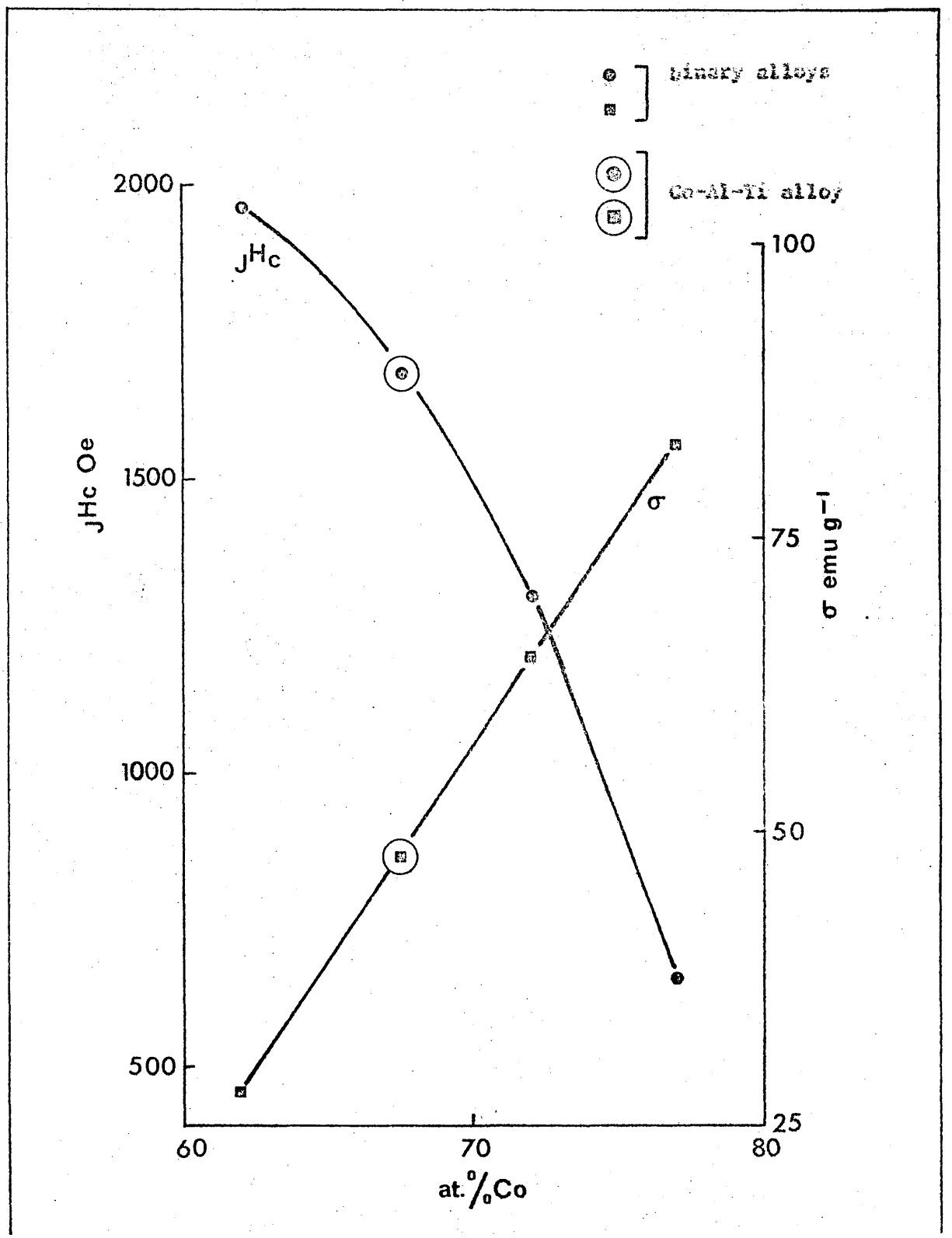

c was detected. The variation of σ and $_{J}H_{c}$ on ageing is shown in Figure 44 and Table 17. Peak $_{J}H_{c}$ was 1680 Oe (267 hours at 450°C) and σ reached a minimum value of around 48 emug^{-1}.

It is interesting to compare maximum $_{J}H_{c}$ and minimum σ of this alloy with those from the original binary alloys (section 3.2.3.). These values are plotted against cobalt content in Figure 45. It can be seen that the point representing σ of the ternary alloy falls exactly on the straight line connecting the points for the binary alloys, while a smooth curve can be drawn joining all four $_{J}H_{c}$ points. Thus, in the present work, the addition of titanium at the expense of cobalt resulted in increased coercivity but the effect on both coercivity and σ was not significantly different from that which might be anticipated if aluminium content was increased to a similar extent, i.e. to give a 32.5% Al binary alloy.

It has been suggested that $_{J}H_{c}$ is influenced by activation energy. If, therefore, the Co-Al-Ti alloy is assumed to be equivalent to a 32.5% Al binary alloy, E_{A} for the reaction might be expected to be intermediate between the values for the 28% and 38% Al alloys (19,000 and 25,000 cal/mole respectively). E_{A} was determined for the Co-Al-Ti alloy by plotting log t versus $1/T^{o}$ where t was the time for σ to fall to 57 emug^{-1} (Figure 46). The relationship was approximately linear and from the slope, E_{A} was calculated as 27,500 cal/mole, which is higher than anticipated.

In contradiction to the present work, Masumoto et al[45] showed that there was considerable benefit, in terms of coercivity due to the addition of titanium. The Co-Al-Ti alloy with the highest coercivity is that stated earlier, i.e. 67.6% Co (80.55 wt.%), 27.4% Al (14.82 wt.%), 5.0% Ti (4.6 wt.%). This can be compared with a binary alloy with the same atomic cobalt content, i.e. 67.6% Co (82 wt.%), 32.4% Al (18 wt.%). The properties of these alloys after heat treatment to give maximum coercivity were given by Masumoto et al as follows

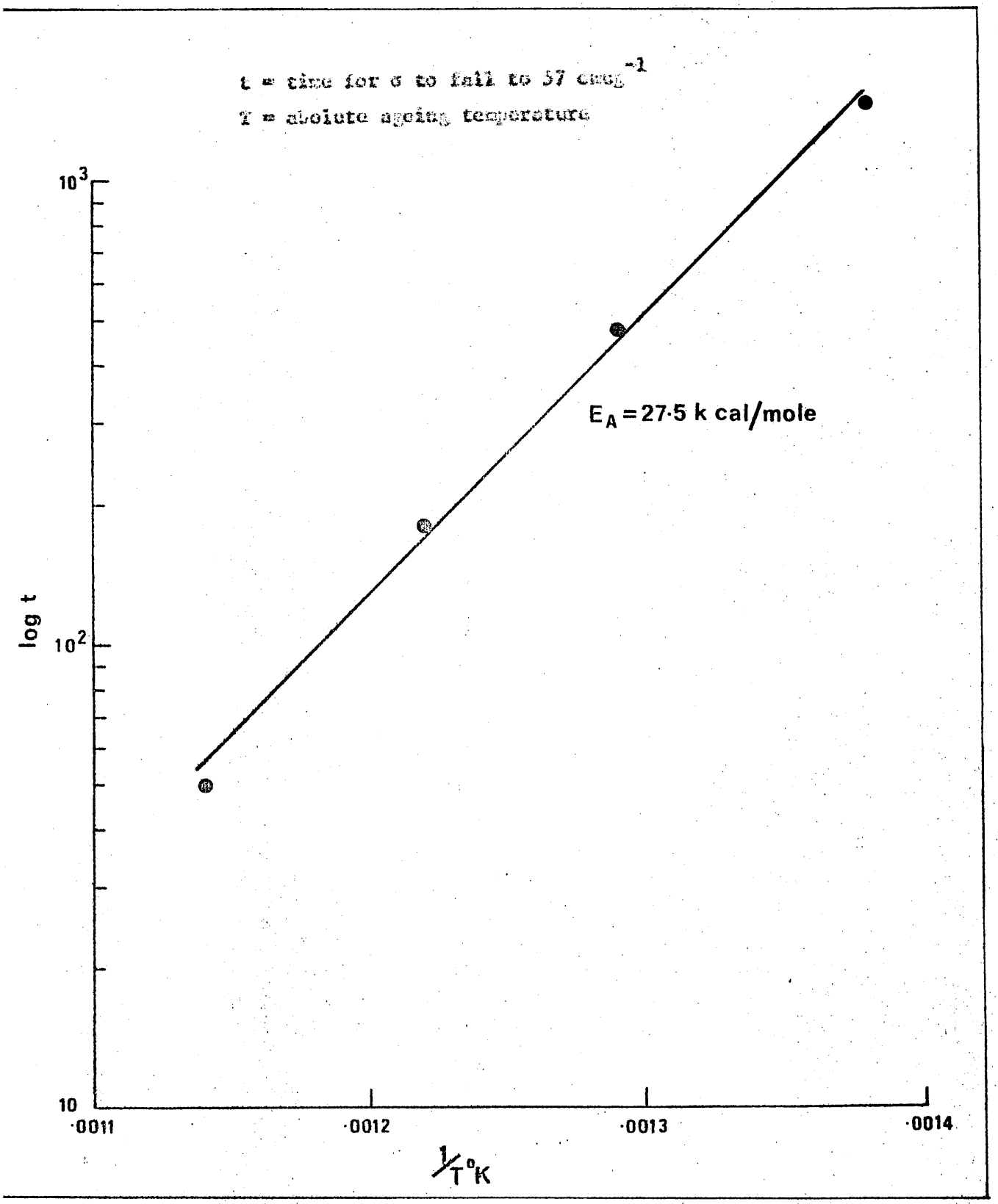
t = time for σ to fall to 57 ohm^{-1}
T = absolute ageing temperature
10^3
10^2
10
log t
E_A = 27·5 k cal/mole
·0011
·0012
·0013
·0014
$\frac{1}{T}$°K

Fig. 47 - Derived demagnetisation curves for a 32.4% Al binary Nelcolloy alloy (based on the results of Masumoto et al [41])

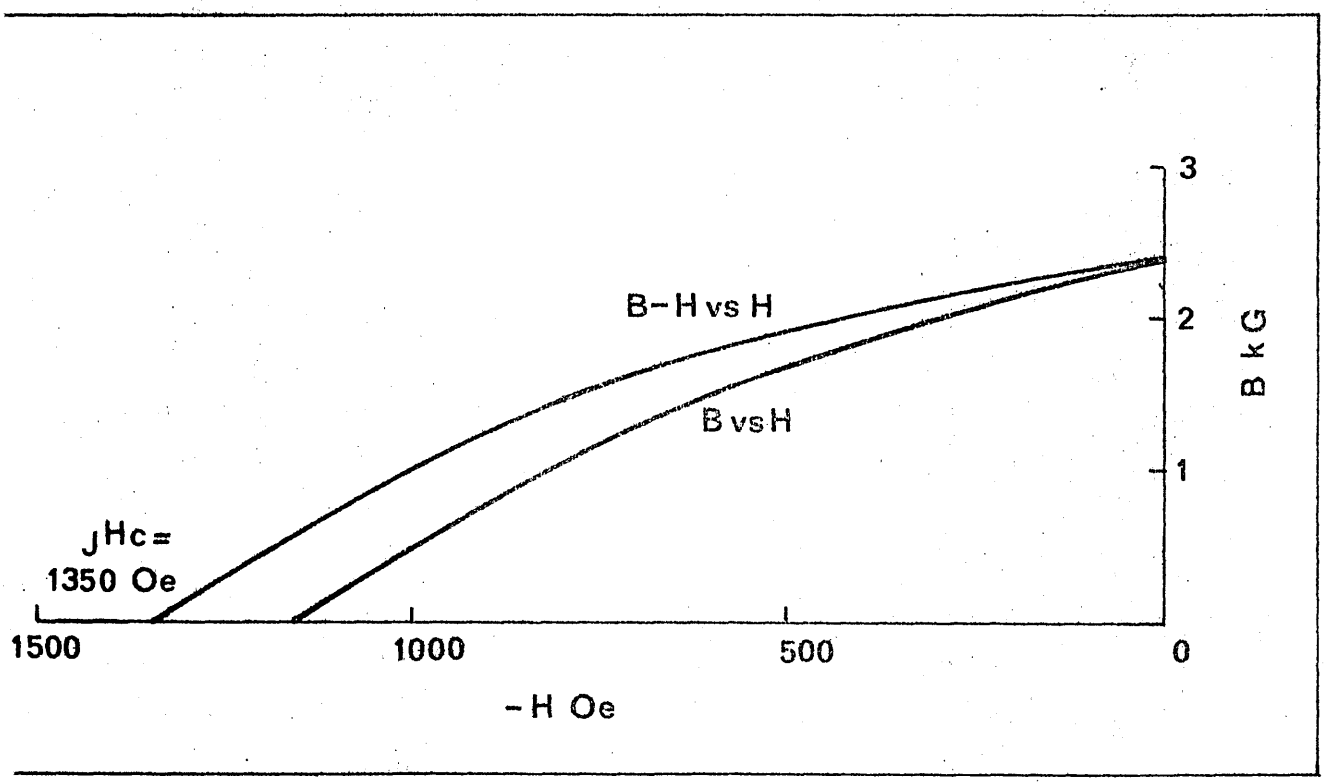

	$4\pi J_s$	B_r	$(BH)_{max}$	H_c	$_JH_c$	$\frac{B_r}{4\pi J_s}$
	G	G	MGO	Oe	Oe	
Co-Al-Ti[45]	4220	2850	1.40	1550	1675	0.68
Co-Al[41]	4800	2400	0.90	1160	not stated	0.5

$_JH_c$ of the binary alloy is not stated but in Figure 47 a demagnetisation curve, (B v.s. H), with B_r, H_c and $(BH)_{max}$ as given by Masumoto et al for the binary alloy, is constructed. From this an intrinsic demagnetisation curve (B-H v.s. H) has been derived and this can be extrapolated to give a $_JH_c$ value of about 1350 Oe. The value may not be accurate because the precise form of the demagnetisation curve is not known. It is clear, however, that $_JH_c$ of the binary alloy must have been considerably lower than that of the alloy with titanium. As noted above, activation energy derived in the present work was rather higher, in the presence of titanium, than would be expected for the equivalent binary alloy. No corresponding increase in $_JH_c$ was observed but it is possible that increased activation energy due to the presence of titanium might be responsible for the increased $_JH_c$ obtained by Masumoto et al.

4.3. Modifications to Increase Remanence

4.3.1. The addition of Iron

The saturation magnetisation of iron at room temperature is greater than that of cobalt (σ Fe = 217, σ Co = 161). The partial replacement of the cobalt content of Malcolloy by iron might be expected, therefore, to increase σ of the precipitate and, consequently B_r of the material after ageing.

A cast of commercial purity constituents was induction melted under argon as described previously. Analysed composition was -

Co 65.2% (by difference), Al 30.2%, Fe 4.6%

The composition is marked on the Co-Al-Fe phase diagram in Figure 48. The phase boundaries shown are those at 800°C derived by Edwards[73] whose

Fig. 48 - Aluminium Cobalt Iron phase diagram at 800°C (after Edwards [73]).
The asterisk marks the composition of the alloy discussed in the script

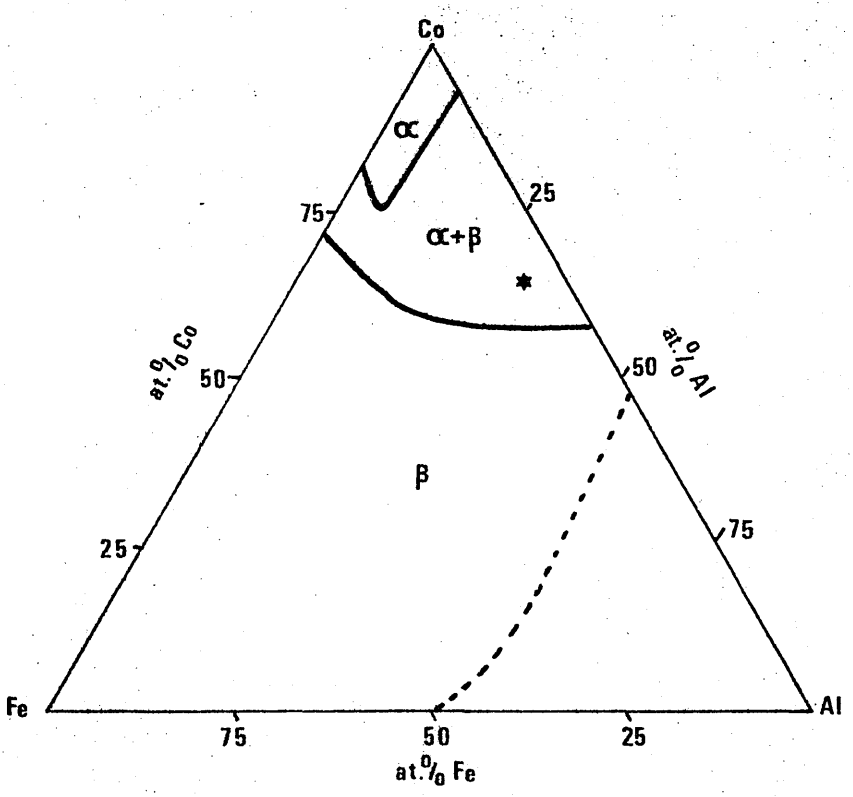

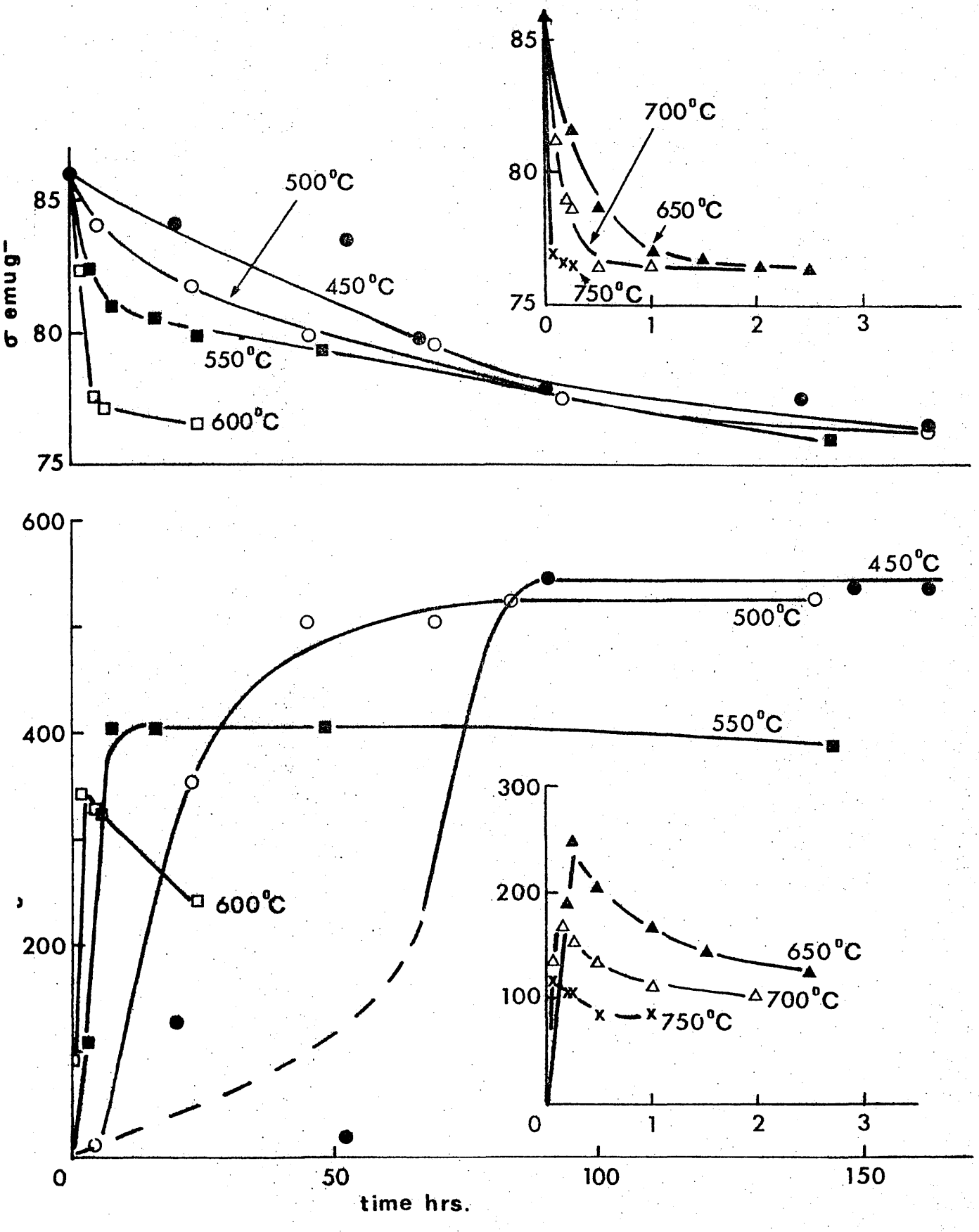
σ emug⁻
85
80
75
500°C
450°C
550°C
600°C
700°C
650°C
750°C
0
1
2
3
600
400
200
300
100
450°C
500°C
550°C
600°C
650°C
700°C
750°C
0
50
100
150
time hrs.

TABLE 18

THE EFFECT OF AGEING ON $_{J}H_{c}$ AND σ OF THE Co-Al-Fe ALLOY

450°C			500°C			550°C		
Time hrs.	$_{J}H_{c}$ Oe	σ emug^{-1}	Time hrs.	$_{J}H_{c}$ Oe	σ emug^{-1}	Time Hrs.	$_{J}H_{c}$ Oe	σ emug^{-1}
0	<2	86.0	0	<2	86.0	0	<2	86.0
20	127	84.1	5	10	84.1	3	108	82.4
52	50	83.5	23	355	81.8	7½	401	81.0
66	219	79.8	45	502	79.9	16	401	80.6
90	545	77.9	69	502	79.6	24	401	79.9
138	535	77.5	93	524	77.4	48	404	79.4
162	535	76.5	141	525	76.9	144	388	76.1
190	530	76.6	162	520	76.3			
270	528	76.5						

600°C			650°C			700°C		
0	< 2	86.0	0	<2	86.0	0	< 2	86.0
1	89	-	10 min	190	-	5 min	136	81.3
2	341	82.4	15 "	248	81.5	10 min	170	79.0
3	323	-	½	205	78.8	15 "	154	78.6
4	326	77.6	1	165	77.0	½	136	76.5
6	321	77.2	1½	143	76.8	1	112	76.6
24	245	76.6	2½	125	76.3	2	103	76.6
			25	101	76.5			

750°C		
0	< 2	86.0
5 min	120	77.0
10 "	105	76.6
15 "	103	76.6
½	85	76.3
1	85	76.4

work shows that this alloy will contain two phases, $\alpha + \beta$, at temperatures below 800°C and only β, at temperatures above 1300°C. Solution treatment and ageing to precipitate cobalt was therefore feasible.

Samples were solution treated at 1380°C to give σ between 85.5 and 87 $emug^{-1}$ and ${}_JH_c < 2$ Oe. Metallographic and X-ray diffraction examination revealed the anticipated single phase β structure. The change in ${}_JH_c$ and σ on ageing at temperatures between 450°C and 750°C is shown in Figure 49 and Table 18. As with the binary alloys the precipitate was ϵ below 650°C and $\alpha + \epsilon$ at higher temperatures. Comparing the properties with those for the binary alloys (Figures 9-12) it is seen that, in the alloy with iron, maximum ${}_JH_c$ is lower and more dependent on ageing temperature in the range 450-600°C than was the case for the binary materials. Also, the minimum value of σ (about 76 $emug^{-1}$) is rather higher than would be expected for a corresponding binary alloy. Thus, σ was increased by the addition of iron but only at the expense of ${}_JH_c$.

The reason for the reduced ${}_JH_c$ was easily established. In Figure 50 σ, T curves for Co-Al-Fe samples aged for various times at 450°C are plotted. These were produced as described in section 3.6. and indicate clearly the presence of two magnetic phases (α and β) in all cases. Thus even after 162 hours at 450°C β remained strongly magnetic at room temperature. From Table 18 it can be seen that more prolonged ageing at 450°C did not result in any significant change in ${}_JH_c$ or σ. It must be concluded, therefore, that the precipitation reaction was essentially complete after 162 hours and that the magnetic β present was in metastable equilibrium with the ϵ dispersion.

Analysis of the curves in Figure 50 using the approach described in section 3.6. is possible. The results can only be approximate, however, for two reasons. First, the composition and, therefore, the σ of the dispersion is not known. Second, the Curie temperature of the β present is much higher than was the case for the binary samples studied.

Fig. 50 - σ, T curves for Co-Al-Ni samples after ageing at 450°C

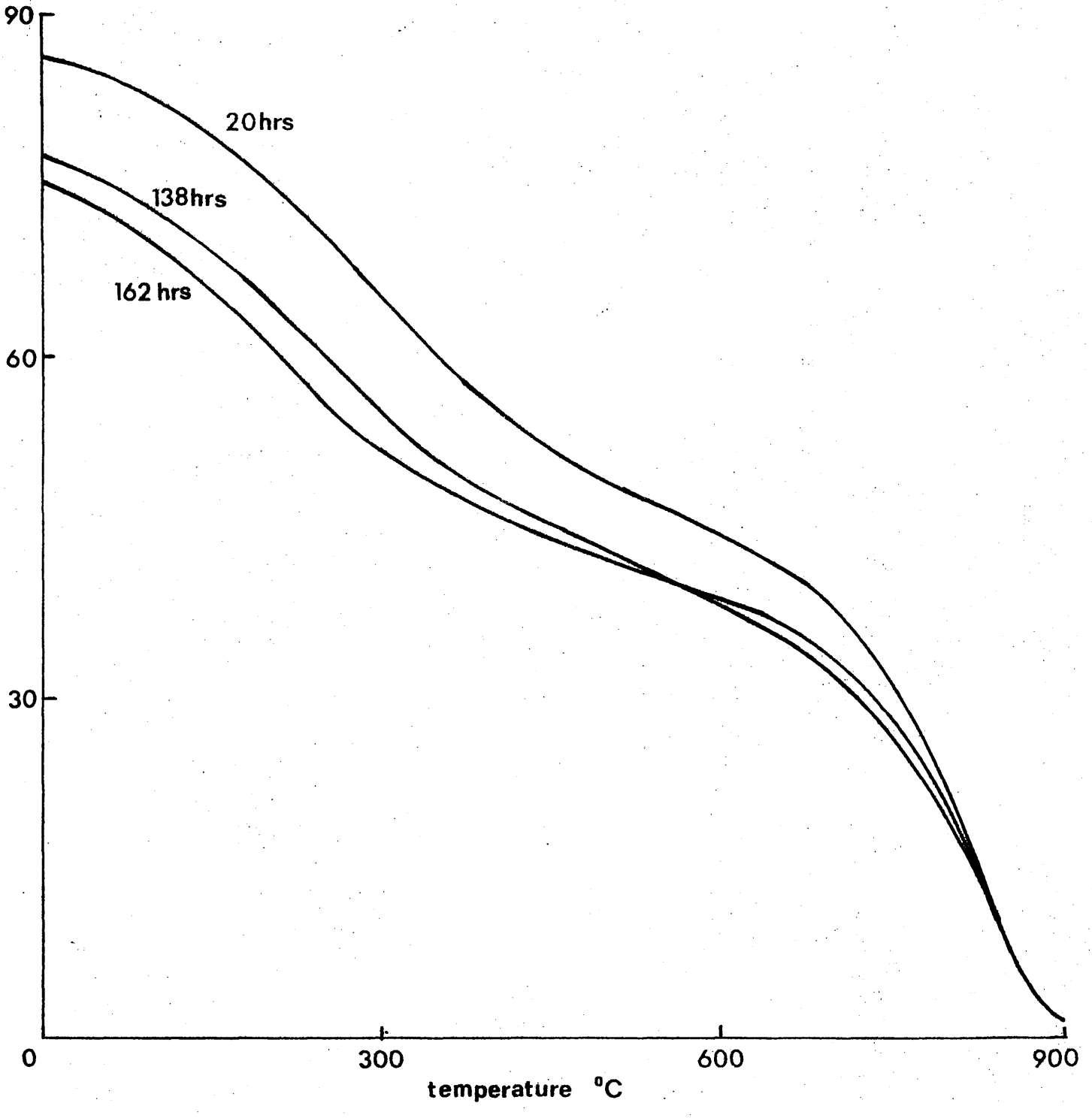

As a result it is not possible to select a temperature at which the influence of β on the magnetisation is negligible without moving into the range where the ε to α transition, with consequent solution of aluminium is likely. Assuming the CoFe dispersion contains about 5% Fe, σ would be about 165 $emug^{-1}$ at room temperature (σ Co at room temperature is 161 $emug^{-1}$) and 146 $emug^{-1}$ at 500°C (σ Co at 500°C is 144 $emug^{-1}$). It can be calculated, as in section 3.6., that in the case of the sample aged 162 hours at 450°C the weight fractions of precipitate and β present are approximately 0.3 and 0.7 respectively. σ of β is then 34 $emug^{-1}$. The contribution of β to the total magnetisation (at saturation) is, therefore, about 24 $emug^{-1}$ while that of the precipitate (at remanence) is about 26 $emug^{-1}$.

According to the discussion in section 3.6. an even lower coercivity than that observed might be anticipated because of the relatively large ratio of the β and precipitate contributions. However, in view of the various inaccuracies involved in calculating the contributions it seems unwise to draw more than the general conclusion that the low $_{J}H_{c}$ can be attributed to the persistence of the magnetic β matrix.

4.3.2. Attempts to induce particle alignment

As stated earlier, the remanent magnetisation (B_r) of a permanent magnet consisting of randomly aligned single domain particles is approximately equal to half the saturation magnetisation[13], the properties being equal in all directions. If the particles are aligned with their easy axes of magnetisation parallel, however, the properties of the assembly are anisotropic and in the direction parallel to the preferred axes of the particles, B_r is equal to saturation magnetisation. Thus, although in other directions properties are reduced relative to those of a randomly aligned system, there is a great improvement in B_r and, therefore, $(BH)_{max}$ in the preferred direction.

A number of experiments were, therefore, carried out with the aim of inducing some degree of alignment in the ε precipitate in Malcolloy.

a. Magnetic field heat treatment

In the Alnico alloys (see Table 1) a high coercivity is derived from a magnetic, single domain precipitate with a b.c.c. structure, present in a non-magnetic, b.c.c. matrix; the precipitate particles are elongated parallel to <001> matrix directions and thus exhibit shape anisotropy. The two phase structure is produced by spinodal decomposition during heat treatment, the precise nature of the treatment being dependent on the composition of the alloy[74]. If the reaction is initiated in the presence of a magnetic field, elongation of the magnetic component along those <001> matrix directions which are parallel to the field direction is favoured. If the material has a randomly oriented grain structure it is unlikely that many grains will have <001> matrix directions parallel to the field, elongation thus takes place along those <001> directions most nearly parallel and a limited degree of alignment is obtained. Greater alignment and superior anisotropic properties are achieved if the matrix grains are oriented with <001> axes parallel and if the field during heat treatment is applied in this direction. The Alnico alloys, with either randomly oriented (equiaxed) or oriented (columnar) grain structures (the latter produced by exothermic casting as described in section 3.6.) are almost invariably manufactured as anisotropic field treated magnets.

In the case of Malcolloy the precipitate is h.c.p. ε in which the preferred direction of magnetisation at room temperature is <0001>. Superior anisotropic properties would, therefore, be induced if the <0001> axes of the particles were parallel. Unfortunately the results of Honda and Masumoto[32] indicate that at temperatures above 250°C the anisotropy of the structure changes so that the principal directions in the basal plane become preferred directions of magnetisation. The variation of $_{J}H_{c}$ with temperature of Malcolloy (section 3.3.) is not entirely consistent with these observations but it seems likely that within the range of temperature used for ageing these alloys (450-600°C) <0001>ε will not be the preferred direction of magnetisation.

There is no reason to suppose, therefore, that field heat treatment would favour precipitation with <0001> c (directions) parallel to the field. Assuming that the type of anisotropy detected by Honda and Masumoto between 250°C and 400°C also exists at higher temperatures, the most likely effect of ageing in a field is that precipitation with (0001) c (planes) parallel to the field would be encouraged.

In section 3.4. the crystallographic orientation relationship between c precipitate and β matrix was defined as (0001) c parallel to (011)β. In the same section it was shown that in castings consisting of columnar crystals the <001> β was approximately parallel to the columnar axis. It follows that (011) β (planes) were parallel, perpendicular or at 45° to this axis. On application of a field parallel to the columnar axis during ageing, two of the (011) β planes in each crystal would be approximately parallel to the field; precipitation of c with (0001) c parallel to these (011) β planes would, therefore, be favoured. Since the columnar grains were, apart from the correspondence of <001> β axes, randomly oriented, the <0001> c directions would lie in a plane perpendicular to the field direction.

The effect in terms of magnetic properties would be to decrease B_r, $(BH)_{max}$ and H_c in the field direction, which would contain no <0001> c directions, but to give some improvement in all directions perpendicular to the field. Since <0001> c directions would be distributed at random within the plane perpendicular to the field only a small improvement would be anticipated.

In equiaxed castings (with randomly oriented grains) few (011) β planes would be parallel to the field and any anisotropy arising from field heat treatment would be less marked than for columnar samples.

In fact, as shown in Table 19, the properties of equiaxed and columnar samples, aged in a magnetic field, showed no sign of anisotropy and were identical to those of samples aged without a field. The equiaxed

TABLE 19

THE PROPERTIES OF EQUIAXED AND COLUMNAR HALCOLLOY AFTER AGEING FOR 6 HOURS AT 550°C WITH AND WITHOUT THE APPLICATION OF A MAGNETIC FIELD

	Crystal Structure	Test Direction	B_r G	$(BH)_{max}$ MGO	H_c Oe
No Field	equiaxed	-	3400	1.20	1110
	equiaxed	perpendicular to above	3350	1.25	1125
	columnar	parallel to columnar crystals	3300	1.20	1120
	columnar	perpendicular columnar crystals	3400	1.24	1120
Field	equiaxed	parallel to field	3350	1.22	1125
	equiaxed	perpendicular to field	3450	1.25	1115
	columnar	parallel to field	3400	1.21	1115
	columnar	perpendicular to field	3350	1.25	1120

material was from the 28% Al alloy and the columnar samples (also nominally 28% Al) were from the cast described in section 3.4. All samples were solution treated at 1300°C for ½ hour and water quenched. Magnetic field ageing, for 6 hours at 550°C , was carried out in a small furnace inside a water cooled solenoid which provided a field of about 6000 Oe. In the case of the columnar samples, the field was applied parallel to the columnar axis.

Since no anisotropy whatsoever was detected after field heat treatment, it must be concluded that the increase in magnetic energy associated with a particle forming with unfavourable orientation relative to the field was insufficient to inhibit nucleation and growth.

b. Mechanical work

It is well known that plastic deformation can induce preferred orientation and it seemed worthwhile as part of the present work to examine the effect of mechanical work on the Malcolloy alloys.

This approach was completely unsuccessful. Attempts were made to forge samples from the 23%, 28% and 38% Al alloys at all stages of the heat treatment process, i.e. before and after solution treatment and after ageing. The samples were pre-heated to various temperatures up to 1400°C, and forged by hand, using a hammer and an anvil. In every case, the first blow of the hammer shattered the specimen and only in those samples heated to either 1200°C or 1400°C were signs of plastic deformation observed. The alloys were thus found to be unforgeable. This is not in agreement with Masumoto et al who reported alloys containing between about 20% and 25% Al to be "forgeable", those between about 25% and 30% Al to be "somewhat forgeable" and only those above 30% to be "unforgeable".

4.3.3. Increased B_r due to the presence of magnetic ζ

It has been suggested in section 3.6.4. that because of the influence of local fields, the ratio $B_r/4\pi J_s$ for Malcolloy samples may be increased to considerably greater than 0.5 (the expected value for isotropic materials) if the matrix phase ζ is magnetic. It may be that the properties obtained

by Masumoto et al[41], who reported B_r and $(BH)_{max}$ rather higher than those measured in the present work (Table 10) were influenced by magnetic β in this way. In 3.6.2. and 3.6.3., however, it has been shown that the main effect of magnetic β is to reduce $_JH_c$. It is nevertheless possible that some increase in $(BH)_{max}$ could be obtained if heat treatment was carefully controlled so that the effect of magnetic β on $_JH_c$ was minimised while retaining some improvement in B_r. The limited scope of this possibility is demonstrated by the demagnetisation curves in Figure 34 for samples from the 28% Al alloy aged for 1 hour and 169 hours respectively at 500°C. In the sample aged for 1 hour σ_β was 25 emug^{-1} and after 169 hours σ_β was zero (Table 14). B_r was higher after 1 hour and $B_r/4\pi J_s$ was reduced to 0.56 in the 169 hour sample. At the same time, however, the presence of magnetic β has restricted $_JH_c$ of the sample aged for 1 hour, to 524 Oe (Table 8). Clearly, therefore, since σ_β must be very low in order to give high $_JH_c$, any improvement in B_r due to this mechanism is likely to be small. No experiments specifically aimed at exploring this effect have been carried out. Nevertheless it can be seen from the results in Table 10 for the 28% Al alloy aged at 500°C that optimum B_r and $(BH)_{max}$ do not correspond to maximum $_JH_c$. Thus, the best $(BH)_{max}$ (1.30 MGO) was obtained after 12½ hours at 500°C when $_JH_c$ was only 1215 Oe, σ_β (Table 14) was 12.3 emug^{-1} and $B_r/4\pi J_s$ was 0.57.

Fig. 51 - Co/Ti phase diagram. According to Fountain and Forgeng [75].

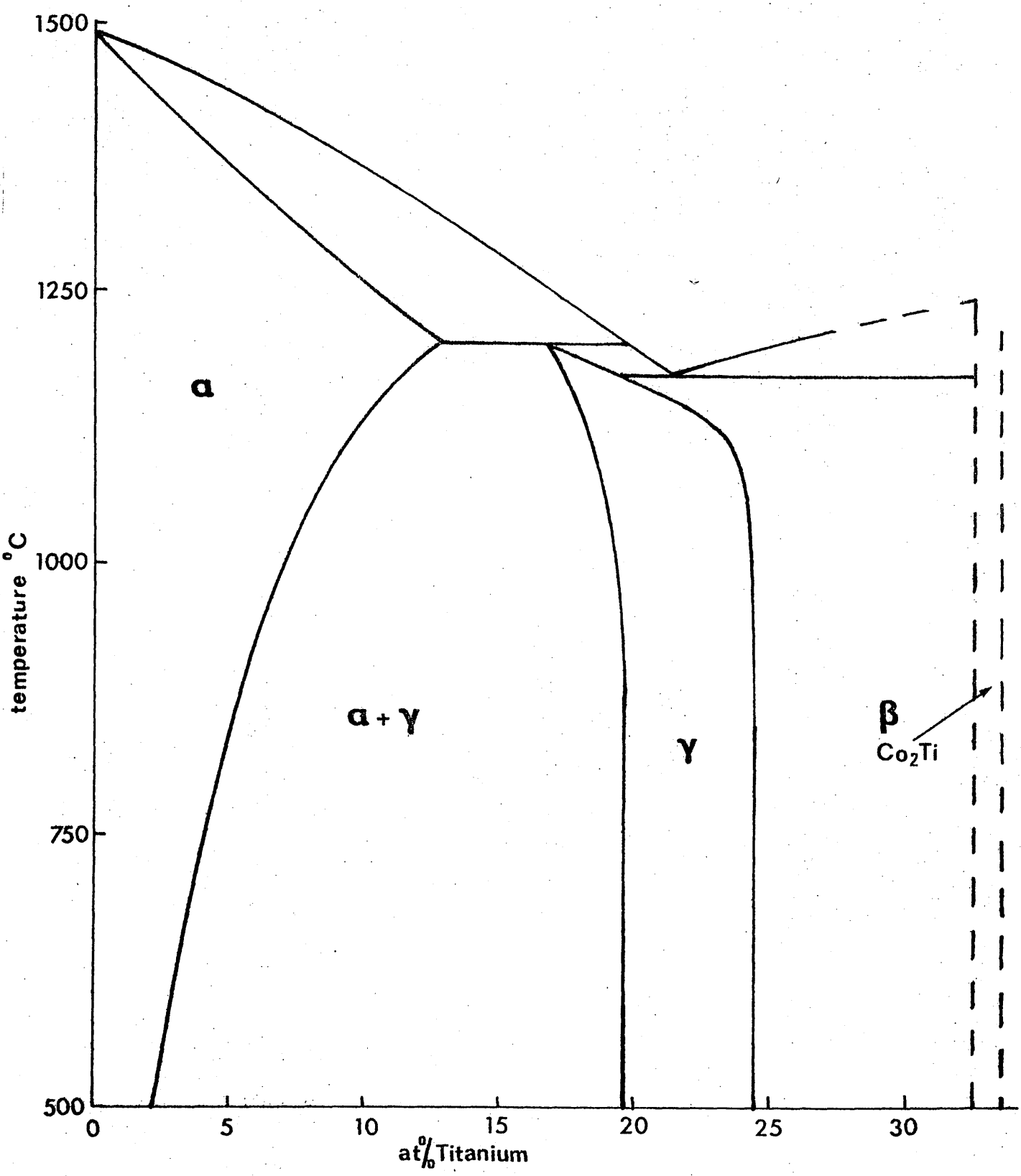

5.1. Introduction

The high cobalt section of the cobalt titanium phase diagram according to Fountain and Forgeng[75], is shown in Figure 51. It can be seen that, as with the Co-Al system, it is possible to take a certain amount of the primary, cobalt rich phase (α) into solution in an intermediate phase which in this case is f.c.c. γ.

Thus, alloys containing between about 17 and 20% Ti should be amenable to solution treatment within the γ phase field, at temperatures between about 1050 and 1175°C, followed by ageing in the two phase, α + γ, field to precipitate α. The fraction of the cobalt rich phase available for precipitation in these alloys is much less than in the two lower aluminium (28% and 23% Al) Malcolloy alloys; saturation magnetisation will, therefore, be lower and B_r, $(BH)_{max}$ and H_c will be inferior to those of the Malcolloy alloys. In the context of the present work, however, Co Ti alloys are of interest because of the similarity between the crystal structures of the intermediate phase γ and the f.c.c. allotrope of cobalt, α. Thus, f.c.c. α cobalt has a lattice parameter of 3.5441Å[50], while that of f.c.c. γ was shown by Fountain and Forgeng[75] to vary between 3.604Å (20% Ti) and 3.614Å (24% Ti). In view of the similarity between the two structures and bearing in mind the sluggish nature of the f.c.c. to h.c.p. transition in cobalt (Appendix I), it seems inevitable that on ageing at temperatures above the transition temperature, the cobalt rich precipitate will form as the stable f.c.c. allotrope and that this structure will be retained on cooling to room temperature. The CoTi alloys thus provide an opportunity to examine the properties of a f.c.c. cobalt precipitate produced under similar conditions to those under which the h.c.p. precipitate is formed in Malcolloy.

5.2. Preparation and Heat Treatment of the Alloys

5.2.1. Preparation of the alloys

Two casts were prepared from commercial purity constituents (99.5 wt.%). Melting procedure was identical to that used for the Malcolloy alloys i.e. under half an atmosphere of argon, in a pure alumina crucible contained in an induction heated graphite susceptor. The casts were allowed to solidify in the crucible and, after solidification, were re-melted to ensure satisfactory mixing. Nominal Ti contents were 17.5% and 20%, analysed compositions, including Fe present as impurity were as follows.

Ti at %	Fe at %	Co (by difference) at %
17.3	0.2	82.5
20.1	0.25	79.65

The 17.5% Ti alloy was subsequently used for solution treatment and ageing experiments. The 20% Ti material was aimed to give single phase γ approximately of the composition which, according to the phase diagram (Figure 51), would come into equilibrium with α in the 17.5% Ti alloy on ageing at temperatures below 900°C. Thus it was possible to assume that the structure and magnetic properties of the 20% Ti alloy were similar to those of the matrix in the 17.5% Ti alloy after ageing to give complete precipitation of α.

5.2.2. Heat treatment of the Alloys

Both alloys were initially subjected to a homogenising treatment of 6 hours at 1160°C, (i.e. within the γ phase field in both cases, see Figure 51), followed by water quenching. Atmospheric protection was provided by a continuous flow of purified hydrogen. Subsequent examination of both casts by optical microscopy showed the 20% Ti material to be single phase but revealed a multi-phase structure of cored dendrites in a eutectic matrix in the 17.5% Ti alloy. Unlike the Malcolloy alloys both CoTi casts were found to be forgeable and a single phase structure was ultimately achieved in the 17.5% Ti alloy by forging prior to solution treatment.

Forging was carried out by hand after pre-heating to 1160°C. Metallographic examination after forging to give about 80% reduction showed the dendritic structure to be heavily deformed but indicated no sign of re-crystallisation. Subsequent solution treatment at 1160°C followed by water quenching produced the desired single phase structure.

No further treatment was applied to the 20% Ti material but samples from the 17.5% Ti cast were subjected to a variety of ageing treatments at temperatures between 450°C and 750°C as shown in Table 20. Ageing at all temperatures was carried out without atmospheric protection and the samples were quenched to room temperature after ageing.

5.3. Results and Discussion

Both alloys were examined by X-ray diffraction in the single phase condition. In both cases the structure was identified as f.c.c. γ, with lattice parameter of 3.608Å in the 20% Ti alloy and 3.600 Å in the 17.5% Ti alloy. These values are in good agreement with those of Fountain and Forgeng[75]. During ageing of the 17.5% Ti alloy, at all the temperatures shown in Table 20, lines appeared representing f.c.c. α. These were weak, due to the small amount of the phase available for precipitation (see Figure 51) and were positioned close to the γ lines. This was to be expected in view of the similarity between the two crystal structures. Some line broadening was observed in the patterns of both phases. It seems likely in view of the crystallographic similarity between α and γ that this was due to mutual strain and that the two structures were completely or partially coherent.

$_{J}H_{c}$ and σ were determined for both casts in the single phase condition. The 20% Ti material had σ of 47.5 emug^{-1} while that of the 17.5% Ti alloy was 60.5 emug^{-1}. In each case, these values are the mean of ten determinations where the range was about ±1 emug^{-1}. As with Malcolloy σ was measured on small solid samples. $_{J}H_{c}$ ranged from 45 to 56 Oe with a mean of 49 Oe for the 20% Ti alloy and from 50 to 67 Oe with a

TABLE 20

VARIATION OF J^{H}_{c} AND σ OF THE 17.5% TI ALLOY ON AGEING

450°C			500°C			550°C		
Time hrs.	J^{H}_{Oc}	σ emug^{-1}	Time hrs.	J^{H}_{Oc}	σ emug^{-1}	Time hrs.	J^{H}_{Oc}	σ emug^{-1}
0	60	60.5	0	60	60.5	0	60	60.5
5	69	60.2	2	71	-	1	69	61.0
10	77	62.1	5	82	-	5	101	-
20	89	61.9	10	101	60.0	24	154	-
66	140	60.7	23	135	-	48	160	-
90	195	61.3	47	189	-	96	231	60.3
114	229	60.4	71	201	61.1	102	232	-
138	220	61.1	95	233	-	126	202	60.0
			101	230	60.7			

700°C			750°C		
0	60	60.5	0	60	60.5
½	154	60.1	½	114	-
1	174	-	1	185	-
2	223	-	2	190	-
5	223	-	5	170	61.1
10	207	60.9			

room of 60 Oe for the material with 17.5% Ti. In each case the $_{J}H_{c}$ of five different samples was determined. During ageing $_{J}H_{c}$ and σ of the 17.5% Ti alloy varied as shown in Table 20.

It can be seen that there was no significant change in σ during ageing. $_{J}H_{c}$ increased and then decreased reaching a peak value of about 230 Oe at all temperatures except 750°C where the peak value was 190 Oe.

The lack of variation in σ can be explained as follows. According to the phase diagram the weight fraction of α after full precipitation in the 17.5% Ti alloy, is about 0.13. σ of the precipitate will be a little lower than that of pure cobalt because of about 2% titanium in solution, 158 emug^{-1}, is a reasonable estimate based on a linear dilution law. Assuming σ of the matrix phase γ to be equal to that of the 20% Ti alloy, i.e. 45.5 emug^{-1} it is easily shown that σ of the 17.5% alloy after full precipitation of α should be about 63 emug^{-1}, i.e. very similar to the solution treated value.

The relatively low level of $_{J}H_{c}$ achieved is not surprising in view of the magnetic matrix. Furthermore, if coercivity was due to the presence of the α precipitate which is f.c.c. and thus has low crystal anisotropy, a very small particle size of less than 200Å would be necessary to give single domain behaviour and high coercivity (see section 3.7.1. and Figure 39).

Unlike the Malcolloy alloys, where $_{J}H_{c}$ in the solution treated condition was too small to be measured, (<2 Oe), both the cobalt-titanium alloys exhibited significant coercivity, (>45 Oe), after solution treatment to give single phase γ. It cannot be assumed, therefore, that the coercivity of γ, after precipitation of α in the 17.5% Ti alloy, was insignificant in relation to the coercivity of the α particles. Indeed, since lattice strain can hinder domain boundary movement and thus increase coercivity (section 1.2), it is conceivable that coherency strain, which it has been suggested above, is induced in γ during precipitation, might result in the coercivity of γ increasing during ageing. It would not be impossible, therefore, for the

coercivity of the γ matrix to be greater than that of the α precipitate if the latter was larger than single domain size.

Unfortunately, therefore, because of the presence of the magnetic γ matrix and the uncertainty regarding the precise source of the coercivity it is difficult to interpret the properties of the cobalt-titanium alloys in the same terms as the Malcolloy alloys and no useful parallels can be drawn.

6.1. Introduction

A finely dispersed mixture of phases can be obtained in alloys of eutectic or eutectoid composition. Lamellar spacings of less than 1 μm are frequently observed. Tiller[76] and Chilton and Winegard[77] have shown that lamellar spacing in eutectics decreases as solidification rate increases. Thus, in the lead tin eutectic Chilton and Winegard observed a spacing of 1.5 μm in a directionally solidified sample, grown at 1.5 mm per minute; this spacing decreased to 0.5 μm, when the growth rate was increased to 18 mm per minute. Such a dispersion would be too coarse for single domain behaviour in either f.c.c. cobalt (d_o = 0.02 μm) or h.c.p. cobalt (d_o = 0.2 μm), but by suitable control of solidification conditions it is feasible that some approach to a single domain system might be achieved particularly in the case of the h.c.p. allotrope.

A number of workers[78-80] have reported the magnetic properties of eutectic alloys containing a ferromagnetic phase. The magnetic component, frequently iron but in some cases nickel or cobalt, was produced as elongated particles by directional solidification. The aim was to obtain shape anisotropic particles, approximating to single domains, and thus having high coercivity, but in most cases coercivity was low, i.e. <20 Oe. Exceptional results were those of Livingston[40], who achieved a coercivity of 925 Oe in the gold cobalt eutectic by cold drawing a directionally solidified sample (see section 1.2.2.), and those quoted in a patent specification[81] by Magnetfabrik Bonn where coercivities up to 700 Oe were reported for various, directionally solidified iron based eutectics. Much of this work has been reviewed by Calasso[39]. In every case, the observed coercivity was attributed to shape anisotropic particles and there was no suggestion, even when the magnetic component of the eutectic was cobalt, that crystal anisotropy might be primarily responsible.

In the case of the iron based eutectics patented by Magnetfabrik [81] the iron component of the eutectic structure must, presumably, have been sufficiently finely divided to approximate to a single domain system in order to give the reported coercivity. Since iron has low crystal anisotropy single domain size is small, i.e. around 200Å and high coercivity is only achieved with elongated particles. If a eutectic structure with this degree of sub-division, together with particle elongation, can be obtained, it seems likely that the conditions necessary to give high coercivity in a dispersion of h.c.p. cobalt, i.e. particles with diameter about 2000Å should be fairly easily achieved. Since the particles need not be elongated there should be no necessity for directional solidification.

In the majority of eutectic and eutectoid structures, the phases are distributed with a lamellar or rod-like structure, this is not ideal for high coercivity behaviour in a material with high crystal anisotropy because shape anisotropy may oppose crystal anisotropy and thus reduce coercivity. Furthermore, although lamella thickness may approach the diameter of a single domain particle, the dimensions in the perpendicular directions will be very much greater and the formation and movement of domain boundaries within the lamellae seems likely. Nevertheless, in view of the high levels of coercivity reported by Livingston[40] and Magnetfabrik[81], an examination of cobalt based eutectic and eutectoid alloys was thought to be worthwhile.

6.2 Structure and Magnetic Properties of the Eutectic Alloys

6.2.1. Alloy composition and preparation

Eutectic alloys were prepared to several compositions.

(i) The eutectic in the cobalt antimony system (Figure 52a [82]) at 25% (41 wt.%) Sb.

(ii) That in the cobalt niobium system (Figure 52b [83]) at 15% (21.5 wt.%) Nb.

(iii) The cobalt carbon eutectic (Figure 52c [84]) at 12.5% (2.9 wt.%) C.

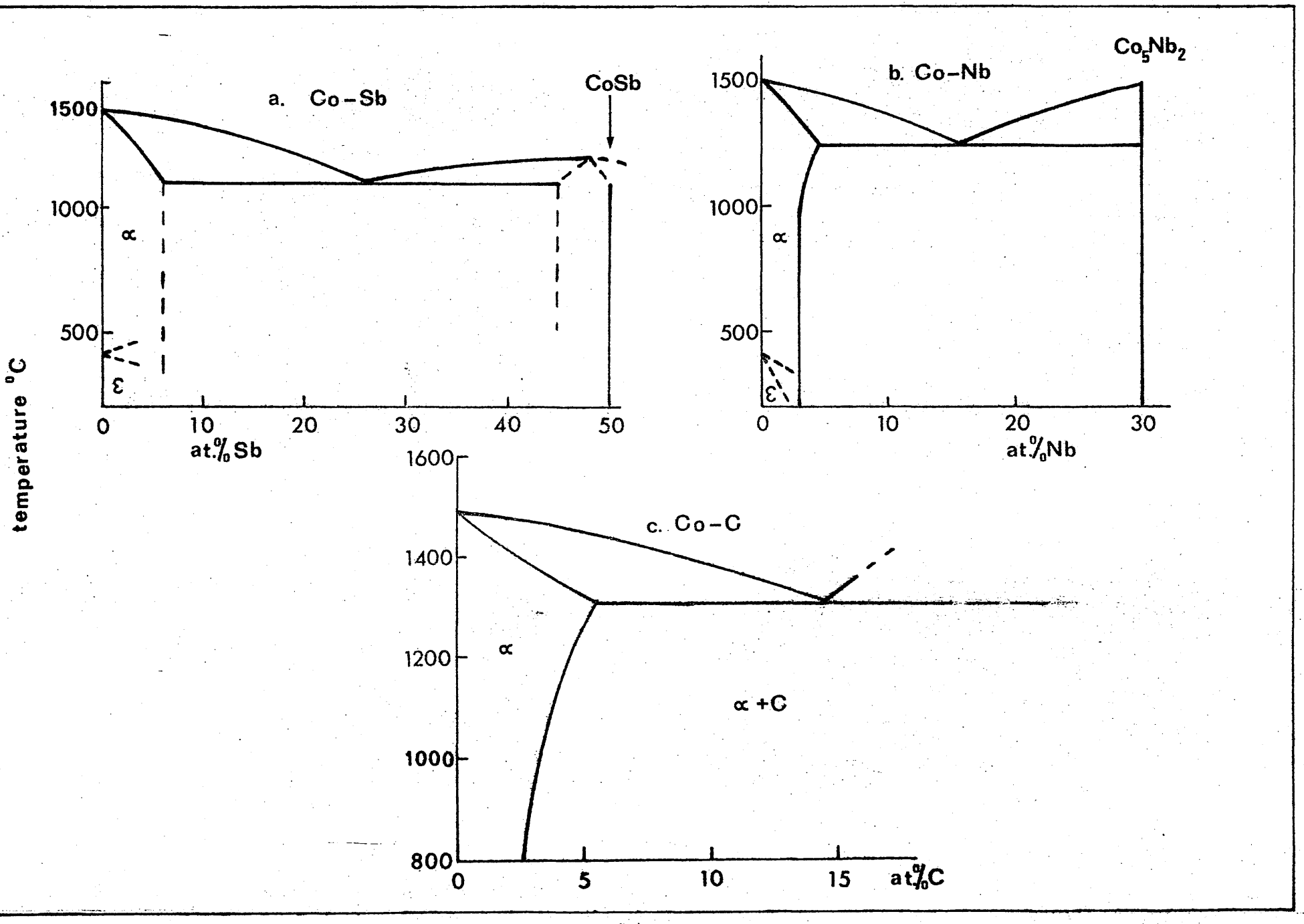
a. Co-Sb
CoSb
1500
1000
500
α
ε
0
10
20
30
40
50
at.% Sb
b. Co-Nb
Co_5Nb_2
1500
1000
500
α
ε
0
10
20
30
at.% Nb
temperature °C
c. Co-C
1600
1400
1200
1000
800
α
α +C
0
5
10
15
at.% C

Fig. 33 - Eutectic Alloys

a

Co Sb eutectic

x 1,500

b

Co C eutectic

x 1,500

c

Co C eutectic + 0.5% Fe/Si

x 1,500

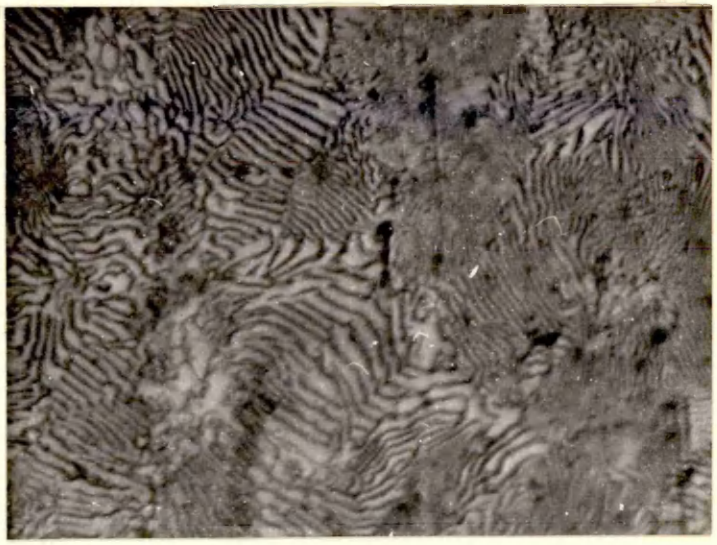

(iv) Four alloys approximating to the Co C eutectic but containing 0.25, 0.5, 1.0 and 2.0 wt.% ferro-silicon, (70 wt.% Si) respectively.

The alloys, of commercial purity (about 99.5 wt.%) were melted by induction heating under argon. The addition of Fe-Si to four of the Co C casts was based on the fact that Fe-Si has the effect of refining the iron graphite eutectic in grey cast iron[85]. It was possible that a similar effect might result from the addition of Fe-Si to the Co C eutectic alloy.

Because solidification rate was expected to influence the nature of the eutectic structure, samples of each molten alloy were allowed to solidify under different conditions. One sample from each was poured into a sand mould, another was chill cast in a small steel ingot mould and the third was shotted by pouring into water. The average cooling rates induced by sand and chill casting were measured as 4°C per second and 26°C per second, respectively. The shotted material, which was obtained by pouring into water with a depth of 90 cm from a height of 60 cm above the water surface, consisted of spheroidal granules ranging in diameter from 1 cm to 0.1 cm. The cooling rate was not measured but was certainly much greater than 500°C per second. The alloys were not analysed but metallographic examination confirmed that in each case the structure consisted almost entirely of the eutectic.

6.2.2. Structure and properties of the as cast eutectic alloys

The micro structures of the Co Sb and Co Nb alloys were normal eutectic structures; that of the Co Sb alloy after chill casting is shown in Figure 53 . The phases appeared to be in the form of lamellae or plates rather than rods. The Co C and Co C + Fe-Si alloys had an anomalous eutectic structure consisting of graphite flakes in a cobalt matrix; Figures 53b and 53c show the chill cast structures of the Co C and the Co C + 0.5% Fe Si alloys.

Using a calibrated eye-piece graticule it was possible to

TABLE 21

PROPERTIES OF COBALT BASED EUTECTIC ALLOYS IN THE AS CAST CONDITION AND AFTER HEAT TREATMENT FOR 30 HOURS AT 375°C.

Alloy	Condition	Sand Cast		Chill Cast		Shotted	
		σ emu$_{-1}$	J^H_c Oe	σ emu$_{-1}$	J^H_c Oe	σ emu$_{-1}$	J^H_c Oe
Co Sb	as cast	55.9	42	56.4	66	56.0	78
	30 hr. 375°C	56.1	43	56.2	73	57.0	109
Co Nb	as cast	72.1	36	71.6	49	71.0	67
	30 hr. 375°C	70.9	49	70.9	54	70.3	79
Co C	as cast	152.1	4	148.0	12	155.4	11
	30 hr. 375°C	153.0	6	150.2	18	153.0	15
Co C+	as cast	155.1	9	158.2	11	153.0	12
0.25 wt.% FeSi	30 hr. 375°C	-	19	-	18	-	20
Co C+	as cast	154.0	15	148.0	18	156.1	20
0.5 wt.% FeSi	30 hr. 375°C	-	23	-	35	154.7	44
Co C+	as cast	151.7	18	149.3	19	150.2	15
1.0 wt.% FeSi	30 hr. 375°C	-	29	-	22	-	40
Co C+	as cast	154.0	14	150.7	7	150.9	19
2.0 wt.% FeSi	30 hr. 375°C	-	31	-	19	-	37

obtain an approximate measure of the degree of sub-division in the various structures. In the lamellar Co Sb and Co Nb eutectics lamellar thickness decreased from an average of about 2μm in the sand cast samples to about 1μm in the shot.

In the case of the Co C and Co C + Fe-Si alloys average spacing between graphite flakes was measured. It can be seen from Figure 53 that the spacing within individual samples was very variable. The measurements are, therefore, regarded as giving only approximate indication of the degree of sub-division. As with the lamellar eutectics, the structure became finer as cooling rate increased. Thus in the Co C material (without Fe-Si) flake spacing decreased from about 8μm in the sand casting to about 4μm in the chill cast sample. There was, however, little or no difference between the chill cast and shotted structure. Fe Si had the anticipated effect of refining the structure. The average spacing was reduced by about a half at each of the cooling rates regardless of the size of the Fe Si addition. An additional effect was the appearance of clearly defined eutectic colonies (Figure 53c), flake spacing within the colonies was much lower than the average and in the shotted and chill cast samples was estimated as about 1μm.

$_{J}H_{c}$ and σ of all samples were determined and are shown in Table 21. Neither cooling rate nor the addition of Fe-Si had a consistent effect on σ but there was some variation in $_{J}H_{c}$. In general, this property increased as the structures became finer, but the highest value obtained was 78 Oe (Co Sb shot).

X-ray diffraction examination showed the cobalt rich phase in all the alloys to be a mixture of ε and α; ε predominated but the amount of α increased with cooling rate.

6.2.3. Properties of the eutectic alloys after heat treatment

Since the single domain size for ε is greater than that for α it was likely that $_{J}H_{c}$ might be increased if the cobalt rich components

Fig. 54 - Co-Si phase diagrams

(a) Vogel and Rosenthal [87] and Hashimoto [88]

(b) Köster and Schmid [89]

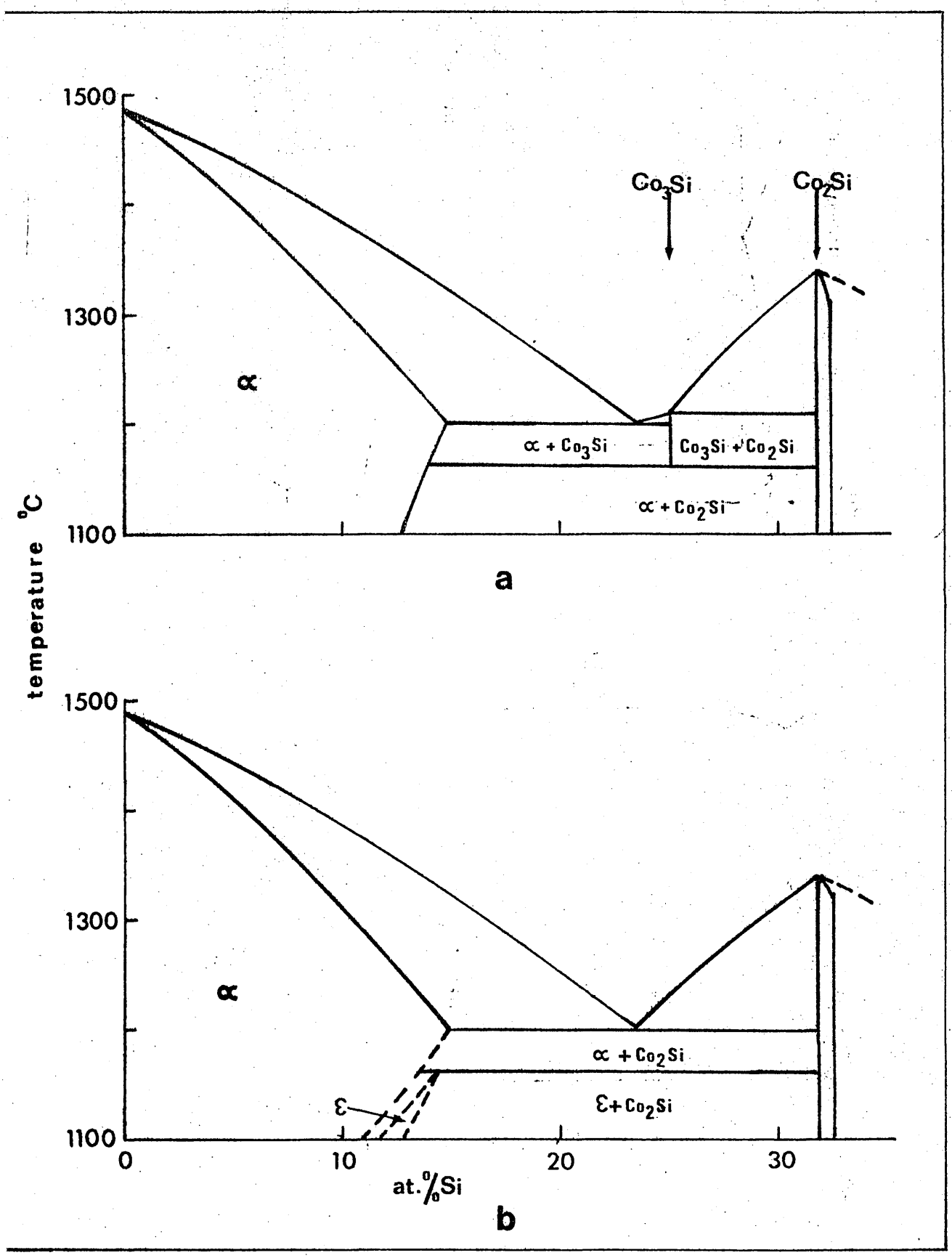

of the structures could be transformed entirely to ε. All the samples were, therefore, heat treated for 39 hours at 375°C and furnace cooled. Only very small traces of α were detected after heat treatment and as shown in Table 21 there was an increase in $_{J}H_{c}$ giving in the best case, the Co Sb shot, $_{J}H_{c}$ of 109 Oe.

6.3. Structure and Magnetic Properties of the Cobalt Silicon Eutectic/Eutectoid Alloy

6.3.1. The cobalt-silicon phase diagram

The earliest version of the cobalt silicon phase diagram derived by Lewkonja[86] (1908), indicates a eutectic reaction at 1205°C in which liquid containing 26.5% Si solidified to give α (f.c.c. cobalt rich solid solution) plus the intermetallic compound Co_2Si. Later workers[87,88,89] obtained similar temperatures for the reaction but placed the eutectic composition between 22.0 and 24.0% Si and detected a second isothermal reaction at 1160°C. The form of the diagram according to Vogel and Rosenthal[87] and Hashimoto[88] is shown in Figure 54a. According to these authors, the eutectic reaction produces α and the intermetallic compound Co_3Si, the latter decomposing eutectoidally to α and Co_2Si at 1160°C. Vogel and Rosenthal[87] observed the phase Co_3Si in quenched samples but do not report its crystal structure. Köster and Schmid[89] did not detect Co_3Si and interpreted the isothermal reaction at 1160°C as the peritectoid transformation of α + Co_2Si to ε, (Figure 54b).

In the context of the present work, the reactions proposed by Vogel and Rosenthal[87] and Hashimoto[88] (Figure 54b) are of particular interest. If, as they suggest, the eutectic reaction is followed by eutectoid decomposition of one of the components of the eutectic it is possible that the resulting structure may be sufficiently fine for an approach to be made to single domain behaviour in the cobalt rich phase.

Fig. 55 - Co Si Eutectic/Eutectoid Alloys

a

x 60

sand cast

x 1,500

b

shotted

x 1,500

c

sand cast
aged 56 hours
at 800°C

x 1,500

d

shotted
aged 166 hours
at 800°C

x 1,500

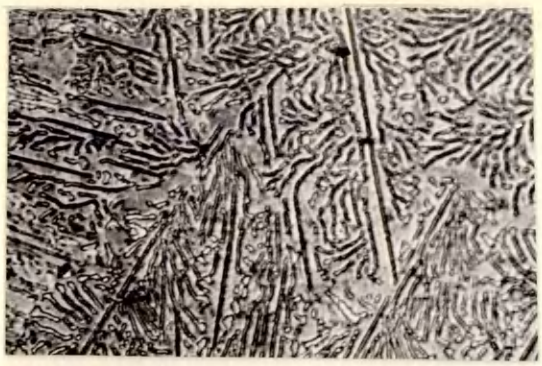

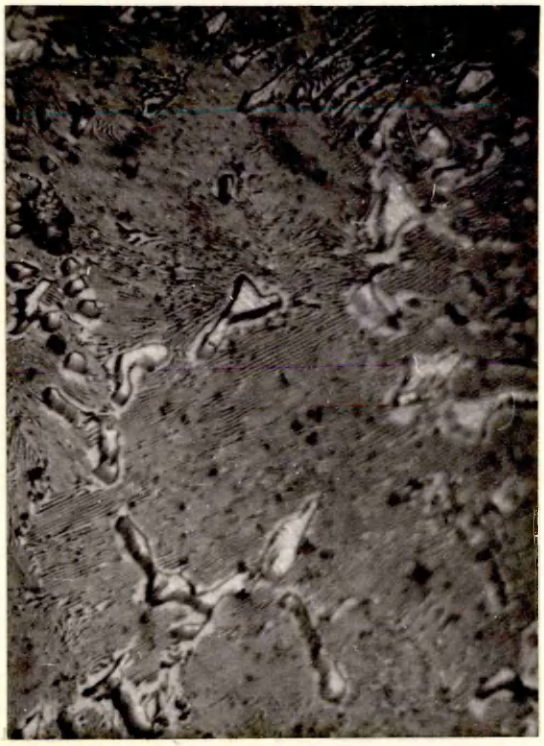

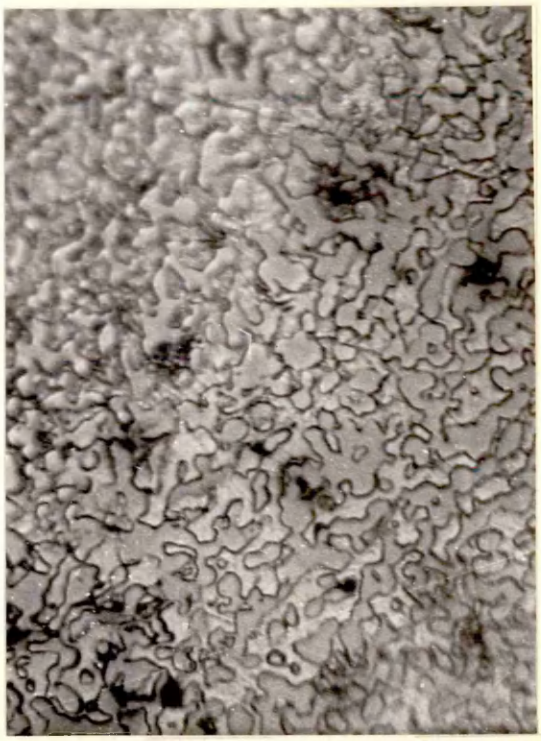

6.3.2. Structure and properties of as cast cobalt silicon alloys

Two casts were prepared using the technique described in section 6.2.1. One was sand cast and the other shotted. The analysed silicon content of the sand cast sample was 23.0% Si while that of the shot was 24.1% Si. The microstructure of the two casts are shown in Figures 55a (sand cast) and 55c (shot). The eutectic structure in the sand casting was much coarser than that of the shot but eutectoid decomposition of one of the eutectic phases was visible in the sand cast alloy. The eutectoid structure was clearly lamellar but the eutectic phases appeared to be rather more rod-like. (In Figure 55a the section photographed at high magnification was perpendicular to that at low magnification and a number of apparently equiaxed particles are present which may be sections through elongated rods). The phases present in both casts were identified by X-ray diffraction as cobalt (predominantly ε with only traces of α) and Co_2Si. (The latter was shown by Calle[90] to be orthorhombic with the following parameters, a = 7.095Å, b = 4.908Å, c = 3.730Å).

J^R_c and σ were 68 Oe and 56.2 $emug^{-1}$ respectively in the sand casting and 93 Oe and 58.2 $emug^{-1}$ in the shot.

6.3.3. Structure and properties of heat treated cobalt silicon alloys

(a) Structure

From the micro structures it appeared that eutectoid decomposition was incomplete in the sand cast material and completely suppressed in the shot (Figure 55a and c). Both casts were, therefore, heat treated at 800°C with the aim of bringing the eutectoid reaction to completion. The samples were quenched to room temperature periodically for magnetic testing and metallographic examination. In the sand casting an increasing amount of eutectoid decomposition was observed metallographically during heat treatment; the reaction appeared to be complete after 56 hours at 800°C (Figure 55b). The eutectoid structure did not appear in the shotted alloy but as treatment progressed, the eutectic phases became rather coarser

TABLE 22

THE EFFECT OF AGEING AT 800°C ON THE PROPERTIES OF COBALT SILICON EUTECTIC/EUTECTOID ALLOYS

Sand cast			Slotted		
heat treatment hrs. at 800°C	J^{M}_{c} Oe	σ emu$_{g}^{-1}$	heat treatment hrs. at 800°C	J^{R}_{c} Oe	σ emu$_{g}^{-1}$
0	68	56.2	0	93	58.2
4	73	55.9	1	137	-
16	86	55.8	8	112	-
32	84	56.3	32	88	57.8
36	82	56.0	64	85	-
56	81	55.8	128	75	-
64	78	56.0	168	70	58.4

and the colony structure was lost (Figure 55d). $_{J}H_{c}$ and σ at various stages during heat treatment are shown in Table 22. Little variation in σ was observed but in both alloys $_{J}H_{c}$ initially increased and then decreased as treatment was continued. It can be seen that $_{J}H_{c}$ of the shot was higher and showed a greater initial increase during heat treatment than that of the sand cast alloy. Since the eutectoid structure in the sand casting was finer than the eutectic in the shot, these results are not consistent with the degree of sub-division of the phases. This is not particularly surprising since, at such relatively low levels of coercivity, other factors, such as strain and particle shape may have a significant influence.

X-ray diffraction examination after heat treatment indicated the phases present in both alloys to be ε (plus traces of α) and Co_2Si. There were no lines which could be attributed to the compound Co_3Si. In the as cast condition Co_2Si was the predominant phase but during heat treatment the intensity of the ε lines increased while that of the Co_2Si pattern decreased. It was concluded that the amount of ε increased at the expense of Co_2Si during heat treatment. This suggests that Co_2Si, supersaturated with cobalt, was retained on casting, and that cobalt was precipitated during subsequent heat treatment. A reaction of this type is not predicted by either of the phase diagrams in Figure 54 and is difficult to reconcile with the apparently eutectoid structure in the sand cast material.

Two samples from the shotted alloy were heat treated for 1 hour at 1175°C under argon and quenched. One sample, containing granules up to 1 cm in diameter was water quenched and the other, consisting of smaller granules between 0.1 and 0.5 cm diameter, was quenched in liquid nitrogen to give a more rapid cooling rate. According to Vogel and Rocenthal[87] and Nishirota[88] (Figure 54a) the structure of the alloy at 1175°C should be largely Co_3Si which would be expected either to be retained by quenching

a

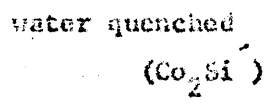
water quenched
(Co_2Si')

x 500

b

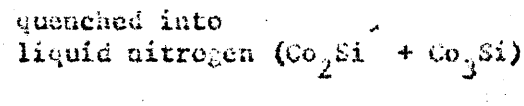
quenched into
liquid nitrogen (Co_2Si' + Co_3Si)

x 500

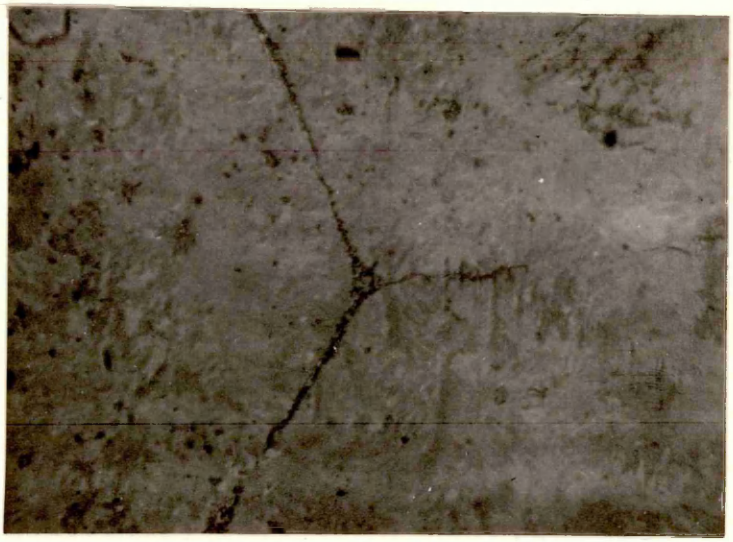

or to decompose to give the eutectoid of cobalt and Co_2Si. It was possible that, if a single phase could be retained by quenching, the eutectoid components might be produced as a fine dispersion on subsequent heat treatment.

The structures produced by quenching were quite surprising. The water quenched material contained isolated pools of a light etching phase in a matrix which appeared to have formed by a massive transformation, (Figure 56a). Electron metallography using carbon replicas showed the matrix to be a single phase- X-ray diffraction indicated the presence of a small amount of h.c.p. and f.c.c. cobalt (presumed to be the light etching phase) but the predominant pattern was almost identical to that of Co_2Si. This phase, which could not be stoichiometric Co_2Si will be referred to as Co_2Si'. It is interesting to note that the phase thought by Vogel and Rosenthal [87] to be Co_3Si was described as "a grey phase", this may well have been Co_2Si'. The structure at the centre of the small granule quenched into liquid nitrogen was identical to that of the water quenched samples but nearer the surface the structure was as shown in Figure 56b. This photograph can be interpreted as showing the growth of Co_2Si' from another phase partially retained by the quench. Using the Beaumaris camera it was possible to obtain a diffraction pattern from the surface of one of the granules. The existence of a small amount of Co_2Si' was confirmed but a number of other lines were present which presumably represented the new phase. A certain amount of line broadening made precise analysis of the unknown pattern difficult but it was possible to index all the lines as a tetragonal phase with the approximate parameters $a = 8.41\text{Å}$, $c = 5.81\text{Å}$. It is reasonable to suppose that this phase was Co_3Si partially retained at room temperature by the very rapid quench. No previous reference to the structure and lattice parameter of Co_3Si has been found.

(b) Magnetic properties after quenching

$_JH_c$ and σ were measured on granules from both samples. The water quenched material (largely Co_2Si') had relatively high $_JH_c$ with some variation between different granules, values ranging between 190 and 245 Oe.

TABLE 23

THE EFFECT OF AGEING ON THE PROPERTIES OF COBALT SILICON SHOT QUENCHED FROM 1175°C

Water Quenched (to give Co_2Si).

450°C			500°C			550°C			650°C		
Time hrs.	J^H_{Oe}	σ emug^{-1}	Time hrs.	J^H_{Oe}	σ emug^{-1}	Time hrs.	J^H_{Oe}	σ emug^{-1}	Time hrs.	J^H_{Oe}	σ emug^{-1}
0	198	58.1	0	190	57.8	0	245	58.7	0	232	58.0
10	206	-	4	210	-	4	262	-	1	245	-
50	214	-	9	228	-	10	272	-	4	190	-
90	215	58.4	17	226	-	20	272	-	8	192	-
150	220	-	40	235	-	44	275	-	24	187	-
198	202	-	64	239	57.4	68	254	58.1	48	178	57.7
			88	242	-	92	202	-	72	156	58.2
			136	221	-	116	120	58.4	100	90	57.6

Quenched into liquid nitrogen (to give predominantly Co_3Si)

300°C			400°C			500°C			700°C		
0	111	66.0	0	110	65.7	0	109	66.2	0	111	66
1	190	58.0	1	256	55.2	1	285	54.3	1	188	54.3
2	194	57.7	2	256	-	2	257	-	3	168	-
7	207	-	5	255	56.1	5	256	-			
20	215	57.2	90	260	-	30	249	53.8			
						65	247	-			
						89	242	54.1			

There was no relationship between ${}_JH_c$ and granule size. σ varied between 57.8 and 58.7 $emug^{-1}$. The properties of the sample quenched into liquid nitrogen were even more variable but ${}_JH_c$ was consistently lower (between 85 and 140 Oe) and σ consistently higher (between 62 and 72 $emug^{-1}$) σ was highest and ${}_JH_c$ lowest in the smallest granules which contained a minimum of Co_2Si'. It was concluded that the σ of Co_3Si was considerably greater than that of Co_2Si'. ${}_JH_c$ of Co_2Si' was relatively high and it is likely that the coercivity of the liquid nitrogen quenched samples, which contained both phases, was due to Co_2Si' and that ${}_JH_c$ of Co_3Si was quite low.

(c) Effect of ageing quenched cobalt silicon samples

Samples consisting of the smallest liquid nitrogen quenched granules (diameter less than 0.2 cm), containing largely Co_3Si, and samples of the water quenched material (Co_2Si'), were aged at various temperatures between 300°C and 650°C. Samples were water quenched to room temperature periodically for magnetic testing and metallographic examination. Values of σ and ${}_JH_c$ obtained are shown in Table 23. In the case of the material containing Co_2Si' (water quenched) there was no variation in σ but ${}_JH_c$ first increased and then decreased at all temperatures. After 48 hours at 650°C and 68 hours at 550°C the first signs of eutectoid decomposition to Co_2Si and ε were observed by optical metallography and X-ray diffraction. As the eutectoid reaction progressed during further treatment there was a rapid decrease in ${}_JH_c$. The properties of the Co_3Si samples (nitrogen quenched) changed, after only 1 hour at all the temperatures explored, to values typical of Co_2Si' i.e. σ decreased and there was a substantial increase in ${}_JH_c$. Metallographic and X-ray examination after 1 hour at 300°C confirmed that transformation to Co_2Si' had taken place. During subsequent ageing the properties varied in a similar manner to that observed for the water quenched material.

6.3.4. Summary

In general values of $_{J}H_{c}$ associated with the eutectic and eutectoid structures in cobalt silicon alloys were at a similar level to those measured on the cobalt antimony eutectic discussed earlier. It was, however, possible to achieve a much higher $_{J}H_{c}$ up to 285 Oe, by quenching from 1175°C and ageing. The effect of quenching from this temperature was either to produce a phase with a crystal structure similar to Co_2Si but containing excess cobalt (Co_2Si'), or, if the quench was sufficiently rapid, to retain a different phase thought to be tetragonal Co_3Si. The c of Co_2Si' was lower than that of Co_3Si but $_{J}H_{c}$ of Co_2Si' was relatively high (up to 245 Oe in the quenched condition). On heat treatment Co_3Si transformed very readily to Co_2Si' and the $_{J}H_{c}$ of Co_2Si' increased slightly giving the best values observed for this system, (up to 285 Oe). This increase was not associated with the appearance of the eutectoid constituents. The eutectoid reaction did not occur until much later in the heat treatment process and resulted in a decrease in $_{J}H_{c}$.

The reason for the relatively high $_{J}H_{c}$ of Co_2Si' has not been established. Since, this material was shown to have a single phase structure it is clear that single domain particle processes are not involved. Presumably, therefore, the coercivity must arise due to inhibited domain boundary movement. Various factors such as inhomogeneous strain, the presence of structural defects, etc., could be responsible (see section 1.1.2.) It should also be pointed out that the orthorhombic crystal structure of Co_2Si' might well exhibit significant magneto-crystalline anisotropy. If this is the case, domain boundary energy would be high relative to that in a cubic structure and a boundary would have a greater tendency to remain at a low energy site. Coercivity would, therefore, be relatively high if boundary 'pinning sites' were present.

Footnote:

The results in section 6.3.3.(a) which confirm the existence of a compound Co_3Si are substantiated in recent work by J. Van Den Boomgaard and F. H. A. Carpay, (Acta Met. 20 473 (April) 1972. These authors did not observe either Co_2Si or Co_3Si but inferred the existence of the latter from eutectic plus eutectoid structures similar to those shown in Figures 52a and 52b of this Thesis. Thermal analysis showed Co_3Si to form, on cooling, by a peritectic reaction at about 1210°C followed by eutectoid decomposition at about 1170°C.

6.4. The Properties of Cobalt Based Eutectic Alloys After Comminution

Apart from the relatively high $_jH_c$ of the Co_2Si' phase in quenched cobalt silicon samples the properties of the eutectic and eutectoid alloys studied were disappointing with $_jH_c$ not exceeding about 100 Oe. The Co C and Co C + Fe-Si alloys were particularly poor with $_jH_c$ not exceeding 50 Oe. In addition to being too coarse for single domain behaviour to occur it is significant that the Co C eutectic consisted of a continuous cobalt matrix only partially divided by graphite flakes. From the observed coercivity it is clear that the formation and movement of domain boundaries were largely unrestricted in this type of structure. It was possible, however, that if the continuity of the cobalt matrix could be reduced, domain boundaries would move less freely and coercivity would be increased. This was easily achieved by taking advantage of the brittleness of the graphite flake structure. A sample was crushed and milled with the aim of causing fractures associated with the graphite flakes and thus obtaining discrete cobalt particles at least as small as the flake spacing in the bulk material. The alloy used was the Co C + 0.5% Fe-Si shot after 30 hours at 375°C. Samples from the Co Sb shot after 30 hours at 375°C, and the sand cast Co Si alloy after 64 hours at 800°C (eutectoid decomposition complete) were subjected to the same treatment with the similar aim of breaking up the lamellae in the eutectic and eutectoid structures. In addition a sample of Co Si shot after water quenching from 1175°C (Co_2Si') was milled. In this case the aim was to examine the properties of Co_2Si' in finely divided form.

Crushing was carried out by hand, in a hardened steel pestle and mortar, until the material would pass a 200 mesh sieve (particles about 80 μm diameter). Further size reduction was achieved in an attrition mill in which the powder, mixed with a large number of 3 mm diameter,

TABLE 24

PROPERTIES OF EUTECTIC AND EUTECTOID ALLOYS AFTER COMMINUTION

Co C + 0.5% Fe-Si shot
30 hrs. at 375°C
(anomalous eutectic)

Condition	$J_{0c}^{H_c}$	σ emu g^{-1}	size μm
Bulk	44	154.7	-
Crushed	212	153.0	-200 mesh
Milled 8 hrs.	185	110	4.5
" 16 hrs.	210	103	2.5
" 20 hrs.	283	84	2.0
" 24 hrs.	335	74	1.7
" 32 hrs.	386	56	~1.0
" 48 hrs.	458	40	1.5
" 56 hrs.	460	38	~1.0
" 72 hrs.	572	21	~1.0

Co Sb shot
30 hrs. at 375°C
(normal eutectic)

Condition	$J_{0c}^{H_c}$	σ emu g^{-1}	size μm
Bulk	109	57.0	-
Crushed	187	58.1	-200 mesh
Milled 4 hrs.	317	46.9	1.8
" 16 hrs.	435	19.2	1.0

Co Si sand cast
64 hrs. at 800°C
(eutectoid)

Bulk	78	56.0	-
Crushed	261	56.2	-200 mesh
Milled 1 hr.	263	55.5	12
Milled 3 hrs.	259	54.6	8
" 5 hrs.	259	54.2	6
" 13 hrs.	272	48.9	3
" 20 hrs.	292	39.7	2

Co Si shot
1175°C water quench
(Co_2Si*)

Bulk	145	52.8	-
Crushed	323	65.3	-200 mesh
Milled 4 hrs.	245	50.6	1.5
" 14 hrs.	203	47.8	1.4
" 30 hrs.	236	10.0	1.0

Co Si sand cast
64 hrs. at 800°C
properties of size fractions

	$J_{0c}^{H_c}$	σ emu g^{-1}	size μm
Milled 3 hours			
coarse fraction	236	54.3	12
fine fraction	321	53.0	4
very fine fraction	341	50.7	2
Milled 5 hours			
coarse fraction	230	54.2	7
fine fraction	300	51.6	5
very fine fraction	343	45.3	2
Milled 13 hours			
coarse fraction	268	50.1	4
fine fraction	349	48.6	2
very fine fraction	372	38.4	1.5

hardened steel balls was stirred at 250 rpm by a stainless steel paddle. The mixture of balls and powder, together with petroleum ether as a milling medium were contained in a 600 ml. stainless steel beaker. Argon was passed into the beaker during milling to minimise oxidation of the powder.

Milling was interrupted periodically for the determination of σ, $_JH_c$ and particle size. The technique used for estimating average particle size on mounted powder samples has been described in section 2.4.2. The values obtained together with magnetic properties are shown in Table 24.

In all the alloys there was a large decrease in σ during milling, which could only be attributed to oxidation of cobalt. The presence of large amounts of Co_3O_4 was detected by X-ray diffraction in extensively milled samples and a very fine black constituent, assumed to be oxide, was observed metallographically. The water quenched Co Si shot differed from the other alloys in that there was an initial increase in σ. This could not be correlated with any phase change detectable by X-ray diffraction and, apart from the appearance of the oxide, no phase changes were observed in any of the alloys during milling. There was, however, increased line broadening as milling progressed, this was presumably due to mechanically induced strain. Quite large increases in $_JH_c$ were induced by crushing alone and, with the exception of the water quenched Co Si sample, $_JH_c$ continued to rise during milling. The atypical behaviour of the water quenched Co Si alloy in terms of both σ and $_JH_c$ was not surprising since this material had the orthorhombic Co_2Si structure whereas the magnetic component in the other alloys was h.c.p. cobalt. In all cases particle size was reduced by milling and in the Co + 0.5% Fe-Si alloy, which was subjected to the most prolonged milling treatment, the ultimate value was much lower than the flake spacing in the bulk alloy. It is possible that the extensive oxidation, indicated by X-ray diffraction and by the very marked fall in σ was a contributory factor in reducing the size of the metal particles.

Fig. 37 Intrinsic coercivity vs particle size of milled eutectic and eutectoid alloys

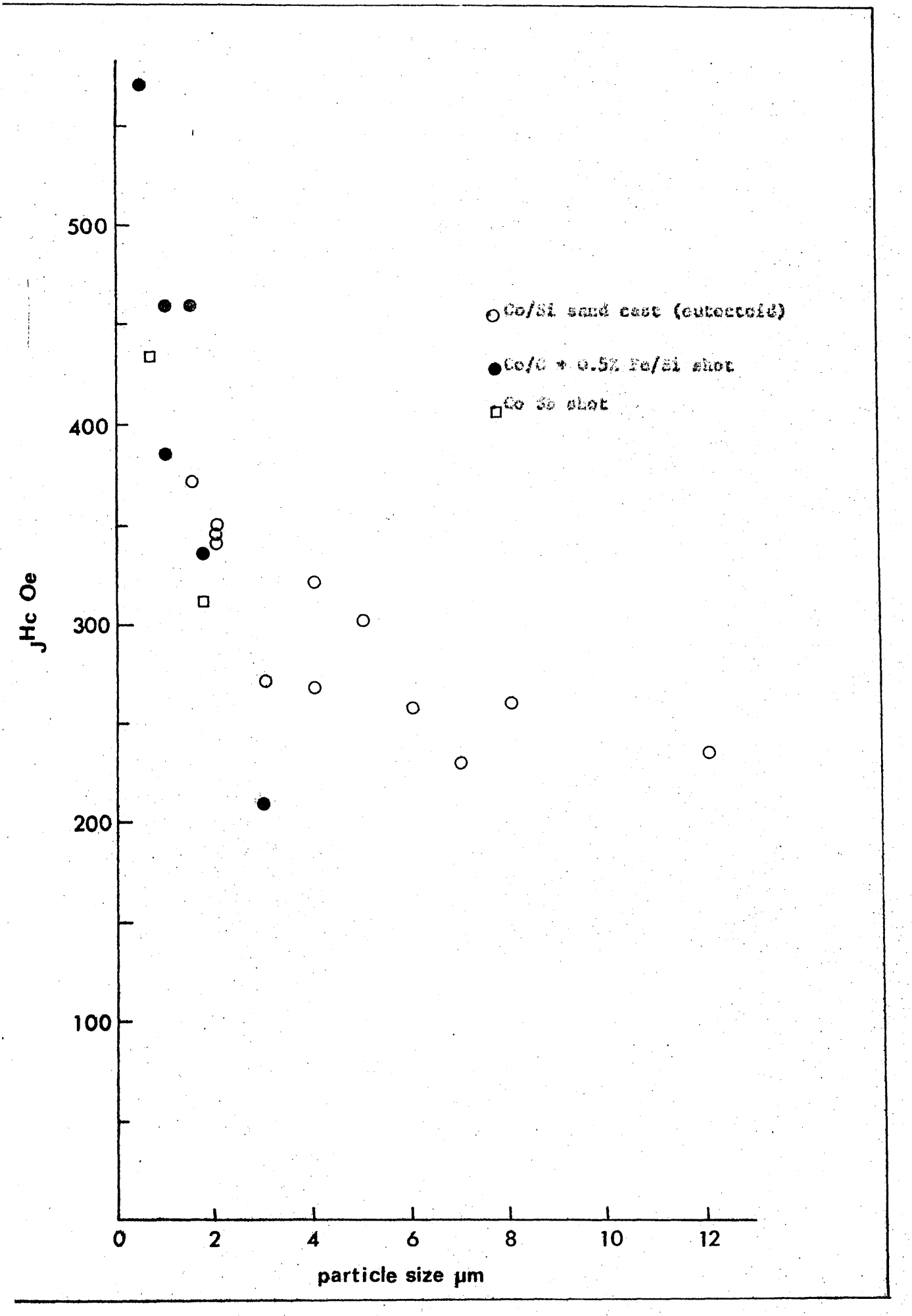

In the early stages of milling a wide range of particle sizes was observed. This was particularly true in the case of the sand cast Co Si powder and an attempt was made to separate this material into size fractions in order to obtain a more realistic relationship between particle size and coercivity. This was achieved by stirring the powder into a fairly viscous mixture of equal parts of ethanol and glycerol. The powder was allowed to settle for a few seconds after which the liquid, along with a fine fraction of the powder, was decanted. The liquid and fines were then re-stirred and held for a rather longer period before the liquid containing the finest fraction was again decanted. By selecting suitable settling times it was thus possible to obtain three approximately equal fractions. Particle size, d and $_{J}H_{c}$ of fractions from samples milled for 3, 5, and 13 hours are shown at the end of Table 24.

In Figure 57 values of $_{J}H_{c}$ for the Co Si sand cast size fractions, the Co C + 0.5% Fe-Si shot and the Co Sb shot, are plotted against average particle diameter. It can be seen that the results show a logical trend with $_{J}H_{c}$ increasing rapidly as particle diameter falls below about 2μm.

6.5. Temperature Dependence of $_{J}H_{c}$ of Eutectic Alloys

In the case of the Malcolloy alloys, discussed earlier, it was possible to evaluate the influence of the crystal anisotropy of ε on the permanent magnet properties by measuring the reversible temperature dependence of $_{J}H_{c}$, (section 3.3.). The results of similar measurements made on some of the eutectic and eutectoid alloys are shown in Table 25 and Figure 58. It can be seen that in all cases $_{J}H_{c}$ varied with temperature and that the changes were largely reversible. With the exception of the water quenched Co Si alloy, which consisted largely of the phase Co_2Si', the magnetic component in the samples tested was cobalt, with the h.c.p.(ε) structure predominating. The influence of the crystal anisotropy of this phase was indicated by the continuous decrease in $_{J}H_{c}$ with increasing

Fig. 56 - Temperature dependance of $_jH_c$ of eutectic and eutectoid alloys

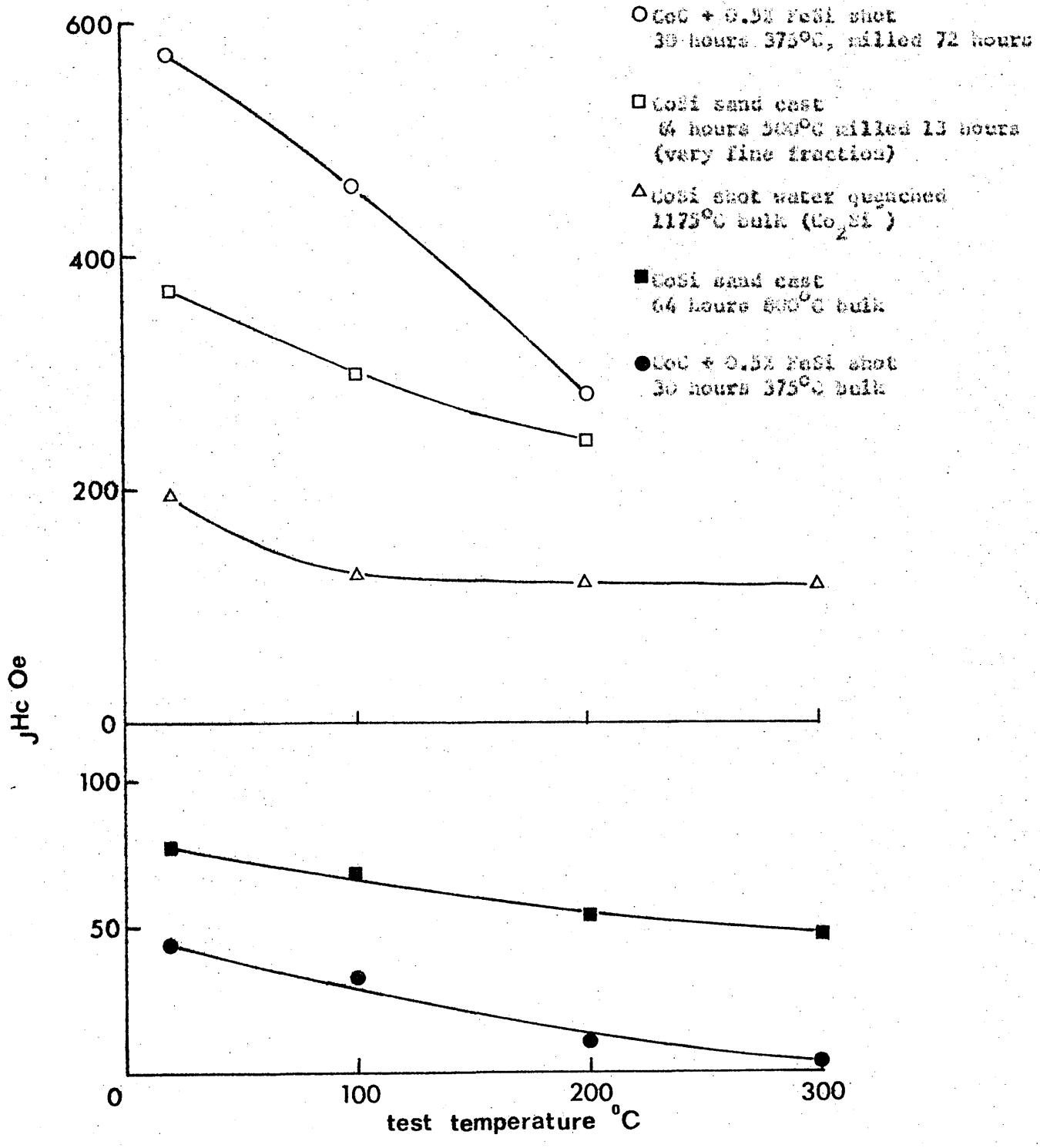

TABLE 25

TEMPERATURE DEPENDANCE OF $_{J}{}^{H}{}_{c}$ OF EUTECTIC AND EUTECTOID ALLOYS

CoC + 0.5% Fe-Si shot 30 hours at 375°C			Co Si sand cast 64 hours at 800°C		
Temp. °C	$_{J}{}^{H}{}_{c}$ Bulk, Oe	Milled 72 hours	Temp. °C	$_{J}{}^{H}{}_{c}$ Bulk, Oe	Milled 13 hours (very fine fraction)
20 (RT)	44	572	20 (RT)	78	372
100	34	460	100	69	300
200	10	280	200	54	243
300	4	-	300	40	-
20 (RT)	45	567	20 (RT)	72	371

CoSi shot, water quenched 1175°C (Co_2Si)

Temp. °C	$_{J}{}^{H}{}_{c}$ Bulk, Oe
20 (RT)	198
100	127
20 (RT)	193
200	120
20 (RT)	195
300	116
20 (RT)	188

temperature. Even in the case of the Co C + 0.5% Fe-Si alloy, where $_{J}H_{c}$ at room temperature was only 44 Oe, the observed temperature dependence can be interpreted in terms of the anisotropy of c.

It has been suggested that the orthorhombic structure of Co_2Si' (water quenched Co Si alloys) might exhibit significant crystal anisotropy and that this may be, in part, responsible for the relatively high $_{J}H_{c}$ (up to 285 Oe) of this phase. The crystal anisotropy of magnetic materials other than c is known to be temperature dependant. The nature of the dependence in the case of Co_2Si' is unpredictable but the fact that there was a reversible decrease in $_{J}H_{c}$ between room temperature and 100°C supports the possibility that $_{J}H_{c}$ was influenced by crystal anisotropy.

7.1. The Malcolloy Alloys

A large part of this thesis (chapters 3 and 4) has dealt with a detailed examination of the Malcolloy alloys. Experiments aimed at improving the permanent magnet properties of these materials were largely unsuccessful but the mechanisms responsible for the observed properties and the main factors affecting the coercivity are now understood.

The work confirms the general conclusion of Masumoto et al[41-49] that the high coercivity induced in the Malcolloy alloys during ageing is due to the precipitation of a fine dispersion of cobalt. In all the alloys (Figures 9-13, 44 and 49), the highest values of $_{J}H_{c}$ were obtained by ageing at temperatures below 600°C. The cobalt precipitate present at room temperature after ageing at these temperatures was ε, and high temperature X-ray diffraction showed that this phase was precipitated at the ageing temperature despite the fact that α was the thermodynamically stable form. Prolonged ageing of the 28% Al alloy at 600°C resulted in the eventual transition of an initially ε precipitate to α and in the higher temperature range, 650-750°C, both allotropes were precipitated with the amount of α increasing as ageing time and temperature were increased. Thus, in all the alloys the highest values of $_{J}H_{c}$ were observed when the precipitate was entirely ε. Electron metallography (Figure 8) showed the ε particle size in samples with high $_{J}H_{c}$ to be of the right order for single domain behaviour (less than 0.2 μm), and the reversible temperature dependence of $_{J}H_{c}$, although influenced by other factors which are not fully understood, was found to be roughly compatible with the variation of the crystal anisotropy of ε with temperature. It was concluded, therefore, that the coercivity of these alloys is due to the presence of a fine dispersion of ε approximating to a single domain system and exhibiting high crystal anisotropy.

The possibility of deriving high coercivity from the crystal anisotropy of ε has been recognised for many years and was discussed in some detail by McCaig[31]. The Malcolloy alloys are, however, the only permanent magnet materials known to derive their properties from this factor. The properties of the 28% Al binary alloy are a little lower than those calculated in section 1.2.1. for randomly aligned, single domain particles of ε with about 50% volume packing. This is consistent with the phase diagram of the Co-Al system which indicates a precipitate volume fraction of around 0.4 in the 28% Al alloy, (Figures 3 and 27). Maximum $_JH_c$ achieved in practice, (approaching 2000 Oe in the 38% Al alloy), was much lwer at room temperature than predicted by theory for single domain particles of ε (in excess of 4000 Oe, Figure 17). Several reasons for this (non-coherent rotation of magnetisation, presence of multi-domain particles, particle imperfection, etc.,), have been discussed and in fact, the approach to the theoretical level is probably as close as that achieved in any known permanent magnet material.

Because the properties of these alloys depend on the formation of a metastable precipitate of ε rather than stable α the mechanism by which the h.c.p. allotrope is formed is of interest. Using an X-ray technique similar to the rotating crystal method it was possible to show that the ε precipitate was oriented relative to the b.c.c. (β) matrix in a manner approximating to the Burgers relationship, i.e. {0001} ε approximately parallel to {110} β and $\langle 11\bar{2}0\rangle_\varepsilon$ approximately parallel to $\langle 111\rangle_\beta$. One feature of this relationship is that $\{1\bar{1}00\}$ ε is parallel to $\{112\}_\beta$, and Figure 24 shows that the atomic arrangements on these two planes are similar with mismatch less than 2%. It would thus be possible for $\{1\bar{1}00\}_\varepsilon$ and $\{112\}_\beta$ to form a partially coherent interface between precipitate and matrix. Examination of the atomic arrangement in planes of low indices (up to {221}) in α and β shows that in no case is mismatch less than about 12%. Coherency between α and β is, therefore, unlikely. Since surface energy makes an important contribution to the total energy of small particles

it is concluded that metastable ε forms preferentially to stable α because of the lower surface energy associated with a partially coherent interface.

The effect of metastable precipitation on the compositions and amounts of phases produced during ageing was explored using magnetic and X-ray phase analysis. It was shown that the ε precipitate was essentially pure cobalt and the β in metastable equilibrium with ε had a higher aluminium content than that predicted by the equilibrium phase diagram for β present after precipitation of stable α, (Figure 27).

In the solution treated condition (single phase β) the alloys were strongly magnetic at room temperature. During ageing T_c of β approached room temperature and $\sigma\beta$ at room temperature decreased. Thus during precipitation the high coercivity cobalt dispersion was in the presence of a low coercivity magnetic β matrix. It was shown, using magnetic analysis, (σ, T curves, Figure 30), that the effect of this phase was to suppress the high coercivity of the ε dispersion until late in the precipitation process when $\sigma\beta$ was very low. The observed relationship between $_JH_c$ and $\sigma\beta$ x weight fraction β was explicable in terms of a simple model based on the mixing of phases with widely differing coercivities, (Figure 31). Because the ε dispersion might reach optimum particle size and maximum coercivity at an early stage of precipitation when β remained strongly magnetic it was possible that a reduced $_JH_c$ would be detected as an apparent maximum later in the process when $\sigma\beta$ had decreased but particle size had increased. That this was the case in the 28% Al binary alloy was inferred from the nature of the temperature dependence of $_JH_c$ of a sample aged for 3 hours at 500°C, (Figure 15), and from the fact that Br of this alloy reached a peak much earlier than $_JH_c$ during ageing at 500°C. The variation in peak $_JH_c$ with composition of the binary alloys is thought to be due to the varying influence of the magnetic matrix rather than any fundamental difference in the properties of the cobalt dispersion, (Figure40).

Clearly the small amount of cobalt available for precipitation in alloys with low cobalt content would restrict particle growth and, therefore, increase the possibility of optimum particle size corresponding to the approach of σ_β to zero. It was also noted that activation energy for precipitation decreased as cobalt content increased. If it is assumed that this implies increased activation energy of diffusion it follows that the tendency for precipitate growth to occur will increase with increasing cobalt content.

The replacement of about 5% of the cobalt content of the 28% Al alloy by iron resulted in β remaining magnetic after ageing (Figure 50); there was a corresponding decrease in peak coercivity relative to that of the binary alloy, (Figure 49). The addition of titanium at the expense of cobalt, which according to Masumoto et al, has the effect of increasing coercivity, was, in the case of the particular alloy examined, almost exactly equivalent, in terms of the effect on $_JH_c$ and σ, to a similar increase in aluminium content (Figures 44 and 45). There was, however, a small increase in activation energy and it is possible that the beneficial effects reported by Masumoto et al for various ternary additions are due to restricted particle growth associated with increased activation energy of diffusion.

In an examination of the influence of solution treatment on maximum $_JH_c$ achieved during ageing at 450°C, it was found that the maximum value first increased and then decreased as solution treatment temperature and time were increased (Figures 42 and 43). The improvement was attributed to increased homogeneity which eliminated regions with high cobalt content in which relatively rapid particle growth could occur. At the same time, however, since equilibrium vacancy concentration increases with temperature, the number of vacancies retained on quenching could be increased so that diffusion and particle growth on ageing would be easier. The observed effects can be understood in terms of these two conflicting influences.

Attempts to induce anisotropic permanent magnet properties by means of field heat treatment of equiaxed and columnar samples were completely unsuccessful as were experiments aimed to give preferred orientation through mechanical work. The latter resulted in shattering of the specimens during forging at temperatures up to 1400°C.

It was noted that in the work of Masumoto et al and to a lesser extent in the present work, the ratio $B_r/4\pi J_s$ was frequently greater than the value of 0.5 expected for random assemblies of anisotropic single domain particles. This is thought to arise when the matrix phase is slightly magnetic and is magnetised by local fields associated with the cobalt particles. The result was that maximum $(BH)_{max}$ during ageing occurred while the matrix was still weakly magnetic and before peak $_JH_c$.

7.2. Cobalt, 17.5% Ti alloy

The 17.5% Ti alloy, which was the subject of a brief examination, was similar to Malcolloy in that cobalt can be precipitated from solid solution by a suitable heat treatment process. In this case, however, the precipitate was α and the $_JH_c$ was low. It is probable that the α particles were too large for single domain behaviour, i.e., greater than 200 Å, although this has not been confirmed. The matrix in this alloy remained magnetic throughout the ageing process but, after solution treatment, had a $_JH_c$ much greater than that of the matrix phase in Malcolloy. Since $_JH_c$ of the matrix may have increased during ageing it was difficult to define the influence of this phase on the magnetic properties of the material as a whole.

7.3. Eutectic and Eutectoid Alloys

In general, quite low values of coercivity were associated with the eutectic and eutectoid structures in the bulk condition but $_JH_c$ could, to some extent, be correlated with the degree of sub-division of the cobalt rich component of the structure and in some of the alloys

(Co Sb, Co Nb and Co C) there was a significant increase in $_JH_c$ when this phase was transformed, during heat treatment at 375°C, from a mixture of ε and α to give largely ε, (Tables 21 and 22). The temperature dependance of $_JH_c$ of the Co C + 0.5% FeSi shot (anomalous eutectic) and the CoSi sand casting (eutectoid), (Figure 58) was sufficiently marked to suggest the influence of the crystal anisotropy of ε.

The highest levels of coercivity (200-300 Oe) were achieved by quenching CoSi samples of eutectoid composition to give a phase (Co_2Si') with the crystal structure of the compound Co_2Si but with composition closer to Co_3Si. If a sufficiently rapid quench was employed, the phase retained was tetragonal Co_3Si which had low coercivity but this transformed readily to Co_2Si' on heat treatment at temperatures as low as 300°C. The reason for the rehtively high $_JH_c$ of Co_2Si' is not clear but it is pointed out that the orthorhombic structure of this phase is likely to exhibit some form of magneto-crystalline anisotropy. There was a reversible decrease in $_JH_c$ on heating from room temperature to 100°C, (Figure 58) which might be interpreted as indicating the influence of this factor.

Substantial improvement in the $_JH_c$ of eutectic and eutectoid alloys was achieved by comminution (Table 24). Initial increases, giving $_JH_c$ between 200 and 300 Oe, which were induced by crushing to -200 mesh, were attributed to a reduction in the continuity of the cobalt rich component of the structures. Further gains after prolonged milling were associated with decreasing particle size, (Figure 57), but were only achieved at the expense of σ. The fall in σ was due to oxidation of the cobalt rich phase and it is probable that particle size reduction was facilitated by the oxidation process. As with the bulk materials, the $_JH_c$ of the powdered alloys was found to vary with temperature in a manner compatible with the influence of the crystal anisotropy of ε.

7.4. General Conclusions

It is clear from this work that particles of ε approximating to single domains can be utilised as the basis of permanent magnet materials. However, magnets primarily based on cobalt must, because of the relatively high cost of this metal, have properties which are in some respect superior to those of existing materials if they are to be of practical use. In this respect the properties of finely divided ε dispersions present in high cobalt alloys have proved disappointing. Thus, in Malcolloy alloys, although ${}_{J}H_{c}$ approached 2000 Oe, B_r, $(BH)_{max}$ and H_c were low. These properties are related to $4\pi J_s$ which is dependant upon the volume fraction of precipitate present. In the highest cobalt Malcolloy alloy volume fraction of precipitate is limited to about 0.5 and even if the high B_r of such an alloy could be combined with the high ${}_{J}H_{c}$ associated with low cobalt contents, the overall isotropic properties would be inferior to those of a number of cheaper materials. The material would be greatly improved if these particles were aligned with <0001> axes parallel, giving anisotropic properties. Field heat treatment with this aim proved completely ineffectual and, because the crystal anisotropy of ε at elevated temperatures is quite different from that exhibited at room temperature, this technique would, at best, give <0001> ε directions parallel to a plane rather than inducing full alignment and the benefit in terms of magnetic properties would be small. The two problems of particle packing and particle alignment appear to set a limit to the properties of Malcolloy and no approach by which significant improvement might be achieved is obvious.

In the eutectic and eutectoid alloys ${}_{J}H_{c}$ was relatively low. Only a small number of alloys were studied and it is possible that other materials might have superior properties. It is likely, however, that even if ${}_{J}H_{c}$ was high the difficulties encountered in Malcolloy, i.e., particle packing and alignment, would arise. It may be that, if oxidation was avoided, powders with high ${}_{J}H_{c}$ and σ could be prepared by milling

eutectic or eutectoid alloys. In this respect the Co C (or Co C + FeSi) alloys would be the most useful since the carbon content in terms of weight is only 2.5% and σ is only a little lower than that of pure cobalt. Furthermore, the brittle graphite flake structure of these materials enables comminution to be more easily accomplished than would be the case for pure cobalt.

Whether produced by milling a eutectic alloy or by some other powder metallurgical technique, it seems that high coercivity ε powders in the form of aligned compacts with high density are more likely to give useful permanent magnet properties than are bulk alloys. The process used for powder preparation would need to be such as to favour the h.c.p. rather than the f.c.c. form of cobalt and in this respect milling is attractive since mechanical work tends to induce transition of f.c.c. α to h.c.p. ε. Probably other techniques such as electrodeposition or oxide reduction could be controlled to give the required crystal structure. If high coercivity ε powder could be obtained it is reasonable to hope that aligned, pressed compacts could be prepared by field pressing techniques of the type used for barium ferrite and rare-earth cobalt permanent magnets[25-28]. Sintering to increase densification would probably not be possible because of the ε to α transition and the fact that fine particles of α do not transform readily to ε on cooling. Nevertheless, the introduction of a suitable bonding material should enable mechanically strong compacts to be produced. On this basis useful permanent magnets based on finely divided cobalt remain a distinct possibility.

Acknowledgements

This work is connected with a programme of research into cobalt permanent magnets, which is sponsored by the Centre d'Information du Cobalt and is currently in progress at the Central Research Laboratory of the Permanent Magnet Association.

I would like to express my gratitude to the Permanent Magnet Association and in particular Mr. J. E. Gould, Director of Research, for generously allowing a great deal of time to be spent both on the experimental work and on the preparation of the thesis. It also gives me great pleasure to thank Dr. H.W. Rayson of Sheffield Polytechnic and Mr. W. Wright of the Permanent Magnet Association, Central Research Laboratory, for invaluable advice and encouragement throughout, and to acknowledge the many helpful discussions with Dr. H.McCaig and Mr. C. J. Fellows, both of the Permanent Magnet Association, Central Research Laboratory.

REFERENCES

1 WEISS, P., J. Phys., 6, 661 (1907)

2 HONDA, K. and KAYA, S., Sci. Rep. Tôhoku Imp. Univ., 15, 721 (1926)

3 KAYA, S., Sci. Rep. Tôhoku Imp. Univ., 17, 639 (1928)

4 SUCKSMITH, W. and THOMPSON, J.E., Proc. Roy. Soc., 225, (A), 362 (1954)

5 BRADLEY, A.J. and TAYLOR, A., Nature, 140, 1012 (1937)

6 KERSTEN, M., Phys.Z., 44, 63 (1943)

7 BECKER, R. and DÖRING, W., "Ferromagnetismus", Springer, Berlin (1939)

8 NÉEL, L., Ann. Univ. Grenoble, 22, 299 (1946)

9 ROSENITZ, E., "Ferromagnetic Properties of Metals and Alloys", Oxford University Press (1952)

10 STONER, E.C., "Ferromagnetism Magnetization Curves", Reports on Progress in Physics XIII, 83 (1950)

11 WENT, J.J., RATHENAU, G.W., GORTER, E.W. and VAN OOSTERHOUT, G.W., Phil. Tech. Rev., 13, 194 (1952)

12 KITTEL, C., Rev. Mod. Phys., 21, 541 (1949)

13 STONER, E.C. and WOHLFARTH, E.P., Phil. Trans., 240, 599 (1948)

14 BEAN, C.P. and JACOBS, I.S., J.App. Phys. 27, 1448 (1956)

15 KNEI, E.H., SHTRIKMAN, S. and TREVES, D., Phys. Rev. 106, 446 (1957)

16 WOHLFARTH, E.P., and TONGE, D.G., Phil.Mag., 2, 1333 (1957)

17 RATHENAU, G.W., Smit, J. and STUIJTS, A.L., Z.Phys., 133, 250 (1952)

18 AHARONI, A., J. App. Phys., 30, 70 S (1959)

19 BROWN, W.F., "Micromagnetics" (New York: Interscience Publishers), 66 (1963)

20 WOHLFARTH, E.P., "Hard Magnetic Materials", Phil.Mag., Supp., 6 87 (1959)

21 McCURRIE, R.A., Phil. Mag., 22, 1013 (1970)

22a NÉEL, L., C.R. Acad. Sci., Paris, 224, 1550 (1947)

22b NÉEL, L., C.R.,Acad. Sci.,Paris 228, 664 (1949)

23 De VOS, K.J., "The Relationship Between Microstructure and Magnetic Properties of Alnico Alloys", Thesis, Eindhoven (1966)

24 LEBORSKY, F.E., PAINE, T.O., and MENDELSOHN, L.I., Powder Met.Bull., (4), 57 (1959)

25 BUSCHOW, K.H.J., NAASTEPAD, P.A. and WESTENDORP, F.F., J.App.Phys., 40, 4029 (1969)

26 TSUI, J. and STENAT, K., App. Phys. Letters, 18, 107 (1971)

27 MARTIN, D.L. and RENZ, M.C., Cobalt, 50, 11 (1971)

28 JOHNSON, R.E. and YELLOWS, C.J., Cobalt, No.53, 191 (1971)

29 ZIJLSTRA, H., J. App.Phys., 41, 4881 (1970)

30 SCHWEIZER, J., STENAT, K.J. and TSUI, J.B.Y., I.E.E.E. Trans.Mag., MAG-7, page (1971)

31 McCAIG, M., Cobalt, 31, 83 (1966)

32 HONDA, K. and MASUMOTO, H., Sci.Rep. Tohoku Imp. Univ.,20, 323 (1931)

33 GERLING, W., Z. Angew. Phys., 28, 1 (1969)

34 MEIKLEJOHN, W.H., Rev. Mod. Phys., 25, 302 (1953)

35 WEIL, L., J.Phys., Radium, 12, 437 (1951)

36 LAVIN, F.A., Cobalt, 43, 87 (1969)

37 BATE, G., SCHOFIELD, D. and SUCKSMITH, W., Phil.Mag., 46, 621 (1955)

38 SUCKSMITH, W., J.Phys. Radium, 20, 290 (1959)

39 GALASSO, F.S., J.Metals, 19, 17 (1967)

40 LIVINGSTON, J.D., J.A.P., 41, 197 (1970)

41 MASUMOTO, H., KOBAYASHI, T.,AND WATENABE, K., Jap. Inst.Metals., 6, 187 (1965)

42 MASUMOTO, H., KOBAYASHI, T., and WATENABE, K., ibid, 7, 286 (1966)

43 MASUMOTO, H., KOBAYASHI, T., and WATENABE, K., ibid, 8, 8 (1967)

44 MASUMOTO, H., KOBAYASHI, T., and WATENABE, K., ibid, 8,100 (1967)

45 MASUMOTO, H., KOBAYASHI, T., and WATENABE, K., ibid, 8, 167 (1967)

46 MASUMOTO, H., KOBAYASHI, T., and WATENABE, K., ibid, 8, 259 (1967)

47 MASUMOTO, H., KOBAYASHI, T., and WATENABE, K., ibid, 9, 1 (1968)

48 MASUMOTO, H., KOBAYASHI, T., and WATENABE, K., ibid, 9, 6 (1968)

49 British Patent, 1,087,064

50 SCHRAMM, J., Z.Metalk., 33, 381 (1941)

51 OWEN, E.A., and MADOC-JONES, D., Proc.Phys.Soc., 67, (8), 456 (1954)

52 NEWKIRK, J.B. and GEISSLER, A.H., Acta Met., 1, 456 (1953)

53 HESS, J.B. and BARRETT, C.S., Trans.Amer.Inst.Min.Met.Eng., 194, 645 (1952)

54 KERSTEN, H., Physics, 2, 274 (1932)

55 KRAJEWSKI, W., KRIIGER, J. and WINTERHAGER, H., Cobalt, 47, 81 (1970) and 48, 120 (1970)

56 KLITZING, K.H., Z.Inst., 65, 4 (1957)

57 BUCKSMITH, W., Proc. Roy. Soc., 170, 551 (1939)

58 SCHOLES, R., J.Sci.Inst., 1, 1016 (1968)

59 COOPER, P., Phil. Mag., 8, 805 (1963)

60 WEIL, L., MARFOURE, S and BERTAUT, F., J.Phys.Radium, 9, 203 (1948)

61 BOZORTH, R.M., "Ferromagnetism", D.Van Nostrand Co.Ltd., 265 (1951)

62 [illegible]SKA, C.R., AVERBACH, B.L. and COHEN, M., Acta Met., 8, 81 (1960)

63 BURGERS, W.G., Physica, 1, 561 (1934)

64 KURDJUMOW, G. and SACHS, G., Z.S. f.Phys., 64, 325 (1930)

65 BRADLEY, A.J. and SEAGER, G.C., J.Inst.Metals., 64, 81 (1939)

66 MYERS, H.P. and BUCKSMITH, W., Proc.Roy.Soc., 207A, 427 (1939)

67 McCAIG, M., "Permanent Magnets and Magnetism", (Ed. D.Hadfield), London (Iliffe Books Ltd.) 87 (1962)

68 GERLACH, W., "Probleme der Technischen Magnetisierungskurve" (Ed.E. Becker) Berlin (Verlag Julius Spreinger) 141 (1938)

69 WOHLFARTH, E.P., Research, 7, A1 (1954)

70 LEAK, G.P., J. App. Phys., 26, 1361 (1955)

71 ISHIKA, F.D., WALTENBERG, R.C. and SCOTT, H., Trans.Amer.Inst.Min. Met.Eng., 64, 41 (1921)

72 SMITH, G.C., Prog.,Met., Phys., 1, 176 (1949)

73 EDWARDS, G.S., J.Inst.Met., 67, 68 (1941)

74 De VOS, K.J., "Magnetism and Metallurgy", ed. Berkowitz, A. and Kneller, E., (Academic Press) 473 (1969)

75 FOUNTAIN, R.W. and FORGENG, W.D., Trans.Met.Soc., A.I.M.E., 215, 996 (1959)

76 TILLER, W.A. "Liquid Metals and Solidification" Cleveland Ohio (Amer. Soc. Met.) (1958)

77 CHILTON, J.P. and WINEGARD, W.C., J.Inst. Met. 89, (1961)

78 ALBRIGHT, D.L., Thesis Lehigh Univ. (1965)

79 ALBRIGHT, D.L., and KRAFT, R.W., Trans. A.I.M.E., 236, 998 (1966)

80 GALASSO, F.S., DOUGLAS, F.S., BARRY, W. and BATT, J.A., J.A.P. 38, 5241 (1967)

81 B.P. 1,116, 848

82 ROSENQUIST, T., Acta Met. 1, 701 (1953)

83 KOSTER, W. and MULFINGER, W. Z. Metallkunde 30, 345 (1938)

84 HASHIMOTO, T., KINZOKU no KENKYU, 9, 57 (1932)

85 MONROE, M., J.I.S.I., 206, 1 (1961)

86 ISHIKAWA, K., Z. Anorg.Chem. 59, 327 (1908)

87 VOGEL, R., and ROSENTHAL, K., Arch. Eisenhuttenw. 7, 689 (1934)

88 HASHIMOTO, T., Nippon Kinzoku Gakkai-Shi 1, 135 (1937)

89 KOSTER, W., and SCHMID, E., Z.Metallkunde 29, 232 (1937)

90 CALLO, S., La Metallurgia Italiana, Jan. 1958 p.15

APPENDIX I

THE ALLOTROPES AND ALLOTROPIC TRANSFORMATION OF COBALT

The Allotropes of Cobalt

The fact that cobalt can exist in two allotropic forms, close packed hexagonal and face centred cubic, was first discovered by Hull[A1] in 1921. Since then a great deal of work has been published aimed at measuring accurately the lattice parameters of the allotropes and establishing their stability relative to temperature.

The lattice parameters suggested by "Cobalt Monograph" [A2] as being probably the most accurate are as follows, for the low temperature h.c.p. modification (ε) $a = 2.5071$ Å, $c = 4.0686$ Å, $c/a = 1.6226$[A3], for the high temperature f.c.c. form (α) $a = 3.5441$ Å [A4]. It is interesting to note that several authors [A5-A7] have obtained consistently high values around 3.56 Å for α. Owen and Madoc-Jones[A4] found that annealing cobalt filings caused a progressive increase in lattice parameter from about 3.55 Å up to about 3.56 Å after 88 hours at 595°C and 14 hours at 836°C. Further treatment at 836°C produced no further increase, but 1 hour at 906°C caused reversion to the smaller lattice. They conclude that the large lattice is some type of metastable constituent. It seems likely that this phenomenon is partly responsible for the large range of published values.

The transformation on heating and cooling is subject to considerable hysteresis and is influenced by the history of the materials. A precise transformation temperature cannot be defined but it is now accepted that ε is stable below about 400°C and α is stable at higher temperatures up to the melting point.[A9-A12].

Various workers have made the comment that the X-ray diffraction pattern of the c.p.h. form shows signs of line broadening. Edwards, Lipson and Wilson [A10] explained this by suggesting the presence of faults in the

hexagonal atomic arrangement resulting in a sequence of planes such as ABABACACBCBCABC etc. Edwards and Lipson [A17] were able to show that a structure containing a small number of faults would have a slightly lower free energy than the perfect structure, and that, providing the change in free energy on transformation was very low, this may become a significant factor in determining the atomic arrangement.

In a more recent investigation, Mouska et al [A18] describes two types of fault, growth faults and deformation faults, which they depict as follows:-

Both may be produced by the growing together of two out of phase c.p.h. lattices, while the deformation fault may also form by partial slip converting A planes into C planes and B planes into A planes. They find these faults not to be distributed randomly but to form regions such that, while some regions contain both types, others contain only deformation faults. It is postulated that the latter represent those areas of c.p.h. material which form in the early stages of transformation when transformation strains are readily accommodated by deformation faulting in both phases. During the later stages of the transformation, the growth of c.p.h. areas is more restricted resulting in the appearance of growth and deformation faults where out of phase c.p.h. lattices grew together.

The Allotropic Transformation

Although not completely suppressed in coarse grained material, the transformation f.c.c.→h.c.p. on cooling is sluggish and is subject to the influence of a number of metallurgical variables. This can be

accounted for in terms of the low driving force which in turn is associated with the free energy change involved in the reaction. Heidenreich and Shockley[A19] estimated from the transition temperature a free energy change, ΔG of 100 cal/mole. Other investigations[A19,20,21] have obtained values between 105 and 108 cal/mole at 700°K, although Adams and Altstetter[A21] go on to show that in single crystals the value is variable dependent on the history of the material, and suggest that the number and type of defects has a significant effect.

Hysteresis Effects

Huss and Barrett[A9] showed that by lightly deforming the metal it was possible to bring about the $a \rightarrow \epsilon$ transformation at similar temperatures, 417 ± 7°C, on heating and cooling. This is unusual in that the transformation is generally subject to considerable hysteresis[A12,A22,A23] Typical results are those of Sebilleau and Bibring[A22] who carried out a series of dilatometric experiments on cold worked cobalt. They found that a number of cycles through the transition temperature were necessary before a stable dilatometric curve was produced. This stabilisation corresponded to the completion of re-crystallization. The form of the stable curve, as shown in Figure A1, indicates transformation temperatures of 430°C on heating, and 390°C on cooling. These temperatures were independent of heating and cooling rates, but the ranges of temperature over which transformation took place ($\Delta T1$ and $\Delta T2$) were reduced by reduced heating and cooling rates. If heating or cooling was stopped within a transition range, the transformation stopped. If the direction of treatment was then reversed, the reverse change did not occur until the normal transformation temperature was reached.

Effect of Grain Size and Particle Size

The extent to which cobalt is sub-divided into grains or discrete particles has an important effect on the incidence of the transformation.

Owen and Madoc-Jones[A4] report the retention of α in finely divided cobalt after annealing and quenching from temperatures up to 600°C, and note the appearance of ε after quenching from higher temperatures. These results are similar to those of a number of other workers [A12,A13-15,A23], and some authors [A13-15] have suggested the existence of a second allotropic change (f.c.c.→h.c.p.) between 800°C and 1150°C. However, Newkirk and Geissler [A9] showed that, although both allotropes were produced on quenching from 1220°C, the f.c.c. form alone was present when examined in a high temperature X-ray diffraction camera at a similar temperature. It seems, therefore, that the α→ε transformation, which is sluggish in bulk material, is completely suppressed in fine grained samples but that annealing at high temperatures causes sintering and grain growth, thus producing suitable conditions for the appearance of a certain amount of ε on cooling. The majority of the results concern samples quenched from the annealing temperature, but it has also been shown [A4] that similar suppression of the reaction occurs on furnace cooling.

The Effect of Mechanical Work

Hess and Barrett [A8] have shown that a small amount of deformation has the effect of decreasing the amount of hysteresis between the heating and cooling reactions. They go on to show, however, that severe deformation of the cubic form produced considerable lowering of the f.c.c. → h.c.p. transformation temperature, possibly due to the hindering effect of the increased number of dislocations on the growth of h.c.p. nuclei.

It is well established that moderate deformation at room temperature will convert retained f.c.c. material to h.c.p. Sykes [A24] reports that h.c.p. material so formed persists even after prolonged treatment at 1000°C, but this seems unlikely and is not substantiated by Troiano and Tokich [A12], who found that the amount of the f.c.c. phase began to increase on treatment at 320°C, and that samples became entirely cubic at 475°C.

Sebilleau and Bibring [A23] showed that, after severe cold working of the hexagonal structure, recrystallization began around 350°C, and that annealing at 300°C resulted only in the recovery of the material. Samples previously allowed to recover at 300°C were found on recrystallization at 350°C to be entirely h.c.p. while recrystallization without prior recovery produced a certain amount of the f.c.c. form. Apart from a small difference in temperature, this effect is similar to that observed by Troiano and Tokich and is thought, according to Sebilleau and Bibring, to be connected with the energy introduced into the metal by plastic deformation, which may be close to the free energy difference between the two phases, and which would be reduced by recovery prior to recrystallization.

Cobalt Produced by Electrolysis and by Oxide Reduction

Hull [A1] was able to show that cobalt produced by electrolysis of the sulphate contained both types of lattice while Kersten [A25] found that at values of pH around 5-6, the cobalt deposited was completely hexagonal, and that reducing the pH by the addition of H_2SO_4 resulted in the appearance of increasing amounts of the f.c.c. lattice.

Several workers, including Hendricks et al [A15], and Sykes [A24], have found that the crystal form of the cobalt produced by the reduction of Co_3O_4 is dependent on the temperature such that c.p.h. is present below 400°C, f.c.c. up to about 1000°C, and h.c.p. above 1000°C. Since 400°C is below the equilibrium transformation temperature the appearence of c.p.h. material is straightforward; the presence of the cubic form between 400°C and 1000°C is probably due to the suppression of the transformation on cooling, while the re-appearance of the hexagonal form above 1000°C can be attributed to grain growth as discussed earlier.

Influence of Alloy Additions and Impurities

Gianni et al [A26] discuss the allotropic transformation in cobalt rich solid solutions. They first consider the transformation as martensitic

occurring at temperatures M_s on cooling and A_s on heating. These temperatures can be affected in three possible ways, as represented in Figure A2. It should be stressed that these temperatures are influenced by variables such as grain size and previous history, and should not be included as part of an equilibrium phase diagram. With regard to the thermodynamic stability of the allotropes, two basic possibilities exist, these being as shown in Figure A3, the constriction or enlargement of the f.c.c. field.

Considering the possible combinations of these diagrams in real systems, it is pointed out that the M_s temperature must always lie within the equilibrium h.c.p. (ε) field and A_s within the f.c.c. (α) field. Thus a type I equilibrium diagram may appear in combination with type b or c M_s and A_s temperatures, and type II with type a or c M_s and A_s temperatures. In most practical cases the reaction will take place martensitically at the M_s or A_s temperature, but this is not necessarily the case, particularly in type I equilibrium when the transformation temperatures are increased and a diffusion type mechanism may take precedence. Two schematic representations of equilibrium diagrams plus M_s and A_s temperatures are presented by Gianni et al, as shown in Figure A4.

A comprehensive review of the effect of alloy additions on the transformation in cobalt has been published by Krajewski et al [A27].

The Transformation Mechanism

The reaction α → ε on cooling is characterized by a number of features which have led to its being classified as martensitic; these may be summarized as follows:-

(i) The transformation is, under most circumstances, athermal in nature [A17,A22,A23];

(ii) retained f.c.c. material is converted to h,c.p. on moderate deformation at or below room temperature [A12];

(iii) the reaction temperature is not lowered by increasing the cooling velocity [A12,A23];

(iv) the amount of f.c.c. material retained at room temperature is dependent on the time and temperature of heat treatment (therefore effectively on the grain, or particle size) not on the cooling velocity [A12];

(v) tranformation markings indicating surface tilts and upheavals associated with a shear mechanism are commonly observed in pure cobalt [A26].

The crystallographic relationship between the two allotropes is given by Christian [A28] as

$$\{111\}_\alpha \;//\; \{0001\}_\varepsilon,\ \langle 110\rangle_\alpha \;//\; \langle 11\bar{2}0\rangle_\varepsilon$$

The transformation f.c.c. → h.c.p. can be brought about by a simple shear in the {111} planes of the f.c.c. structure such that every alternate atomic plane is displaced through a distance $a/\sqrt{6}$ in the $[11\bar{2}]$ direction where 'a' is the lattice parameter of the f.c.c. unit cell.

Various authors have discussed mechanisms for the transformation in some detail.

Christian [A28] considers the reaction to be nucleated from a dislocation in the (111) plane with Burgers' vector $a/\sqrt{2}\ [10\bar{1}]$ which splits into the two partial dislocations $a/\sqrt{6}\ [11\bar{2}]$. These are mutually repulsive, and on moving apart produce a small region of atoms with the h.c.p. structure. If the temperature is such that the f.c.c. form is stable, the width of this extended dislocation will be restricted and will have an equilibrium width dependent on temperature. As the temperature is lowered towards the transformation temperature, the restrictive forces approach zero and the width of the dislocation will

tend to increase. Below the equilibrium transformation temperature, assuming the absence of other restraining forces associated with structural imperfections, the two partials will move steadily apart, under a driving force associated with the lower free energy of the h.c.p. structure. They will thus ultimately arrive at a grain boundary or free surface, at which point reflection will occur.

Christian goes on to point out that, due to the displacement involved not being a lattice vector, reflection back along the slip plane would result in an energetically unfavourable proximity between adjacent atoms. However, atoms in neighbouring slip planes which also tend to overshoot are not restrained in this way, and reflections on these may be possible. In fact, reflection on the next (111) plane would disturb the stable h.c.p. atomic arrangement produced by the passage of the original dislocation, and is thus unfavourable, while reflection on the next but one plane would cause an increase in the amount of h.c.p. material and propogation of the transformation.

It is thus possible to envisage complete transformation on this basis. The presence of faults may be accounted for by the reflection of partial dislocations along the next, instead of the next but one, plane to the original slip plane. The athermal nature of the transformation is explained since the transformation, once initiated, will proceed until halted by force fields associated with stationary dislocations and imperfections. This resistance is overcome by the increase in driving force produced by lowering the temperature. The extent of the transformation thus depends on temperature rather than on time at temperature or cooling rate.

The lowering of the transformation temperature and the general sluggishness of the reaction in fine grained poly-crystalline material is explained by Christian as being due to the tendency of dislocations to lose kinetic energy on arrival at grain boundaries, resulting in their

being more easily stopped, on reflection, by opposing force fields. Similarly, a dislocation may be completely absorbed at a grain boundary and thus contribute no further to the reaction. It may also be postulated that insufficient suitable dislocations are present in very fine particles or grains to efficiently nucleate the transformation, and that those which are present tend to have a lower kinetic energy than in coarse grained material due to the shorter distance through which they have travelled on arrival at a free surface or grain boundary.

A slightly different type of mechanism is proposed by Seeger [A29], Sebilleau and Bibring [A30], and Bilby [A31]. Again, the transformation on cooling is nucleated by a region of h.c.p. material present between two partial dislocations in the f.c.c. lattice. Growth of the stacking fault is, however, accomplished by rotation around a dislocation with a screw component of $2a/3$ <111>. The failure of the reaction to occur in finely divided material is assumed to be due to a lack of sufficient suitable dislocations in individual particles or grains.

REFERENCES (Appendix I)

A1 Hull, A.W., Phys. Rev., 17 (ii), 571 (1921)

A2 "Cobalt Monograph", Ed. Centre d'Information du Cobalt, Brussels 1960

A3 Anantharaman, T.R., Current Sci., 27, 51, (1958)

A4 Owen, E.A., and Madoc-Jones, D., Proc. Phys. Soc., 67 (B), 456 (1954)

A5 Sekito, S., Sci. Rep.Tohoku Univ., 16, 565 (1927)

A6 Wyckoff, R.W.G., The Structure of Crystals (New York Chemical Catalog. Co.Inc.), 204 (1931)

A7 Marick L., Phys. Rev., 49, 831 (1936)

A8 Hess, J.B., and Barrett, C.S., Trans. Amer.Inst.Min.Met.Eng., 194, 645 (1952)

A9 Newkirk, J.B., and Geissler, A.H., Acta Met., 1, 456 (1953)

A10 Marick, L., Phys. Rev., 49 (ii), 831 (1936)

A11 Meyer W.F., Z. Krist., 97, 145 (1937)

A12 Troiano, A.R., and Tokich, J.L., Trans. Amer. Inst.Min.Met.Eng., 175, 728 (1948)

A13 Metcalfe, A.G., Proceedings First World Metallurgical Congress, Detroit 1951, Amer.Soc. Metals, 177 (1952)

A14 Metcalfe, A.G., Acta Met., 1, 669 (1953)

A15 Hendricks, S.B., Jefferson, M.E., and Schultz, J.E., Z. Krist., 73, 376 (1930)

A16 Edwards, O.S., Lipson H., and Wilson, A.J.C., Proc. Roy.Soc. A, 180, 268 (1942)

A17 Edwards, O.S., and Lipson, H., J.Inst.Metals, 69, 177 (1943)

A18 Houska, C.R., Averback, B.L., and Cohen, M., Acta Met., 8, 81 (1960)

A19 Heidenreich, R.D., and Schockley, W., "Strength of Solids", (The Physical Society, London) 57, (1948)

A20 Kelley, K.K., U.S. Bureau Mines, Bull. No. 584, 59 (1960)

A21 Adams, L., and Altstetter, C., Trans. Met. Soc. A.I.M.E., 242, 139 (1968)

A22 Myers, H.P., and Sucksmith, W., Proc. Roy. Soc. A, 207, 427 (1951)

A23 Seuilleau, F., and Dibring, H., The Allotropic Transformation of Cobalt, Inst. of Metals Monograph and Rep. Series No. 18, London 299 (1956)

A24 Sykes, W.P., Trans. Amer. Soc. Steel Treating, 21, 385 (1933)

A25 Kersten, M., Physica, 2, 274 (1932)

A26 Gianni, A., Burma, J., and Preisc, E.J., Cobalt No.39 (1968)

A27 Krajewski, W., Kruger, J and Winterhager, H., Cobalt No.47 81 and No.48, 120 (1970)

A28 Christian, J.W., Proc. Roy. Soc., A. 206, 51 (1951)

A29 Seeger, A., Z. Metallkunde, 47, 653 (1956)

A30 Bibring, H., and Sebilleau, F., Rev. Met., 52, 569 (1955)

A31 Bilby, B.A., Phil. Mag., 44, 782 (1953)

Fig. A 1 - Temperature hysteresis of α ⇌ ε transformation [A22]

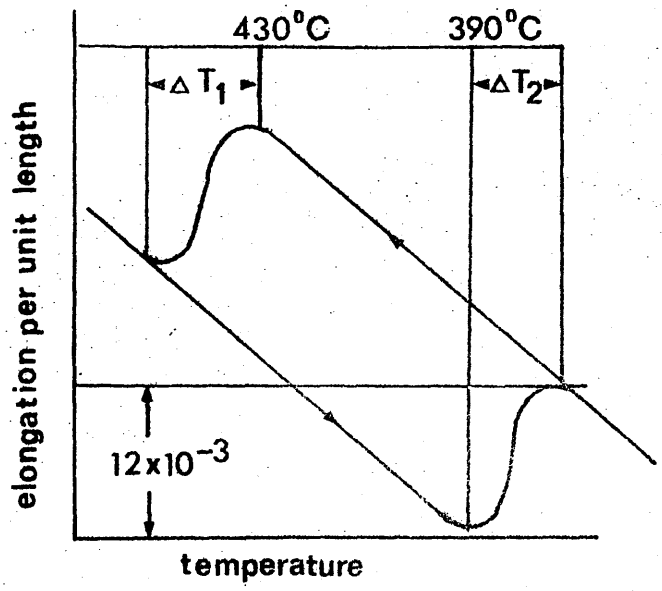

Fig. A 2 - Effect of alloy additions on martensitic α ⇌ ε transformation (schematic) [A26]

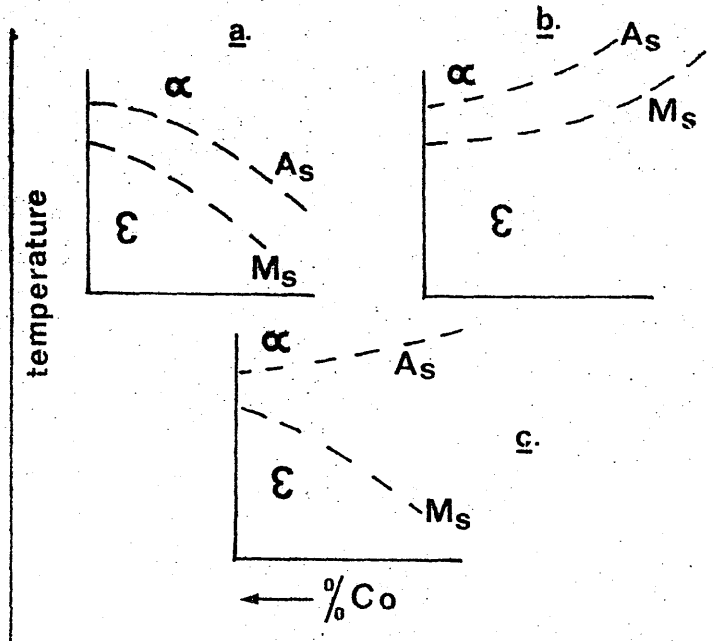

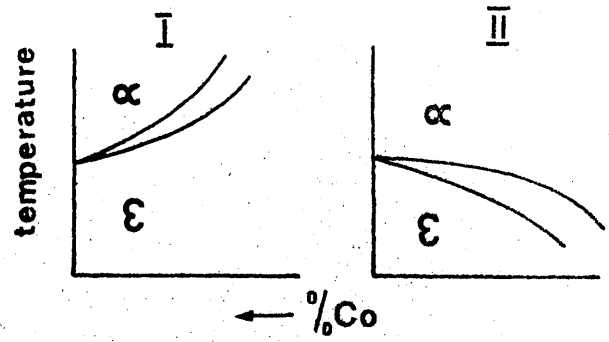

Fig. A 3 - Effect of alloy additions on the equilibrium stability of α and ε, (schematic) [A26]

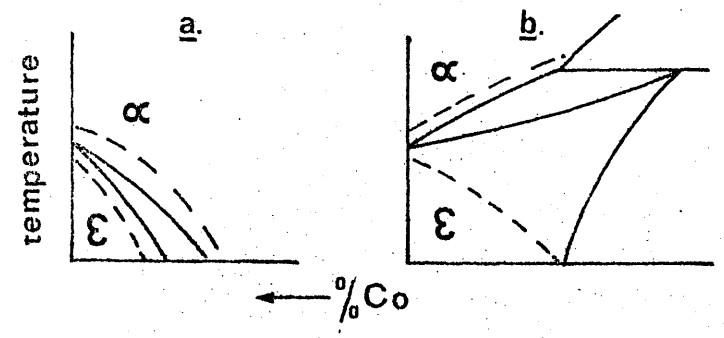

Fig. A 4 - Schematic phase diagrams with A_s and M_s temperatures superimposed [A26]

(a) Cobalt based alloys with nickel or iron

(b) Cobalt based alloys with the refractory metals

APPENDIX II

Summary of a recent X-ray diffraction study of Halcolloy

Arbuzmov, M.P., Pavlyukov, A.A. and Opanasenko, O.S., Fiz. Metal Metalloved., 28, 787 (1969), (in Russian). Phys. Metals and Metallography 28, 21 (1971) (in English).

Pavlyukov, A. A., Opanasenko, O.S., and Sobolevskaya, V.I., Fiz. Metal Metalloved., 29, 888, (1970). (in Russian). Phys Metals and Metallography, 29, 220 (1971), (in English).

These reports came to the attention of the author when published in English translation during 1971, at which time the work described in this thesis was largely complete. The papers are concerned largely with a study of the crystallography of the Halcolloy alloys and substantially confirm several of the conclusions reached in the present work.

Using X-ray diffraction photographs obtained in a rotating crystal camera with single crystal specimens rotating, rocking and fixed, the phases present in an alloy of cobalt plus 27.5 at% aluminium, in the quenched and aged condition, were studied. On ageing at up to 700°C a h.c.p. phase with lattice parameters, $a = 2.50$ Å, $c = 4.0$ Å, $c/a = 1.60$ was precipitated. This phase was called α' to differentiate it from the f.c.c., α solid solution of aluminium in cobalt which precipitated on ageing at 750°C. The h.c.p. form of cobalt, ε, has parameters, $a = 2.5071$ Å, $c = 4.0686$ Å, $c/a = 1.6228$ Å. It seems reasonable to suppose, therefore, that the h.c.p. α' phase detected by Arbuzov et al is, essentially, ε. The parameters of α' are thus rather smaller than those normally accepted for ε but the fact that values are quoted to only two decimal places in the case of a and only one place in the case of c, suggests that the accuracy of the measurements was not very great and it is doubtful whether any significance should be attached to the small difference observed.

These results thus confirm, in general terms, the conclusion reached in this thesis that ε is precipitated in Malcolloy at ageing temperatures for which α is the stable form. It is not clear at what temperature f.c.c. α was detected in addition to h.c.p. α′ (ε) but both phases were present after ageing at 700°C the amount of α increasing as the time was extended from half-an-hour to one hour.

The orientation relationship between h.c.p. α′ (ε) and the b.c.c. matrix (β) was determined as,

$$(0001)_{\alpha'} \;//\; (01)_{\beta} \qquad \langle 11\bar{2}0\rangle_{\alpha'} \;//\; \langle 111\rangle_{\beta}$$

This is the Burgers relationship and substantiates the results of the present work. It is also interesting that, from the form of diffuse scattering regions associated with the matrix reflections, Arbuzov et al deduced that the matrix was strained, due to coherency with the h.c.p. precipitate, so that the cubic lattice was distorted into a monoclinic structure. The effect was not observed when the precipitate was α. This is again in agreement with the present work where line broadening in the diffraction pattern of β in the presence of ε was attributed to strain. Furthermore, strain due to coherency between $(1\ \bar{1}00)_{\varepsilon}$ and $(112)_{\beta}$, (the planes suggested in the thesis as being likely to form a coherent interface between ε and β), would result in a reduction in the interplaner spacing of one set of {110} planes in the β lattice, thus giving a monoclinic type of structure.